Design and synthesis of biocompatible fluorescent semi-conductor nanocrystals for *in-vivo* and *in-vitro* imaging/sensing applications

by

Wenhao Liu

B.A. Chemistry, B.A. Integrated Science
Northwestern University
Evanston, IL
2005

Submitted to the Department of Chemistry in
Partial Fulfillment of the Requirements for the Degree of

DOCTOR OF PHILOSOPHY

at the

MASSACHUSETTS INSTITUTE OF TECHNOLOGY

March 2010
[June 2010]

Signature of Author _____
Department of Chemistry
March 20, 2010

Certified By _____
Moungi G. Bawendi
Lester Wolfe Professor of Chemistry
Thesis Supervisor

Accepted By _____
Robert W. Field
Chairman, Department Committee of Graduate Students

This doctoral thesis has been examined by a committee of the Department of Chemistry as follows:

Professor Andrei Tokmakoff _____ Chairman

Professor Moungi G. Bawendi _____ Thesis Supervisor

Professor Alice Y. Ting _____ Department of Chemistry

Design and synthesis of biocompatible fluorescent semi-conductor nanocrystals for *in-vivo* and *in-vitro* imaging/sensing applications

by

Wenhao Liu

Submitted to the Department of Chemistry on March 3, 2010 in partial fulfillment of the requirements for the degree of Doctor of Philosophy in Chemistry

ABSTRACT

Quantum dots (QD) are unique materials in which their optical properties are decoupled from their solution properties via the tunability of surface ligands. The primary focus of this thesis is the design and synthesis of new ligand coatings to render QDs water soluble, pushing the boundaries of QD applications in biology both in-vivo and in-vitro. On the in-vivo front, ultra-small QDs (~5 nm hydrodynamic diameter) were synthesized via the use of Cysteine as a zwitterionic ligand coating to generate the smallest biocompatible QDs known to date, allowing for the first time collection of quantitative in-vivo renal clearance data of inorganic nanoparticles in a mouse as a model for design of future clearable nanoparticle in-vivo probes and drug delivery vehicles.

On the in-vitro front, a suite of multifunctional ligands were synthesized to produce QDs that exhibit low non-specific binding to cells, small hydrodynamic diameter (HD), tunable surface charge, high quantum yield, and good solution stability across a wide pH range. These ligands feature dihydrolipoic acid for tight binding to the QD surface, a short poly(ethylene glycol) (PEG) spacer for water solubility and biocompatibility, and an amine or carboxylate terminus for covalent derivatization. We successfully demonstrated covalent attachment of energy acceptor dyes to enable sensing applications via Forster Resonance Energy Transfer (FRET), and attachment of proteins to enable high-affinity cell labeling and single particle tracking. In addition, QDs solubilized with these ligands could be derivatized via metal-affinity driven conjugation chemistry with polyhistidine-tagged proteins, which facilitated the purification of monovalent QDs for the first time via gel electrophoresis.

Further improvement on ligand stability focused on addressing the problem of thiol oxidation, and a new class of multifunctional polymer ligands were developed featuring multiple imidazole moieties for multidentate interactions with the QD surface. The polymers are synthesized via reversible addition-fragmentation chain transfer (RAFT)-mediated polymerization to produce molecular weight controlled monodisperse random copolymers from three types of monomers that feature imidazole groups for QD binding, polyethylene glycol (PEG) groups for water solubilization, and either primary amines or biotin groups for derivatization.

Thesis Supervisor: Moungi G. Bawendi, Ph.D.
Title: Lester Wolfe Professor of Chemistry

Preface

Chapters from this thesis were reproduced in part from the following references:

Liu W, Greytak AB, Lee JM, Wong CR, Park J, Marshall LF, Jiang W, Ting AY, Nocera DG, Fukumura D, Jain RK, Bawendi MG. Compact biocompatible quantum dots via RAFT-mediated synthesis of imidazole-based random copolymer ligand. *J Am Chem Soc* 2009, **132**: 472-483

Liu W, Howarth M, Greytak AB, Zheng Y, Nocera DG, Ting AY, Bawendi MG. Compact Biocompatible Quantum Dots Functionalized for Cellular Imaging. *J Am Chem Soc* 2008, **130**: 1274 -1284.

Howarth M, **Liu W**, Puthenveetil S, Zheng Y, Marshall LF, Schmidt MM, Wittrup KD, Bawendi MG, Ting AY. Monovalent, reduced-size quantum dots for imaging receptors on living cells. *Nature Methods* 2008, **5**: 397-399

Liu W, Choi HS, Zimmer JP, Tanaka E, Frangioni JV, Bawendi MG. Compact Cysteine-Coated CdSe(ZnCdS) QDs for In Vivo Applications. *J Am Chem Soc* 2007, **129**: 14530.

Choi HS, **Liu W**, Misra P, Tanaka E, Zimmer JP, Kandapallil B, Bawendi MG, Frangioni JV. Renal Clearance of Nanoparticles. *Nature Biotech* 2007, **25**: 1165 - 1170.

To My Family and Friends

Table of Contents

Table of Figures

Chapter 1: Introduction to Semiconductor Nanocrystals and Their Applications in Biology

1.1 *From the Bulk to the Nanoscale*

The electronic structure of a bulk semiconductor is characterized by valence and conduction bands with continuous density of states increasing as $E^{1/2}$. The effect on the density of states as dimensional constraints are increasingly imposed on the carriers is illustrated in Figure 1-1. As the dimensionality decreases from the bulk to a thin film quantum well, to a 1D quantum wire, and finally to a zero-dimensional quantum dot (QD), the energy levels become

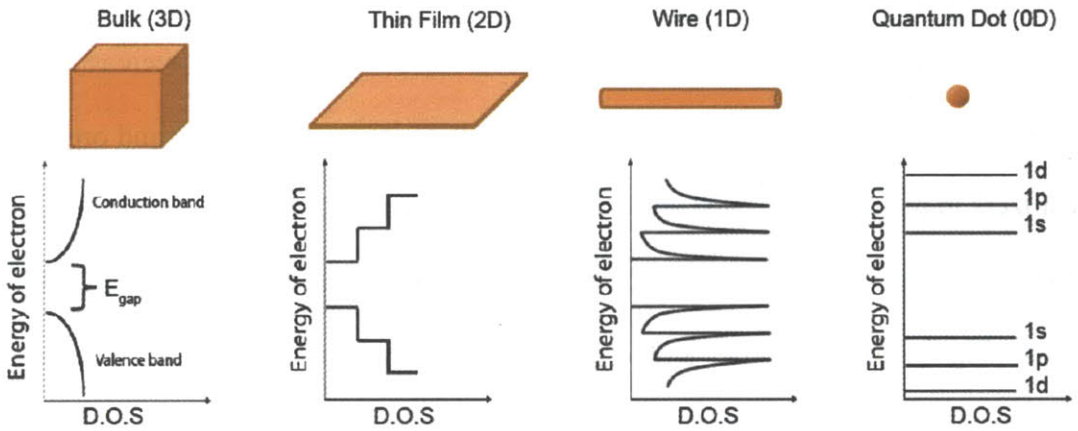

Figure 1-1 Illustration of the quantum size effect on the density of states. The density of states for a semiconductor is shown qualitatively from the bulk material, to a 2D thin film, to a 1D quantum wire, and fibnally to a 0D quantum dot, showing atomic-like states.

increasingly discretized with increasingly sharp transitions. In the extreme case of 0D confinement, the once-continuous density of states in the bulk become discrete atom-like states (Figure 1-1). The physical size at which this extreme quantum confinement regime takes place depends on the characteristic exciton Bohr radius of the particular semiconductor material. In the case of CdSe, which is the primary focus of this thesis, the Bohr radius is ~5.6 nm. Indeed,

the size range of CdSe QDs accessible using modern synthetic techniques can range from a radius of ~1 – 5 nm. In this strong confinement regime in which the nanocrystal size is smaller than the exciton Bohr radius, the bandgap energy is strongly influenced by the nanocrystal size. A more quantitative and detailed theoretical treatment of this quantum size effect can be found in reference [1]. A simple "particle in a sphere" model can be used to approximate the bandgap energy, which is found to be proportional to $1/r^2$. Thus, as the QD becomes smaller, the bandgap energy increases to produce a blue-shift in the optical spectra. The unique optical tunability of QDs as a function of size is one of the properties that make QDs especially attractive for numerous technological applications.

1.2 *Overview of Nanocrystal Synthesis*

Over the past 15 years, QDs have proven to be useful in an increasing number of technological applications, such as in the active emitting layer of inorganic and organic LEDs,[2, 3] as sensitizers in photovoltaic cells[4] and photodetectors[5], and as imaging agents in biology.[6, 7] The key driver enabling the application of QDs in such a diverse range of fields lies in the ability to synthesize highly monodisperse and crystalline nanocrystals in a colloidally stabilized and solution processable system. Having highly monodisperse and crystalline nanocrystals enables detailed studies of their photophysical properties, and also yields QDs with exceptionally narrow emission spectra on the order of 25 – 30 nm full-width at half-maximum (FWHM) in the case of CdSe, which is critical for technological applications where color purity and the ability for multiplexing are important. In addition, QDs as synthesized are colloidally stabilized by organic capping ligands, which make them amenable to solution processing techniques such as spin casting, drop casting, and ligand exchange for dispersibility in a wide variety of both non-polar and polar solvents. The versatility of this nanocrystal system, in which the optical properties (i.e.

emission color) are decoupled from the physical properties (i.e. solubility, surface charge, surface functionality, etc.) has enabled the numerous applications outlined above and continue to act as the driving force for future applications.

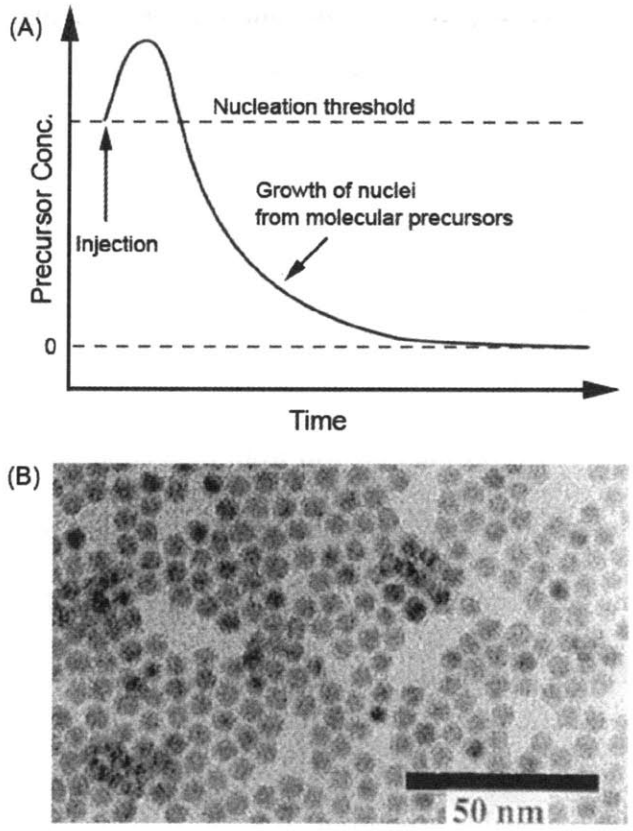

Figure 1-2 Nucleation model and TEM of CdSe nanocrystals. (A) LaMer and Denegar model for nucleation and growth of nanocrystals.[8] Rapid injection of precursors triggers a discrete nucleation event, followed by slow growth of the nuclei via the diffusive addition of molecular precursors. (B) TEM of CdSe nanocrystals synthesized in the manner described in (A), showing highly monodisperse size distribution.[9] Image reproduced from C. B. Murray, Ph.D. Thesis, MIT, 1995.

One of the early investigations of colloidal nanocrystals was made in the 1980s, where small nanocrystallites were synthesized via an arrested precipitation method followed by aging via Ostwald ripening, which produced CdS clusters with relatively broad size distribution.[10-12] A breakthrough in nanocrystal synthesis came in the early 1990s with the development of a LaMer and Dinegar type synthesis[13] of CdSe nanocrystals. In 1950, LaMer and Dinegar formulated a theory on the formation of monodisperse colloids, in which a temporally distinct

nucleation event is induced by the critical supersaturation of solution precursors. The formation of nuclei relieves the critical supersaturation thereby rapidly arresting nucleation to produce a population of homogenous nuclei, from which controlled growth of the nanoparticle occurs via addition from molecular precursors in solution, yielding highly monodisperse sulfur hydrosols (Figure 1-2A). This same type of synthesis was achieved for CdSe using a highly reactive organometallic precursor dimethylcadmium ($CdMe_2$), along with trioctylphosphine-Se (TOP-Se) as the selenium source, injected rapidly and simultaneously into a high temperature (~300 °C) coordinating solvent to induce a homogenous nucleation event.[9] This injection of room temperature precursors quickly lowers the solvent temperature to below the nucleation threshold (~260 °C), whereupon controlled growth from molecular precursors commences in the presence of a trioctylphosphine/trioctylphosphine oxide (TOP/TOPO) coordinating solvent system. Alkylphosphosphic acid impurities inherently present in the TOP/TOPO solvent system are critical at this stage both for colloidally stabilizing the nanocrystals and for providing the steric barrier needed for slowing the growth kinetics allowing for controlled growth. In this fashion, CdSe nanocrystals of tunable size from ~15-100 Å with narrow size distributions (5-10% dispersity) can be synthesized efficiently and reproducibly (Figure 1-2B). Figure 1-3 shows the typical experimental apparatus for this type of synthesis.

However, due to the acute toxicity, instability, and pyrophoric nature of $CdMe_2$, other less reactive precursors were soon developed. For instance, $Cd(acac)_2$ was developed as an alternative Cd source by reduction of Cd^{2+} to elemental cadmium using dodecanal in a solution of TOP, forming a yellow colored homogenous solution.[14] This elemental Cd precusor solution was then introduced along with TOP-Se into TOP/TOPO at high temperature, following the

same type of reaction pathway shown in Figure 1-2 to produce monodisperse and crystalline nanocrystals, while utilizing a much less reactive and safer Cd starting material.

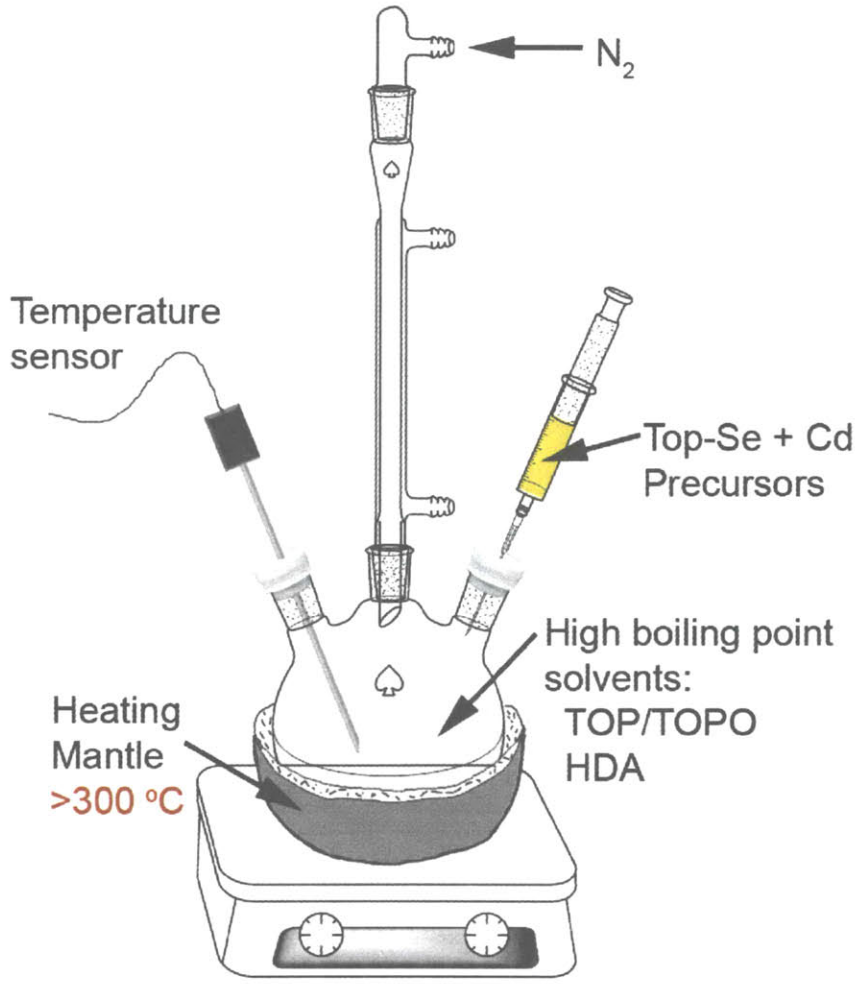

Figure 1-3 Schematic of reaction setup for typical nanocrystals synthesis. Cd and Se precursors are loaded into a syringe and rapidly injected into a bath of high boiling-point solvents at >300 °C.

Later work by Peng et al. showed that $CdMe_2$ decomposes rapidly in hot TOPO to Cd-phosphonic acid complexes, suggesting also that $CdMe_2$ may not be necessary. Indeed, a Cd-phosphonic acid complex could be generated first by heating CdO, an inert and non-pyrophoric precursor, with tetradecylphosphonic acid (TDPA) in TOP/TOPO.[15] Subsequent injection of a selenium source at high temperature also produced high quality CdSe nanocrystals with excellent size distribution and size control. Peng et al also introduced the use of non-coordinating solvents

such as 1-octadecene, while relying on the addition of coordinating ligands such as fatty amines and fatty acids to achieve controlled growth.[16, 17] These and other methods utilizing both non-pyrophoric Cd precursors and more benign non-coordinating solvents have enabled the scale-up of QD synthesis for industrial applications.

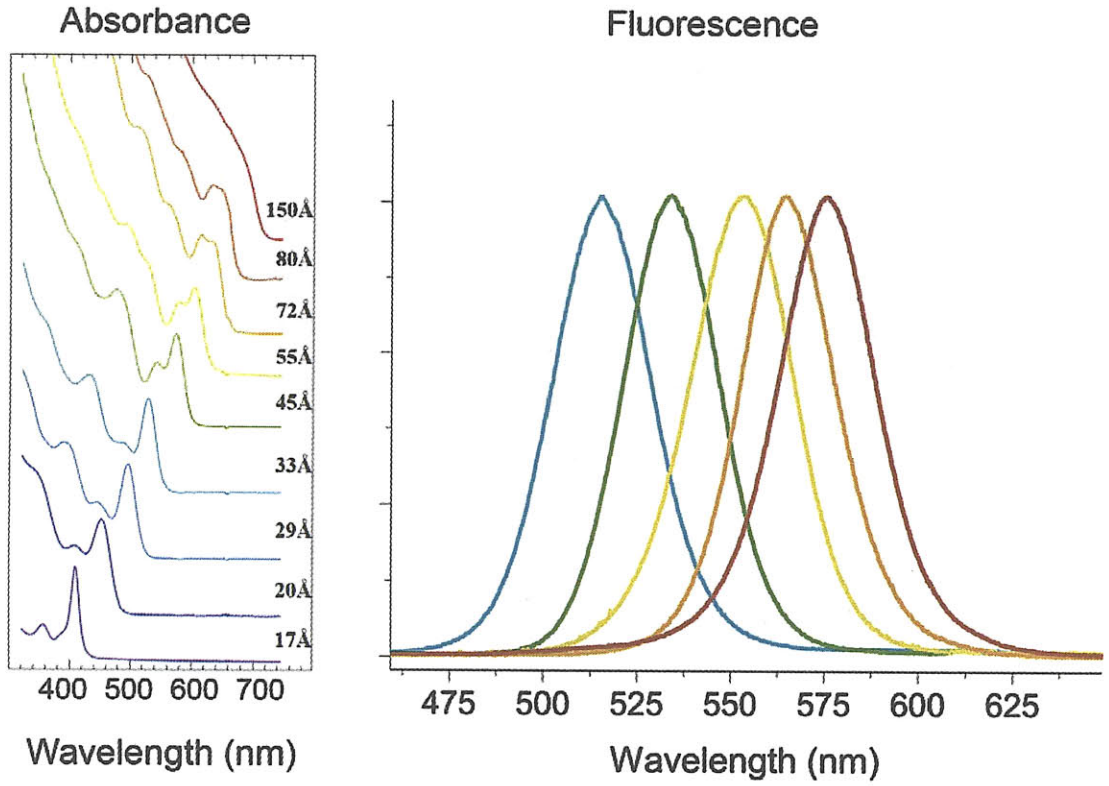

Figure 1-4 Absorbance and emission spectra of a CdSe size series. Left: Absorbance of a size series of CdSe QDs. Figure reproduced from C. B. Murray, Ph.D. Thesis, MIT, 1995. Right: Emission spectra of a separate size series of QDs, showing tunability of the emission spectrum with narrow FWHM (25-30 nm).

Figure 1-4 shows the optical spectra of a representative CdSe size series synthesized using the Dinegar and LaMer-type pathway. Due to the narrow size distribution, the absorbance spectra of these QDs show at least three clearly resolved transitions, and the quantum size effect can also be clearly observed in the red-shift of the first absorbance and emission peaks as a function of nanoparticle size.

1.3 *QD Surface Passivation*

QD cores as synthesized often contain surface defects acting as trap states, typically manifested in the emission spectrum as a broad shoulder to the red of the main band-edge emission peak. These trap states also lead to significant non-radiative recombination of excitons, resulting in low photoluminescence quantum yields (QY) of <10%. Passivation of these trap states can be achieved by the growth of a semiconductor shell material onto the core following two considerations: (1) the shell material must be of sufficient lattice match to the core material

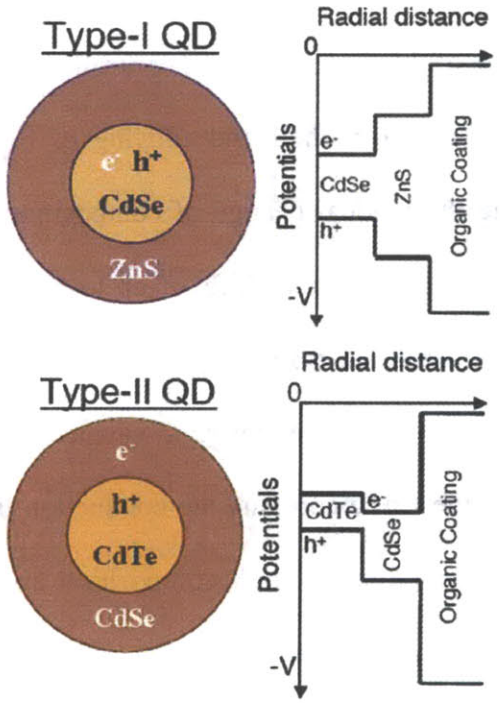

Figure 1-5 Band structures of Type I and Type II QDs. Top: CdSe(ZnS) core(shell) QDs exhibiting a Type I band structrure and emitting in the visible region. Bottom: CdTe(CdSe) core(shell) QDs exhibiting a Type II band structure, in which the hole is confined to the core, while the electron is delocalized to the shell, emitting in the NIR region. In this case, radiative recombination occurs at the core/shell interface.

to allow for epitaxial growth, and (2) the shell material must chosen to have the correct band off-set to either (2a) effectively confine electron-hole pair to the core, or (2b) confine one of the

electron or hole to the core, while allowing the other to delocalize into the shell. Considerations 2a and 2b form what are known as Type I and Type II band structures, respectively (Figure 1-5). The growth of a shell not only serves to passivate trap states and drastically enhance the quantum yield, but it is also a method for tuning the spectral properties of the final core/shell nanocrystal. For instance, Type I CdSe(ZnS) core(shell) QDs can access the visible region between ~530-650 nm with radiative recombination occurring across the bandgap of the CdSe core. When overcoating with a few layers of ZnS, a small red-shift of 5-10 nm is observed in the emission spectrum from the initial cores. This is mainly due to a partial leakage of the wave function into the ZnS matrix.[18] The degree of this leakage can be controlled by varying the shell composition. For instance, by growing a $Zn_xCd_{1-x}S$ shell, the alloying of Cd into the core can effectively increase the core size, while the gradual change of composition allows further leakage of the wavefunction into the shell, resulting in red-shifts of up to 50 nm. On the other hand, type II CdTe(CdSe) QDs can access emission wavelengths in the NIR with radiative recombination occurring at the core/shell interface and the emission wavelength determined by the band offset between the valence band of the CdTe core and the conduction band of the CdSe shell (Figure 1-5).[19] By the choice of the appropriate shell composition and band offset, a large spectral window can be accessed for various applications.

This thesis mainly describes the use of CdSe cores overcoated with various combinations of CdS and ZnS in a Type I band structure. Typically, a pure ZnS shell of 2-5 monolayers can effectively passivate the surface, increasing the QY of CdSe core QDs from near zero to up to 50% for CdSe(ZnS) core(shell) QDs. However, due to a lattice mismatch of ~12% between CdSe and ZnS, shell thicknesses of >5 monolayers can impose significant lattice strain on the system leading to formation of defect dislocations.[18] These defects can act as trap sites and

contribute to non-radiative recombination, thus lowering the QY. In our experience, we find that a shell of ~3 monolayers offers the highest QY. Notwithstanding, a further improvement in shell quality can be achieved by using an alloyed $Zn_xCd_{1-x}S$ shell, which reduces the lattice strain, allowing for growth of a thicker and more robust shell and provides better passivation of interfacial trap states. Having a thick and robust shell is critical not only for high QY in organic solution, but also for preserving the QY after further solution processing such as ligand exchange to make the QDs water soluble for biological applications.[20-22] In the case of either the $Zn_xCd_{1-x}S$ alloy or pure CdS shell, the additional CdS material also contributes to a higher absorbance cross section, which can greatly increase the effective brightness of the QDs.

Shell synthesis (i.e. overcoating) is typically achieved by careful addition of the highly reactive precursors diethylzinc ($ZnEt_2$) and TMS_2S using syringe pumps to CdSe QD cores that have been purified via precipitation and redispersion into a solvent of TOP/TOPO. The addition of a long-chain amine such as hexadecylamine (HDA) during overcoating also serves to passivate the QD surface resulting in higher QY. The greatest degree of control in terms of shell growth can be achieved via the SILAR (successive ion layer adsorption and reaction) method, by which cationic and anionic precursors are added alternately and allowed to react to achieve a layer-by-layer epitaxial growth of a high quality shell.[22, 23] Modification of literature procedures using Cd-oleate and TMS_2S as the precursors for a CdS shell on CdSe using the SILAR approach has enabled synthesis of QDs with QYs approaching unity.

The resulting QDs have a structure shown in Figure 1-6, in which the core is surrounded by an epitaxially grown shell with an organic long-chain alkyl ligand shell providing colloidal stability and solubility in organic solvents. The next section explores how the native QD ligands

can be exchanged to give QDs different solvent properties, including solubility in water for biological applications.

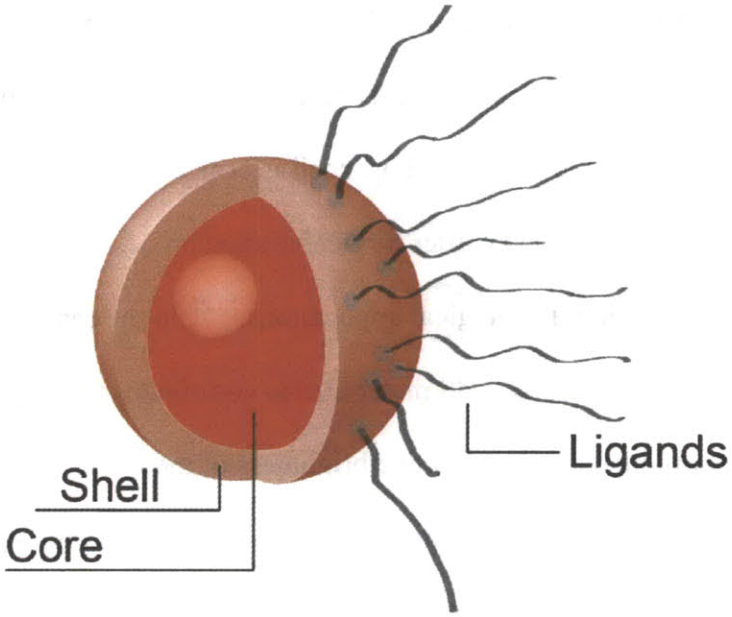

Figure 1-6 Schematic of QDs as synthesized from organic solution. The core(shell) structure is capped with organic long-chain alkyl ligands.

1.4 *Water Solubilization and Derivatization Strategies for QDs*

QDs are fluorophores with narrow emission spectra tunable through visible and near-infrared wavelengths, exceptional resistance to photobleaching compared to organic dyes, and high quantum yields.[9, 24, 25] The advent of water solubilization strategies to render QDs biocompatible has lead to a recent surge in the application of QDs for labeling and optical sensing in biological,[6, 7, 26-29] biomedical,[30-33] and environmental[34-36] contexts. However, the optimal design of QDs for single molecule imaging in live cells presents a unique set of challenges. Ideally, the nanoparticle should be (1) easily derivatizable such that various secondary reporters or biomolecules can be appended to the QD to allow for sensing capabilities and/or targeting to cellular receptors of interest. At the same time, the QD must achieve this while maintaining the properties of (2) low non-specific binding to cells, (3) small hydrodynamic

size, (4) high quantum yield, and (5) good pH stability. Since the solution properties of QDs ultimately depend on the ligands coating its surface, the challenge of synthesizing a nanocrystal to satisfy the above criteria must be addressed through rational ligand design and as of 2007 was not yet been met by any existing ligand system to our knowledge.

QDs initially synthesized are incompatible with the cellular environment due to the hydrophobic ligands, typically alkylphosphonic acids, which coat the QD surface. The following sections will outline the various strategies that have thus far been developed for the water solubilization and biological targeting of QDs along with the shortfalls of each method in the context of cell labeling, stressing the need for the development of new ligand systems.

1.4.1 Ligand Encapsulation

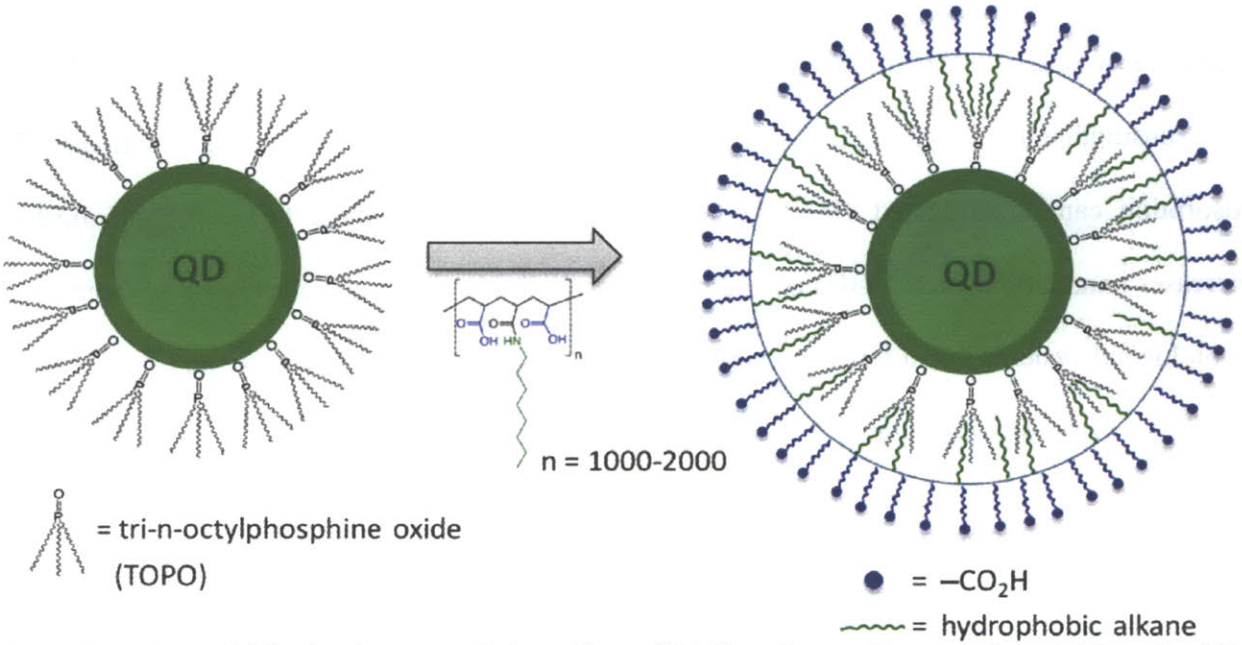

Figure 1-7 Water solublization by encapsulation with amphiphilic polymers. Encapsulation of QDs using 30% octylamine modified polyacrylic acid. The polymer forms a micelle around the QD, in which the hydrophobic alkyl chains interact with the TOPO, and the carboxylic acid groups interact with the aqueous environment for solubility.

Presently, the dominant class of QDs used for single molecule cellular imaging are those which retain hydrophobic surface ligands from synthesis and are encapsulated in amphiphilic polymer shells, typically consisting of high molecular weight polyacrylic acid partially modified with n-octylamine (Figure 1-7).[6, 37-40] The non-polar alkyl chains interact with the hydrophobic TOPO ligand on the QD surface, while the carboxylic acid groups render the QD water soluble. Such encapsulated QDs benefit from high quantum yield (QY), but the polymeric shell produces large hydrodynamic diameters (HDs) on the order of 15-30 nm for an inorganic core/shell diameter of only 4-6 nm.[41] The size of polymer-coated QDs, which is often much larger than the receptors being labeled, has been a major barrier to the widespread use of QDs in biological imaging, potentially interfering with the function of labeled proteins and limiting access to hindered spaces such as neuronal synapses.[27, 42] Furthermore, amphiphilic polymer coatings are often highly charged, which contributes to non-specific binding to cell membranes, rendering them unsuitable for single-particle imaging where low background is essential. Non-specific adsorption can be mitigated via PEGylation of polymer-encapsulated QDs, but this further increases nanoparticle size.[43] QDs coated with phospholipids or silica shells have also been used in biological systems but suffer from similar limitations of inherently large size and the need for a bulky PEG passivating layer.[7, 44]

1.4.2 Ligand Exchange

The size of water-soluble QDs can be dramatically reduced, while maintaining derivatizability, by displacing the native hydrophobic coating with carboxylate-bearing small molecule alkane-thiols such as mercaptoacetic acid (MAA), mercaptopropionic acid (MPA), or cysteine (Figure 1-8A).[45-48] Conjugation to amine bearing biomolecules is typically achieved using carbodiimide coupling chemistry to the carboxylic acid group of MAA. Although MAA-

capped QDs have HDs of only ~6-8 nm, they are inherently unstable due to weak ligand-QD interactions, leading to QD precipitation on the time-scale of several hours under ambient conditions.[41,45] In addition, the water solubility of MAA-capped QDs relies critically on the ionization state of the carboxylic acid group, and such QDs are only stable at basic pH when the carboxylate is sufficiently deprotonated. The negative charge required to keep the QDs water

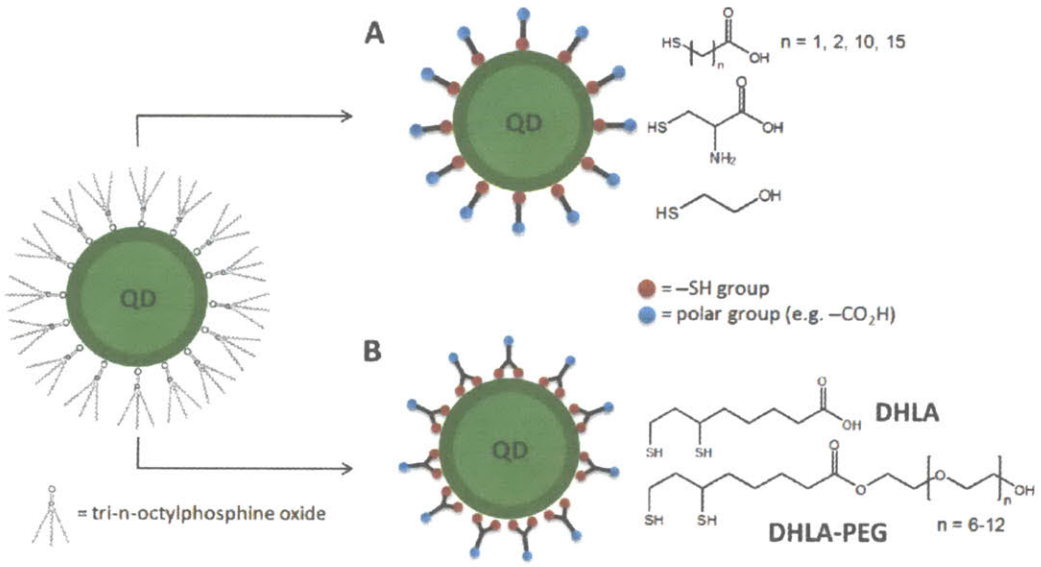

Figure 1-8 Water solubilization via ligand exchange. Ligand exchange can be performed using (A) monothiol and (B) dithiol derivatives.

dispersible also promotes non-specific binding to cells via electrostatic interactions.[43, 49]

Dithiol ligands, such as dihydrolipoic acid (DHLA), are much more stable with respect to ligand dissociation, but still yield QDs that precipitate under weakly acidic conditions (Figure 1-8B).[46, 50] Furthermore, DHLA-coated QDs also exhibit high non-specific binding, rendering them unusable for single particle tracking applications. In previous reports, ligand exchange with esters of DHLA appended to various length PEGs yielded QDs that were highly stable in aqueous solution and suitable for live cell imaging.[31, 51] However, the hydroxyl-terminated surface of these DHLA-PEG QDs lacks the functionality for efficient and selective covalent

derivatization under mild conditions, for example with targeting biomolecules for receptor labeling on cells.

1.4.3 Derivatization strategies for QDs

While the nature of the ligand coating dictates the size and solution properties of QDs for cell labeling, the various methods of derivatization enabled by the coating must also be considered in the design of a new ligand system for cell labeling. Presently, two commonly employed QD derivatization strategies are (1) direct covalent modification of QDs using common bioconjugation methods such as 1-ethyl-3-(3-dimethylaminopropyl) carbodiimide (EDC) and N-hydroxysulfosuccinimide (Sulfo-NHS) mediated cross-coupling between amino and carboxyl functionalities (Figure 1-9A),[6, 38, 47, 52] and (2) self-assembly of biomolecules onto QDs using a poly-histidine (His_6) tag expressed at the terminus of a protein, which associates to the QD through metal-affinity interactions between the nitrogen group on the imidazole of

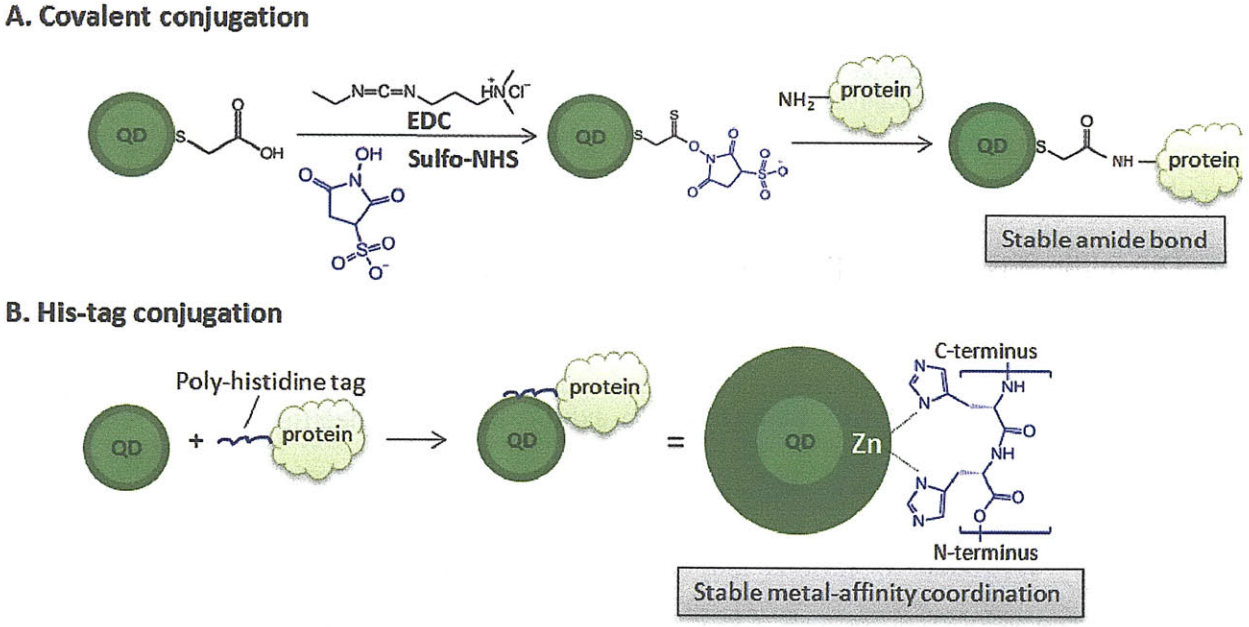

Figure 1-9 QD derivatization strategies. (A) Covalent conjugation to carboxy-functionalized QDs using EDC/Sulfo-NHS ester formation followed by reaction with an amine functionalized biomolecules to form a stable amide bond. (B) Metal affinity coordination using a protein fused to a poly-histidine (His6) tag.

histidine and the Zn on the QD ZnS shell (Figure 1-9B).[53-55]

QDs encapsulated in polymeric shells, or ligand exchanged with short alkane thiols are usually derivatized by covalent conjugation. QDs capped with DHLA or DHLA-PEG are amenable to metal-affinity driven self-assembly of His_6-tagged proteins, leading to stable conjugates that retain both QD luminescence and functionality of the coordinated biomolecule.[56] However, there is currently no robust strategy which combines the ability for covalent and His_6-tag conjugation onto the same nanoparticle, while maintaining the properties of small size, low non-specific binding, and solution stability. Such a strategy would allow for greater control in the composition of functional surface molecules used on QDs for sensing and cell labeling applications, and is the direction in which we are pursuing.

A summary of QD aqueous solution properties conveyed by various types of ligands surveyed in the literature is given in Figure 1-10. As illustrated, there was no single ligand system before this thesis which provides for all of the properties desirable for robust cell labeling. Clearly, new ligand design is necessary to address this gap in QD water solubilization technology. This thesis is partially about a journey to develop a set of ligands to fulfill all of these criteria simultaneously, the details of which will be addressed in Chapters 4 and 6.

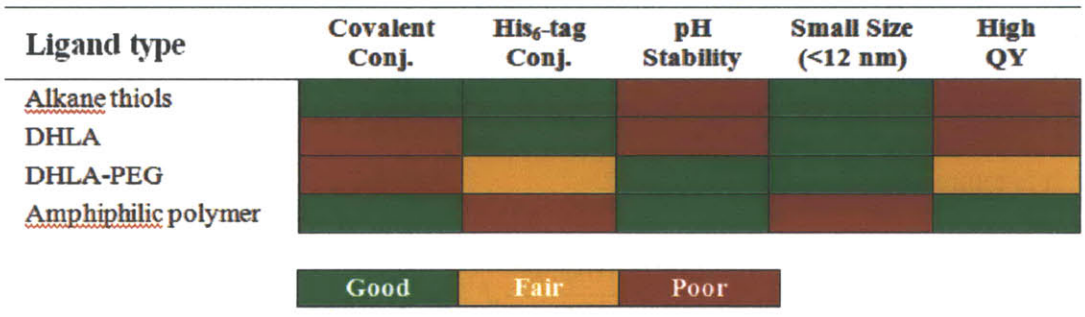

Figure 1-10 Summary of the solution properties for QDs capped with various ligands with respect to parameters desired for an ideal in vitro fluorescent QD probe.

1.5 *QDs as FRET Sensors*

1.5.1 Introduction to FRET

Another one of our goals is to develop stable aqueous core(shell) QDs which are not only compatible for cell labeling, but can also sense their environment with optical read-out of environmental parameters such as analyte binding or solution pH. However, the emission center of CdSe QDs is highly isolated from the external environment due to the presence of a higher band-gap ZnS shell, which confines the excitons to the QD core. Thus, the optical spectra of QDs are highly insensitive to fluctuations in the surrounding solution environment, making the semiconductor material itself a poor sensor. The primary mechanism by which QDs can communicate to the environment is through fluorescence resonance energy transfer (FRET), a process in which the energy from a photo-excited donor is non-radiatively transferred to an energy acceptor, which can then emit the photon energy. The rate of energy transfer from donor (D) to acceptor (A) is expressed as

$$k_{DA} = \frac{1}{\tau_D}\left(\frac{R_0}{r}\right)^6 \qquad \textbf{(1.1)}$$

where τ_D is the donor excited state lifetime, and R_0 is a characteristic separation distance at which the FRET rate is equal to the radiative decay rate ($k_{DA} = 1/\tau_D$). In other words, R_0 is the distance at which 50% of the energy is emitted by the donor and 50% is transferred to the acceptor. It is expressed as

$$R_0 = \frac{9000\ln(10)\phi_D\kappa^2}{128\pi^5 n^4 N_A} J \qquad \textbf{(1.1)}$$

where ϕ_D is the quantum yield of the donor, n is the refractive index of the medium, N_A is Avogadro's number, and κ takes into account the relative orientations of the donor and acceptor

dipoles. J is the overlap integral which takes into account the spectral overlap between donor emission and acceptor absorbance

$$J = \int_0^\infty f_D(\nu) \cdot \varepsilon_A(\nu) \cdot \nu^4 d\nu \qquad \textbf{(1.2)}$$

where $f_D(\nu)$ is the normalized emission spectrum of the donor in cm^{-1}, and $\varepsilon_A(\nu)$ is the extinction coefficient of the acceptor in $M^{-1}cm^{-1}$. The FRET efficiency, which is the fraction of photons transferred to the acceptor non-radiatively, can be expressed as

$$E = \frac{k_{DA}}{k_{DA} + \tau_D^{-1}} = \frac{R_0^6}{R_0^6 + r^6} \qquad \textbf{(1.4)}$$

In the case where there are multiple identical acceptors arranged uniformly around a single donor, the FRET efficiency becomes[57]

$$E = \frac{nR_0^6}{nR_0^6 + r^6} \qquad \textbf{(1.5)}$$

where n is the number of acceptors. Thus, high FRET efficiency is achieved when there is good spectral overlap between donor emission and acceptor absorbance according to Eq. (1.2) and (1.3), and when there are multiple copies of an acceptor around a single donor according to Eq. (1.5). The FRET efficiency is also highly distance dependent, falling off as $1/r^6$. Thus, altering either the distance or spectral overlap between donor and acceptor will modulate the FRET efficiency and can be exploited to construct a variety of sensors. We will consider the latter case of modulating spectral overlap in the demonstration of a QD FRET pH sensor.

1.5.2 QDs as FRET based pH sensors

A ratiometric QD pH sensor based on FRET from a QD to a dye was recently developed in collaboration with the lab of Professor Daniel Nocera.[34] A generalized FRET sensor construct

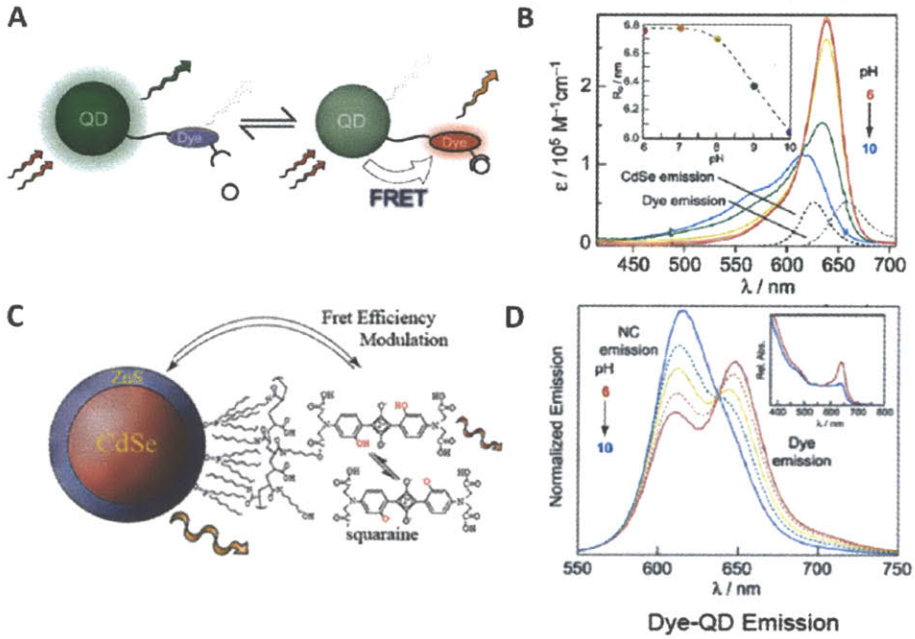

Figure 1-11 QD ratiometric pH sensor. (A) Schematic for a QD-based FRET sensor. A FRET acceptor dye with an analyte-dependent absorbance spectrum is used to modulate FRET efficiency. Presence of analyte can activate FRET to produce a positive signal. (B) Absorbance spectrum of squaraine dye as a function of pH. Inset shows calculated R0 as a function of pH, with indicated CdSe emission used to compute the spectral overlap. (C) Schematic of a polymer encapsulated QD covalently bound to squaraine dye. (D) Emission of QD-dye construct as a function of pH, showing ratiometric signal (from Ref. [34])

consists of a QD tethered to a dye which has an absorbance spectrum that changes in response to some environmental stimuli, such as analyte binding or solution pH (Figure 1-11A). A change in the absorbance spectrum alters the overlap integral to produce a measureable change in the FRET efficiency. Certain organic dyes, such as squaraine, exhibit pH dependent absorbance spectra (Figure 1-11B), which was used as a basis for the modulation of FRET efficiency as a function of pH.[34] We have previously demonstrated a functional pH sensor by covalently attaching squaraine to QDs coated with an amphiphilic polymer shell (**Figure** 1-11C). Modulation of FRET efficiency manifests as a change in the ratio of the donor and acceptor fluorescence intensities (Figure 1-11D). At low pH, greater spectral overlap translates to higher FRET efficiency, resulting in decreased emission from the QD donor and an enhancement of emission from the dye acceptor. At high pH, decreased spectral overlap leads to an enhancement of QD

emission over the dye emission. By monitoring the QD and dye channels separately, a ratiometric signal can be computed as a function of pH, which provides a method for calibration.

However, the dye illustrated here is attached to a QD encapsulated with an amphiphilic polymer shell and as previously discussed is not optimal for cell labeling studies due to large size and potential non-specific binding to cells. This again highlights the need for the development of new ligand systems for QD water solubilization to generate QDs that are biocompatible and can also function as FRET sensors. Even after developing such a biocompatible QD pH sensor, there still remains the problem of how to target QDs specifically to cellular receptors of interest.

1.6 *QDs for specific targeting and single particle tracking of cellular receptors*

1.6.1 Limitations of current labeling strategies using antibody interactions

The most commonly used method of targeting QD to specific cellular receptors is shown in Figure 1-12, and relies on the streptavidin/biotin interaction. Streptavidin is a protein which has femtomolar binding affinity to the small molecule biotin. Their association is one of the strongest non-covalent interactions known in nature. To achieve specific binding, the cellular receptor of interest is first targeted using a primary antibody, followed by a biotinylated secondary antibody. The addition of streptavidin conjugated QDs enables specific binding of the QD to the biotinylated antibody, thus indirectly labeling the receptor of interest. However, this method of labeling suffers from many limitations, as shown in Figure 1-12. Of particular concern is the large size of the QD labeling construct, which is on the order of 50 nm, and also the weak primary-secondary antibody interaction, which can lead to dissociation of the QD from the target. In addition, multiple copies of Streptavidin and multiple binding sites per Streptavidin can lead to multivalent interactions between QDs and multiple receptors, leading to crosslinking,

which can unintentionally trigger cellular signaling pathways and alter receptor behavior. These concerns are currently barriers against the ubiquitous use of QDs for cellular labeling applications.

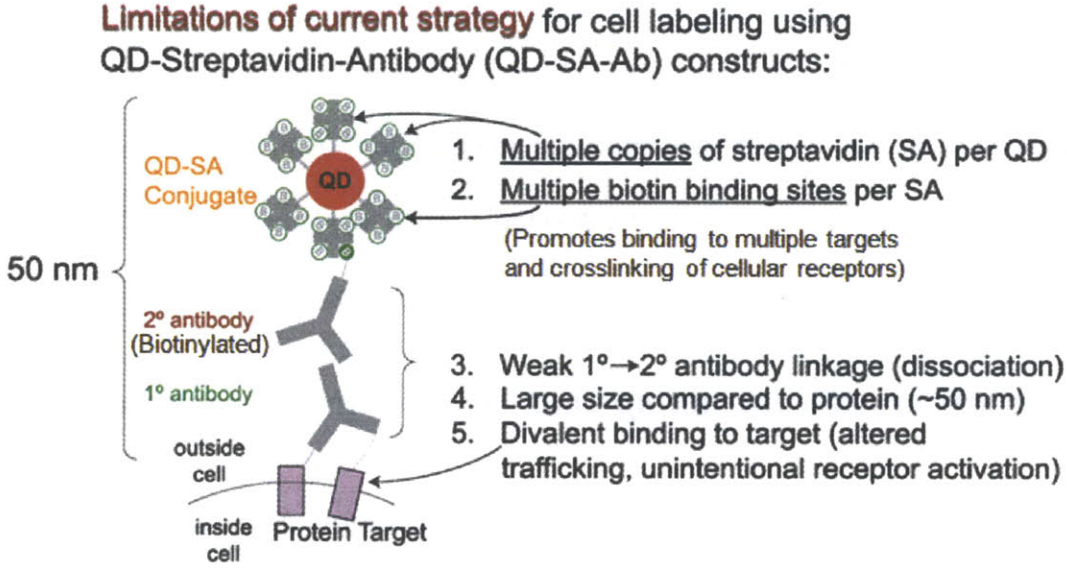

Figure 1-12 Strategy for targeting QDs to cell surface proteins. Protein of interest is fused to a 15 amino-acid recognition sequence (AP), which is specifically biotinylated by the addition of biotin ligase (BirA), biotin and ATP. Addition of commercial QDs conjugated to streptavidin (QD-SA) enables specific labeling.

1.6.2 Cell targeting using biotin ligase

A new strategy for cell labeling was recently developed in the lab of our collaborator Professor Alice Ting, chosen to minimize the size of the labeling construct by binding the QD directly to cell membrane proteins via the streptavidin/biotin interaction, without the need for bulky intermediary primary and secondary antibodies (Figure 1-13).[27] The elimination of antibodies simultaneously solves the issue of probe dissociation, since labeling is achieved by direct binding of streptavidin to biotinylated target proteins. This method of labeling was made possible by the discovery of the protein biotin ligase (BirA), which can site-specifically biotinylate a 15 amino-acid recognition sequence called the acceptor peptide (AP) fused to either terminus of a receptor of interest .[27] The addition of recombinant BirA, and biotin-AMP to the

cell medium enables specific and efficient biotinylation of the AP tag, and QDs conjugated to

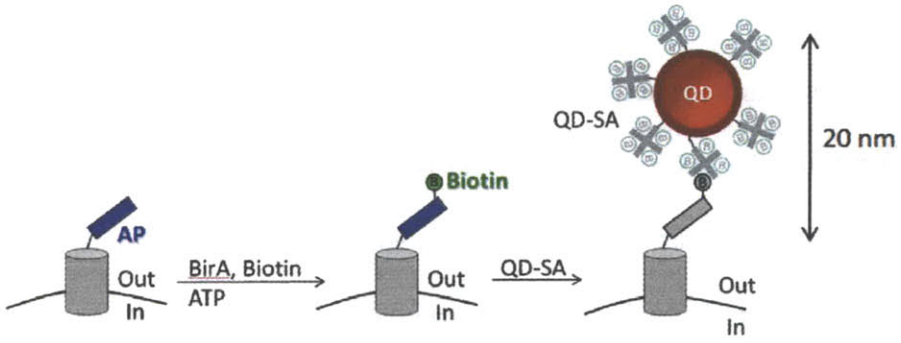

Figure 1-13 Strategy for targeting QDs to cell surface proteins. Protein of interest is fused to a 15 amino-acid recognition sequence (AP), which is specifically biotinylated by the addition of biotin ligase (BirA), biotin and ATP. Addition of commercial QDs conjugated to streptavidin (QD-SA) enables specific labeling.

streptavidin (QD-SA) can then be applied to visualize the biotinylated protein population. However, this labeling construct is still 20 nm in size, and is excluded from crowded regions such as the neuronal synapse.[27] The majority of this size is due to the polymer-encapsulated commercial QDs used in labeling. Thus, a further decrease in size to allow improved access to the synapse must be addressed through the synthesis of more compact ligand coatings. In addition to a decrease in size, enabled by the development of new ligands, the other challenge is to produce monovalent QDs which possess just a single binding site per QD for single molecule tracking applications. The development of such small and monovalent QDs is another focus of this thesis and will be addressed in Chapter 5.

1.6.3 Single particle tracking of cellular receptors

Single-particle tracking can give unprecedented understanding of the motion of cell surface proteins, free from the simplification of ensemble averaging. The large absorbance cross-section, photostability, and high quantum yield of QDs allow them to be easily imaged on a single molecule level, a feat which is difficult to achieve using fluorescent organic dyes or

proteins. For instance Dahan et al. used QDs to track diffusion of glycine receptors on neurons to reveal their lateral dynamics within the neuronal membrane.[39] Ehlers et al used QDs to study the mobility of GluR1 AMPA receptors within synapses as a function of synaptic activity,[58] and Lidke et al was able to study the active transport of the epidermal growth factor receptor (EGFR) along the cellular filopodia upon specific ligand binding.[59] In all of these studies, commercial QDs with HD between 20-30 nm were used, and in some studies conclusions were drawn based upon the measured diffusion coefficients for receptors labeled with these QDs. The major concern is that the large QD size will hinder the diffusion of the labeled receptor and alter the results. The large size of QDs is most evident in the labeling of receptors within the neuronal synapse. Single particle studies by Howarth et al. have shown that QDs are significantly excluded from certain synaptic regions, principally due to their large size.

To address the issue of large QD size potentially interfering with the function (i.e. diffusion) of labeled receptors and to improve QD access to the synapse, smaller biocompatible QDs need to be developed, further emphasizing the need for new ligand design.

1.6.4 QDs as In Vivo Probes

Just as with in-vitro imaging of cells, synthesis of nanomaterials for in-vivo imaging has its own set of design parameters. Chief among those are the particles' size and charge. Before getting into the effect of these two parameters on QD biodistribution, let us first consider the motivations for using QDs for in-vivo imaging, of which there are many.

First, the emission of QDs can act as fluorescent reporters upon systemic injection into a complex organism such as a mouse, providing insight into the biodistribution of nanomaterials on the size range between 10 – 100 nm. Size probes from 10 – 30 nm can be synthesized from QDs of various core(shell) compositions and surface coatings,[41] while sizes larger than 30 nm

can be achieved by embedding QDs into a larger host material such as silica.[60] In both size regimes, what is of interest is that the emission from the QDs acting as a convenient reporter of its location, allowing for detailed biodistribution studies. In addition, because QDs are such robust fluorophores, their emission can be tracked in animals on time scales of days and even months. [7, 30]

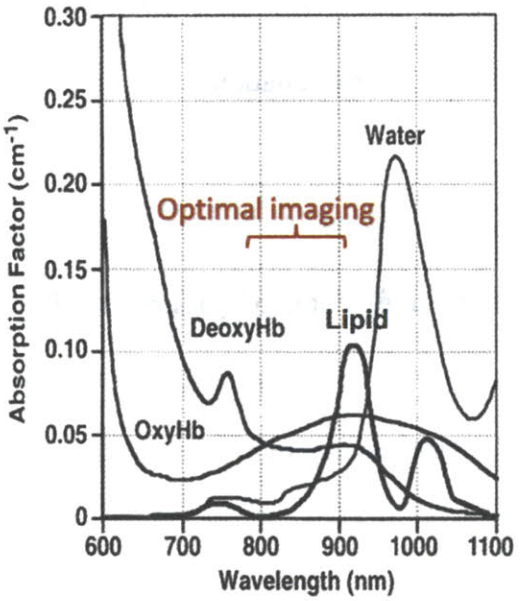

Figure 1-14 Optimal imaging window for in vivo studies in the NIR. The optimal range occurs in the 750 – 850 nm range, where there is minimal absorbance from blood, tissue, and water.

Second, because optical properties of QDs are decoupled from their surface properties due to the ability to modify the organic capping layer, the QD surface can be altered to study the effect of chemical functionality on biodistribution. For instance, it has been shown that nanoparticles with different length poly(ethylene glycol) coatings accumulate differently in the bone marrow and liver of mice.[30] In addition, the surface of QDs can be modified with biomolecules for targeting specific tissues or cells within the body. For instance, QDs conjugated to small molecules, peptides or antibodies that bind to known cancer biomarkers can selectively

accumulate at a tumor site, providing a means of optically marking tumors for study or resection.[32, 61, 62]

Third, because QDs are spectrally tunable, they can be made to emit at the optimal window for in-vivo imaging, which is in the near infrared (NIR) where there is minimal absorbance from tissue, blood and water, providing significantly improved imaging depth (Figure 1-14). Furthermore, because QDs have such high two-photon absorbance cross-section compared to organic dyes, the use of two-photon NIR excitation can further enhance the imaging depth of QDs for in-vivo applications.

The above-mentioned advantages of QDs for in-vivo studies can assist in the understanding of nanomaterial biodistribution as a function of parameters like size and charge, the most relevant application of which is to assist in the building of models for nanoparticle drug delivery vehicles, which are of the similar size regime, in order to better design the drug carriers to reach their intended targets.

So far, studies of nanoparticle size on biodistribution have identified a number of size regimes. Large QDs on the order of 20 – 30 nm tend to be taken up by the lungs, liver, spleen, and lymphatic system when injected intravenously.[30, 63] When injected subcutaneously, QDs of the size regime from 15 – 20 nm have been shown to accumulate in the sentinel lymph nodes, which is important in the diagnosis of breast cancer.[25] The sentinel lymph node is the first lymph node encountered by metastasizing cancer cells from a primary tumor. If a biopsy identifies malignant cells in the sentinel lymph node, then it's likely that the cancer has metastasized. Traditional sentinel lymph node biopsy relies on the injection of a radioactive tracer along with a dye, which provides the surgeon with a rough idea as to the region of the sentinel lymph node. The surgeon will remove all lymph nodes in that region for biopsy. The advantage of using QDs

for this application is that the sentinel lymph node can be targeted and imaged directly through the skin, and can be easily removed via optically guided surgery, paving the way for a potential clinical application of QDs in human surgery. For this study, type II CdTe(CdSe) QDs emitting in the optimal NIR window were utilized.[25]

Smaller QDs on the order of 10 nm have been found to extravasate out of blood vessels into interstitial fluid.[31] The biodistribution of even smaller QDs has not been explored prior to this thesis, and one aspect of our work has focused on the development of these QDs that are biocompatible for in-vivo imaging and small enough to explore the renal clearance threshold (Chapters 2 and 3).

The motivation is that below a certain size threshold of ~5 nm, it is known that proteins and small molecules are cleared from the body through the kidneys and exit through urine. Due to the inherent toxicity of heavy metal containing QDs, it would be highly advantageous to synthesize QDs that are below this renal size filtration threshold so that they can be efficiently cleared from the body after imaging for safety and regulatory reasons. Proving that QDs can clear through this mechanism would also serve as a framework in the development of future drug delivery vehicles that can deliver a drug and then degrade into components that are small enough to clear from the body completely. How small the degradation components must be can be determined by a detailed study using QDs as a size probe.

Another aspect of QD design for in-vivo imaging lies in the ability to control the particle charge and hydrophilicity. Studies have found that a neutral hydrophilic poly(ethylene glycol) coating can prevent the uptake of QDs into the reticuloendothelial (RES) system, including the liver, spleen, and lymph nodes,[30] and that neutral particles of different hydrophilicity tuned via the length of the poly(ethylene glycol) coating can also greatly affect uptake in the liver,

pancreas, kidneys and lymph nodes.[64] Charged particles invariably end up binding non-specifically to serum proteins,[31] thus increasing their size and facilitating their uptake to the lungs, liver, and other organs. Thus, for biocompatibility reasons, it is important to design an in vivo probe with neutral surface charge to prevent biofouling, although it is a challenge to do so while also keeping the size small. This is a challenge that is addressed in this thesis in Chapter 2.

1.7 *Thesis Overview*

The next two chapters of this thesis address the challenge of how to synthesize extremely small QDs in the 5 – 10 nm size regime, while maintaining low non-specific binding and biocompatibility for in-vivo applications. Chapter 2 deals with the synthesis and characterization of such ultra-small QDs, and Chapter 3 will go in depth into the application of these QDs to probe for the first time the renal filtration threshold in mice. This work paves the way for future design of nanoparticle drug delivery vehicles can safely and effectively clear from the body.

Chapters 4 and 5 describe our attempts at solving the major challenge outlined in section 1.4. That is, how to design a ligand to satisfy the 5 most important criteria for an in vitro fluorescent QD probe: (1) small size, (2) facile derivatizability, (3) high QY, (4) low non-specific binding, and (5) high stability. Prior to this thesis, there was a lack of any single ligand system that could fulfill all five criteria simultaneously, and all five are important if we are to do robust single molecule imaging on live cells. Using this ligand platform, we demonstrate the prototype for a ratiometric QD pH sensor via the coupling of a pH sensitive dye, and we also demonstrate robust cell labeling and single molecule imaging via two conjugation methods of QDs to streptavidin. Chapter 5 extends the work of Chapter 4 by using the same ligand system to develop a purification method for the generation of monovalent QD probes, which addresses one of the last great problems of using QDs for cell labeling – the crosslinking of receptors due

to multivalency. We show that by using monovalent QDs, we alter the labeling pattern of EphA3 on live cells and prevent triggering of signaling pathways due to receptor clustering versus using multivalent QDs.

Chapter 6 discusses a new ligand system based on a polymeric imidazole multidentate binding group to render more stable water soluble QDs for in vitro and in vivo applications. This polymer system was designed to be modular and expandable to a wide variety of mixed polymer systems, with the potential to generate QD surface coatings of great variety. We demonstrate the utility of this next-generation coating via dye conjugation, high affinity cellular labeling, and in-vivo imaging of the tumor vasculature.

1.8 *References*

1. Efros, A. L.; Rosen, M., The electronic structure of semiconductor nanocrystals. *Annu. Rev. Mater. Sci.* **2000,** 30, 475-521.

2. Caruge, J. M.; Halpert, J. E.; Wood, V.; Bulovic, V.; Bawendi, M. G., Colloidal quantum-dot light-emitting diodes with metal-oxide charge transport layers. *Nat. Photonics* **2008,** 2, (4), 247-250.

3. Coe, S.; Woo, W. K.; Bawendi, M.; Bulovic, V., Electroluminescence from single monolayers of nanocrystals in molecular organic devices. *Nature* **2002,** 420, (6917), 800-803.

4. Lee, H. J.; Yum, J. H.; Leventis, H. C.; Zakeeruddin, S. M.; Haque, S. A.; Chen, P.; Seok, S. I.; Grazel, M.; Nazeeruddin, M. K., CdSe quantum dot-sensitized solar cells exceeding efficiency 1% at full-sun intensity. *Journal of Physical Chemistry C* **2008,** 112, (30), 11600-11608.

5. McDonald, S. A.; Konstantatos, G.; Zhang, S. G.; Cyr, P. W.; Klem, E. J. D.; Levina, L.; Sargent, E. H., Solution-processed PbS quantum dot infrared photodetectors and photovoltaics. *Nature Materials* **2005,** 4, (2), 138-U14.

6. Wu, X.; Liu, H.; Liu, J.; Haley, K. N.; Treadway, J. A.; Larson, J. P.; Ge, N.; Peale, F.; Bruchez, M. P., Immunofluorescent labeling of cancer marker Her2 and other cellular targets with semiconductor quantum dots. *Nat. Biotechnol.* **2003,** 21, (1), 41-46.

7. Dubertret, B.; Skourides, P.; Norris, D. J.; Noireaux, V.; Brivanlou, A. H.; Libchaber, A., In Vivo Imaging of Quantum Dots Encapsulated in Phospholipid Micelles. *Science* **2002,** 298, (5599), 1759-1762.

8. LaMer, V. K.; Dinegar, R. H., Theory, Production and Mechanism of Formation of Monodispersed Hydrosols. *J. Am. Chem. Soc* **2002,** 72, (11), 4847-4854.

9. Murray, C. B.; Norris, D. J.; Bawendi, M. G., Synthesis and characterization of nearly monodisperse CdE (E = sulfur, selenium, tellurium) semiconductor nanocrystallites. *J. Am. Chem. Soc.* **1993,** 115, (19), 8706-8715.

10. Rossetti, R.; Nakahara, S.; Brus, L. E., Quantum size effects in the redox potentials, resonance Raman spectra, and electronic spectra of CdS crystallites in aqueous solution. *The Journal of Chemical Physics* **1983,** 79, (2), 1086-1088.

11. Brus, L., Electronic wave functions in semiconductor clusters: experiment and theory. *J. Phys. Chem.* **1986,** 90, (12), 2555-2560.

12. Bawendi, M. G.; Kortan, A. R.; Steigerwald, M. L.; Brus, L. E., X-Ray Structural Characterization of Larger Cdse Semiconductor Clusters. *Journal of Chemical Physics* **1989,** 91, (11), 7282-7290.

13. LaMer, V. K.; Dinegar, R. H., Theory, Production and Mechanism of Formation of Monodispersed Hydrosols. *J. Am. Chem. Soc* **1952,** 72, (11), 4847-4854.

14. Stott, N. E. Novel synthetic routes to high-quality II-VI colloidal nanocrystals: controlled growth using mild precursors in the presence of selected ligands. Ph.D. Thesis, Massachusetts Institute of Technology, 2004.

15. Peng, Z. A.; Peng, X., Formation of High-Quality CdTe, CdSe, and CdS Nanocrystals Using CdO as Precursor. *J. Am. Chem. Soc* **2000,** 123, (1), 183-184.

16. Yu, W. W.; Peng, X. G., Formation of high-quality CdS and other II-VI semiconductor nanocrystals in noncoordinating solvents: Tunable reactivity of monomers. *Angewandte Chemie-International Edition* **2002,** 41, (13), 2368-2371.

17. Pradhan, N.; Reifsnyder, D.; Xie, R.; Aldana, J.; Peng, X., Surface Ligand Dynamics in Growth of Nanocrystals. *Journal of the American Chemical Society* **2007,** 129, (30), 9500-9509.

18. Dabbousi, B. O.; Rodriguez-Viejo, J.; Mikulec, F. V.; Heine, J. R.; Mattoussi, H.; Ober, R.; Jensen, K. F.; Bawendi, M. G., (CdSe)ZnS Core-Shell Quantum Dots: Synthesis and Characterization of a Size Series of Highly Luminescent Nanocrystallites. *J. Phys. Chem. B* **1997,** 101, (46), 9463-9475.

19. Kim, S.; Lim, Y. T.; Soltesz, E. G.; De Grand, A. M.; Lee, J.; Nakayama, A.; Parker, J. A.; Mihaljevic, T.; Laurence, R. G.; Dor, D. M.; Cohn, L. H.; Bawendi, M. G.; Frangioni, J. V., Near-infrared fluorescent type II quantum dots for sentinel lymph node mapping. *Nat Biotechnol* **2004,** 22, (1), 93-7.

20. Manna, L.; Scher, E. C.; Li, L. S.; Alivisatos, A. P., Epitaxial Growth and Photochemical Annealing of Graded CdS/ZnS Shells on Colloidal CdSe Nanorods. *J. Am. Chem. Soc.* **2002,** 124, (24), 7136-7145.

21. Yu, Z.; Guo, L.; Du, H.; Krauss, T.; Silcox, J., Shell Distribution on Colloidal CdSe/ZnS Quantum Dots. *Nano Lett.* **2005,** 5, (4), 565-570.

22. Xie, R.; Kolb, U.; Li, J.; Basche, T.; Mews, A., Synthesis and Characterization of Highly Luminescent CdSe-Core CdS/Zn0.5Cd0.5S/ZnS Multishell Nanocrystals. *J. Am. Chem. Soc.* **2005,** 127, (20), 7480-7488.

23. Li, J. J.; Wang, Y. A.; Guo, W. Z.; Keay, J. C.; Mishima, T. D.; Johnson, M. B.; Peng, X. G., Large-scale synthesis of nearly monodisperse CdSe/CdS core/shell nanocrystals using air-stable reagents via successive ion layer adsorption and reaction. *J. Am. Chem. Soc* **2003,** 125, (41), 12567-12575.

24. Chan, W. C. W.; Nie, S., Quantum Dot Bioconjugates for Ultrasensitive Nonisotopic Detection. *Science* **1998,** 281, (5385), 2016-2018.

25. Kim, S.; Lim, Y. T.; Soltesz, E. G.; De Grand, A. M.; Lee, J.; Nakayama, A.; Parker, J. A.; Mihaljevic, T.; Laurence, R. G.; Dor, D. M.; Cohn, L. H.; Bawendi, M. G.; Frangioni, J. V., Near-infrared fluorescent type II quantum dots for sentinel lymph node mapping. *Nat. Biotech.* **2004,** 22, (1), 93-97.

26. Bruchez, M., Jr.; Moronne, M.; Gin, P.; Weiss, S.; Alivisatos, A. P., Semiconductor Nanocrystals as Fluorescent Biological Labels. *Science* **1998,** 281, (5385), 2013-2016.

27. Howarth, M.; Takao, K.; Hayashi, Y.; Ting, A. Y., Targeting quantum dots to surface proteins in living cells with biotin ligase. *Proc Natl Acad Sci USA.* **2005,** 102, (21), 7583-7588.

28. Gao, X.; Chan, W. C. W.; Nie, S., Quantum-dot nanocrystals for ultrasensitive biological labeling and multicolor optical encoding. *J. Biomed.Opt.* **2002,** 7, (4), 532-537.

29. Anikeeva, N.; Lebedeva, T.; Clapp, A. R.; Goldman, E. R.; Dustin, M. L.; Mattoussi, H.; Sykulev, Y., Quantum dot/peptide-MHC biosensors reveal strong CD8-dependent cooperation between self and viral antigens that augment the T cell response. *Proc. Natl Acad. Sci. USA* **2006,** 103, (45), 16846-16851.

30. Ballou, B.; Lagerholm, B. C.; Ernst, L. A.; Bruchez, M. P.; Waggoner, A. S., Noninvasive Imaging of Quantum Dots in Mice. *Bioconjug. Chem.* **2004,** 15, (1), 79-86.

31. Zimmer, J. P.; Kim, S.-W.; Ohnishi, S.; Tanaka, E.; Frangioni, J. V.; Bawendi, M. G., Size Series of Small Indium Arsenide-Zinc Selenide Core-Shell Nanocrystals and Their Application to In Vivo Imaging. *J. Am. Chem. Soc.* **2006,** 128, (8), 2526-2527.

32. Gao, X.; Cui, Y.; Levenson, R. M.; Chung, L. W. K.; Nie, S., In vivo cancer targeting and imaging with semiconductor quantum dots. *Nat Biotechnol* **2004,** 22, (8), 969-976.

33. So, M.-K.; Xu, C.; Loening, A. M.; Gambhir, S. S.; Rao, J., Self-illuminating quantum dot conjugates for in vivo imaging. *Nat Biotechnol* **2006,** 24, (3), 339-343.

34. Snee, P. T.; Somers, R. C.; Nair, G.; Zimmer, J. P.; Bawendi, M. G.; Nocera, D. G., A Ratiometric CdSe/ZnS Nanocrystal pH Sensor. *J. Am. Chem. Soc.* **2006,** 128, (41), 13320-13321.

35. Medintz, I.; Clapp, A.; Brunel, F.; Tiefenbrunn, T.; Tetsuo Uyeda, H.; Chang, E. L.; Deschamps, J. R.; Dawson, P. E.; Mattoussi, H., Proteolytic activity monitored by fluorescence resonance energy transfer through quantum-dot-peptide conjugates. *Nat. Mater.* **2006,** 5, (7), 581-589.

36. Zhang, C. Y.; Yeh, H. C.; Kuroki, M. T.; Wang, T. H., Single-quantum-dot-based DNA nanosensor. *Nat. Mater.* **2005,** 4, 826-831.

37. Medintz, I.; Uyeda, H.; Goldman, E.; Mattoussi, H., Quantum dot bioconjugates for imaging, labelling and sensing. *Nat. Mater.* **2005,** 4, 435-446.

38. Zhou, M.; Nakatani, E.; Gronenberg, L. S.; Tokimoto, T.; Wirth, M. J.; Hruby, V. J.; Roberts, A.; Lynch, R. M.; Ghosh, I., Peptide-Labeled Quantum Dots for Imaging GPCRs in Whole Cells and as Single Molecules. *Bioconjug. Chem.* **2007,** 18, (2), 323-332.

39. Dahan, M.; Levi, S.; Luccardini, C.; Rostaing, P.; Riveau, B.; Triller, A., Diffusion Dynamics of Glycine Receptors Revealed by Single-Quantum Dot Tracking. *Science* **2003,** 302, (5644), 442-445.

40. Courty, S.; Luccardini, C.; Bellaiche, Y.; Cappello, G.; Dahan, M., Tracking Individual Kinesin Motors in Living Cells Using Single Quantum-Dot Imaging. *Nano. Lett.* **2006,** 6, (7), 1491-1495.

41. Smith, A. M.; Duan, H.; Rhyner, M. N.; Ruan, G.; Nie, S., A systematic examination of surface coatings on the optical and chemical properties of semiconductor quantum dots. *Phys. Chem. Chem. Phys.* **2006,** 8, 3895-3903.

42. Groc, L.; Heine, M.; Cognet, L.; Brickley, K.; Stephenson, F. A.; Lounis, B.; Choquet, D., Differential activity-dependent regulation of the lateral mobilities of AMPA and NMDA receptors. *Nat Neurosci* **2004,** 7, (7), 695-696.

43. Bentzen, E. L.; Tomlinson, I. D.; Mason, J.; Gresch, P.; Warnement, M. R.; Wright, D.; Sanders-Bush, E.; Blakely, R.; Rosenthal, S. J., Surface Modification To Reduce Nonspecific Binding of Quantum Dots in Live Cell Assays. *Bioconjug. Chem.* **2005,** 16, (6), 1488-1494.

44. Parak, W. J.; Gerion, D.; Zanchet, D.; Woerz, A. S.; Pellegrino, T.; Micheel, C.; Williams, S. C.; Seitz, M.; Bruehl, R. E.; Bryant, Z.; Bustamante, C.; Bertozzi, C. R.; Alivisatos, A. P., Conjugation of DNA to Silanized Colloidal Semiconductor Nanocrystalline Quantum Dots. *Chem. Mater.* **2002,** 14, (5), 2113-2119.

45. Aldana, J.; Wang, Y. A.; Peng, X., Photochemical Instability of CdSe Nanocrystals Coated by Hydrophilic Thiols. *J. Am. Chem. Soc.* **2001,** 123, (36), 8844-8850.

46. Mattoussi, H.; Mauro, J. M.; Goldman, E. R.; Anderson, G. P.; Sundar, V. C.; Mikulec, F. V.; Bawendi, M. G., Self-Assembly of CdSe-ZnS Quantum Dot Bioconjugates Using an Engineered Recombinant Protein. *J. Am. Chem. Soc.* **2000,** 122, (49), 12142-12150.

47. Algar, W. R.; Krull, U. J., Adsorption and Hybridization of Oligonucleotides on Mercaptoacetic Acid-Capped CdSe/ZnS Quantum Dots and Quantum Dot-Oligonucleotide Conjugates. *Langmuir* **2006,** 22, (26), 11346-11352.

48. Liu, W.; Choi, H. S.; Zimmer, J. P.; Frangioni, J. V.; Bawendi, M. G., *Compact Cysteine-Coated CdSe(ZnCdS) QDs for In Vivo Applications* **2007,** Submitted.

49. Xue, F.; Chen, J.; Guo, J.; Wang, C.; Yang, W.; Wang, P.; Lu, D., Enhancement of Intracellular Delivery of CdTe Quantum Dots (QDs) to Living Cells by Tat Conjugation. *J. Fluoresc.* **2007,** 17, (2), 149-154.

50. Pons, T.; Uyeda, H. T.; Medintz, I. L.; Mattoussi, H., Hydrodynamic Dimensions, Electrophoretic Mobility, and Stability of Hydrophilic Quantum Dots. *J. Phys. Chem. B* **2006,** 110, (41), 20308-20316.

51. Uyeda, H. T.; Medintz, I. L.; Jaiswal, J. K.; Simon, S. M.; Mattoussi, H., Synthesis of Compact Multidentate Ligands to Prepare Stable Hydrophilic Quantum Dot Fluorophores. *J. Am. Chem. Soc.* **2005,** 127, (11), 3870-3878.

52. Yan Zhang; Min-kyung So; Andreas M. Loening; Hequan Yao; Sanjiv S. Gambhir; Rao, J., HaloTag Protein-Mediated Site-Specific Conjugation of Bioluminescent Proteins to Quantum Dots. *Angew. Chem. Int. Ed.* **2006,** 45, (30), 4936-4940.

53. Goldman, E. R.; Balighian, E. D.; Mattoussi, H.; Kuno, M. K.; Mauro, J. M.; Tran, P. T.; Anderson, G. P., Avidin: A Natural Bridge for Quantum Dot-Antibody Conjugates. *J. Am. Chem. Soc.* **2002,** 124, (22), 6378-6382.

54. Sapsford, K. E.; Pons, T.; Medintz, I. L.; Higashiya, S.; Brunel, F. M.; Dawson, P. E.; Mattoussi, H., Kinetics of Metal-Affinity Driven Self-Assembly between Proteins or Peptides and CdSe-ZnS Quantum Dots. *J. Phys. Chem. C.* **2007,** 111, (11528-11538).

55. Delehanty, J. B.; Medintz, I. L.; Pons, T.; Brunel, F. M.; Dawson, P. E.; Mattoussi, H., Self-Assembled Quantum Dot-Peptide Bioconjugates for Selective Intracellular Delivery. *Bioconjugate Chem.* **2006,** 17, (4), 920-927.

56. Medintz, I. L., Self-assembled nanoscale biosensors based on quantum dot FRET donors. *Nature Mater.* **2003,** 2, 630-638.

57. Medintz, I. L.; Clapp, A. R.; Mattoussi, H.; Goldman, E. R.; Fisher, B.; Mauro, J. M., Self-assembled nanoscale biosensors based on quantum dot FRET donors. *Nat. Mater.* **2003,** 2, (9), 630-638.

58. Ehlers, M. D.; Heine, M.; Groc, L.; Lee, M.-C.; Choquet, D., Diffusional Trapping of GluR1 AMPA Receptors by Input-Specific Synaptic Activity. *Neuron* **2007,** 54, (3), 447-460.

59. Lidke, D. S.; Lidke, K. A.; Rieger, B.; Jovin, T. M.; Arndt-Jovin, D. J., Reaching out for signals: filopodia sense EGF and respond by directed retrograde transport of activated receptors. *J. Cell. Biol.* **2005,** 170, (4), 619-626.

60. Popovic, Z.; Liu, W.; Chauhan, V. P. S.; Wong, C. R.; Greytak, A. B.; Jiang, W.; Fukumura, D.; Jain, R. K.; Bawendi, M. G., Nanoparticle size series for in vivo imaging. *In Preparation* **2010**.

61. Akerman, M. E.; Chan, W. C. W.; Laakkonen, P.; Bhatia, S. N.; Ruoslahti, E., Nanocrystal targeting in vivo. *PNAS* **2002,** 99, (20), 12617-12621.

62. Choi, H. S.; Liu, W.; Liu, F.; Nasr, K.; Misra, P.; Bawendi, M. G.; Frangioni, J. V., Design considerations for tumour-targeted nanoparticles. *Nat Nano* **2010,** 5, (1), 42-47.

63. Fischer, H. C.; Liu, L. C.; Pang, K. S.; Chan, W. C. W., Pharmacokinetics of nanoscale quantum dots: In vivo distribution, sequestration, and clearance in the rat. *Advanced Functional Materials* **2006,** 16, (10), 1299-1305.

64. Choi, H. S.; Ipe, B. I.; Misra, P.; Lee, J. H.; Bawendi, M. G.; Frangioni, J. V., Tissue- and Organ-Selective Biodistribution of NIR Fluorescent Quantum Dots. *Nano Letters* **2009,** 9, (6), 2354-2359.

Chapter 2: Ultra-Compact Aqueous QDs for In Vivo Applications*

2.1 *Background and Motivation*

This chapter describes a method by which the 5-10 nm hydrodynamic diameter regime was achieved in water using CdSe(CdZnS) core(shell) QDs for in vivo imaging applications. This size regime is of interest for studying the threshold for renal filtration, which has never before been investigated using monodisperse nanometer-sized probes. The ligand exchange method is used here utilizing the thiol group of the cysteine molecule in order to achieve a compact structure via ligand displacement of the native QDs ligands. The challenge was in demonstrating that such small zwitterionic ligands were sufficiently biocompatible as to not bind non-specifically to native serum proteins. As it turns out, this process is highly pH dependent as one might expect from the pKa values of the zwitterionic groups. Described herein is the synthesis, characterization, and application of such small probes to demonstrate for the first time clearance of inorganic nanomaterials through the kidneys of a mouse.

QDs are usually described as fluorophores having remarkable photostability, large absorption cross sections, and tunable emission peaks. Equally important, QDs also serve as versatile nanoscale objects of precisely tunable size and morphology, having exceptionally narrow size distributions.[1,2] Size is an especially important parameter in the design of nanomaterials for applications in biology, for both in-vitro and in-vivo applications. In cell labeling applications, for example, size can affect endocytosis or limit access to receptors of interest, such as those in the neuronal synapse.[3] In live animals, particle size can dramatically affect biodistribution and pharmacokinetics.[4,5] In any case, the optimal size depends on the

* Much of this chapter has appeared in print. It is reproduced with permission from *J Am Chem Soc* 2007, **129**: 14530.

application. For example, it has been previously shown that Type II CdTe(CdSe) core(shell) QDs with a hydrodynamic diameter (HD) of ~19 nm can be used to selectively map sentinel lymph nodes.[6] More recently, we have also shown that 8.7 nm HD Type I InAs(ZnSe) QDs allowed the mapping of multiple lymph nodes and also showed the potential extravasation of QDs from the vasculature.[7] It is generally much more difficult to minimize QD HD than to maximize it. Moreover, reducing HD could increase the in-vivo bioavailability of QDs and lead to an improved understanding of clearance mechanisms. In this chapter, we demonstrate bio-compatible fluorescent QDs with an exceptionally small HD of ~6 nm using a CdSe(ZnCdS) core(shell) structure coated with DL-cysteine and show renal clearance of these QDs in rat models.

2.2 *Synthesis of Cysteine Coated CdSe(CdZnS) QDs*

2.2.1 Results and discussion

Cysteine-coated nanocrystals have been demonstrated previously with CdS QDs synthesized directly from aqueous solution in the presence of L-cysteine hydrochloride.[8] However, these QDs suffered from low QY (6-8%) and broad fluorescence (FWHM >100 nm) due to emission from surface trap sites. We report the synthesis of high-quality cysteine-coated CdSe(ZnCdS) core(shell) QDs using well-developed nanocrystal synthesis procedures, in which cores are formed through the rapid injection of metal and chalcogenide precursors into hot solvent and then overcoated with a thin shell of a higher band gap material. Finally, the native ligands are exchanged with DL-cysteine to yield water dispersible QDs (QD-Cys).

Ligand exchange with cysteine was achieved using a biphasic exchange method in which QDs dispersed in chloroform were mixed with a solution of cysteine in phosphate buffered saline

(PBS). This biphasic mixture was stirred vigorously at room temperature, and phase transfer of QDs from the organic to the aqueous phase occurred over ~2 h, leaving a colorless chloroform

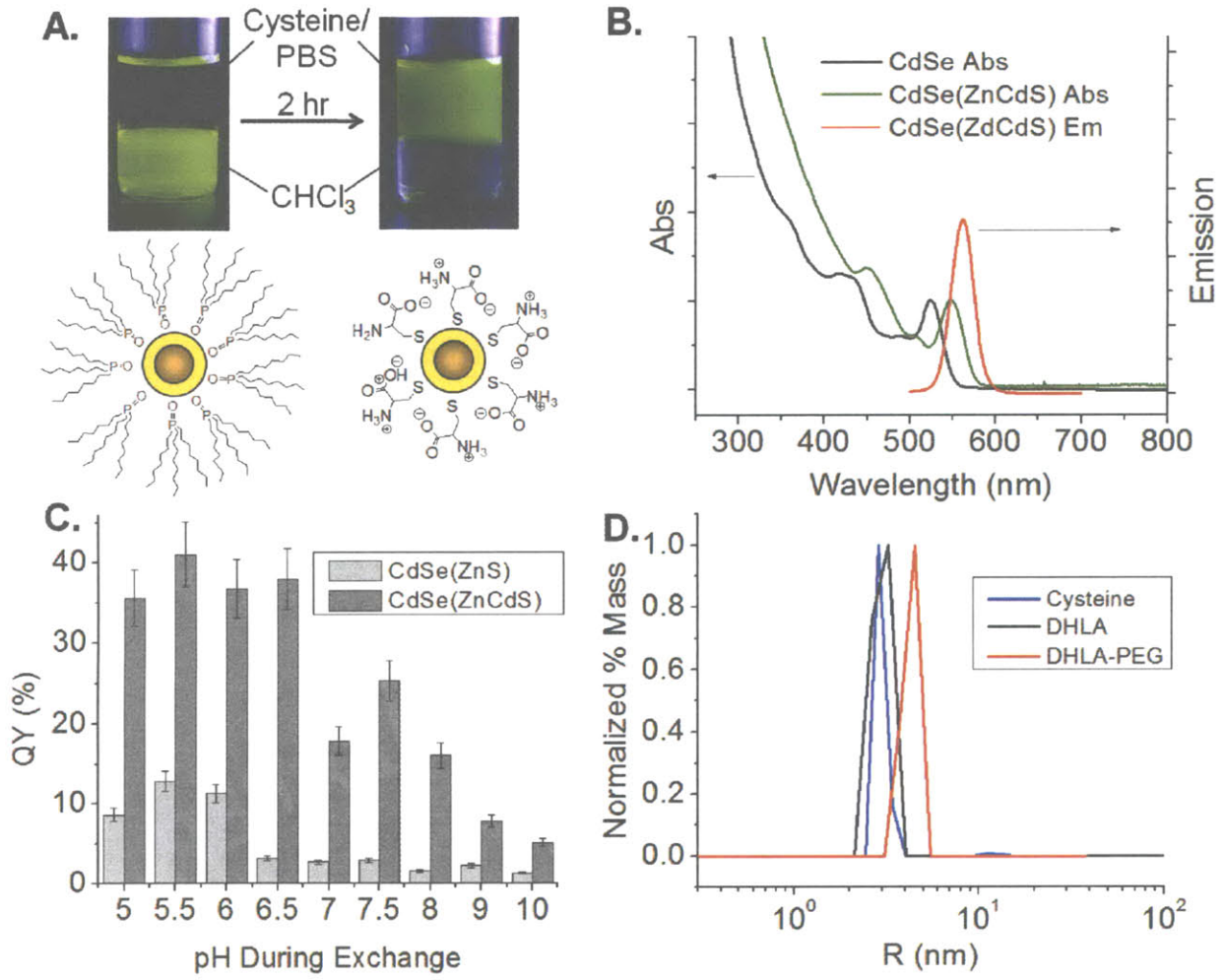

Figure 2-1 Characterization of CdSe(CdZnS) core(shell) QDs ligand exchanged with DL-Cysteine. (A) Schematic and image of QDs before and after ligand exchange with DL-cysteine. (B) QD absorption and emission spectra before and after overcoating with ZnCdS alloy shell. (C) QY as a function of pH for ZnS and ZnCdS alloy shell structures. (D) DLS data for QD565 coated with the indicated ligands, showing HDs in PBS of 5.95 nm (cysteine), 6.02 nm (DHLA), and 8.60 nm (DHLA-PEG).

layer (Figure 2-1A). The QDs were precipitated twice with ethanol and re-dispersed in PBS at pH 7.4 for analysis. QD-Cys as synthesized formed macroscopic aggregates upon standing at room temperature overnight. Storing the samples in the dark at 4°C only extended their stability to ~24 h. QD-Cys precipitation was attributed to dissociation of the ligand from the QD followed

by spontaneous oxidation to form cysteine dimers (cystine), which do not reattach to the QD surface, resulting in QD aggregation. By introducing a reducing agent, such as sodium borohydride or dithiothreitol (DTT) to prevent cystine formation, the stability of QD-Cys increased to ~1 week under ambient conditions (Figure 2-2) and to at least three months when stored in the dark at 4 °C.

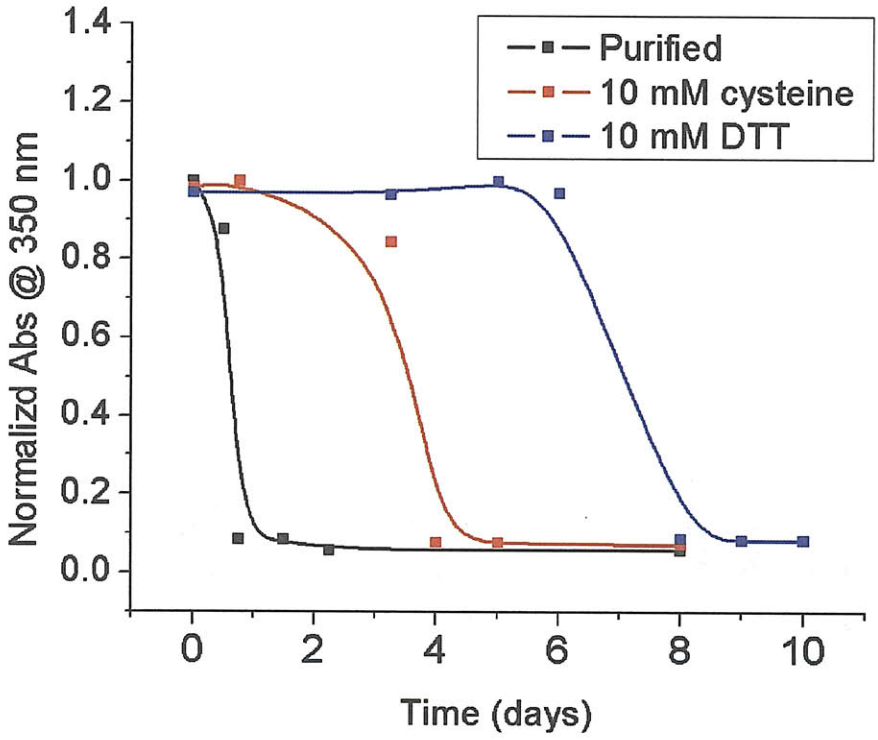

Figure 2-2 Stability of QD-Cys over time under various conditions. High absorbance at 350 nm indicates well dispersed sample, while low absorbance indicates aggregation and precipitation of QD-Cys.

Following phase transfer to water, the QDs exhibited decreased quantum yield (QY), consistent with previous reports of ligand exchange with monothiol ligands.[9] The final QY was highly sensitive to both the quality of the inorganic shell and the pH of the aqueous solution during ligand exchange. The most robust inorganic shells were obtained by the formation of a $Zn_xCd_{(1-x)}S$ alloy, as we previously reported.[10] The large red-shift of the absorbance maximum

upon overcoating evidenced the presence of an alloy shell (Figure 2-1B). To illustrate the dramatic difference a robust shell makes on the QY, ligand exchange with cysteine was

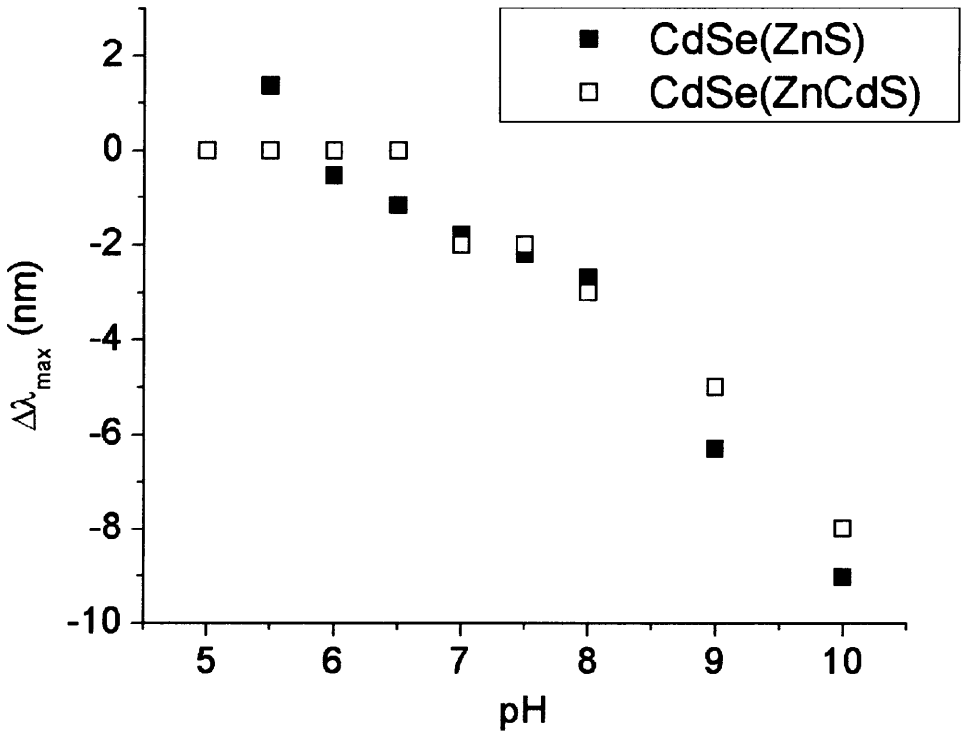

Figure 2-3 Blueshift of emission spectrum as a function of pH during ligand exchange. CdSe cores with ZnS or ZnCdS alloy shell both exhibited similar amounts of blue-shift, indicative of etching, but the alloyed shell QDs preserved much higher QY.

performed with CdSe QDs bearing 3 monolayers of either a pure ZnS or an alloy ZnCdS shell (30% Cd by mass). While the QY of the CdSe(ZnS) QDs dropped from ~68% in growth solution to ~13% in water, the QY of the CdSe(ZnCdS) QDs dropped from ~66% in growth solution to ~40% in water after ligand exchange under identical conditions. To test the effect of pH during ligand exchange on QY, exchange with cysteine was performed in aqueous buffer ranging from pH 5 to pH 10. The resulting QD-Cys were precipitated with ethanol and re-dispersed in PBS at

pH 7.4 for analysis. The maximum QY was achieved at pH 5.5, with QY dropping drastically beyond pH 6.0 (Figure 2-1C), which was correlated with a blue-shift in the absorbance spectrum, indicative of shell degradation (Figure 2-3). This degradation may be due to the formation of the reactive thiolate ion on cysteine at more basic pH, which can etch the shell during exchange. The more robust CdSe(ZnCdS) QDs showed the same pH dependent blue-shift in the absorbance spectrum as CdSe(ZnS) QDs, but exhibited >2-fold higher QY across the pH range tested, suggesting that the alloyed shell is not more resistant to etching, but is better at passivating surface trap sites. Similar alloy shells could help maintain the QY of QDs capped through ligand exchange with other mono-thiol ligands as well.

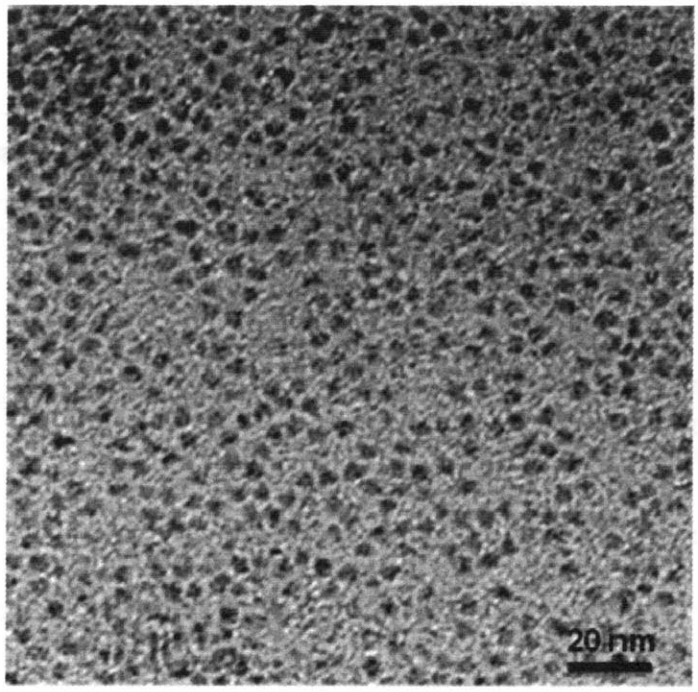

Figure 2-4 TEM of CdSe(ZnCdS) QDs drop-cast from hexane solution

The HD of QD-Cys was 5.95 nm by dynamic light scattering (DLS) (Figure 2-1D). Transmission electron microscopy (TEM) showed an inorganic particle size of 3.62 nm (Figure

2-4), indicating that the cysteine coating contributes ~1.2 nm to the overall radius, which is reasonable given the small extended size of cysteine (~0.6 nm) plus a hydration shell. By comparison, the same QD cores exchanged with dihydrolipoic acid (DHLA) and DHLA conjugated to a short polyethylene glycol (n=8; DHLA-PEG) showed HDs of 6.02 and 8.60 nm,

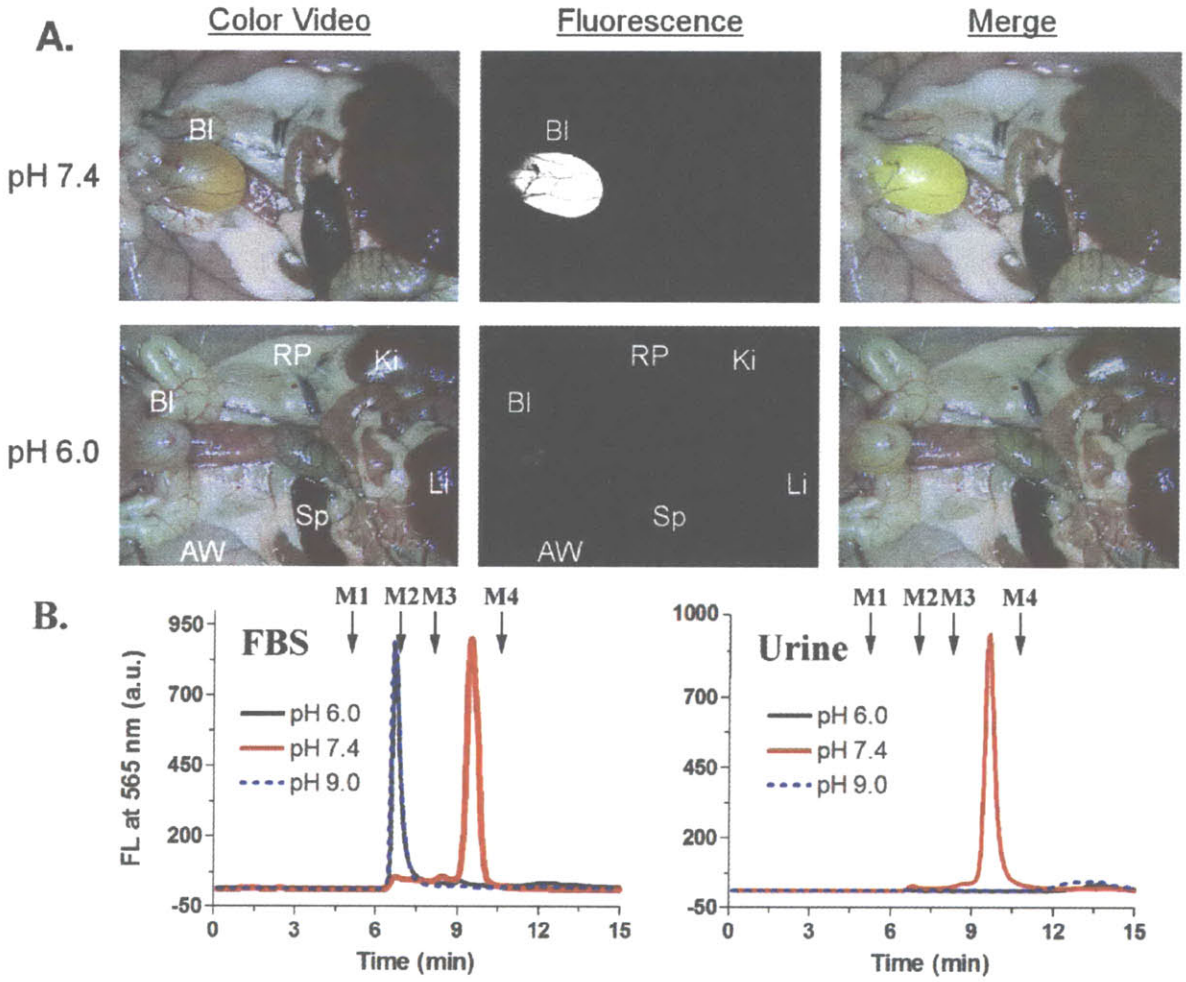

Figure 2-5 Renal clearance and GFC analysis of DL-cysteine coated QDs. (A) Fluorescence images of rats injected with QD-Cys incubated in FBS at the indicated pH, 4 h postinjection (Bl, bladder; Ki, kidneys; Li, liver; RP, retroperitoneum; AW, abdominal wall, and Sp, spleen.): color video (left), 565 nm fluorescence (middle), merged (right). (B) GFC analysis of QD-Cys incubated in FBS at various pH (left), and in urine (right) 4 hours postinjection (fluorescence detection at 565 nm). Mw markers M1 (thyroglobulin, 670 kDa), M2 (γ-globulin, 158 kDa), M3 (ovalbumin, 44 kDa), and M4 (myoglobin, 17 kDa) are shown by arrows.

respectively (Figure 2-1D). Incubation of DHLA-coated QDs in fetal bovine serum (FBS) for 4 h at 37 °C resulted in a large increase in size to >15 nm (data not shown) due to non-specific

protein binding, consistent with previous reports of proteins binding to QDs bearing charged ligands.[7,11] Incubation of QD-Cys in FBS under the same conditions did not alter the size of the QD, indicating that QD-Cys does not aggregate or bind proteins in serum (Figure 2-5B), which is attributed to the zwitterionic nature of the ligand at pH 7.4, rendering the QD surface effectively charge neutral. Indeed, changing the pH of the FBS to favor positively or negatively charged forms of cysteine at low and high pH, respectively, induced protein binding as seen by the same large increase in size after serum incubation (Figure 2-5B).

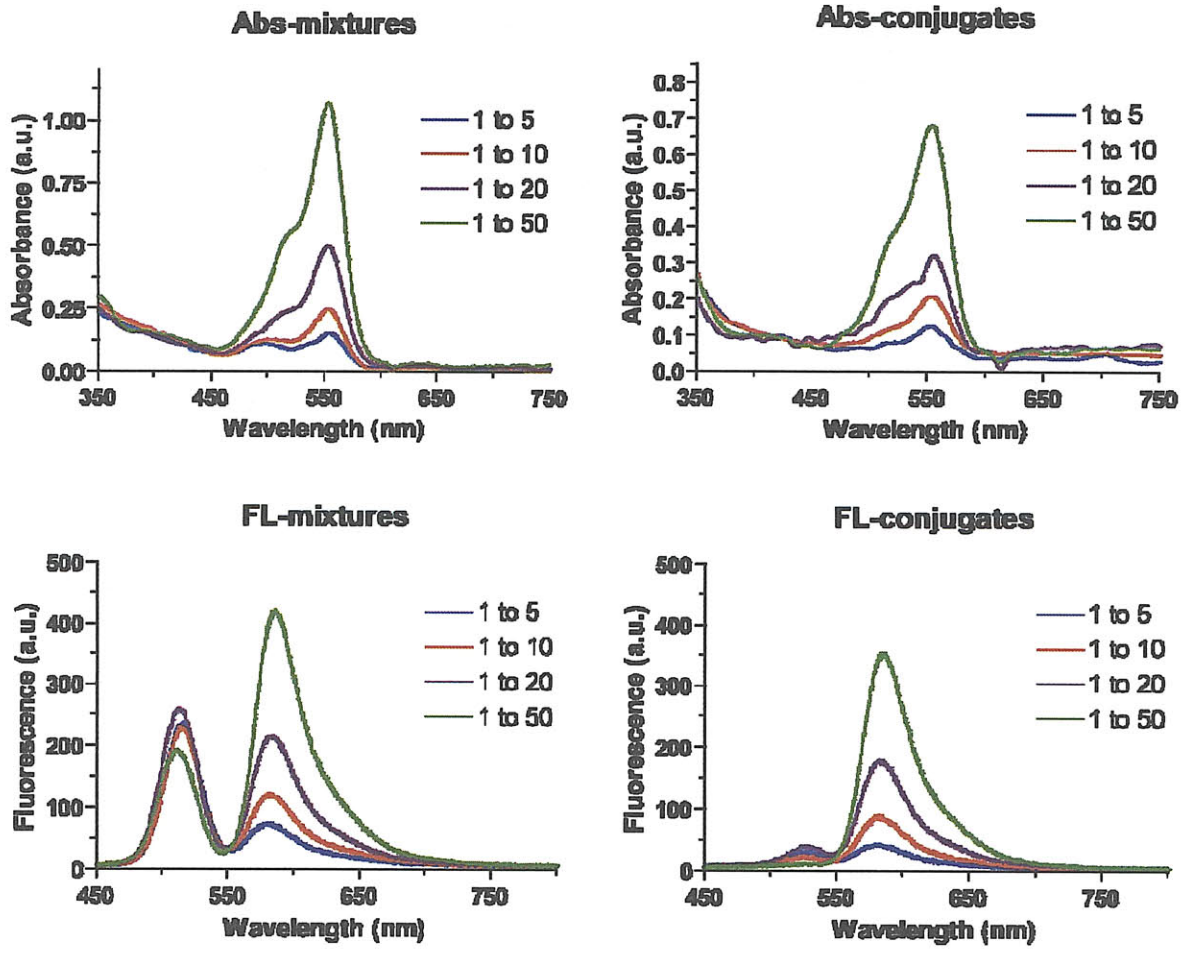

Figure 2-6 Absorbance and emission spectra of QD-dye conjugates. Absorbance (top row) and fluorescence (bottom row) spectra of Alexa, QD-Alexa mixtures, and QD-Alexa conjugates after purification, from left to right. Each graph shows 5 different QD:dye ratios. Fluorescence spectra were measured with excitation at 414 nm.

The exceptionally small size of QD-Cys and their stability in serum enabled us to observe interesting, new *in vivo* behavior. When injected into rats intravenously, QD-Cys accumulated mainly in the bladder 4 h postinjection, indicating that the QDs were near or below the size threshold for renal clearance (Figure 2-5A). Gel filtration chromatography (GFC) analysis of the

Mixed Dye:QD Ratio	QD Abs @ 350	QD Conc (μ M)	Dye Abs @ 555	Dye Conc (μ M)	Purified Dye:QD Ratio
5	0.22	0.51	0.09	0.58	1.13
10	0.22	0.51	0.16	1.07	2.08
20	0.13	0.30	0.25	1.65	5.43
50	0.19	0.44	0.62	4.1	9.32

Table 2-1 QD-cys Alexa conjugation ratios. Concentrations were measured based on εdye = 150,000 cm-1M-1 at 555 nm for Alexa 555, and εQD = 420,000 cm-1M-1 at 350 nm for QD515.

urine confirmed the presence of QDs in the bladder (Figure 2-5A). Injecting protein-bound QD-Cys (incubated with FBS at pH 6.0 or 9.0 for 4 h) showed no renal clearance 4 h postinjection, suggesting both that protein-QD complexes are stable over this time scale and that renal clearance is largely dependent on the size of the QD. By systematically altering the core(shell) size of QD-Cys, it is possible to precisely determine the size threshold for renal filtration.[12]

In addition, active constructs for in-vivo targeting and sensing can potentially be obtained by covalently conjugating other species to QD-Cys through the C-terminus of the cysteine residue. To demonstrate, we conjugated 515 nm emitting QD-Cys to Alexa fluor 555 through carbodiimide coupling chemistry and purified the construct with three cycles of spin filtration through a 10 kDa M_w cutoff filter. By altering the initial ratio of dye to QD, the average number of dye molecules ultimately attached to each QD was tuned from <1 to 9, as determined by UV-Vis absorption. Excitation of the QD at a wavelength with minimal dye absorption resulted largely in dye fluorescence and quenched QD emission, suggesting efficient fluorescence resonance energy transfer (FRET) between QD and dye (Figure 2-6).

In summary, we have developed a versatile nanoparticle construct using a compact cysteine coating on a highly robust CdSe(ZnCdS) core(shell) structure to form aqueous QDs that are biologically compatible, extraordinarily compact, highly fluorescent, and easily functionalized. These properties, combined with the observation of renal clearance, open up the possibility of functionalized nanocrystals for in-vivo targeted imaging, in which small molecules can be conjugated to QD-Cys for targeting, and unbound QDs can be rapidly cleared to achieve high signal/noise ratios and to reduce background toxicity.

2.2.2 Experimental Details

Materials and Methods. Trioctylphosphine oxide (TOPO), hexadecylamine (HDA), decylamine, and dodecanal (DDA) were purchased from Sigma Aldrich and used as received. Selenium shot, cadmium 2,4-pentanedionate ($Cd(acac)_2$), and n-hexylphosphonic acid (HPA) were purchased from Alfa Aesar (Ward Hill, MA). Dimethylcadmium ($CdMe_2$) and diethylzinc ($ZnEt_2$) were purchased from Alfa Aesar and Fluka, respectively. Both were filtered through a 0.2 μm syringe filter and stored at -30°C under inert atmosphere. Trioctylphosphine (TOP) and tributylphospine (TBP) were purchased from Strem Chemicals (Buchs, Switzerland). Tributylphosphine selenide (TBP-Se) was prepared by dissolving 0.15 mmol of selenium shot in 100 mL of TBP under inert atmosphere and stirring vigorously overnight, forming a 1.5 M TBP-Se solution. All air sensitive materials were handled in an Omni-Lab VAC glove box under dry nitrogen atmosphere with oxygen levels < 0.2 ppm. All solvents were spectrophotometric grade and purchased from EMD Biosciences. UV-Vis absorbance spectra were taken using an HP 8453 diode array spectrophotometer. Photoluminescence spectra were recorded with a SPEX FluoroMax-3 spectrofluorimeter. The absorbance of all solutions was kept below 0.1 OD to avoid inner-filter effects.

CdSe(ZnCdS) QD Synthesis. Core(shell) CdSe(ZnCdS) nanocrystals were synthesized via modification of previously reported procedures.[13,14] Briefly, a precursor solution comprising of $Cd(acac)_2$ (155 mg, 0.5 mmol) and DDA (0.25 mL) in TOP (2.8 mL) was degassed at 100°C for 1 hr, followed by the addition of TBP-Se (1.5M, 3.3 mL) after cooling to room temperature. This mixture was loaded into a syringe under dry N_2 atmosphere. In a separate 3-neck round bottom flask, 90% TOPO (6.25 g) and 90% HDA (5.75 g) were degassed at 135°C for 2 hr and backfilled with N_2. The temperature was increased to 360°C before rapidly injecting the precursor solution. The cores were grown at 280°C until the desired emission wavelength was reached. The typical full width at half maximum (FWHM) of the emission spectrum was 28 nm for the cores. After cooling to 80°C, butanol (4 mL) was added to prevent solidification of the product. The core stock solution was allowed to settle for 1 hr at RT and then centrifuged at 3000 g for 4 min. The pellet was discarded and the supernatant was precipitated twice with the addition of acetone followed by centrifugation. The pellet was redispersed in hexane, filtered through a 0.2 μm filter, and injected into a degassed solution of 99% TOPO (10 g) and n-hexylphosphonic acid (0.4 g). After removal of the hexane under reduced pressure at 80°C, the flask was back-filled with dry N_2 and the temperature increased to 130°C before adding 0.25 mL of decylamine and stirring for 30 min. Precursor solutions of $ZnEt_2/CdMe_2$ and $(TMS)_2S$ were prepared by dissolving the appropriate amounts of each in 4 mL of TOP and loading them into two separate syringes under inert atmosphere. The amount of $ZnEt_2$ was calculated by assuming a 3 monolayer overcoat according to the methods of Dabbousi et al., comprising 30% $CdMe_2$ by mass.[13] Typical masses were 56 mg and 14 mg for $ZnEt_2$ and $CdMe_2$, respectively. Two equivalents of $(TMS)_2S$ were used. The precursor solutions were injected simultaneously into the 130°C bath at a rate of 4 mL/hr and annealed overnight at 80°C. QD stock solutions were

stored under ambient conditions in a solution of butanol (4 mL) and centrifuged once more before use.

Preparation of water solublized CdSe(ZnCdS) nanocrystals. To an aliquot of QDs in growth solution (0.5 mL) was added acetone to the first sign of turbidity. Centrifugation at 3500 g for 4 min yielded a highly colored supernatant. The pellet was discarded and the supernatant was precipitated once more in this fashion. The resulting supernatant was precipitated with the addition of excess methanol. Centrifugation and decantation yielded a colored pellet to which chloroform (0.4 mL) was added. To this solution was added 1 mL of a 40 mg/mL solution of cysteine in phosphate buffered saline (PBS) to form a biphasic system. The mixture was stirred vigorously at RT for 2 hr, or until the chloroform layer became clear. The solution was centrifuged at 3000 g for 4 min to achieve phase separation. The organic layer was removed by pipette and any residual chloroform was removed from the aqueous phase by evaporation with stirring under reduced pressure. The QDs were precipitated twice with the addition of ethanol and redispersed in PBS buffer at pH 7.4. The QD solution was stabilized with the addition of DTT (10 mM) to prevent the dimerization of cysteine. QD formulations treated in this fashion were stable for up to 1 week under ambient conditions, and for at least 3 months when stored in the dark at 4 °C. Prior to any conjugation chemistry, free ligand was removed by three cycles of dilution/concentration through a Vivaspin 6 10,000 Da M_w cutoff filter (Goettingen, Germany).

QD-Cys stability measurements. An aqueous solution of QD-Cys was left under ambient conditions in the presence of 10 mM cysteine, 10 mM DTT, or free of excess ligand by dialysis. At set time intervals, the solution was centrifuged to remove any QDs that had precipitated due to instability. A small aliquot of the supernatant (50 uL) was then diluted in 1 mL of PBS buffer, and the absorbance at 350 nm was measured (Figure S1).

QD-Cys Alexa conjugation. The synthesized QD-Cys was conjugated to Alexa Fluor 555 cadaverine (Molecular Probes). Conjugation of the single nucleophile-containing molecule was performed using standard carbodiimide chemistry. QD-Cys was resuspended in 0.1 M MES (2-(N-morpholino)ethanesulfonic acid), pH 6, and treated with 100 equivalents (per particle) of the carbodiimide 1-ethyl-3-(3-dimethyllaminopropyl)carbodiimide (EDC; Pierce) and 250 equivalents (per particle) of sulfo-NHS (Pierce). The suspension was incubated for 15 min, and excess reagents removed by ultrafiltration. Between 5-50 equivalents of the Alexa fluor 555 was dissolved in PBS, pH 8.0, and mixed with the MES solution, resulting in a final pH of 7.4. After 4 hr of conjugation, QD-Cys was subjected to ultrafiltration with Tris, pH 8.0 to remove any unconjugated dye and to quench unreacted NHS. An aliquot of the final material was analyzed by UV-Vis absorption to determine the number of ligand molecules conjugated to the QD surface. Based on the extinction coefficients for Alexa 555 and QD-Cys, <1 to 9 dye molecules were conjugated to the surface of the QD-Cys (Table S1).

Transmission Electron Microscopy. The inorganic size of CdSe(ZnCdS) QDs was determined using a JEOL 200CX TEM operating at 200 kV. One drop of a dilute sample of QDs in hexane precipitated two times using acetone was placed onto a Formvar coated copper grid, allowed to settle for 20 seconds, and wicked away using an absorbent tissue. Size analysis was performed on captured digital images using ImageJ 1.34s.

GFC analysis. In order to measure stability in fetal bovine serum (FBS), QD-Cys were incubated for 4 hours at various pH ranges and analyzed by RP-HPLC on a 8 x 300 mm, 200 Å Diol (YMC, Japan) size-exclusion column. For the mobile phase, pH 7.4 PBS containing 1 mM cysteine was used with a flow rate of 1 mL/min. Calibration of HD was performed by injecting 50 μL of gel filtration protein standards from Bio-Rad (cat. 151-1901) containing thyroglobulin

(669 kDa, 18.8 nm HD), γ-globulin (158 kDa, 11.1 nm HD), ovalbumin (44 kDa, 6.1 nm HD), myoglobin (17 kDa, 3.8 nm HD), and vitamin B_{12} (1.4 kDa, 1.67 nm HD). On-line, full spectrum analysis of absorbance (model 2487, Waters) and fluorescence (model 2475, Waters) permits collection of desired fractions.

Animal models. Animals were housed in an AAALAC-certified facility staffed by full-time veterinarians, and were studied under the supervision of an approved institutional protocol. Sprague-Dawley (SD) male rats were purchased from Taconic Farms (Germantown, NY) at 300–350 g size. All animals acclimated to the animal facility for at least 48 hr prior to experimentation. For surgery, rats and mice were anesthetized with 65 mg/kg intraperitoneal pentobarbital. For the biodistribution test, 1 mL of 3 μM QDs was injected intravenously into the rats. After each study, anesthetized rats were euthanized by intraperitoneal injection of 200 mg/kg pentobarbital, a method consistent with the recommendations of the Panel on Euthanasia of the American Veterinary Medical Association.

Intraoperative fluorescence imaging systems. Intraoperative fluorescence imaging systems optimized for animal surgery have been described in detail previously.[6,12,15-17] For fluorescence excitation, 100 mA LEDs with 470 ± 20 nm excitation filters were used, and 560 ± 20 nm bandpass filters were used for fluorescence emission. The exposure time (200 ms) and normalizations were the same for all fluorescence images. Simultaneous photon collection for color video and fluorescence images is achieved with custom-designed optics. After computer-controlled camera acquisition via custom LabVIEW (National Instruments, Austin, TX) software, anatomic (white light) and functional (fluorescent light) images can be displayed separately and merged. All images are refreshed up to 15 times per second. The entire apparatus

is suspended on an articulated arm over the surgical field, thus permitting noninvasive and nonintrusive imaging.

Dynamic Light Scattering. Light scattering analysis was performed using a DynaPro Dynamic Light Scatterer. All QD samples were between 2-3 μM in concentration and filtered through a 0.02 μm filter before analysis. Typical count rates were between 100-300 kHz. Each autocorrelation function (ACF) was acquired for 10 seconds, and averaged for 10 minutes per measurement. A software filter was employed to discard all ACF fits with sum of squares errors > 15. All measurements were taken in triplicate, and the resulting ACF was fitted using the Dynamics V6 software employing a non-negative least squares fitting algorithm. HD data were obtained from a mass weighted size distribution analysis.

Quantum yield (QY) of QDs. The QY of QD565 was measured relative to Rhodamine 590 (QY 99% in ethanol) with excitation at 490 nm. Solutions of QDs in PBS and dye in ethanol were optically matched at the excitation wavelength. Fluorescence spectra of QD and dye were taken under identical spectrometer conditions in triplicate and averaged. The optical density was kept below 0.1 at the λ_{max}, and the integrated intensities of the emission spectra, corrected for differences in index of refraction and concentration, were used to calculate the quantum yields using the expression $QY_{QD} = (\text{Absorbance})_{dye}/(\text{Absorbance})_{QD} \times (\text{Peak Area})_{QD}/(\text{Peak Area})_{Dye} \times (n_{QD\ solvent})^2/(n_{Dye\ solvent})^2 \times QY_{Dye}$.[18]

2.3 *References*

1. Murray, C. B.; Norris, D. J.; Bawendi, M. G. *J. Am. Chem. Soc.* **1993**, *115*, 8706-8715.

2. Wu, X.; Liu, H.; Liu, J.; Haley, K. N.; Treadway, J. A.; Larson, J. P.; Ge, N.; Peale, F.; Bruchez, M. P. *Nature Biotechnol.* **2003**, *21*, 41-46.

3. Howarth, M.; Takao, K.; Hayashi, Y.; Ting, A. Y. *PNAS.* **2005**, *102*, 7583-7588.

4. Caliceti P., V. F. M. *Adv. Drug Delivery Rev.*, *55*, 1261-1277.

5. DeNardo, S. J.; Yao, Z.; Lam, K. S.; Song, A.; Burke, P. A.; Mirick, G. R.; Lamborn, K. R.; O'Donnell, R. T.; DeNardo, G. L. *Clin. Cancer Res.* **2003**, *9*, 3854S-3864.

6. Kim, S.; Lim, Y. T.; Soltesz, E. G.; De Grand, A. M.; Lee, J.; Nakayama, A.; Parker, J. A.; Mihaljevic, T.; Laurence, R. G.; Dor, D. M.; Cohn, L. H.; Bawendi, M. G.; Frangioni, J. V. *Nat. Biotech.* **2004**, *22*, 93-97.

7. Zimmer, J. P.; Kim, S.-W.; Ohnishi, S.; Tanaka, E.; Frangioni, J. V.; Bawendi, M. G. *J. Am. Chem. Soc.* **2006**, *128*, 2526-2527.

8. Chen, J. L.; Zhu, C. Q. *Analytica Chimica Acta* **2005**, *546*, 147-153.

9. Smith, A. M.; Duan, H.; Rhyner, M. N.; Ruan, G.; Nie, S. *Phys. Chem. Chem. Phys.* **2006**, *8*, 3895-3903.

10. Snee, P. T.; Chan, Y.; Nocera, D. G.; Bawendi, M. G. *Adv. Mater.* **2005**, *17*, 1131-1136.

11. Bentzen, E. L.; Tomlinson, I. D.; Mason, J.; Gresch, P.; Warnement, M. R.; Wright, D.; Sanders-Bush, E.; Blakely, R.; Rosenthal, S. J. *Bioconjugate Chem.* **2005**, *16*, 1488-1494.

12. Choi, H. S.; Liu, W.; Misra, P.; Tanaka, E.; Zimmer, J. P.; Kandapallil, B.; Bawendi, M. G.; Frangioni, J. V. 2007.

13. Dabbousi, B. O.; Rodriguez-Viejo, J.; Mikulec, F. V.; Heine, J. R.; Mattoussi, H.; Ober, R.; Jensen, K. F.; Bawendi, M. G. *J. Phys. Chem. B* **1997**, *101*, 9463-9475.

14. Fisher, B. R.; Eisler, H.-J.; Stott, N. E.; Bawendi, M. G. *J. Phys. Chem. B* **2004**, *108*, 143-148.

15. Frangioni, J. V. *Nat Biotech* **2006**, *24*, 909-913.

16. De Grand, A. M.; Frangioni, J. V. *Technol Cancer Res Treat.* **2003**, *2*, 553-562.

17. Nakayama, A.; del Monte, F.; Hajjar, R. J.; Frangioni, J. V. *Mol Imaging* **2002**, *1*, 365-377.

18. Eaton, D. *IUPAC.* **1988**, *60*, 1107-1114.

Chapter 3: Application of Cysteine-Coated QDs in Determination of the Renal Filtration Threshold*

3.1 *Background and Motivation*

In order to meet FDA regulatory approval, any potentially toxic agent injected into the body must satisfy three criteria for clearance, or removal from the body: (1) they can be metabolized by the liver and cleared through the bowel, (2) they can biodegrade into smaller components which then clear through the kidneys, or (3) the whole construct must be small enough to clear through the kidneys. One long term goal is to develop nanocrystals for use in the clinic as a disease diagnostic tool to image tumors, for instance. For nanocrystals, due to their high perceived toxicity, clearance through the liver is not an option, since this can take many days, and even then the clearance is not complete. Biodegradability is also not an option, since most QDs contain heavy-metal components that would be toxic if broken down and released into the body, so the only option is renal clearance. Thus, pinpointing the renal clearance threshold can serve as the basis for the design of future nanocrystals that can potentially be used in the clinic.

Previous clearance data using proteins and small molecules as probes suggested that the renal filtration cut-off is around 5 nm in hydrodynamic diameter (HD). The underlying reason for this size threshold lies in the anatomy of the kidney, in which a structure known as the glomerulus acts as a mechanical size filter.[1] Blood flows into the glomeruous via capillaries, and any foreign objects (small molecules, proteins etc.) that are small enough to physically pass

* Much of this chapter has appeared in print. It is reproduced with permission from *Nature Biotech* 2007, **25**: 1165 - 1170. The in-vivo imaging data in this chapter were the result of a collaboration with the research group of John V. Frangioni at the Beth Israel Deaconess Medical Center.

through the membrane are removed from the blood and take a path leading eventually to the bladder. Previous studies from the literature using proteins as size probes for biodistrubtion suggest that this renal filtration cut-off is around 5 nm HD (Table 3-1).

Molecule	MW (kDa)	HD (nm)	Urine/Blood filterability (%)	Blood Half-life (min)	Whole Body Half-Life (hr)	Ref
Inulin	5.0	3.0	100	8.8	1.9	[2,3]
Lysozyme	15	3.4	80	12	1.3	[4,5]
Myoglobin	17	3.8	75	8.9	2.0	[4,6]
scFv	30	5.3*	74	11	1.4	[7]
Bence-Jones	44	6.1*	10	–	3.0	[8,9]
Fab'	50	6.0	9	28	4.0	[4,10]
$Sc(Fv)_2$	60	7.0*	–	78	5.1	[7]
HSA	67	7.3*	0.3	110	16	[6]
$[sc(Fv)_2]_2$	120	9.3*	–	170	8.9	[7]
IgG	152	11.0	< 0.1	330	730	[4,7]

Table 3-1 Biodistribution and renal filtration as a function of hydrodynamic diameter. *Unknown HDs were calculated using the following power law fit to literature values: HD = A × MW^B + C × MW^D. Where: A = -0.000000002614; B = 3.326; C = 0.9482; D = 0.5001; R2 = 0.999.

In the previous chapter, we established a means of synthesizing ultra-compact biocompatible QDs for in vivo imaging and demonstrated for the first time renal clearance of a nanomaterial. In this chapter, we seek to refine our understanding of the renal filtration threshold via the synthesis of a size series of QDs spanning ~4.5 – 8 nm in hydrodynamic diameter (HD) keeping cysteine constant as the organic coating, but changing the physical inorganic size of the nanocrystals themselves. Currently, many nanoparticle formulations are under development for the treatment of disease, but oftentimes the long-term health effects of such particles in the body is unknown. The determination of this renal filtration threshold is important for nanomedicine because it establishes the size at which nanoparticles can be effectively cleared from the body. Ideally, this research will guide the design of future nanoparticle systems that will either be small enough to be cleared renally, or degrade into components that are small enough to do so.

We chose CdSe as our core material for the size series study because the synthetic protocols are sufficiently mature to generate particles with extremely narrow size distribution with deviations of <5% and also within the size range of interest (between 2-6 nm in diameter). However, the bandgap of CdSe is not optimal for in-vivo imaging due to the high degree of absorbance and scattering from tissue in the visible region. Therefore, in this case, the CdSe particles act only as a size probe and we rely on the conjugation of an additional marker to determine their biodistribution.

3.2 *Synthesis and characterization of a CdSe(ZnS) size series*

3.2.1 Results and Discussion

A size series of CdSe cores were synthesized using previously reported procedures and overcoated with ~3 monolayers of ZnS. The more robust ZnCdS alloy shell reported in the previous chapter was not used because the goal here was to minimize the particle size without regards to QY (*vide infra*). By this method, core(shell) QDs with diameters of 2.9 – 4.3 nm were synthesized. For the smallest sized cores, the CdO protocol developed by Peng et al. was used,[11] and larger sized cores utilized the method of Stott et al.[12] All cores were overcoated by the same method using $ZnEt_2$ and $(TMS)_2S$.

Ligand exchange was performed using a suite of ligands designed to test the effect of charge on non-specific binding to serum proteins. The ligands ranged from anionic, zwitterionic, cationic to neutral (Figure 3-1A). QDs with the various ligand coatings were incubated in fetal bovine serum (FBS) for 4 h to simulate the blood environment and their size analyzed by gel permeation chromatography (GFC). If non-specific binding to serum proteins were to occur, the size should increase after FBS incubation as measured by GFC. Figure 3-1B shows that the zwitterionic DL-cysteine coating and the neutral DHLA-PEG coated QDs both exhibited

negligible non-specific binding, while the anionic and cationic QDs exhibited

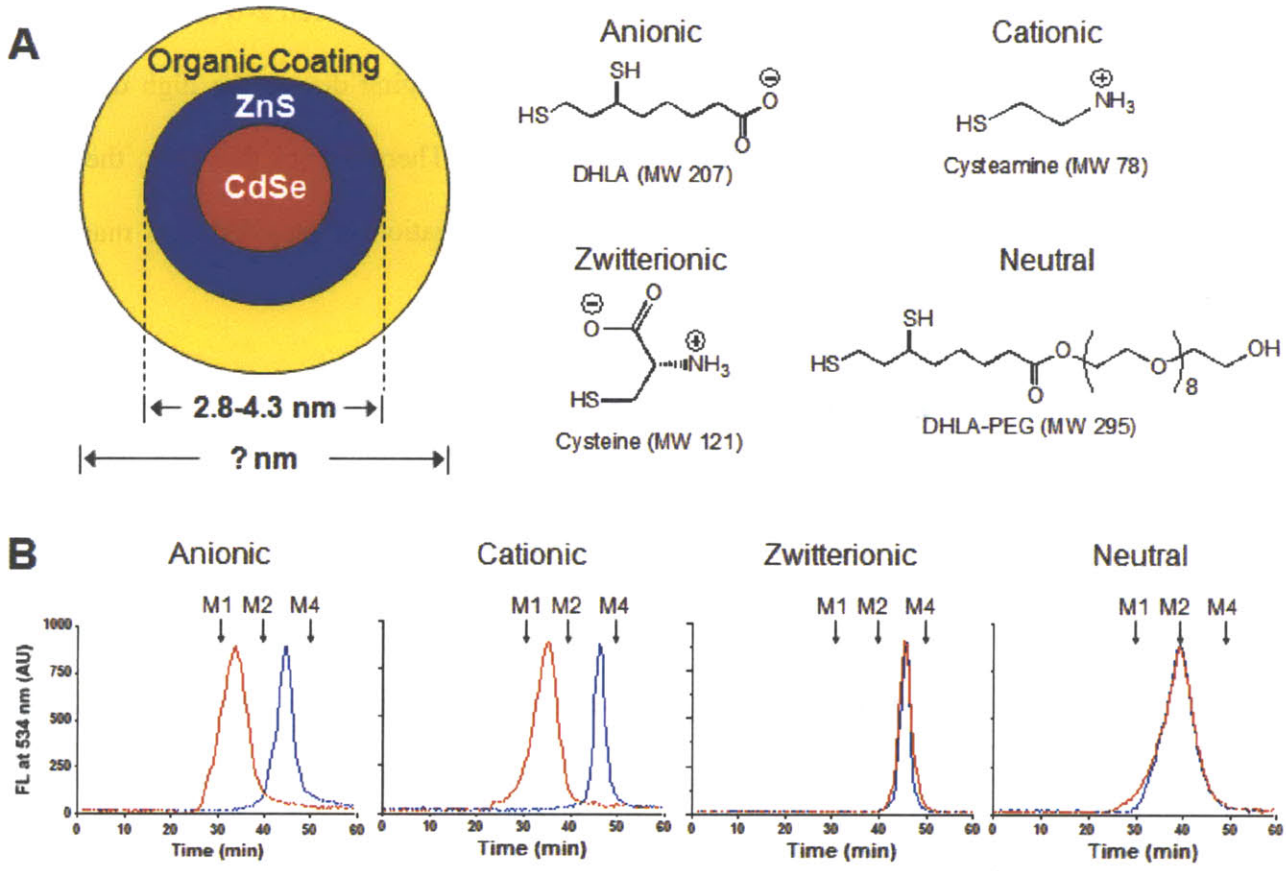

Figure 3-1 Ligand exchange of CdSe(ZnS) core(shell) QDs with various ligands. (A) Schematic of QD structure, with inorganic core(shell) structure and various organic coatings. (B) GFC analysis of QDs coated with various organic coatings after incubation with FBS.

significant amounts of non-specific binding. This observation is consistent with the fact that charged QDs are likely binding to oppositely charged proteins in serum through electrostatic interactions, thereby increasing their size. Thus, only the neutral or zwitterionic surface coatings are suitable here for in vivo applications if one cares to keep the size small. The difference is that the use of the zwitterionc DL-cysteine ligand affords a much more compact coating than a neutral PEGylated coating due to the long length of the PEG chain necessary to keep the QDs water-soluble. The zwitterionic coating therefore affords its advantage in this case and enables

the access to sub-5 nm HD QDs in water, while PEGylated QDs reached HDs of no less than 10 nm.

The size series of QDs were then water solublized with DL-cysteine via the phase-transfer ligand exchange method as described in the previous chapter. The hydrodynamic size of the final QDs in water was measured by both dynamic light scattering (DLS) and GFC. The sizes obtained from both measurements were in acceptable agreement with one another and gave particles in water ranging in size from ~4.6 – 8 nm in diameter (Figure 3-2C). The fluorescence spectrum, representative TEM, and GFC data of the size series can be seen in Figure 3-2. This size series will be then used to probe the renal filtration threshold in mice.

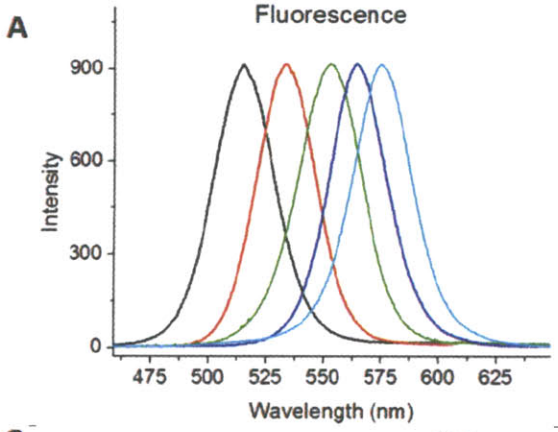

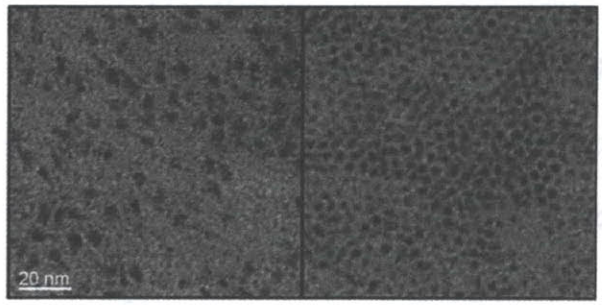

C

QDs	Em Max (nm)	TEM Dia (nm)	DLS		GFC	
			HD (nm)	%PD	HD (nm)	PDI
QD515	515	2.85 ± 0.18	4.64 ± 0.08	20.9	4.41 ± 0.09	1.14
QD534	534	3.02 ± 0.20	4.91 ± 0.05	25.9	4.96 ± 0.18	1.13
QD554	554	3.30 ± 0.25	5.64 ± 0.01	13.1	5.46 ± 0.14	1.13
QD564	564	3.80 ± 0.20	6.40 ± 0.02	24.7	6.51 ± 0.33	1.20
QD574	574	4.31 ± 0.46	7.22 ± 0.20	24.8	8.21 ± 0.52	1.46

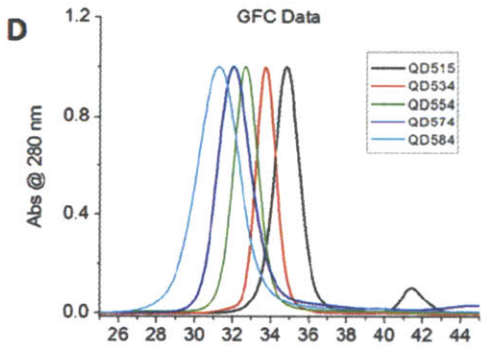

Figure 3-2 Ligand exchange of CdSe(ZnS) core(shell) QDs with various ligands. (A) Schematic of QD structure, with inorganic core(shell) structure and various organic coatings. (B) GFC analysis of QDs coated with various organic coatings after incubation with FBS.

3.2.2 Experimental Details

Synthesis of CdSe/ZnS Core/Shells. CdSe/ZnS Core/shell nanocrystals were synthesized using the following methods: QD515,[13] QD534,[14, 15] QD554,[14, 15] QD564,[14, 15] and QD574.[14, 15] See Supplementary Information for detailed experimental methods.

DHLA and DHLA-PEG Organic Coatings. Dihydrolipoic acid (DHLA) and DHLA conjugated to a polyethylene glycol spacer (n = 8, DHLA-PEG) was prepared using procedures from the literature.[16, 17] Ligand exchange was performed according to reported procedures,[16, 17] with modifications. Briefly, an aliquot of QD growth solution (0.2 mL) was precipitated with the addition of acetone followed by centrifugation at 3500 g for 4 min. The supernatant was discarded, and 50 μL of neat DHLA or DHLA-PEG along with 50 μL of MeOH was added to the pellet. The mixture was stirred at 60°C for 2 hr and precipitated with the addition of ethanol, chloroform, and hexane followed by centrifugation at 3500 g for 4 min. The supernatant was discarded and the QD sample was redispersed in PBS (pH 7.4) for analysis.

Cysteine and Cysteamine Organic Coatings. Ligand exchange with cysteine and cysteamine were carried out using a biphasic exchange method, in which QDs size-selectively precipitated twice using acetone were redispersed in $CHCl_3$ to which a solution of cysteine (40 mg/mL) or cysteamine (50 mg/mL) in PBS (1 mL) was added. This biphasic mixture was stirred vigorously for 2–6 hr until the organic layer became colorless. The $CHCl_3$ phase was removed by pipette, and residual organic solvent removed under reduced pressure. The QDs were precipitated twice with the addition of ethanol and redispersed in PBS (pH 7.4) for analysis. The cysteine-coated QDs (QD-Cys) were stabilized by adding dithiothreitol (DTT, 1 mM) to prevent the dimerization of cysteine. QD-Cys formulations treated in this fashion are stable for up to 1 week in PBS, pH 7.4 storage buffer under ambient conditions, and exhibit quantum yields (QY) between 10-15% (See Supplementary Information for detailed experimental methods). Prior to

conjugation, any free ligands were removed by three cycles of dilution/concentration through Vivaspin 6 (MWCO 10,000) spin concentrators (Vivascience, Stonehouse, UK).

TEM Sizing of QD Core/Shell. The size of CdSe/ZnS core/shell structures was measured using a JEOL 200CX TEM operating at 200 kV. One drop of a dilute sample of QDs in hexane was placed onto a Formvar coated copper grid, allowed to settle for 20 seconds, and wicked away using an absorbent tissue. Size analysis was performed on captured digital images using ImageJ V. 1.34s.

HD Measurements by Dynamic Light Scattering. Light scattering analysis was performed on a DynaPro Dynamic Light Scattering system (Qyatt, Santa Barbara, CA). The concentration of stock QDs was 2–3 μM, and all QDs were filtered through a 0.02 μm filter before analysis. Typical count rates were between 100–300 kHz. Each autocorrelation function (ACF) was acquired for 10 seconds, and averaged for 10 minutes per measurement. A software filter was employed to discard all ACF fits with sum of squares errors >15. The resulting ACF was fitted using the Dynamics V6 software employing a non-negative least squares fitting algorithm. Hydrodynamic size data were obtained from a mass weighted size distribution analysis and reported as the mean of triplicate measurements ± SD.

Gel-Filtration Chromatography (GFC). Details of the custom GFC system, which permits on-line, full-spectrum analysis of QD absorbance and fluorescence, have been published previously.[18] GFC was performed on a Superose-6 10/300 GL column (Amersham Biosciences, Piscataway, NJ) using PBS, pH 7.4 supplemented with 1 mM cysteine as mobile phase. Flow rate was 0.4 mL/min. Calibration of HD was performed by injecting 50 μL of protein standards (cat. 151-1901, Bio-Rad, Hercules, CA) containing thyroglobulin (669 kDa, 18.0 nm HD), γ-globulin (158 kDa, 11.9 nm HD), ovalbumin (44 kDa, 6.13 nm HD), myoglobin (17 kDa, 3.83

nm HD), and vitamin B_{12} (1.35 kDa, 1.48 nm HD). All HD measurements were performed with three independent experiments. For measurement of the effects of serum protein adsorption, 1 μM QDs were incubated in PBS or 100% fetal bovine serum (FBS) for 4 hr at 37°C prior to loading 100 μL onto the GFC column.

3.3 *In Vivo Imaging Using CdSe(ZnS) Size Series*

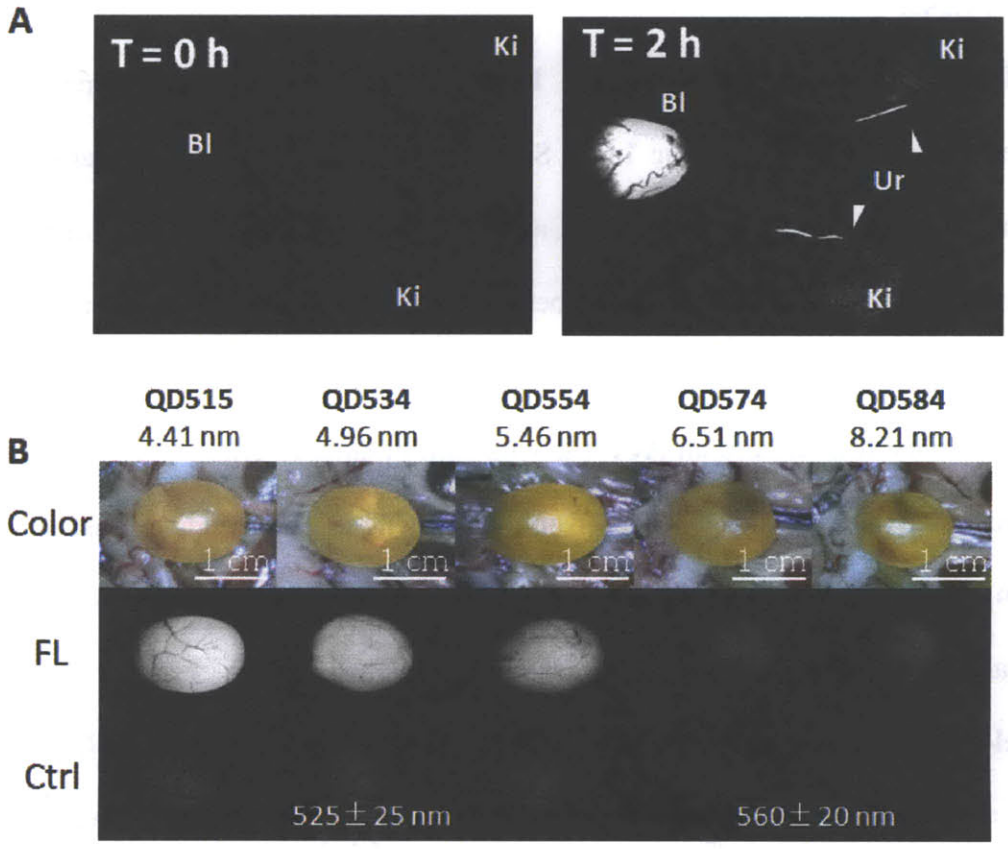

Figure 3-3 Renal excretion of QD-Cys size series by fluorescence imaging. (A) Renal clearance of Cys-QD515 at T = 0 and T = 2 h post-injection, showing active transport of QDs from both kidneys (Ki) to the bladder (Bl) via the ureter (Ur; arrowheads). (B) Images of bladder 4 h post-injection. Top: merged color and fluorescence image. Middle: fluorescence image from the QD channel. Bottom: uninjected control bladder. A 525 ± 25 nm emission filter was used for QD515 and QD534. A 560 ± 20 nm filter was used for QD554 , QD 564, and QD574. The exposure time (200ms) and normalizations were the same for all fluorescence images. Scale bar = 1 cm

3.3.1 Results and Discussion

Each QD in the size series described in the previous section was diluted to ~2 μm concentration using PBS and injected intravenously into different rats. The abdominal region of each rat was surgically exposed and imaged using a custom intraoperative imaging system with excitation using high-powered blue LEDs and image capture using a CCD camera equipped with the proper color filters. For the smallest cysteine-coated 515 nm-emitting QDs (Cys-QD515), QD emission could be visualized directly within the bladder 2 h post-injection, and active transport of QDs from the kidneys into the bladder via both ureters could be seen (Figure 3-3A). For the rest of the size series, the bladder was imaged after 4 h and was observed to become progressively dim (i.e. have less renally cleared QDs) with increasing HD (Figure 3-3B). Clearly, there is a size dependent effect on the degree of renal clearance being observed.

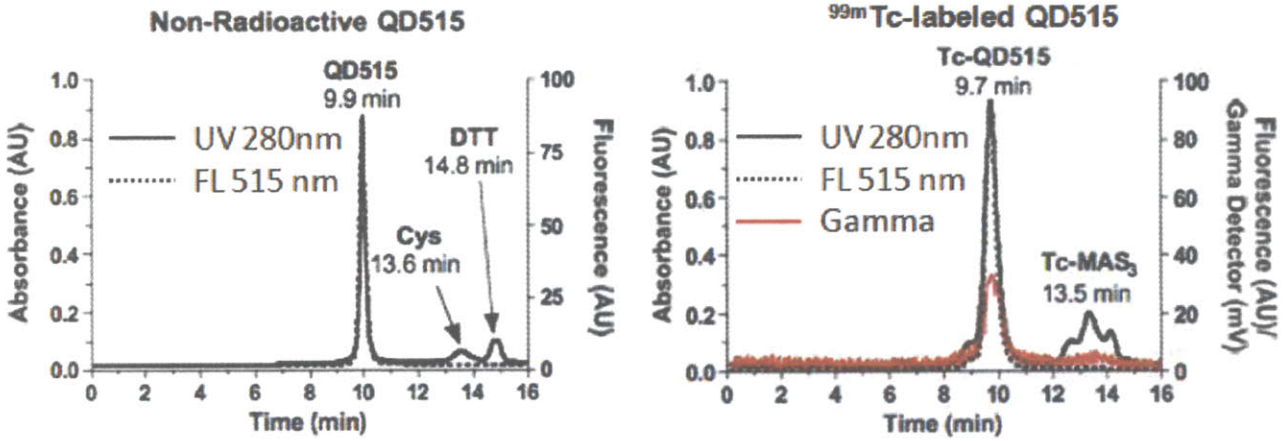

Figure 3-4 Confirmation of ^{99m}Tc conjugation to Cys-QDs by GFC with both fluorescence and gamma detection. Left: control sample. Right: conjugated sample.

In order to quantitatively measure QD biodistribution and assess the degree of renal clearance versus retention of QDs in the body and other organs, we labeled the QDs with a gamma ray-emitting isotope Technicium-99m (^{99m}Tc). This was achieved by covalently conjugating a MAS_3 molecule to the surface of QDs via the amino moiety of cysteine using carbodiimide coupling chemistry. The MAS_3 moeity was then used to chelate ^{99m}Tc, thereby

tethering the radioisotope to the QD surface. QDs after this conjugation chemistry were shown to be radioactive and also retained their original size as measured by size-exclusion HPLC with an in-line gamma-ray counter (Figure 3-4). In order to ensure that ^{99m}Tc atoms were securely tethered to the QD, the conjugates were incubated at room temperature for 4 h and purified via dialysis, showing that more than 90% of the radioisotope remained bound to the QDs after this purification step (data not shown).

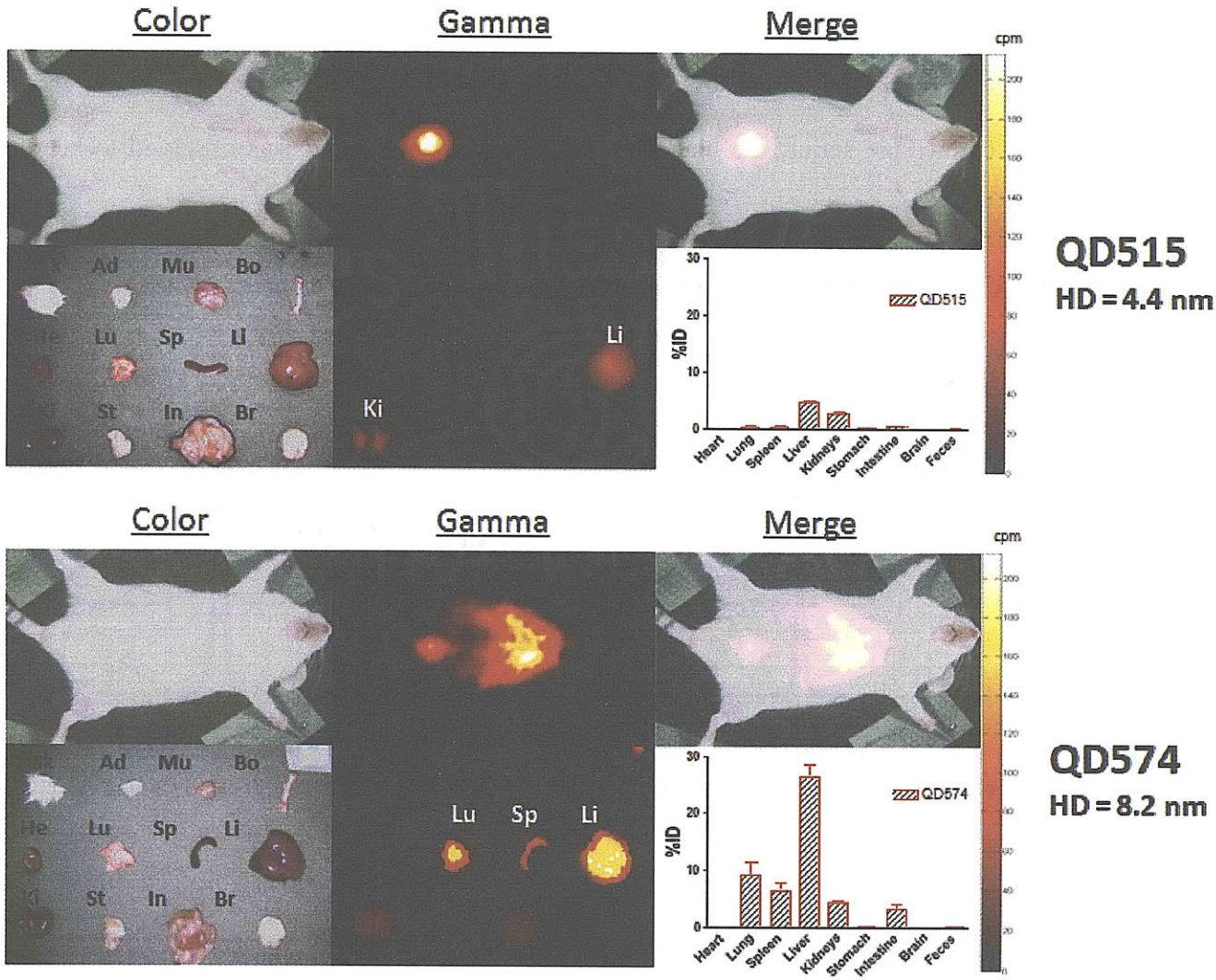

Figure 3-5 Quantitative biodistribution of ^{99m}Tc labeled QDs 4 h post-injection. Top: Cys-QD515 showing highest signal intensity in the bladder, and some accumulation of QDs in the liver (Li) and kidneys (Ki). Bottom: Cys-QD574 showing accumulation in the lungs (Lu), liver (Li), and spleen (Sp).

The radioactively labeled QD size series were injected into different rats intravenously. The blood-halflife was measured by periodically sampling the blood through the tail vein and measuring the radioactivity. The blood half-life can be described in this case by a multi-compartmental model, in which an injected drug distributes rapidly into organs that are vessel rich (α-phase half-life), followed by a slower systemic distribution into peripheral components along with clearance from the body (β-phase half-life).[19] In this case we are interested in whole-body clearance so the β-phase halflife is the relevant parameter. Mathematically, a two compartment model generates a log(concentration) vs time profile which exhibits a rapid fall for the α-phase, followed by a slower constant slope decay (β-phase). By analyzing the blood clearance with respect to this model for each QD in the size series, a large dependence of the β-phase on HD was observed, ranging from $t_{1/2\beta}$ = 48 m to $t_{1/2\beta}$ = 20 h as the HD increased from 4.4 nm to 8.6 nm (Figure 3-6).

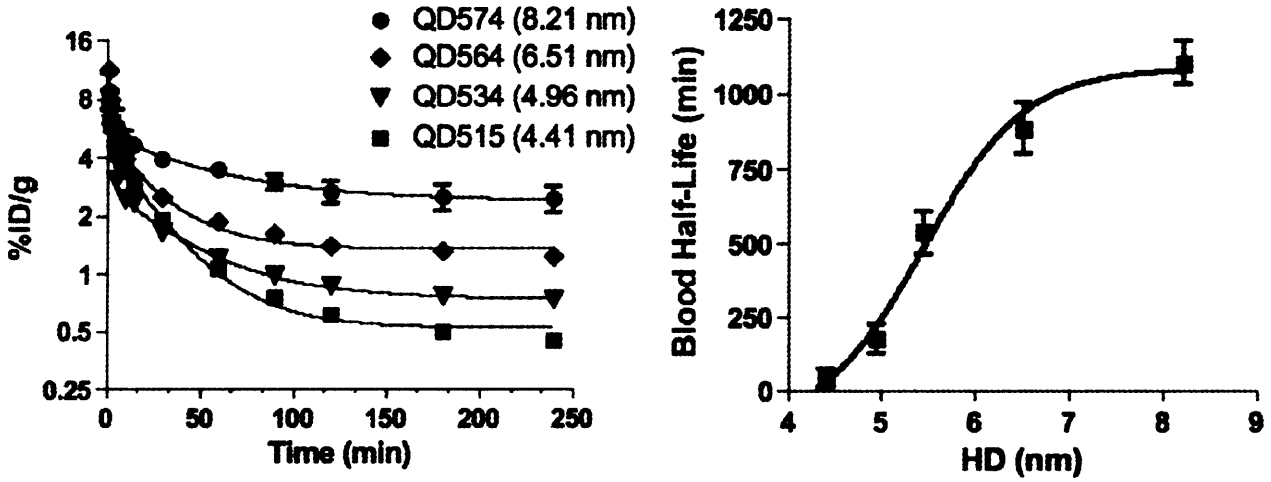

Figure 3-6 Blood clearance halflife of QD size series. Left: % injected dose per gram as a function of time for each QD in the size series. Right: blood halflife as a function of HD. Each data point is the mean ± s.d. from N = 5 animals.

In addition, a quantitative assessment of renally cleared QDs versus biodistribution of QDs in the body as a function of QD size can be performed using the radioisotope signal, which can be spatially resolved to pinpoint the QD location. After four hours post-injection, Cys-

QD515 (HD 4.4 nm) ended up mostly in the bladder, with a small percentage of the injected dose in the liver and kidneys. By contrast, Cys-QD574 (8.6 nm) exhibited appreciable uptake in the liver, lung, and spleen, and a much lower signal in the bladder (Figure 3-5).

In order to validate that the gamma radiation signal coming from the bladder is indeed to QD-bound ^{99m}Tc and not from free ^{99m}Tc that may have dissociated, we performed GFC on the urine sample and confirmed that the QD signal co-eluted with the gamma signal. Also, by comparing the radioactivity measured in the bladder against the signal measured in the individual organs, nearly all of the injected dose could be accounted for. Therefore, the percent renal clearance can be defined as the amount of injected dose found in the urine divided by the total injected dose.

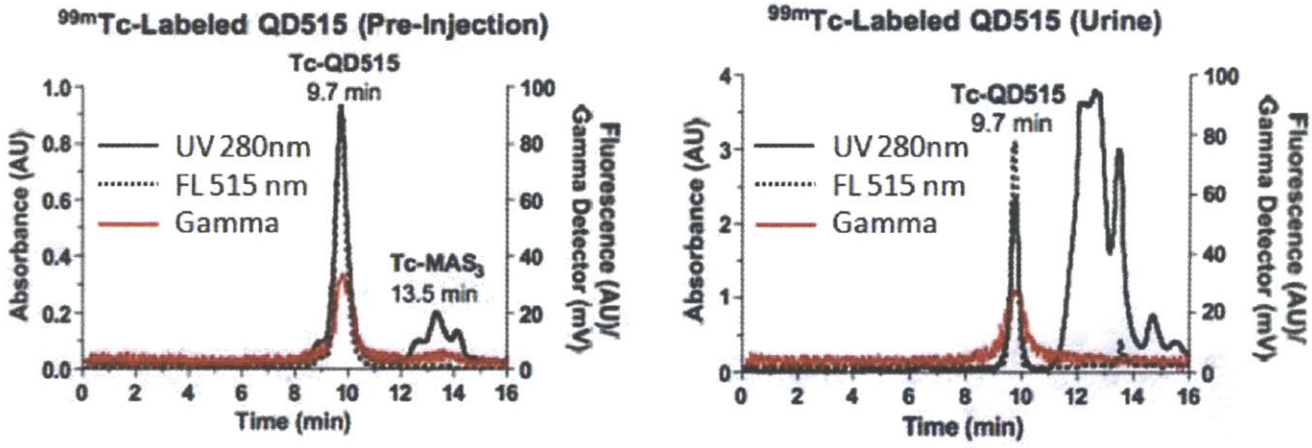

Figure 3-7 GFC of QDs before injection, and of the urine 4 h post-injection, with both fluorescence and gamma detection.

When we plot both the percent injected dose of the urine versus that found within the carcass, we build up a sigmoidal profile shown in Figure 3-8 as a function of HD. From this graph, we can observe that the threshold for renal clearance, in this case defined by the size at which 50% of the injected particles can be cleared from the body within 4 h is around 5.5 nm HD. This size assumes a spherical morphology and we do not know the effect of shape or aspect ratio on renal clearance. This is a topic for future studies.

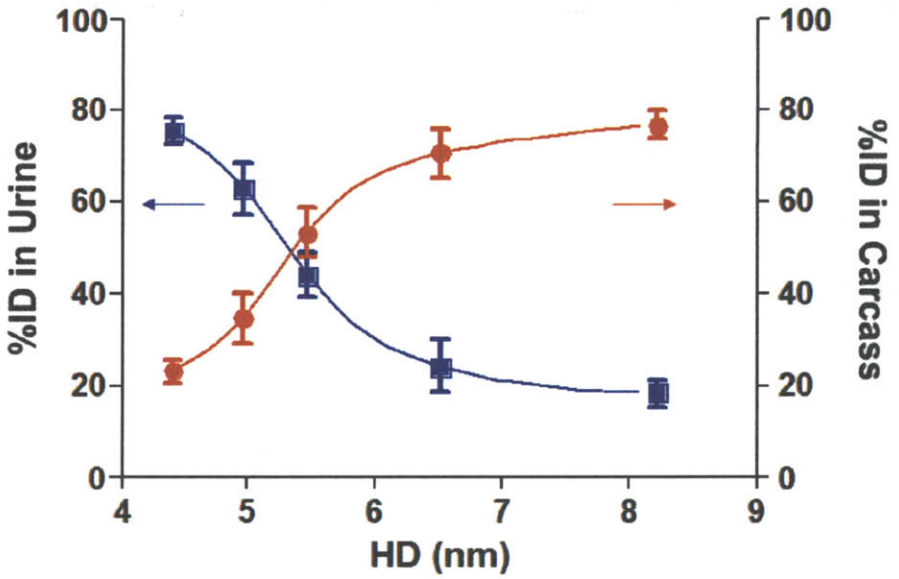

Figure 3-8 Urine excretion (red) and carcass retention (blue) of 99mTc labeled Cys-QDs as a function of HD 4 h post-injection into mice. Each point represents the mean ± s.d. of N = 5 animals.

There are currently two schools of thought on what constitutes an ideal in vivo probe. On one hand, some believe that the probe should be large as possible and heavily PEGylated in order to increase blood circulation half-life.[20, 21] This would be the case if the probe were to carry an expensive drug that should ideally be released gradually. In order to have high efficacy it's desirable to have the nanoparticle releasing the drug to stay in circulation for long as possible. On the other hand, there's the school of thought that the particle ought to be engineered to be as small as possible so that it can be cleared from the body quickly and efficiently. In the first case of drug delivery, long circulation time makes sense as long as the delivery vehicle is non-toxic (i.e. polymer nanoparticles). For the goal of eventually using QDs such as CdSe or InAs as an imaging probe, we want these nanomaterials cleared as quickly as possible due to their potential toxicity. However, the caveat is that the faster the particle clears, the less time it has to perform its function, such as targeting a tumor, for example. The next step is thus to demonstrate that a

small QD probe on the order of 5 nm can both effectively target, and then also effectively clear from the body.

Such a study was recently carried out by Choi et al., demonstrating that small Cys-QDs can indeed target a tumor and also renally clear.[22] The study focused on two small molecules GPI and cRGD, both of which target prostate-specific-membrane-antigen (PSMA). The Cys-QDs were conjugated to one of these small molecules for targeting, and also to a NIR dye for visualization. Both small molecules specifically target PSMA, which is overexpressed on the surface of prostate cancer cells, and upon intravenous delivery these QDs were seen to selectively accumulate at the (+)-PSMA expressing tumor, while minimal signal was observed in the (-)-PSMA expressing tumor. In addition, after 4 h post-injection, the QDs could be clearly seen in the bladder as a sign of successful renal clearance, along with successful tumor targeting. This work demonstrates that a construct which both targets and renally clears is possible and lays down some design rules in terms of particle valency, size, and surface coating, which paves the way for the design of future targetable and clearable nanoparticle imaging or disease treating agents.

3.3.2 Experimental Details

^{99m}Tc-Labeling of QDs. Preparation of high-specific-activity N-hydroxysuccinimide (NHS) ester of ^{99m}Tc-MAS_3, in neat aprotic solvent, has been described previously.[23] See Supplementary Information for detailed experimental methods. ^{99m}Tc-QD conjugation was performed by the addition of 80 μL of ^{99m}Tc-MAS_3-NHS (2 mCi) in DMSO to 1 mL of QDs (1 μM) in PBS, pH 7.8. After stirring for 1 hr, the radiolabeled conjugates were purified by washing five times in Vivaspin concentrators (MWCO 10,000) with pH 7.4 PBS and analyzed by RP-HPLC on a 8 x 300 mm, 200 Å Diol (YMC, Kyoto, Japan) size-exclusion column using PBS, pH

7.4 supplemented with 1 mM cysteine as mobile phase. Details of the RP-HPLC system have been described previously.[24]

QD Biodistribution and Clearance. 100 μL of 3 μM ^{99m}Tc-QDs (~250 μCi) were administered intravenously to N = 5 CD-1 mice per QD. Mice were housed in special cages to allow for the collection of urine and feces. Measurement of blood clearance was performed by intermittent sampling of the tail vein. Mice were sacrificed at 4 hr post-injection. To measure total urinary excretion, the ureters and urethra were ligated with silk sutures, and the bladder removed en masse and combined with excreted urine, prior to measurement of radioactivity in a dose calibrator. The remaining carcass was also measured in a dose calibrator, then the skin, adipose, muscle, bone, heart, lungs, spleen, liver, kidneys, stomach, intestine, brain, and feces were resected, washed twice in PBS, pH 7.4, weighed, and their radioactivity measured on a Wallac Wizard (model 1470, Perkin Elmer, Wellesley, MA) 10-detector gamma counter. Curve fitting was performed using Prism version 4.0a (GraphPad, San Diego, CA) software. Gamma radioscintigraphy was performed with a Research Digital Camera (Isocam Technologies, Castana, IA) equipped with a 1/2" NaI crystal, 86 photomultiplier tubes, and high-resolution (1 mm) low-energy lead collimator.

3.3.3 References

1. Green, P. J. The Kidneys: What ,Where, and How. http://coe.fgcu.edu/faculty/greenep/kidney/index.html (Jan 1, 2007)
2. Pappenheimer, J. R.; Renkin, E. M.; Borrero, L. M., Filtration, diffusion and molecular sieving through peripheral capillary membranes; a contribution to the pore theory of capillary permeability. *Am J Physiol* **1951,** 167, (1), 13-46.
3. Prescott, L. F.; McAuslane, J. A.; Freestone, S., The concentration-dependent disposition and kinetics of inulin. *Eur J Clin Pharmacol* **1991,** 40, (6), 619-24.

4. Olmsted, S. S.; Padgett, J. L.; Yudin, A. I.; Whaley, K. J.; Moench, T. R.; Cone, R. A., Diffusion of macromolecules and virus-like particles in human cervical mucus. *Biophys J* **2001,** 81, (4), 1930-7.

5. Hansen, N. E.; Karle, H.; Andersen, V., Lysozyme turnover in the rat. *J Clin Invest* **1971,** 50, (7), 1473-7.

6. Lund, U.; Rippe, A.; Venturoli, D.; Tenstad, O.; Grubb, A.; Rippe, B., Glomerular filtration rate dependence of sieving of albumin and some neutral proteins in rat kidneys. *Am J Physiol Renal Physiol* **2003,** 284, (6), F1226-34.

7. Goel, A.; Colcher, D.; Baranowska-Kortylewicz, J.; Augustine, S.; Booth, B. J.; Pavlinkova, G.; Batra, S. K., Genetically engineered tetravalent single-chain Fv of the pancarcinoma monoclonal antibody CC49: improved biodistribution and potential for therapeutic application. *Cancer Res* **2000,** 60, (24), 6964-71.

8. Solomon, A.; Waldmann, T. A.; Fahey, J. L.; McFarlane, A. S., Metabolism of Bence Jones Proteins. *J Clin Invest* **1964,** 43, 103-17.

9. Bradwell, A. R.; Carr-Smith, H. D.; Mead, G. P.; Harvey, T. C.; Drayson, M. T., Serum test for assessment of patients with Bence Jones myeloma. *Lancet* **2003,** 361, (9356), 489-91.

10. Chapman, A. P.; Antoniw, P.; Spitali, M.; West, S.; Stephens, S.; King, D. J., Therapeutic antibody fragments with prolonged in vivo half-lives. *Nat Biotechnol* **1999,** 17, (8), 780-3.

11. Peng, Z. A.; Peng, X., Formation of High-Quality CdTe, CdSe, and CdS Nanocrystals Using CdO as Precursor. *J. Am. Chem. Soc.* **2001,** 123, (1), 183-184.

12. Stott, N. E. Novel synthetic routes to high-quality II-VI colloidal nanocrystals: controlled growth using mild precursors in the presence of selected ligands. Ph.D. Thesis, Massachusetts Institute of Technology, 2004.

13. Peng, Z. A.; Peng, X., Formation of high-quality CdTe, CdSe, and CdS nanocrystals using CdO as precursor. *J Am Chem Soc* **2001,** 123, (1), 183-4.

14. Dabbousi, B. O.; Rodriguez-Viejo, J.; Mikulec, F. V.; Heine, J. R.; Mattoussi, H.; Ober, R.; Jensen, K. F.; Bawendi, M. G., (CdSe)ZnS core-shell quantum dots: synthesis and characterization of a size series of highly luminescent nanocrystallites *J Phys Chem B* **1997,** 101, (46), 9463-9475.

15. Fisher, B. R., Eisler, H.-J., Stott, N.E. & Bawendi, M.G., Emission intensity dependence and single-exponential behavior in single colloidal quantum dot fluorescence lifetimes *J Phys Chem B* **2004,** 108, (1), 143-148.

16. Uyeda, H. T.; Medintz, I. L.; Jaiswal, J. K.; Simon, S. M.; Mattoussi, H., Synthesis of compact multidentate ligands to prepare stable hydrophilic quantum dot fluorophores. *J Am Chem Soc* **2005,** 127, (11), 3870-8.

17. Mattoussi, H.; Mauro, J. M.; Goldman, E. R.; Anderson, G. P.; Sundar, V. C.; Mikulec, F. V.; Bawendi, M. G., Self-assembly of CdSe-ZnS quantum dot bioconjugates using an engineered recombinant protein. *J Am Chem Soc* **2000,** 122, (49), 12142-50.

18. Frangioni, J. V.; Kim, S. W.; Ohnishi, S.; Kim, S.; Bawendi, M. G., Sentinel Lymph Node Mapping With Type-II Quantum Dots. *Methods Mol Biol* **2007,** 374, 147-60.

19. Rowland, M.; Benet, L. Z.; Graham, G. G., Clearance concepts in pharmacokinetics. *Journal of Pharmacokinetics and Pharmacodynamics* **1973,** 1, (2), 123-136.

20. Gao, X.; Cui, Y.; Levenson, R. M.; Chung, L. W. K.; Nie, S., In vivo cancer targeting and imaging with semiconductor quantum dots. *Nat Biotechnol* **2004,** 22, (8), 969-976.

21. Ballou, B.; Lagerholm, B. C.; Ernst, L. A.; Bruchez, M. P.; Waggoner, A. S., Noninvasive Imaging of Quantum Dots in Mice. *Bioconjug. Chem.* **2004,** 15, (1), 79-86.

22. Choi, H. S.; Liu, W.; Liu, F.; Nasr, K.; Misra, P.; Bawendi, M. G.; Frangioni, J. V., Design considerations for tumour-targeted nanoparticles. *Nat Nano* **2010,** 5, (1), 42-47.

23. Misra, P.; Humblet, V.; Pannier, N.; Maison, W.; Frangioni, J. V., Production of multimeric prostate-specific membrane antigen small molecule radiotracers using a solid-phase 99mTc pre-loading strategy. *J Nuc Med* **2007,** In Press.

24. Humblet, V.; Misra, P.; Frangioni, J. V., An HPLC/mass spectrometry platform for the development of multimodality contrast agents and targeted therapeutics: prostate-specific membrane antigen small molecule derivatives. *Contrast Media Mol Imaging* **2006,** 1, (5), 196-211.

Chapter 4: QDs Optimized for Live-Cell Imaging via Synthesis of Hetero-bifunctional Multi-dentate Coordinating Ligands*

4.1 *Background and Motivation*

In this chapter, we turn our attention to the optimization of QDs for in-vitro labeling applications. As described in Chapter 1.4, an ideal QD probe for cellular labeling and single particle tracking should be: (1) easily derivatizable such that various secondary reporters or biomolecules can be appended to the QD to allow for sensing capabilities and/or targeting to cellular receptors of interest; at the same time, the QD must achieve this while maintaining the properties of (2) low non-specific binding to cells, (3) small hydrodynamic size, (4) high quantum yield, and (5) good pH stability. Prior to 2007, there was no single ligand system available which could satisfy all five criteria simultaneously, to our knowledge. Commercial QDs based on amphiliphic polymer coatings are stable and derivatizable, but the encapsulation method of water solubilization makes the QDs inherently large.[1-5] Small molecule thiols used for ligand exchange have produced smaller QDs, but they suffer from poor stability and limited derivatizability.[6-10] In each ligand system there existed a set of tradeoffs and compromises. In this Chapter, we seek to address this challenge by designing a QD-ligand system that can satisfy all 5 criteria simultaneously and demonstrate the use of this new system for robust single particle imaging of QDs on live cells.

---

* Much of this chapter has appeared in print. It is reproduced with permission from *J Am Chem Soc* 2008, **130**: 1274 -1284. The cellular imaging data in this chapter were the result of a collaboration with the research group of Alice Y. Ting in the department of Biological Chemistry.

We now demonstrate an efficient route to compact, derivatizable aqueous CdSe(ZnCdS) core(shell) QDs, enabled by a new suite of DHLA-PEG-derived ligands terminating in amine or carboxylic acid functional groups. These ligands feature a dithiol moiety for tight binding to the QD surface, a short poly(ethylene glycol) spacer for water solubility and biocompatibility, and either and amine or carboxyl terminus for derivatization. The quantum yield (QY) of these DHLA-PEG derivatized QDs was enhanced to ~40% via an alloyed $Zn_xCd_{1-x}S$ shell.[11] The QDs display good pH stability, a tunable zeta potential, very low non-specific binding to cells, and an HD between 9 and 12 nm, which is substantially smaller than polymer encapsulated QDs. We demonstrate derivatization of these QDs via both covalent bond formation (to small molecule and protein partners) and His_6-protein coupling for targeted cell labeling. The versatility of this QD system is highlighted by imaging the interaction of epidermal growth factor (EGF) with EGF receptors on live cells, and by simultaneously derivatizing QDs with streptavidin for targeting and an organic fluorophore for potential sensing applications by FRET. The versatile QD scaffold reported here facilitates a highly modular approach for tuning the composition of functional surface molecules on QDs for cellular targeting and sensing applications.

4.1 *Results and Discussion*

4.1.1 Ligand Synthesis and Design

Compounds 3 (aminoPEG) and 6 (carboxyPEG) presented in Scheme 1 were designed with the following considerations in mind: (1) a DHLA moiety provides strong coordination to the QD surface, (2) a PEG spacer conveys water solubility and reduces non-specific binding, and (3) a carboxy or amine functionality enables further covalent derivatization.

The diamine functionalized polyethylene glycol (**1**) was synthesized from commercially available PEG (avg MW 400, $n \approx 8$) via a simple three step reaction in high yield with minimal purification steps required. The overall yield was 89% on a 30 g scale. Synthon **2**, which served as the precursor to both **3** and **6,** was delivered from the reaction of **1** with the N-hydroxysuccinimidyl ester of lipoic acid (LA-NHS). **3** was furnished smoothly from ring opening lipoic acid (LA) to the dihydrolipoate form by reduction with sodium borohydride.[12] Alternatively, **2** could be modified by its reaction with methylmalonylchloride, followed by methylester deprotection to form an amide linkage to a malonic acid group (compound **5**). Reduction with sodium borohydride yielded compound **6**.

Scheme 1

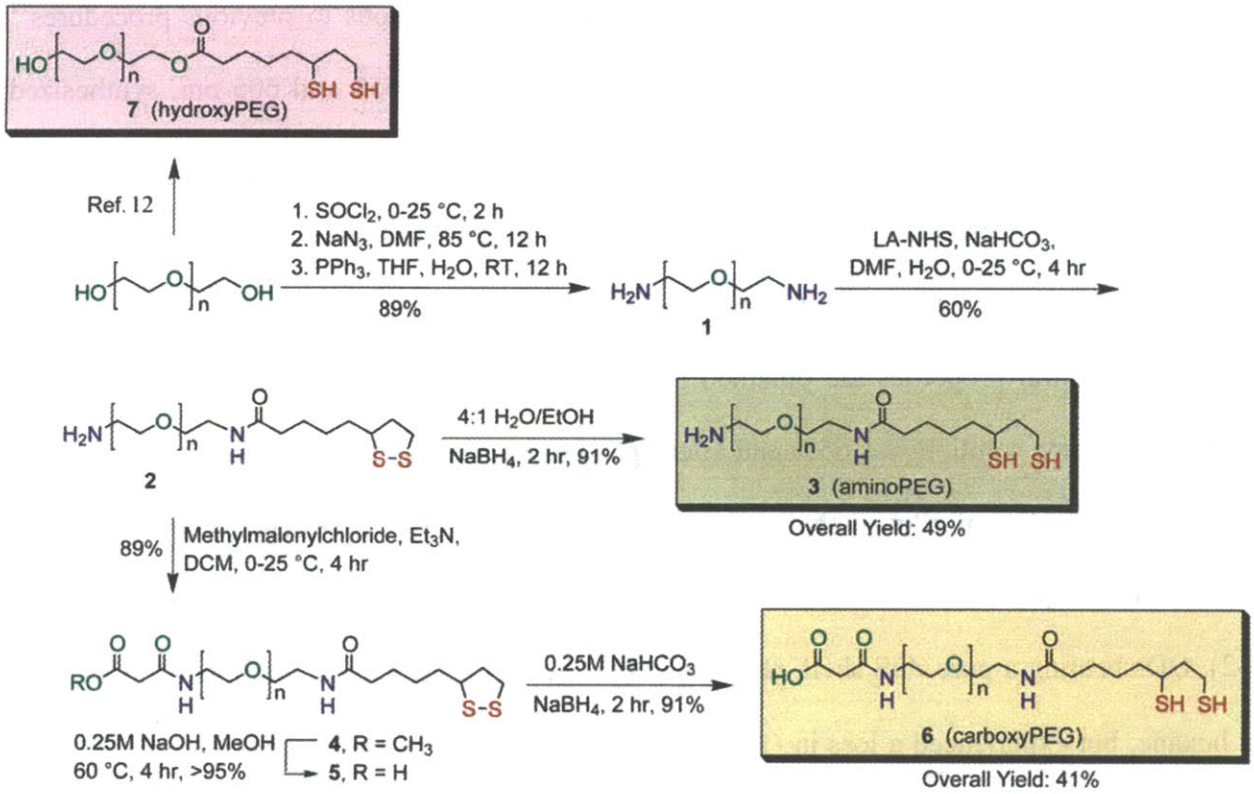

The synthetic strategy of Scheme 1 incorporates several advantages. Precursor **1** is obtained in large quantities without the need for extensive purification. Heterobifunctional ligands were obtained in a straightforward fashion from compound **1**, with a DHLA moiety for robust coordination to the QD surface, a PEG spacer for water solubility, and a head group consisting of a primary amine (compound **2**) or in principle any of a wide variety of derivative forms including carboxylic acid-terminated **6**. Moreover, these ligands feature amide bonds, which are more robust towards hydrolysis than ester bonds.

4.1.2 Ligand Exchange and Characterization of Hydrophilic QDs.

Water-soluble QDs were obtained for displacing the native hydrophobic ligands of CdSe/$Zn_xCd_{1-x}S$ core/shell QDs with aminoPEG, carboxyPEG, hydroxyPEG (compound **7**), or mixtures thereof. Ligand exchange was carried out by modifications to previous procedures[12] using QD samples with selected emission wavelengths between 558 and 605 nm, synthesized according to modified literature procedures.[13, 14]

Figure 4-1A presents the absorption and emission spectra of a representative QD sample with emission centered at 605 nm (QD605) before and after ligand exchange with carboxyPEG **6**. Similar spectral properties are obtained for QDs exchanged with aminoPEG **3**. The QY of QD605 in hexane solution was 65% and after ligand exchange was typically 30 - 40%. We note that the aqueous QY of alloyed shell QDs (CdSe/$Zn_xCd_{1-x}S$, $x = 0.7$) was enhanced by as much as two-fold compared to that of QDs overcoated with a pure ZnS shell ($x = 1$) (Figure 4-1, Figure 4-2). QDs bearing a pure ZnS shell, rather than the alloy $Zn_xCd_{1-x}S$ shell, exhibited similar QYs in hexane, but experienced a loss in QY of up to 75% after ligand exchange with aminoPEG or carboxyPEG. The retention of the high QY values after water solubilization using the alloyed shell was attributed to reduced lattice mismatch between the core and shell, which provides

better passivation of interfacial trap states.[15-17] The samples used in the experiments reported here were overcoated with approximately five monolayers of an $x \approx 0.7$ alloy. The shell was applied with a uniform mole ratio of Cd to Zn precursors throughout the overcoating process, thus we expect Zn and Cd to be present throughout the shell and also on the surface. The formation of the alloy shell in each case was accompanied by a red-shift of the absorbance maximum by approximately 30 nm from that of the CdSe cores.

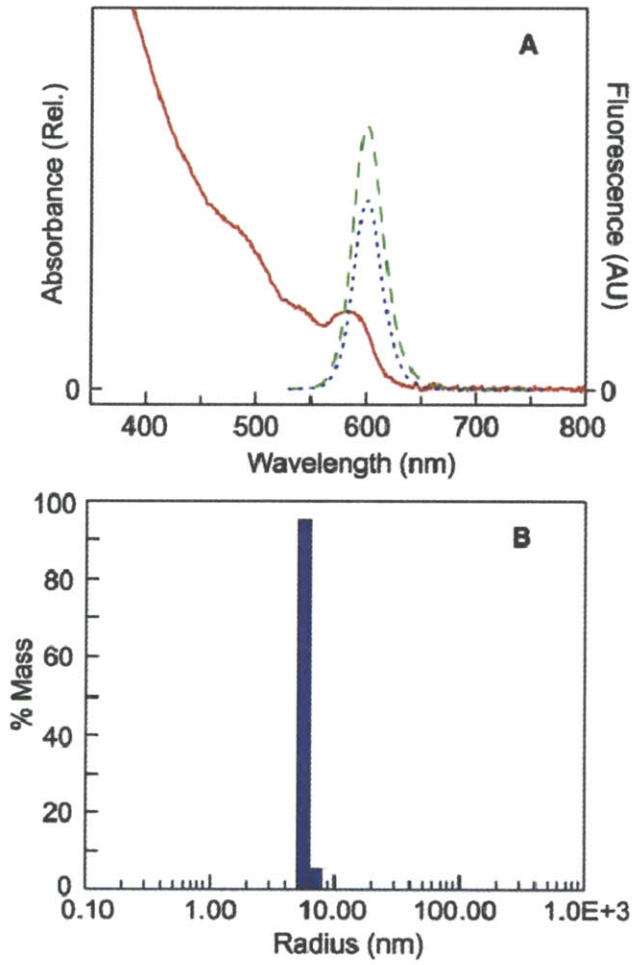

Figure 4-1 Optical and size characterization of QDs in hexanes and after ligand exchange. (A) Absorbance spectrum of CdSe(ZnxCd1-xS) core(shell), QD605, in hexane with x = 0.7 (—, red). Fluorescence spectra with absorption normalized at the excitation (λexc = 520 nm) of QD605 in hexane after one cycle of precipitation (- - -, green, QY = 65%), and in PBS buffer after ligand exchange with aminoPEG (····, blue, QY = 43%), showing a small decrease in QY. (B) Representative dynamic light scattering histogram of QD605 ligand exchanged with aminoPEG in PBS, giving HD = 11.4 nm.

The HD of QDs ligand-exchanged with carboxyPEG (abbreviated carboxyQDs) was measured by dynamic light scattering and found to be ~9.9 nm and ~11.4 nm for QD565 and QD605 (Figure 4-1B), respectively. Similar HDs were found for aminoPEG-functionalized QDs (abbreviated aminoQDs). The HD of these QDs coated with either aminoPEG or carboxyPEG is approximately a factor of two smaller than QDs coated with amphiphilic polymeric shells (e.g. commercial QDs), which have HDs on the order of 14-60 nm.[18] The reduced size of these QDs relative to commonly used commercial QDs makes them attractive for cell labeling applications, as the smaller size reduces the possibility of the probe interfering with receptor function, and potentially increases access of these QDs to more hindered regions, such as the synapse. In addition, the monomodal size distribution shown by the dynamic light scattering histogram indicates that these QDs form well dispersed aggregate-free solutions, which is important for cell labeling and single particle tracking applications.

Faithful imaging and single particle tracking also depends on the ability of QDs to remain well dispersed in solution when exposed to pH fluctuations from pH 7.4 in the cell medium down to pH 5 within lysosomes. DHLA-capped QDs aggregate below pH 6, since their water solubility depends largely on the negative charge of the ionized carboxylic acid group.[12] However, both carboxyQDs and aminoQDs were found to be stable in aqueous solutions between pH 5.0 and pH 9.5 with no significant change in brightness for at least three days (Figure 4-3). We surmise that the PEG linker of aminoQDs and carboxyQDs further enhances water solubility and hence one would expect greater pH stability, similar to what was previously reported for hydroxyQDs.[12]

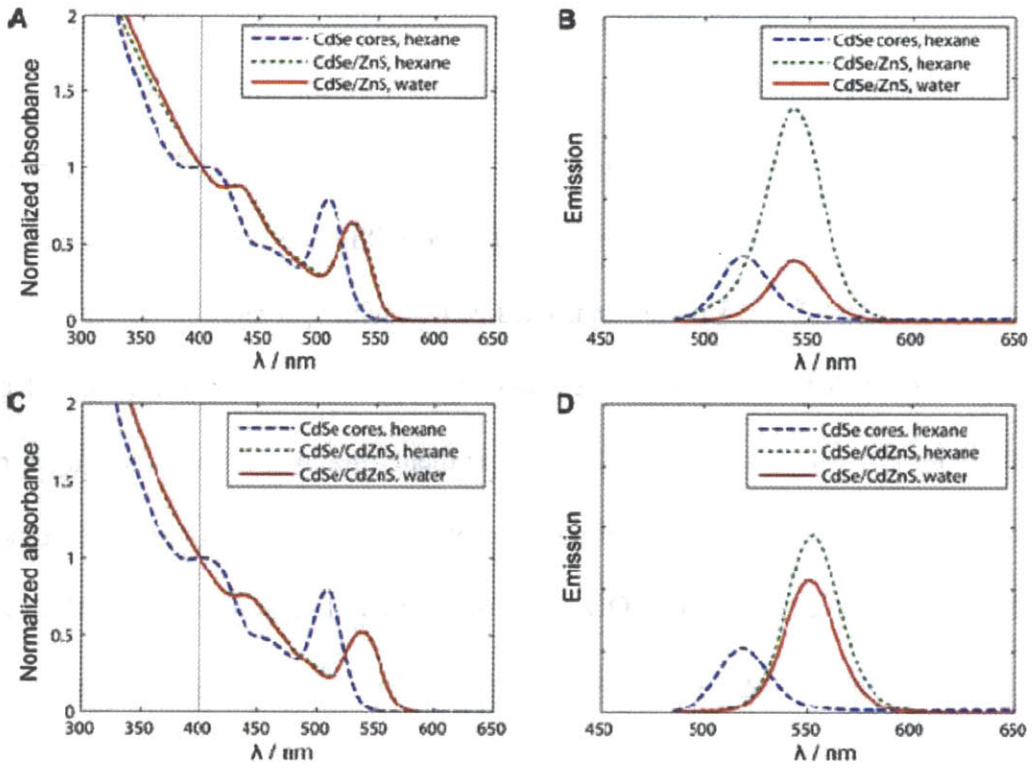

Figure 4-2 Absorption and emission spectra in hexane and in aqueous solution are shown for a representative batch of CdSe QD cores that was split and separately overcoated with either a pure ZnS shell or an alloyed ZnxCd1-xS shell. (A) Absorption before (- - -) and after (—) growth of a pure ZnS shell (estimated thickness 3 monolayers), and after ligand exchange to make 20% aminoQDs (···). Spectra are normalized at 400 nm. (B) Emission spectra of QD samples in (A) under 400 nm excitation. Spectra are normalized according to their absorbance at 400 nm such that their intensities may be compared directly. (C) Absorption spectra, normalized as in (A), before and after growth of a ZnxCd1-xS shell (x = 0.8) and using the same total equivalents of metal precursors as in (A), and after ligand exchange. (D) Emission spectra of QD samples in (C) under 400 nm excitation, normalized as in (B).

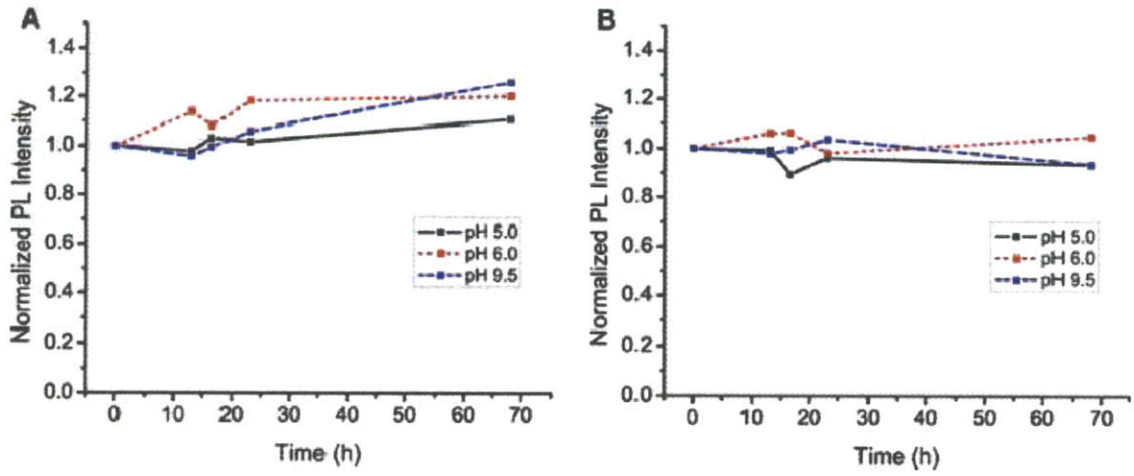

Figure 4-3 pH stability of DHLA-PEG based QDs over time. (A) carboxyQDs and (B) 20% aminoQDs (with 80% hydroxyPEG by mole ratio) at pH 5.0 (—), 6.0 (···), and 9.5 (- - -).

4.1.3 Tuning Surface Charge and Functional Valency of QDs

One of the next major challenges in designing QDs suitable for cell labeling and single particle tracking is non-specific cell binding, which has been partly attributed to electrostatic attraction of the cell surface with charged QD ligand coatings.[19] Therefore, the QD surface charge is a parameter that must be controlled. QDs ligand-exchanged with aminoPEG or carboxyPEG will have surfaces that are positively and negatively charged, respectively, in neutral buffer. Properties of QDs have been tuned using ligand mixtures.[12, 20] Following this lead, we employed a mixture of aminoPEG or carboxyPEG with non-charged hydroxyPEG (compound **7**)[12] in varying mole fractions to control the surface charge of aqueous QDs. For convenience, nomenclature of the mixed ligand system refers to only aminoPEG or carboxyPEG mole fraction with the balance accounted for by hydroxyPEG. For instance, 20% aminoQDs refer to QDs ligand exchanged with 20% aminoPEG and 80% hydroxyPEG by mole fraction.

The surface charge of the resulting QD samples was analyzed by zeta-potential measurements and agarose gel electrophoresis. Figure 4-4A shows that aminoQDs capped with pure (100%) aminoPEG have a zeta-potential of +36.2 mV, which decreases in an approximately linear fashion with decreasing $-NH_2$ composition in the ligand blend. A similar trend in the zeta-potential was observed with decreasing $-CO_2H$ composition in the ligand blend for carboxyQDs. The results from zeta-potential measurements were also mirrored in measurements of the electrophoretic gel mobility (Figure 4-4B). QDs coated with 100% DHLA were also included for comparison, revealing that DHLA-capped QDs have a higher electrophoretic mobility than carboxyQDs, which could result either from the higher ligand packing density or the smaller HD of the DHLA-capped QDs.

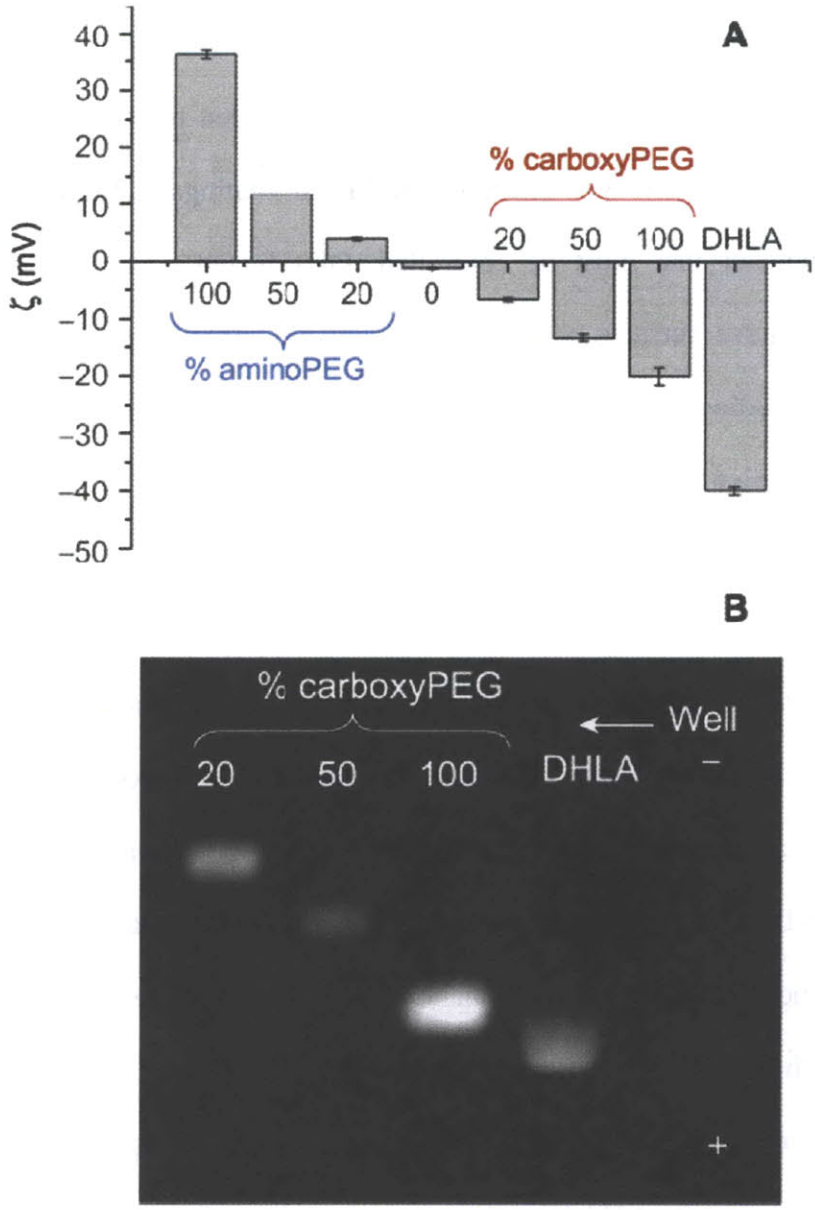

Figure 4-4 Tuning surface charge via ligand exchange using mixed ligands. (A) Zeta-potential measurement of QDs ligand exchanged with various % by mole fraction of aminoPEG or carboxyPEG mixed with hydroxyPEG. DHLA coated QDs shown for comparison. (B) Gel shift of QDs as in (A) with 1% agarose in Tris-acetate-EDTA buffer (pH 8.3).

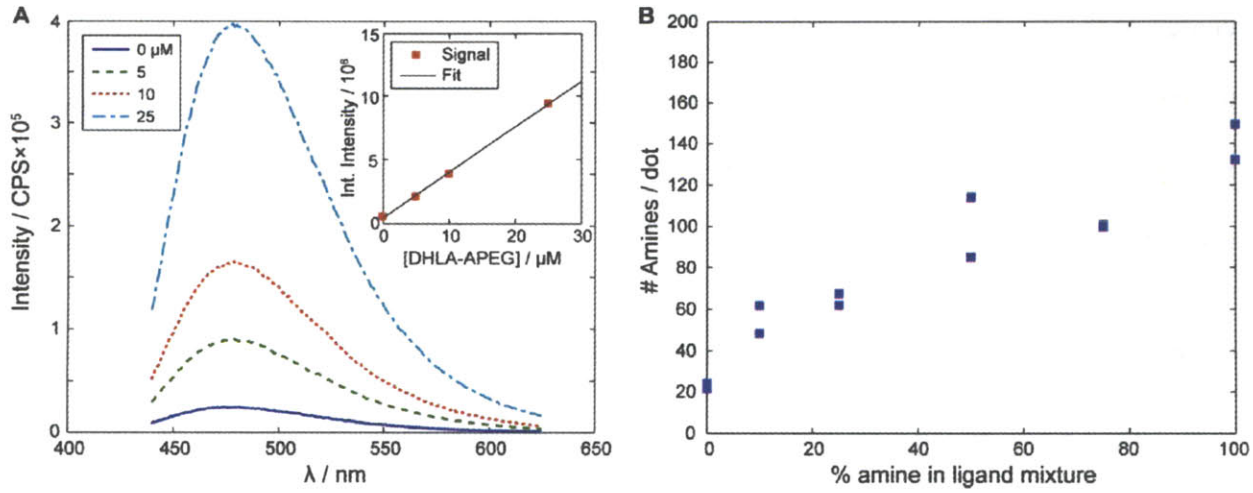

Figure 4-5 Measuring the number of aminoPEG per QD (558 nm emission). (A) Calibration: emission spectra of aminoPEG free ligand solutions in DMF after treatment with fluorescamine (380 nm excitation). Inset: integrated fluorescence intensity of these samples from 460-485 nm, along with a linear fit. (B) Ratio of detected amine concentration to QD concentration versus wt% of amine-terminated ligand in aminoPEG/hydroxyPEG ligand exchange mixtures. Samples were run in duplicate to improve accuracy (in some cases values overlap).

We probed the number of reactive amine functional groups per QD in order to characterize our ability to adjust the QD valency via mixtures of DHLA-PEG derived ligands. Mixed-ligand aminoQDs with 565 nm emission were exposed to fluorescamine, which reacts rapidly with primary amines to form a fluorescent product that can be monitored at 487 nm. The QDs were purified by repeated ultrafiltration to remove free ligand and reacted with excess fluorescamine. By calibrating the fluorescence intensity signal of the fluorescamine after reaction with samples of aminoPEG at known concentration (Figure 4-5A), an estimate of ~140 amines/QD was obtained for 100% aminoQDs, consistent with a previously reported value from a related system.[21] Furthermore, an approximately linear correlation was obtained for the amount of amine detected per QD with the percentage of amine-terminated ligands used in the ligand-exchange blend (Figure 4-5B).

These results suggest that the use of a mixed ligand blend of charged and neutral DHLA-PEG based ligands offers a simple and robust way to tune the final surface composition and

charge of the resulting water-solubilized QDs. The QDs obtained from this method can be tuned to present surface amino or carboxyl groups in high enough numbers for efficient derivatization reactions, while maintaining a minimally charged particle surface to mitigate nonspecific binding for cell labeling applications (*vide infra*).

4.1.4 Mitigation of Non-Specific Cell Binding

In order to directly evaluate the suitability of the charged aminoQDs and carboxyQDs for biological imaging, we investigated the non-specific binding to a human cell-line as a function of ligand composition on the QD surface. Figure 4-6 displays the results. The control sample (Figure 4-6A) shows emission from cell autofluorescence. QDs coated with negatively charged DHLA show significant non-specific binding to both cells and glass (Figure 4-6B) as indicated by the increased fluorescence intensity as compared to the control. Neutral QDs capped with hydroxyPEG (abbreviated hydroxyQDs) show minimal non-specific binding, as expected (Figure 4-6C). Surprisingly, carboxyQDs also showed minimal non-specific cell binding, comparable to hydroxyQDs (Figure 4-6D). The lack of non-specific binding for carboxyQDs, despite the negative charge, highlights the important role of the PEG spacer in reducing non-specific interactions. On the other hand, aminoQDs exhibited severe non-specific binding to cells, which at the same contrast level caused saturation of the imaging field (Figure 4-6E). We ascribe the high level of binding to electrostatic interactions of the highly positively charged QD with the cell surface. The problem is circumvented by coating the QDs with a mixture of 20% aminoPEG and 80% hydroxyPEG (20% aminoQDs), which do not show significantly more non-specific binding than hydroxyQDs (Figure 4-6F).

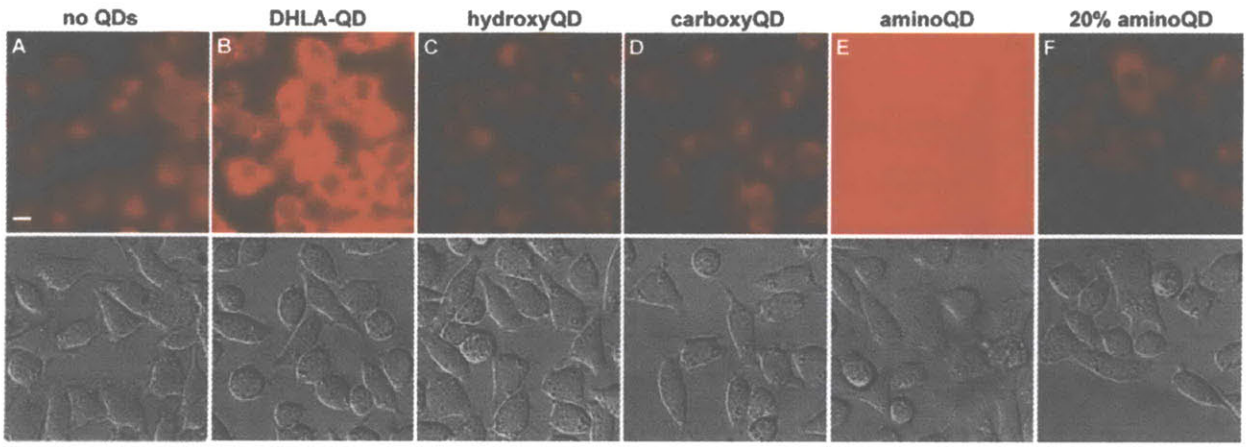

Figure 4-6 Non-specific binding of QD605 to HeLa cells as a function of ligand coating. Top row: fluorescence image with 420 nm excitation, 605 nm emission. Bottom row: differential interference contrast (DIC) image. Cells were incubated with QDs for 10 min at 4 °C, and washed with buffer 4× before imaging. (A) Control sample, showing cell autofluorescence; QDs ligand-exchanged with (B) DHLA, (C) hydroxyPEG, (D) carboxyPEG, (E) aminoPEG, (F) 20% aminoPEG (with 80% hydroxyPEG). Scale bar, 10 μm.

The results of Figure 4-6 indicate that both carboxyQDs and 20% aminoQDs exhibit minimal non-specific binding to cells, making them suitable for cell labeling and single particle imaging applications. We chose the 20% aminoPEG composition in order to provide a reasonable amount of amino groups for covalent derivatization, while sufficiently reducing the surface charge in order to mitigate non-specific interactions with cells. This composition does not necessarily represent an optimized design for non-specific binding, but highlights the advantages of being able to tune the surface composition for a specific application.

4.1.5 Covalent Conjugation to a FRET Acceptor Dye

The suitability of 20% aminoQDs for routine derivatization was evaluated by exposing them to the amine-reactive NHS ester of carboxy-X-rhodamine (ROX), a red-emitting organic

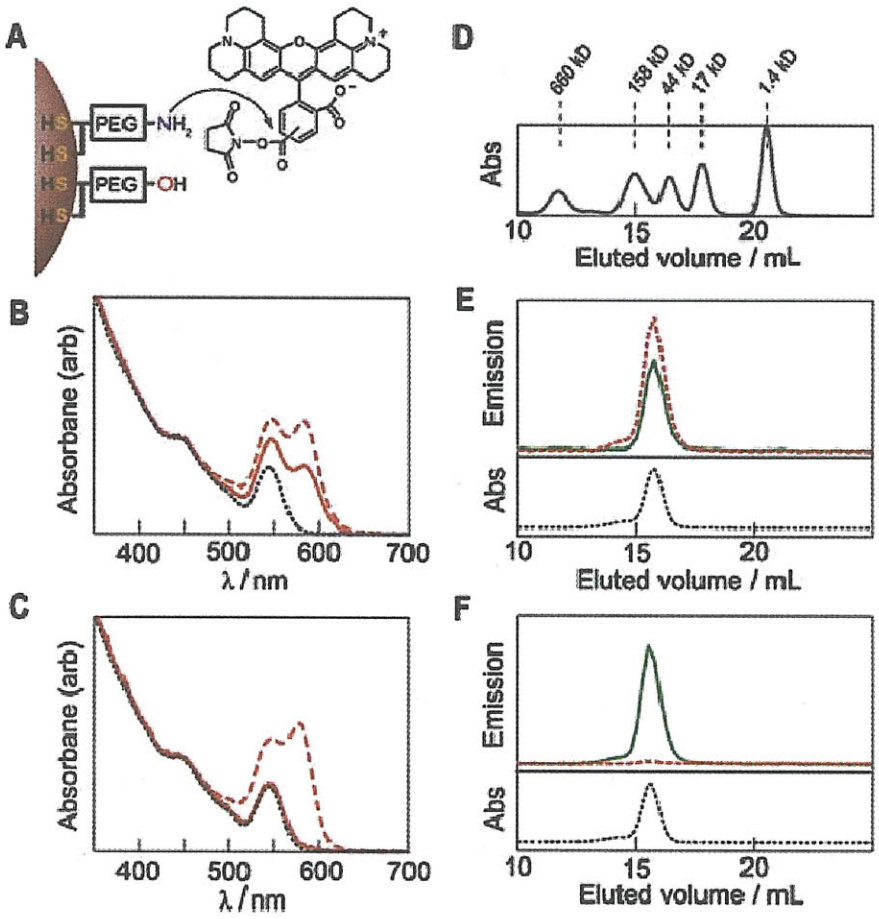

Figure 4-7 Covalent conjugation of dye to amine-functionalized QDs. (A) Derivatization of 20% aminoQDs with the fluorescent dye ROX. (B) Absorption spectra of unconjugated QDs (····, black), QD + dye mixture (----, red) and QD + dye purified (—, red), all normalized at 400 nm. (C) Absorption spectra as in B for control experiment using the unreactive free-acid form of ROX dye: QDs (····, black), QD + dye mixture (----, red) and QD + dye purified (—, red). (D) GFC molecular weight standards. (E) GFC absorbance and fluorescence signals for the QD + dye purified conjugate depicted in (B): QD channel (—, green), ROX channel (----, red) and absorbance at 280 nm (····, black). QD and ROX fluorescence channels are monitored at 558 nm and 610 nm, respectively. (F) GFC absorbance and fluorescence signals for a control sample using a mixture of QD and the free-acid form of ROX dye. Legend is same as in (E).

fluorescent dye (Figure 4-7A). Coupling to a dye offers the advantage of easily monitoring the coupling yield by following the prominent dye absorption feature. Additionally, QD-dye energy transfer systems have recently opened up new possibilities as the basis for optically-reporting chemo/biosensors,[22-25] and the QD-ROX here serves as a model system for a dual-emission

ratiometric FRET sensor platform recently developed and demonstrated for the case of pH sensing.[25, 26]

QDs emitting at 558 nm (QD558) were selected to afford good spectral overlap with the ROX absorbance peak in order to form a donor/acceptor FRET couple. The ROX emission at 610 nm can then be easily monitored independent of the QD emission. Following reaction with the ROX succinimidyl ester, the QDs were separated from unbound dye and NHS byproduct via ultrafiltration. Figure 4-7B shows the absorption spectra of the initial QDs, the reaction mixture, and the purified product, with the dye absorption peak clearly visible. A fit of the spectrum as a sum of QD and dye contributions revealed a dye:QD molar ratio of 5.0 as-mixed, and 2.9 upon purification, indicating a coupling yield of 58%. In a control experiment (Figure 4-7C), a QD sample from the same batch was mixed with the free-acid form of ROX under identical reaction conditions. Upon purification, <3% of the dye remained, indicating minimal non-specific adsorption of the dye onto the QD surface.

The FRET efficiency of the QD-dye couple was estimated to be ~90% by measuring the quenching of QD fluorescence after dye conjugation (Figure 4-8). The Förster distance was calculated to be R_0 = 5.6 nm from the spectral overlap. From the measured FRET efficiency, the measured amount of dye per QD (m) and the calculated R_0, the QD-dye separation distance was calculated to be r = 4.8 nm,[27] which is in good agreement with the hydrodynamic diameter of these QDs (9.9 nm).

The purified QD-ROX conjugate was additionally characterized by gel filtration chromatography (GFC) using a size-exclusion column. Comparison with protein molecular weight (MW) standards (Figure 4-7D) provides an estimate of size for samples under investigation. Figure 4-7E shows the GFC results for the purified QD-ROX conjugate shown in

Figure 4-7B. QD-ROX elutes at 15.7 mL volume, corresponding to a protein-equivalent MW of ~94 kD. The emission spectrum at this volume shows a peak in both QD and ROX channels.

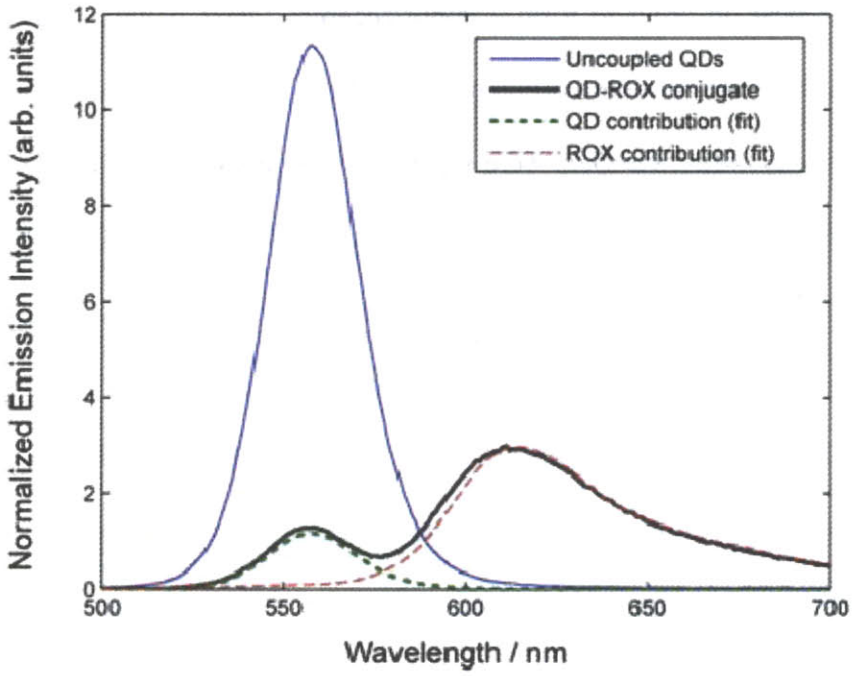

Figure 4-8 Emission spectra of purified QD-ROX conjugate described in the text and of a matching sample prepared with no dye. The spectra have been normalized according to the QD concentration in each sample so that the emission intensities may be directly compared. Fitting the emission spectrum of the conjugate as a linear combination of QD and dye components reveals a quench of the QD emission intensity by approximately 90% versus that in the absence of the ROX dye.

Fluorescence detection at 558 nm (QD emission) and 610 nm (ROX emission) reveals ROX emission at an elution volume corresponding to the QDs, confirming that the QD and dye are indeed bound.

In contrast, GFC of a mixture of free QDs and ROX dye at the same dye:QD ratio as the coupled sample shows UV absorbance and QD emission signals at the same elution volume as the couple, but no dye fluorescence (Figure 4-7F). Indeed, the dye is not detected at all because of its low absorption cross section at the absorbance and excitation wavelengths used by the instrument. The ROX emission is detected in the coupled case because dye molecules bound to

the QD are excited by FRET. Uncoupled QDs run under the same conditions also elute at 15.7 mL in this experiment, suggesting that attachment of a dye does not significantly alter the QD size. Together, the GFC data indicate that small-molecule dyes in NHS ester form can be covalently appended to the mixed ligand QDs without perturbing the QD size, and that control experiments with non-activated dye show no indication of coupling/binding.

4.1.6 Covalent Conjugation to Streptavidin for High Affinity Cell Labeling The scope of covalent derivatization using amine-functionalized QDs was extended by conjugating the protein streptavidin (SA) to provide a method for specific targeting to cellular receptors. SA was conjugated to 605 nm emitting 20% aminoQDs (aminoQD-SA) using EDC/NHS coupling chemistry. QDs modified in this manner showed strong binding to non-specifically biotinylated cells. In control experiments in which the coupling agents or the SA were omitted, QDs showed minimal binding to biotinylated cells (data not shown), confirming the role of covalent bond formation (as opposed to electrostatic interactions) in tethering SA to the QDs. We applied the aminoQD-SA conjugates to specific cell labeling and single particle tracking of EGF receptors (EGFR) on live cells. EGFR is an important activator of cell division and a target for therapy of many cancers.[28] There are still many questions about the mechanism of receptor association and internalization in EGFR signal transduction, which are best addressed through study at the single molecule level. [29, 30]

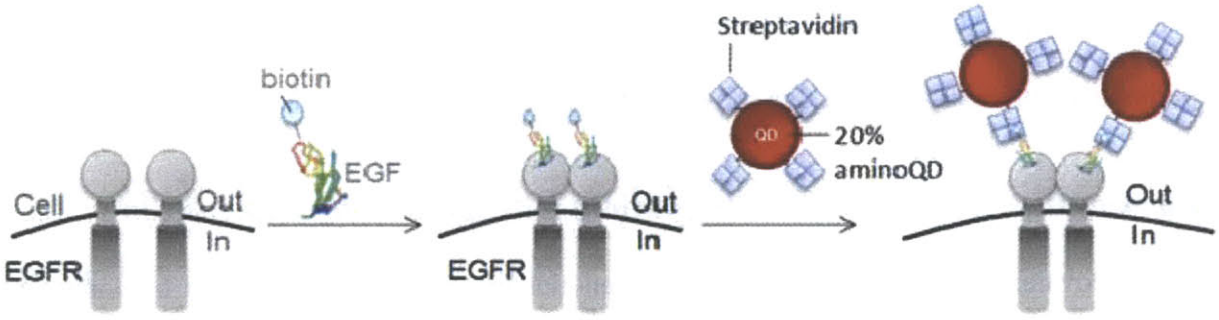

Figure 4-9 Targeting QDs to EGFR. EGFR labeled with biotinylated EGF (bioEGF), followed by staining with aminoQDs covalently conjugated to streptavidin (not drawn to scale).

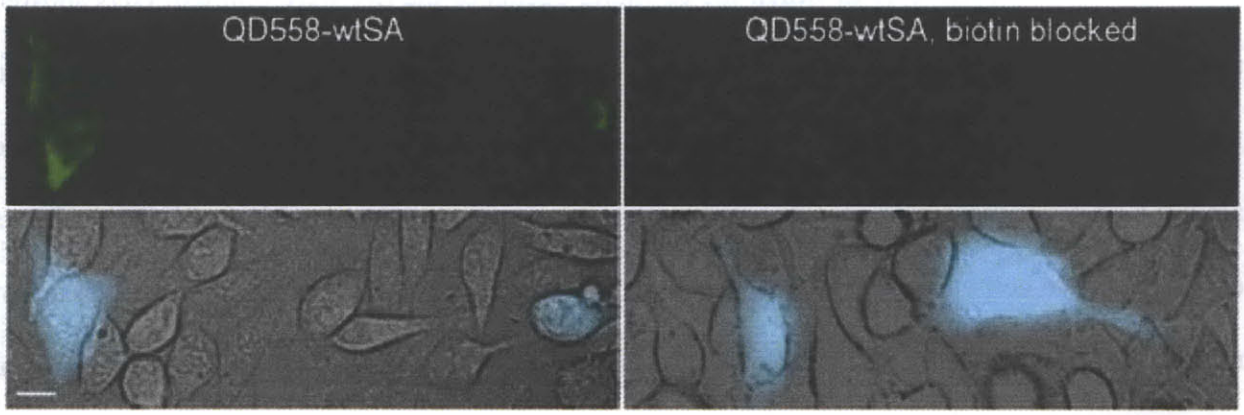

Figure 4-10 Targeting of 20% aminoQD-SA conjugates to EGFR on live cells**.** EGFR expressing cells are indicated by BFP co-transfection marker. Top row: QD558 channel. Bottom row: BFP + DIC channel. Left: EGFR transfected COS7 cells treated with biotinylated EGF and stained with aminoQD-SA. Right: control experiment in which aminoQD-SA was blocked with excess free biotin. Scale bar, 10 μm.

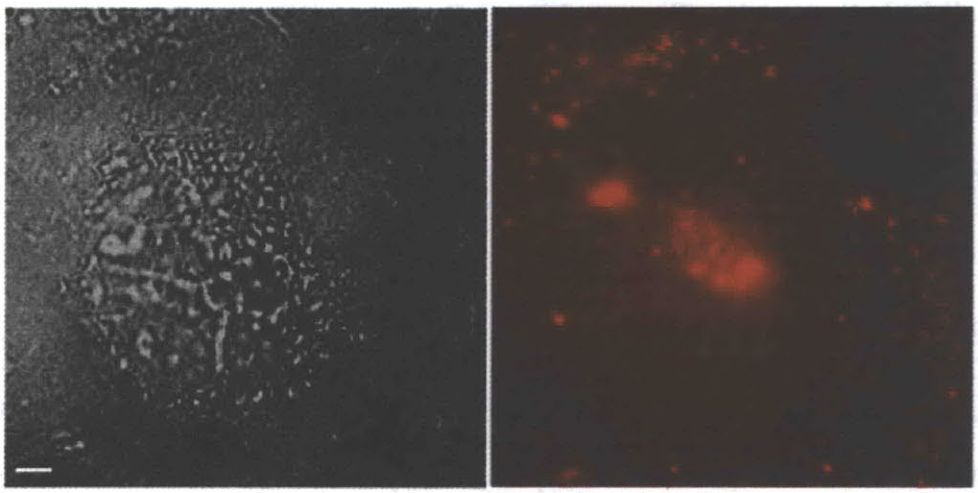

Figure 4-11 Single particle tracking of EGF via low density labeling with 20% aminoQD-SA. Left: DIC channel. Right: QD605 channel. Large patches of brightness represent autofluorescence, bright dots represent clusters of QDs, movie shows fluorescence intermittency of single QDs, which migrate in a manner consistent with active transport of labeled receptors. Scale bar, 5 μm.

Figure 4-9 schematically illustrates the targeting of live cells transfected with human EGFR. COS7 cells were incubated with biotinylated EGF (bioEGF) and then stained with aminoQD-SA. We observed specific binding of the QD to the surface of EGFR transfected cells (Figure 4-10, left), shown by the blue fluorescent protein (BFP) co-transfection marker. Adjacent untransfected cells, indicated by the absence of the BFP marker, did not show QD staining, illustrating the specificity of labeling. Control experiments in which QDs were blocked with excess free biotin also showed no binding (Figure 4-10, right). Furthermore, the photostability, specificity, and high QY of these QDs enabled single particle tracking of EGF interaction with EGFR on the cell surface (Figure 4-11). Individual QDs were identified by their fluorescence intensity and intermittency, or blinking, behavior and could be seen in motion on the surface of cells in a manner consistent with active transport of the labeled receptor.

4.1.7 **Cell Labeling with a Targeted Dual-Emission QD**

Metal affinity coordination and covalent attachment to QDs each has its advantages and limitations. For small molecules such as dyes, a His_6-tagged form is not readily available, and so covalent conjugation is preferable. For recombinant proteins, expression with a His_6-tag is routine and metal affinity conjugation to QDs is convenient due to the high binding affinity, fast kinetics of binding, controlled orientation of the protein on the QD surface, and ease of preparation with little or no purification steps necessary.[31] Here we combine the advantages from both methods of bioconjugation to achieve a versatile nanocrystal that still maintains the desired properties for cell labeling, forming a basis for the realization of QDs with both targeting specificity and environmental sensing capabilities.

To show that aminoQDs bearing alloyed $Zn_xCd_{1-x}S$ shells are amenable to metal affinity driven coordination of His_6-tagged proteins, we incubated 20% aminoQDs with a streptavidin bearing a His_6-tag on one subunit (hSA). Polyhistidine has been shown to associate with CdSe/ZnS core/shell QDs via metal-affinity interactions with Zn ions present at the nanocrystal surface.[31] In the present case, Cd ions present on the surface due to the alloyed shell could also participate in binding.[32] We used hSA-tagged QDs in conjunction with biotinylated EGF for specific labeling of EGFR on live cells (Figure 4-12A, left). The resulting QD-hSA conjugates showed specific binding to biotinylated EGF on EGFR expressing cells, indicated by the green transfection marker (Figure 4-12B, left). We note that previously, an analog of compound **7** with $n \approx 12$ was found to inhibit the binding of a polyhistidine tagged protein to the metal rich QD surface due to steric interference.[12] However, we found that the PEG based ligands described here, with $n \approx 8$, enabled efficient binding to hSA.

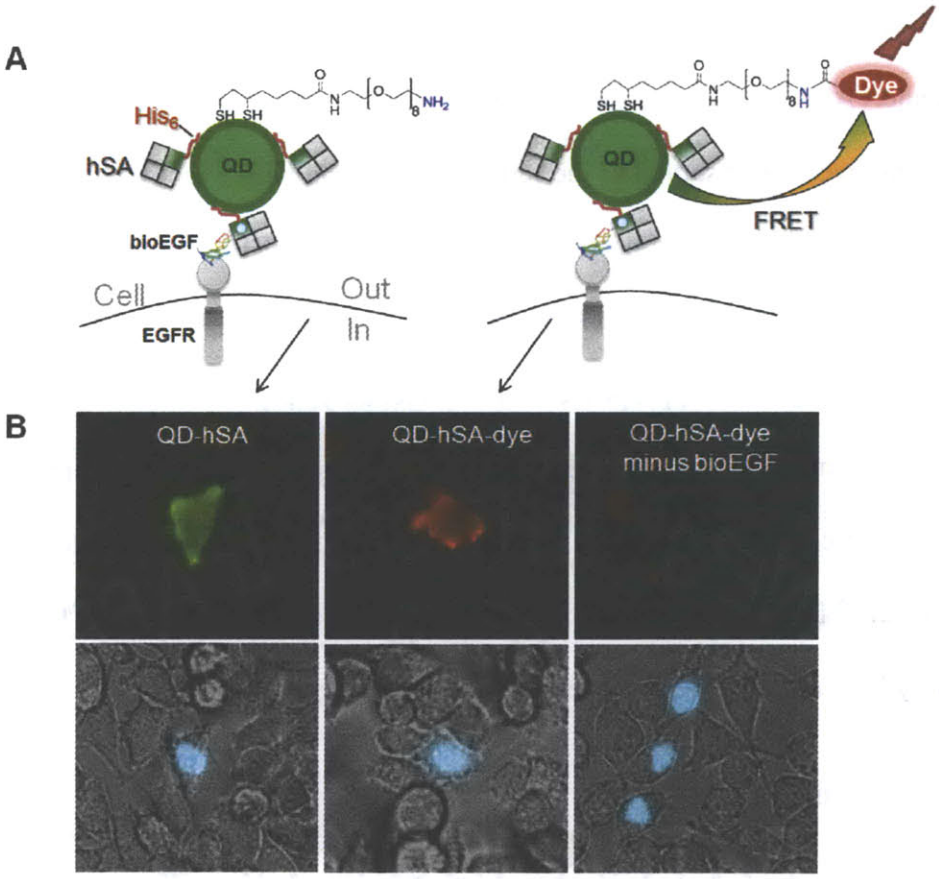

Figure 4-12 Targeting the EGF receptor with a QD-dye conjugate. (A) Schematic showing conjugation of His6-tagged streptavidin (hSA) to 20% aminoQDs (left) or combined hSA conjugation with covalent conjugation of dye to 20% aminoQDs (right) (only one surface ligand shown for clarity). (B) Labeling of EGFR transfected into HeLa cells with biotinylated EGF, followed by staining with QD-hSA (left), QD-hSA-dye (middle), or a control with QD-hSA-dye minus biotinylated EGF (right). Top: fluorescence pseudo-color images showing overlay of 558 nm (QD emission, green) and 605 nm (emission from QD-dye FRET, red). Bottom: phase contrast images showing overlay of YFP (nuclear transfection marker emission, cyan).

To generate aminoQDs bearing both a dye and streptavidin, we conjugated 20% aminoQDs to the photostable AlexaFluor 568 dye using NHS chemistry, giving ~2.3 dye molecules per QD and ~75% FRET efficiency (data not shown). The QD-dye conjugate was then incubated with hSA and applied to HeLa cells displaying EGFR after incubation with biotinylated EGF (Figure 4-12A, right). QD-hSA-dye conjugates bound specifically to EGFR transfected cells and excitation at 405 nm led to emission principally from the dye, as a result of FRET (Figure 4-12B, middle). Analysis of the individual channels (data not shown) show highly

quenched QD emission in the green channel for the QD-hSA-dye conjugate compared to the QD-hSA conjugate. Also, upon intense irradiation of the QD-hSA-dye conjugate at 405 nm, bleaching of the dye was observed in the red channel, along with a recovery of the QD emission in the green channel, further supporting the occurrence of FRET within the targeted QD-dye conjugate on the cell surface (data not shown).

By appending an appropriate environmentally-responsive chromophore, QD-dye conjugates can be made to behave as a FRET-based sensors of their environment (e.g. pH),[26] while the His_6-tag conjugation of hSA provides a means for targeting QDs to cellular proteins with high affinity. Thus, QDs which exclusively sense a targeted receptor's local environment can potentially be realized using this method of dual conjugation.

4.1.8 Conclusions

We have synthesized a series of DHLA-PEG functionalized ligands that produce aqueous derivatizable QDs with small hydrodynamic size, low non-specific binding, high quantum yield, and good solution stability across a wide pH range for cell labeling applications. We demonstrated the ability to tune the QD surface charge and functional valency without sacrificing pH stability by ligand exchange using a mixture of aminoPEG or carboxyPEG with hydroxyPEG. Using 20% aminoQDs, we showed efficient covalent conjugation of a dye using mild carbodiimide coupling chemistry. Furthermore, covalent conjugation of streptavidin to 20% aminoQDs enabled high affinity labeling and single particle tracking of EGF interaction with EGFR on live cells. We further demonstrated the use of both covalent conjugation of a dye and metal affinity driven conjugation of a His_6-tagged streptavidin to create multifunctional nanocrystals with possible application as targeted, optically-reporting nanosensors. In principle, any combination of proteins, peptides, or small molecule reporters can be conjugated to these

QDs covalently and/or via His_6-tag to provide the desired targeting/sensing capabilities, while maintaining the favorable properties for cell labeling applications.

4.2 *Experimental Details*

Materials and Analysis. All chemicals unless indicated were obtained from Sigma Aldrich and used as received. Air sensitive materials were handled in an Omni-Lab VAC glove box under dry nitrogen atmosphere with oxygen levels <0.2 ppm. All solvents were spectrophotometric grade and purchased from EMD Biosciences. Amine-bearing compounds were visualized on thin layer chromatography (TLC) plates using a ninhydrin solution. All other TLC plates were visualized by iodine staining. NMR spectra were recorded on a Bruker DRX 401 NMR Spectrometer. ESI-MS was measured on an Applied Biosystems QTrap mass spectrometer. Samples were dissolved in a solution of acetonitrile, water, and acetic acid (50:50:0.01 v/v) at a concentration of 2.5 pmol/μL and introduced via syringe pump at a flow rate of 10 μL/min. UV-Vis absorbance spectra were taken using an HP 8453 diode array spectrophotometer. Photoluminescence spectra were recorded with a SPEX FluoroMax-3 spectrofluorimeter. The absorbance of all solutions was kept below 0.1 OD to avoid inner-filter effects. Commercial QD605 were obtained from Invitrogen (cat # Q10101MP).

Compound 1 (Diamino-PEG). Neat PEG_8 (average MW 400 g/mol) (20.0 g, 48.3 mmol) was degassed at 80 °C for 1 h with stirring to remove traces of water. The flask was back-filled with N_2 and cooled on an ice bath before thionyl chloride (10.5 mL, 145.0 mmol) was slowly added. The solution was warmed to 25 °C and stirred for 2 h. The conversion was monitored by the disappearance of the broad O-H stretch at 3,500 cm^{-1} and the appearance of a C–Cl stretch at 730 cm^{-1} in the IR spectrum. The product was diluted with DMF (20 mL) and the solvent removed under reduced pressure. This was repeated three times to remove all residual

traces of thionyl chloride. The sample was dissolved in a solution of sodium azide (9.42 g, 145.0 mmol) in 250 mL DMF and stirred overnight at 85 °C. The solvent was removed under reduced pressure and 200 mL of dichloromethane was added. The precipitate was removed by vacuum filtration and the solvent evaporated *in vacuo* to yield the intermediate di-azide. The conversion was confirmed by the appearance of a sharp azide stretch at 2,100 cm^{-1} and the disappearance of the C–Cl stretch at 730 cm^{-1} in the IR spectrum. The sample was dissolved in 300 mL of tetrahydrofuran (THF), and triphenylphosphine (27.9 g, 106 mmol) was added. The solution was stirred at 25 °C for 4 h before adding 4 mL of water and stirring overnight. The THF was removed *in vacuo* and 100 mL of water was added. The precipitate was removed by vacuum filtration and the filtrate washed with toluene (3 × 50 mL). The water was removed *in vacuo* to yield the pure product as light yellow oil (17.8 g, 89%). ESI-MS: *m/z* 457 $[M + H]^+$. ^1H NMR (400 MHz, $CDCl_3$): δ (ppm) 3.53 (m, 28 H), 3.39 (t, *J* = 5.2 Hz, 4H), 2.74 (t, J = 5.2 Hz, 4H), 1.27 (s, 4H).

Lipoic Acid NHS-Ester (LA-NHS). To a solution of lipoic acid (LA, 5.00 g, 24.23 mmol) and N-hydroxysuccinimide (NHS, 3.35 g, 29.1 mmol) in 150 mL tetrahydrofuran at 4 °C was added slowly a solution of dicyclohexylcarbodiimide (6.00 g, 29.1 mmol) in 10 mL tetrahydrofuran. The mixture was warmed to room temperature and stirred for 5 hr. The precipitate was removed by vacuum filtration and the solvent evaporated *in vacuo*. The crude product was redissolved in 100 mL of ethyl acetate and filtered once more by vacuum filtration. The product was recrystallized from a solution of hot ethyl acetate:hexane (1:1 v/v) as a pale yellow solid (5.88 g, 80%). ^1H NMR (400 MHz, $CDCl_3$): δ (ppm) 3.58 (m, 1H), 3.13 (m, 2H), 2.84 (s, 4H), 2.63 (t, *J* = 7.1 Hz, 2H)), 2.50 (m, 1H), 1.99-1.46 (m, 7H).

Compound 2 (LA-PEG-Amine). To a solution of compound 1 (12 g, 29.1 mmol) and sodium bicarbonate (2.44 g, 29.1 mmol) in dimethylformamide/water (100 mL, 50:50 v/v) at 4 °C was added dropwise a solution of LA-NHS (1.60 g, 5.27 mmol) in 10 mL dimethylformamide over 1 hr. The solution was warmed to RT, stirred overnight, and extracted with chloroform (3 x 30 mL). The combined organic extracts were washed with water (3 x 30 mL), dried over sodium sulfate, filtered, and the solvent evaporated. The crude product was purified by alumina column (dichloromethane/methanol 95:5) to give the final product as a yellow oil (1.90 g, 60%). ESI-MS: *m/z* 601 $[M + H]^+$. ^1H NMR (400 MHz, $CDCl_3$): δ (ppm) 3.63 (m, 26H), 3.52 (t, J = 5.2 Hz, 2H), 3.47 (t, J = 5.2 Hz, 2H) 3.10 (m, 2H), 2.86 (t, J = 5.2 Hz, 2H), 2.40 (m, 1H), 2.17 (t, J = 6.5 Hz, 2H), 1.99 – 1.46 (m, 7H).

Compound 3 (aminoPEG). To a solution of **2** (1.50 g, 2.50 mmol) in 4:1 water/ethanol (20 mL) at 4 °C was slowly added 4 equivalents of sodium borohydride over a 30 min period. The solution was stirred for 2 hr at 4 °C, acidified to pH 2 with 3 M HCl, and extracted with chloroform (3 × 15 mL). The combined organics were dried over $MgSO_4$ and filtered. The solvent was removed *in vacuo* to yield the product as a colorless oil (1.37 g, 91%). ESI-MS: *m/z* 603 $[M + H]^+$. ^1H NMR (400 MHz, $CDCl_3$): δ (ppm) 3.84 (m, 2H), 3.61 (m, 36H), 3.52 (m, 4H), 3.13 (m, 2H), 2.84 (m, 2H), 2.62 (m, 2H), 2.19 (m, 2H), 1.99 – 1.46 (m, 9H).

Compound 5 (LA-PEG-CO2H). To a solution of **2** (1.90 g, 3.16 mmol) and triethylamine (0.320 g, 3.16 mmol) in dichloromethane (30 mL) was dripped slowly a solution of methylmalonylchloride (0.475 g, 3.48 mmol) in dichloromethane (10 mL) at 4 °C. The solution was stirred at RT for 4 hr and the solvent removed *in vacuo*. The crude product was purified by silica column (dichloromethane/methanol 95:5) and the solvent evaporated to give the pure product as a yellow oil (1.97 g, 89%). Methylester deprotection was achieved by stirring with 3.5

equivalents of NaOH in methanol for 5 hr at 60 °C. The solvent was removed *in vacuo* after neutralizing to pH 7 with 3M HCl. The product was dissolved in water, acidified to pH 2, and extracted with chloroform (3 x 20 mL) to yield the pure product in quantitative yield. ESI-MS: *m/z* 731 $[M + H]^+$. ^1H NMR (400 MHz, $CDCl_3$): δ (ppm) 3.70-3.52 (m, 36 H), 3.51-3.35 (m, 6H), 3.14 (m, 2H), 2.45 (m, 1H), 2.20 (t, $J = 7.3$ Hz, 2H), 1.96-1.36 (m, 7H).

Compound 6 (carboxyPEG). To a solution of **2** (1.50 g, 2.06 mmol) in 0.25 M sodium bicarbonate buffer (20 mL) at 4 °C was slowly added 4 equivalents of sodium borohydride over a 30 min period. The solution was stirred for 2 hr at 4 °C, acidified to pH 2 with 3 M HCl, and extracted with chloroform (3 × 15 mL). The combined organics were dried over $MgSO_4$ and filtered. The solvent was removed *in vacuo* to yield the product as a colorless oil. ESI-MS: *m/z* 733 $[M + H]^+$. ^1H NMR (400 MHz, $CDCl_3$): δ (ppm) 3.70-3.52 (m, 36 H), 3.51-3.35 (m, 6H), 2.87 (m, 1H), 2.65 (m, 2H), 2.18 (t, $J = 7.3$ Hz, 2H), 1.96-1.36 (m, 9H).

Synthesis of CdSe($Zn_xCd_{1-x}S$) core(shell) QDs. CdSe cores were synthesised according to previously reported procedures.[11] Overcoating with an alloyed shell was carried via modifications to previously reported procedures. Briefly, CdSe cores precipitated from growth solution by the addition of methanol were redispersed in hexane and injected into a degassed solution of 10 g 99% trioctylphosphine oxide (TOPO) and 0.4 g n-hexylphosphonic acid. After removing the hexane under reduced pressure at 80 °C, the flask was back-filled with dry N_2 and the temperature increased to 130 °C before adding 0.25 mL of decylamine and stirring for 30 min. Precursor solutions of diethylzinc ($ZnEt_2$), dimethylcadmium ($CdMe_2$) and hexamethyldisilathiane [$(TMS)_2S$] were prepared by dissolving the appropriate amounts of each in 4 mL of TOP and loading them into two separate syringes for metal and sulfur under inert atmosphere. The molar quantity of $ZnEt_2$ required to achieve the desired shell thickness

(typically 5 monolayers) were calculated according to the methods of Leatherdale.[33] For an alloyed shell, an appropriate mole fraction $ZnEt_2$ was replaced by $CdMe_2$. A two-fold molar excess of $(TMS)_2S$ was used. The precursor solutions were injected simultaneously into the 130 °C bath at a rate of 4 mL/h. The sample was annealed overnight at 80 °C, and 4 mL butanol was added. The QDs were stored in growth solution under ambient conditions and centrifuged once more before use. Typical fluorescence quantum yields were 68% for QD605 in hexane.

Water Solubilization of CdSe(ZnCdS) Core(Shell) QDs. Exchange of the native tri-n-octylphosphine/tri-n-octylphosphine oxide (TOP/TOPO) surface ligands on QDs for the PEG derivatized ligand was carried out according to previously reported procedures, with modifications to masses of reagents used and the incubation times.[12] To 0.2 mL of QDs in growth solution (optical density > 50 at 350 nm) was added acetone to the point of turbidity. Centrifugation and decantation yielded ~10 mg of dry pellet, to which 50 μL of neat DHLA-PEG derivatized ligand and 10 μL of methanol were added. The mixture was stirred gently under N_2 at 60 °C for 2.5 hr and precipitated by adding 0.3 mL ethanol, 0.05 mL chloroform, and 0.5 mL hexane in succession. Centrifugation at 3000 g for 2 min yielded a clear supernatant, which was discarded. The pellet was dispersed in 0.5 mL of PBS and filtered through a 0.2 μm filter. The sample was purified using gel filtration chromatography in order to remove aggregated QDs, and the fractions were concentrated at 3500 g using a Vivaspin-6 10,000 MWCO spin concentrator. Typical concentrations of QD preparations were 8 μM. The QY in water was ~40%.

Quantum Yield Measurement. QY of QD565 and QD605 was measured relative to Rhodamine 590 (λ_{exc} = 490 nm) and Rhodamine 640 (λ_{exc} = 520 nm), respectively. Solutions of QDs in PBS and dye in ethanol were optically matched at the excitation wavelength. Fluorescence spectra of QD and dye were taken under identical spectrometer conditions in

triplicate and averaged. The optical density was kept below 0.1 between 300-800 nm, and the integrated intensities of the emission spectra, corrected for differences in index of refraction and concentration, were used to calculate the quantum yields using the expression $QY_{QD} = QY_{Dye} \times (Absorbance_{dye} / Absorbance_{QD}) \times (Peak\ Area_{QD} / Peak\ Area_{Dye}) \times (n_{QD\ solvent})^2/(n_{Dye\ solvent})^2$.[34]

Gel Filtration Apparatus. GFC was performed using an ÄKTAprime Plus chromatography system from Amersham Biosciences equipped with a Superose 6 10/300 GL column. PBS (pH 7.4) was used as the mobile phase with a flow rate of 0.5 mL/min. Typical injection volumes were 50 μL. Detection was achieved by measuring the absorption at 280 nm, and the fluorescence spectrum in 30 second intervals was simultaneously recorded using an Ocean Optics SD2000 fiber optic spectrometer (λ_{exc} = 460 nm) from an Ocean Optics LS-450 LED light source. The column was calibrated using gel filtration protein standards from Bio-Rad (cat. 151-1901) ranging in MW from 1.3-158 kDa.

Dynamic Light Scattering. Light scattering analysis was performed using a DynaPro Dynamic Light Scatterer. All QD samples were between 0.5-2 μM and filtered through a 0.02 μm filter before analysis. Typical count rates were between 85-150 kHz. Each autocorrelation function (ACF) was acquired for 10 s, and averaged for 10 min per measurement. A software filter was employed to discard all ACF fits with sum of square errors >15. The resulting ACF was fitted using the Dynamics V6 software employing a non-negative least squares fitting algorithm. Hydrodynamic radii were obtained from a mass weighted size distribution analysis and reported as the mean of triplicate measurements.

Agarose Gel Electrophoresis. Electrophoresis of QDs was performed using a Minicell Primo (Thermo) with 1% Omnipur agarose (EMD) in TAE (40 mM Tris-acetate, 1 mM EDTA, pH 8.3) at 7.9 V/cm for 15 min. QDs were diluted to 150 nM in TAE and mixed with 6x loading

buffer (16% sucrose) before loading onto the gel. Gels were visualized under 305 nm UV with a ChemiImager 5500 (Alpha Innotech Corporation).

Zeta-Potential Measurement. Zeta-potential was measured on a Zeta PALS Zeta Potential Analyzer from Brookhaven Instruments Corp. QDs coated with aminoPEG and carboxyPEG (5 μM) were measured in PBS buffer at pH 6.0 and pH 7.4, respectively. AminoQDs were measured at pH 6.0 because the samples were insufficiently ionized at pH 7.4 to yield well resolved data at the different aminoPEG/hydroxyPEG ligand compositions. Values are reported as the average of triplicate runs consisting of 100 scans each.

pH Stability Measurement. 20% aminoQDs and carboxyQDs (554 nm emission) were incubated in PBS buffer ranging from pH 5.0 to pH 7.4, and borate buffer ranging from pH 8.5 to pH 9.5. at room temperature in the dark at 2 uM concentration. At various time intervals, an aliquot was diluted in PBS for fluorescence analysis in a 96-well plate. Fluorescence intensity measurements of QDs were performed on a Tecan XFluor4 plate reader, with excitation at 490 nm and emission detection at 554 nm. The emission intensities were normalized to that from a stock solution of Rhodamine 590.

Covalent Conjugation of Dye Molecules to Ligand-Exchanged QDs. Purified 20% aminoQDs were brought to ~10 μM in sodium bicarbonate buffer (30 mM), and then an aliquot of ROX NHS ester (Molecular Probes), prepared at 5 mM in anhydrous dimethylformamide, was introduced. After 1 hr reaction time at room temperature, the QDs were then separated from unbound material via ultrafiltration. In control experiments, the amine-reactive dye was replaced with the non-activated (free acid) form, or by pure DMF, and the same work-up procedure was applied after the reaction time had elapsed.

Analysis of FRET in Covalently-Linked QD-dye Conjugates. Förster theory predicts an overall efficiency $E = mR_0^6/(mR_0^6 + r^6)$ for the transfer of excitation from a donor to a set of m acceptors separated by a constant distance r, where R_0 is the characteristic distance at which the transfer to a single acceptor would proceed at 50% efficiency. The characteristic distance (in cm) is given by $R_0 = (8.79\times10^{-25}\ \kappa^2\ n^{-4}\ J\ Q_D)^{1/6}$ for donor quantum yield Q_D and spectral overlap integral J, with orientation factor $\kappa^2 = 2/3$ and refractive index $n = 1.33$. For a given sample, E can be obtained from the quench of the QD donor emission with respect to a control prepared with no dye, m is determined from the absorption spectrum with an appropriate estimate of the QD molar extinction coefficient, and R_0 can be calculated from the spectral overlap and measured QD quantum yield. These parameters allow the typical separation r to be estimated and compared with the radius measured by other means, e.g., DLS.

Conjugation of 20% AminoQDs to Streptavidin. SA (50 μL, 10 mg/mL) was first activated using 1000 equivalents of EDC and NHS in MES buffer (100 mM, pH 6.5) for 30 min. Excess coupling reagent was removed by ultrafiltraion through a 10,000 MW cut-off filter (Vivaspin 2). Activated SA (16 μL) was mixed with 20% aminoQDs (50 μL, 7 μM) in sodium bicarbonate buffer (50mM, pH 8.4) and allowed to react for 1 hr. The QD-SA conjugate was purified by ultrafiltration through a 10,000 MW cut-off filter (Vivaspin 6) into PBS (pH 7.4).

Conjugation of 20% AminoQD-wtSA to Non-specifically Biotinylated Cells. HeLa cells were incubated with 1mg/mL of EZ-Link Biotin-Sulfo-NHS (Pierce) in PBS for 15 min at RT. The cells were washed 4 x and incubated with 20% aminoQD-wtSA samples (100 μL, 200 nM) at 4 °C for 10 min. The cells were then washed 4 x with ice cold PBS before imaging.

Conjugation of His_6-Tagged Streptavidin (hSA) to Dye-Functionalized QDs. To conjugate His_6-tagged streptavidin (hSA) (A1D3, as previously described[35]) to the QDs, 5 μL of

3 μM control or dye-conjugated QDs in 10 mM sodium borate pH 7.4 were incubated with 5 μL 27 μM hSA in PBS for 1 hr at RT.

Cell Culture, Labeling and Imaging. HeLa (human carcinoma) and COS7 (African Green Monkey Kidney) cells were grown in DMEM with 5% Fetal Calf Serum, 50 U/mL penicillin and 50 μg/mL streptomycin. Transfections were performed with Lipofectamine 2000 (Invitrogen) according to manufacturer's instructions and cells were imaged the day after transfection. pEYFP-H2B[36] was a kind gift of A.K. Leung (MIT). This encodes histone H2B fused to enhanced yellow fluorescent protein (YFP), as a nuclear-localized co-transfection marker. The cytoplasmic co-transfection marker BFP was a gift from R. Y. Tsien (UCSD). The human EGFR gene in pcDNA3 (Invitrogen) was a gift from K. D. Wittrup (MIT)

QD Non-Specific Binding of QDs. HeLa, cooled to 4 °C in PBS for 5 min to minimize endocytosis, were incubated with 40 nM QDs in PBS with 0.5% dialyzed bovine N,N-dimethyl casein (Calbiochem) for 10 min at 4 °C. Cells were then washed 4x with ice-cold PBS and imaged in PBS.

Fluorescence and Phase Contrast Microscopy. Cells were imaged live using a Zeiss Axiovert 200M inverted epifluorescence microscope with a 40× oil-immersion lens and a Cascade II camera (Photometrics) with intensification set at maximum. Bright field images were collected using differential interference contrast and 30 ms exposure. BFP (420DF20 excitation, 550DRLP dichroic, 575DF40 emission), YFP (495DF10 excitation, 515DRLP dichroic, 530DF30 emission), Alexa Fluor 568 or ROX (560DF20 excitation, 585DRLP dichroic, 605DF30 emission), QD558 (405DF20 excitation, 515DRLP dichroic, 565DF20 emission) and QD605 or QD558/ROX FRET (405DF20 excitation, 585DRLP dichroic, 605DF30 emission) images were collected and analyzed using Slidebook software (Intelligent Imaging Innovations).

Typical exposure times were 0.1-0.5 s. AlexaFluor 568 fluorescence was bleached by 30 s of intense 405DF20 excitation. Fluorescence images were background-corrected. All fluorescence images were captured under identical camera conditions and are displayed at the same contrast level such that they can be directly compared. Movies were acquired with 0.2 s exposure and no delay between frames, using an additional 2.5× Optovar lens.

EGF Receptor Labeling with Streptavidin Linked to QDs by EDC Coupling. COS7 cells were transfected with 0.2 μg pcDNA3 EGFR and 7.5 ng pcDNA3 BFP per well of a 48-well plate. The next day cells were incubated in PBS with 5 mM $MgCl_2$, 0.5% dialyzed casein and 90 nM biotinylated EGF (biotin-XX-EGF from Invitrogen: human EGF conjugated at a single site to biotin via a long spacer arm) for 5 min at RT. Cells were washed four times with PBS and incubated with PBS, 0.5% dialyzed casein and 70 nM 20% aminoQD605-wtSA for 5 min at RT, before washing four times in PBS and imaging in PBS. As a negative control, QD605-wtSA was incubated with a 500-fold excess of free biotin (Tanabe, USA) for 5 min at RT, before adding to cells.For movie imaging, COS7 cells were labeled as above but with 20 nM 20% aminoQD605-wtSA and were maintained in the microscope at 37 °C using an environmental control system (Solent Scientific)

Imaging of FRET between QD and Dye while Bound to EGF Receptor. A five-fold molar excess of hSA in PBS was incubated with 20% aminoQD558 or 20% aminoQD558-Alexa Fluor 568 for 30 min at RT, allowing stable binding of the His_6-tag of hSA to the QD shell. HeLa were transfected with 0.2 μg pcDNA3 EGFR and 5 ng H2B-YFP per well of a 48-well plate. The next day cells were incubated in PBS with 5 mM $MgCl_2$, 0.5% dialyzed casein and 60 nM biotinylated EGF (biotin-XX-EGF from Invitrogen: human EGF conjugated at a single site to biotin via a long spacer arm) for 5 min at 4 °C, to stop receptor internalization. Cells were

washed four times with cold PBS and incubated with PBS, 0.5% dialyzed casein and 40 nM QD558-hSA or QD558-hSA-Alexa Fluor 568 for 5 min at 4 °C, before washing four times in cold PBS and imaging.

4.3 *References*

1. Wu, X.; Liu, H.; Liu, J.; Haley, K. N.; Treadway, J. A.; Larson, J. P.; Ge, N.; Peale, F.; Bruchez, M. P., Immunofluorescent labeling of cancer marker Her2 and other cellular targets with semiconductor quantum dots. *Nat. Biotechnol.* **2003,** 21, (1), 41-46.

2. Medintz, I.; Uyeda, H.; Goldman, E.; Mattoussi, H., Quantum dot bioconjugates for imaging, labelling and sensing. *Nat. Mater.* **2005,** 4, 435-446.

3. Zhou, M.; Nakatani, E.; Gronenberg, L. S.; Tokimoto, T.; Wirth, M. J.; Hruby, V. J.; Roberts, A.; Lynch, R. M.; Ghosh, I., Peptide-Labeled Quantum Dots for Imaging GPCRs in Whole Cells and as Single Molecules. *Bioconjug. Chem.* **2007,** 18, (2), 323-332.

4. Dahan, M.; Levi, S.; Luccardini, C.; Rostaing, P.; Riveau, B.; Triller, A., Diffusion Dynamics of Glycine Receptors Revealed by Single-Quantum Dot Tracking. *Science* **2003,** 302, (5644), 442-445.

5. Courty, S.; Luccardini, C.; Bellaiche, Y.; Cappello, G.; Dahan, M., Tracking Individual Kinesin Motors in Living Cells Using Single Quantum-Dot Imaging. *Nano. Lett.* **2006,** 6, (7), 1491-1495.

6. Aldana, J.; Wang, Y. A.; Peng, X., Photochemical Instability of CdSe Nanocrystals Coated by Hydrophilic Thiols. *J. Am. Chem. Soc.* **2001,** 123, (36), 8844-8850.

7. Mattoussi, H.; Mauro, J. M.; Goldman, E. R.; Anderson, G. P.; Sundar, V. C.; Mikulec, F. V.; Bawendi, M. G., Self-Assembly of CdSe-ZnS Quantum Dot Bioconjugates Using an Engineered Recombinant Protein. *J. Am. Chem. Soc.* **2000,** 122, (49), 12142-12150.

8. Kim, S.; Bawendi, M. G., Oligomeric Ligands for Luminescent and Stable Nanocrystal Quantum Dots. *J. Am. Chem. Soc.* **2003,** 125, (48), 14652-14653.

9. Algar, W. R.; Krull, U. J., Adsorption and Hybridization of Oligonucleotides on Mercaptoacetic Acid-Capped CdSe/ZnS Quantum Dots and Quantum Dot-Oligonucleotide Conjugates. *Langmuir* **2006,** 22, (26), 11346-11352.

10. Liu, W.; Choi, H. S.; Zimmer, J. P.; Frangioni, J. V.; Bawendi, M. G., *Compact Cysteine-Coated CdSe(ZnCdS) QDs for In Vivo Applications* **2007,** Submitted.

11. Snee, P. T.; Chan, Y.; Nocera, D. G.; Bawendi, M. G., Whispering-Gallery-Mode Lasing from a Semiconductor Nanocrystal/Microsphere Resonator Composite. *Adv. Mater.* **2005,** 17, (9), 1131-1136.

12. Uyeda, H. T.; Medintz, I. L.; Jaiswal, J. K.; Simon, S. M.; Mattoussi, H., Synthesis of Compact Multidentate Ligands to Prepare Stable Hydrophilic Quantum Dot Fluorophores. *J. Am. Chem. Soc.* **2005,** 127, (11), 3870-3878.

13. Murray, C. B.; Norris, D. J.; Bawendi, M. G., Synthesis and characterization of nearly monodisperse CdE (E = sulfur, selenium, tellurium) semiconductor nanocrystallites. *J. Am. Chem. Soc.* **1993,** 115, (19), 8706-8715.

14. Dabbousi, B. O.; Rodriguez-Viejo, J.; Mikulec, F. V.; Heine, J. R.; Mattoussi, H.; Ober, R.; Jensen, K. F.; Bawendi, M. G., (CdSe)ZnS Core-Shell Quantum Dots: Synthesis and Characterization of a Size Series of Highly Luminescent Nanocrystallites. *J. Phys. Chem. B* **1997,** 101, (46), 9463-9475.

15. Manna, L.; Scher, E. C.; Li, L. S.; Alivisatos, A. P., Epitaxial Growth and Photochemical Annealing of Graded CdS/ZnS Shells on Colloidal CdSe Nanorods. *J. Am. Chem. Soc.* **2002,** 124, (24), 7136-7145.

16. Yu, Z.; Guo, L.; Du, H.; Krauss, T.; Silcox, J., Shell Distribution on Colloidal CdSe/ZnS Quantum Dots. *Nano Lett.* **2005,** 5, (4), 565-570.

17. Xie, R.; Kolb, U.; Li, J.; Basche, T.; Mews, A., Synthesis and Characterization of Highly Luminescent CdSe-Core CdS/Zn0.5Cd0.5S/ZnS Multishell Nanocrystals. *J. Am. Chem. Soc.* **2005,** 127, (20), 7480-7488.

18. Pons, T.; Uyeda, H. T.; Medintz, I. L.; Mattoussi, H., Hydrodynamic Dimensions, Electrophoretic Mobility, and Stability of Hydrophilic Quantum Dots. *J. Phys. Chem. B* **2006,** 110, (41), 20308-20316.

19. Bentzen, E. L.; Tomlinson, I. D.; Mason, J.; Gresch, P.; Warnement, M. R.; Wright, D.; Sanders-Bush, E.; Blakely, R.; Rosenthal, S. J., Surface Modification To Reduce Nonspecific Binding of Quantum Dots in Live Cell Assays. *Bioconjug. Chem.* **2005,** 16, (6), 1488-1494.

20. Pinaud, F.; King, D.; Moore, H. P.; Weiss, S., Bioactivation and cell targeting of semiconductor CdSe/ZnS nanocrystals with phytochelatin-related peptides. *J. Am. Chem. Soc.* **2004,** 126, 6115-6123.

21. Ballou, B.; Lagerholm, B. C.; Ernst, L. A.; Bruchez, M. P.; Waggoner, A. S., Noninvasive Imaging of Quantum Dots in Mice. *Bioconjug. Chem.* **2004,** 15, (1), 79-86.

22. Medintz, I. L.; Clapp, A. R.; Mattoussi, H.; Goldman, E. R.; Fisher, B.; Mauro, J. M., Self-assembled nanoscale biosensors based on quantum dot FRET donors. *Nat. Mater.* **2003,** 2, (9), 630-638.

23. Medintz, I.; Clapp, A.; Brunel, F.; Tiefenbrunn, T.; Tetsuo Uyeda, H.; Chang, E. L.; Deschamps, J. R.; Dawson, P. E.; Mattoussi, H., Proteolytic activity monitored by fluorescence resonance energy transfer through quantum-dot-peptide conjugates. *Nat. Mater.* **2006,** 5, (7), 581-589.

24. Shi, L.; DePaoli, V.; Rosenzweig, N.; Rosenzweig, Z., Synthesis and Application of Quantum Dots FRET-Based Protease Sensors. *J. Am. Chem. Soc.* **2006,** 128, (32), 10378-10379.

25. Somers, R. C.; Bawendi, M. G.; Nocera, D. G., CdSe nanocrystal based chem-/bio-sensors. *Chem. Soc. Rev.* **2007,** 36, 579-591.

26. Snee, P. T.; Somers, R. C.; Nair, G.; Zimmer, J. P.; Bawendi, M. G.; Nocera, D. G., A Ratiometric CdSe/ZnS Nanocrystal pH Sensor. *J. Am. Chem. Soc.* **2006,** 128, (41), 13320-13321.

27. Clapp, A. R.; Medintz, I. L.; Mauro, J. M.; Fisher, B. R.; Bawendi, M. G.; Mattoussi, H., Fluorescence Resonance Energy Transfer Between Quantum Dot Donors and Dye-Labeled Protein Acceptors. *J. Am. Chem. Soc.* **2004,** 126, (1), 301-310.

28. Moasser, M. M., Targeting the function of the HER2 oncogene in human cancer therapeutics. *Oncogene* **2007,** 26, (46), 6577-92.

29. Lidke, D. S.; Lidke, K. A.; Rieger, B.; Jovin, T. M.; Arndt-Jovin, D. J., *J. Cell. Biol.* **2005,** 170, (4), 619-626.

30. Teramura, Y.; Ichinose, J.; Takagi, H.; Nishida, K.; Yanagida, T.; Sako, Y., Single-molecule analysis of epidermal growth factor binding on the surface of living cells. *EMBO J.* **2006,** 25, (18), 4215-22.

31. Sapsford, K. E.; Pons, T.; Medintz, I. L.; Higashiya, S.; Brunel, F. M.; Dawson, P. E.; Mattoussi, H., Kinetics of Metal-Affinity Driven Self-Assembly between Proteins or Peptides and CdSe-ZnS Quantum Dots. *J. Phys. Chem. C.* **2007,** 111, (11528-11538).

32. Prabhukumar, G.; Matsumoto, M.; Mulchandani, A.; Chen, W., Cadmium Removal from Contaminated Soil by Tunable Biopolymers. *Environ. Sci. Technol.* **2004,** 38, (11), 3148-3152.

33. Leatherdale, C. A.; Woo, W. K.; Mikulec, F. V.; Bawendi, M. G., On the Absorption Cross Section of CdSe Nanocrystal Quantum Dots. *J. Phys. Chem. B.* **2002,** 106, (31), 7619-7622.

34. Eaton, D., Reference Materials for Fluorescence Measurement. *Pure Appl. Chem.* **1988,** 60, (7), 1107-1114.

35. Howarth, M.; Chinnapen, D. J. F.; Gerrow, K.; Dorrestein, P. C.; Grandy, M. R.; Kelleher, N. L.; El-Husseini, A.; Ting, A. Y., A monovalent streptavidin with a single femtomolar biotin binding site. *Nat Meth* **2006,** 3, (4), 267-273.

36. Platani, M.; Goldberg, I.; Lamond, A. I.; Swedlow, J. R., Cajal Body dynamics and association with chromatin are ATP-dependent. *Nat. Cell Biol.* **2002,** 4, (7), 502-508.

4.4 *Appendix: ^{1}H NMR and ESI MS Spectra of Compounds*

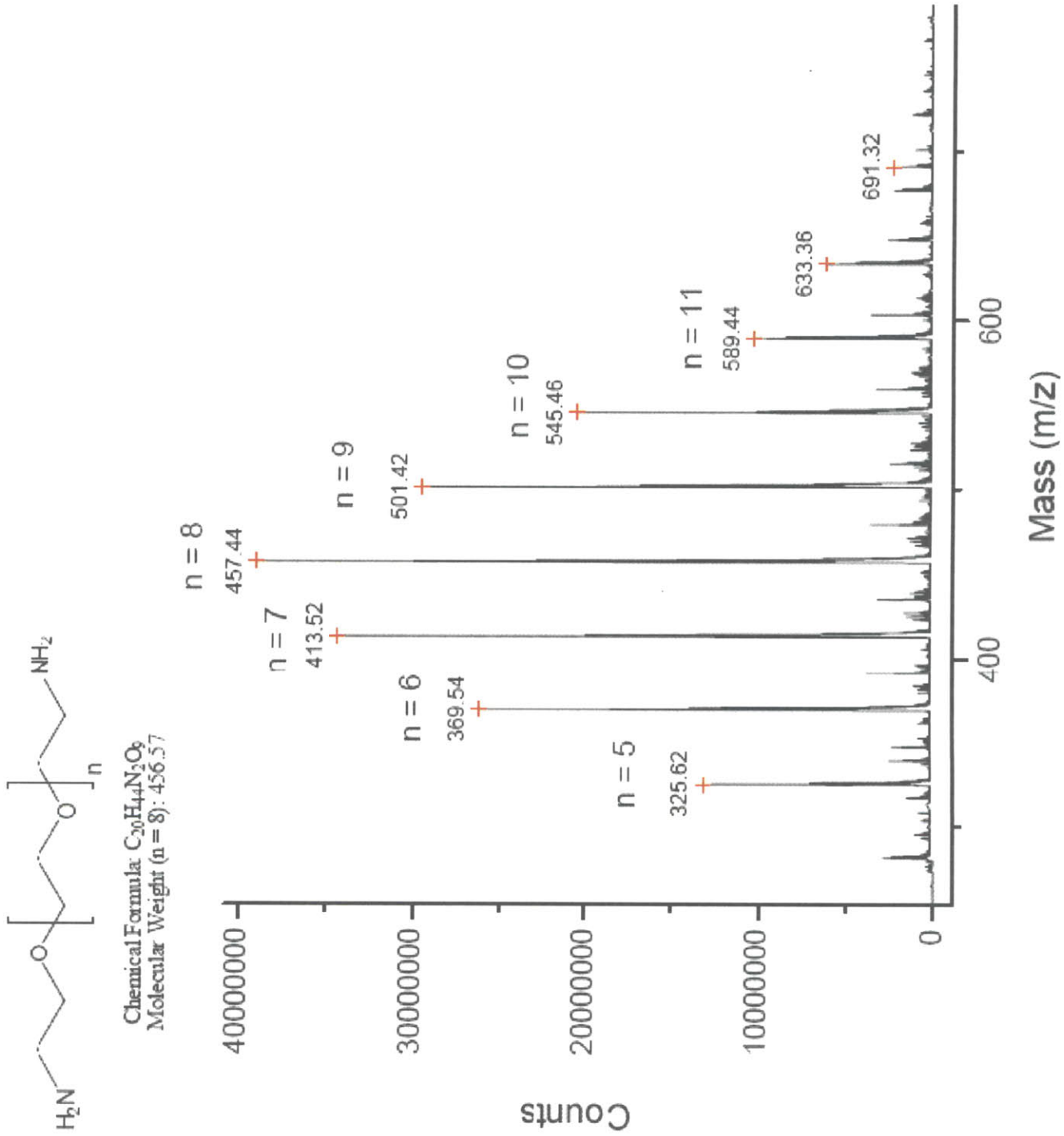

^{1}H-NMR (compound 1)

3.582
3.578
3.133
2.842
2.628
1.934
1.788
1.763
1.585
S
S
O
O
N
O
O
3.50
3.00
2.50
2.00
1.50
ppm

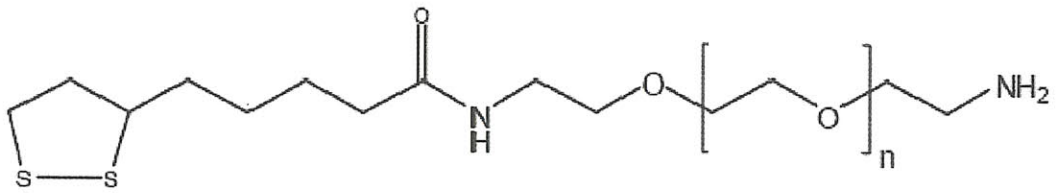

Chemical Formula: $C_{28}H_{56}N_2O_{10}S_2$
Molecular Weight (n = 8): 644.88

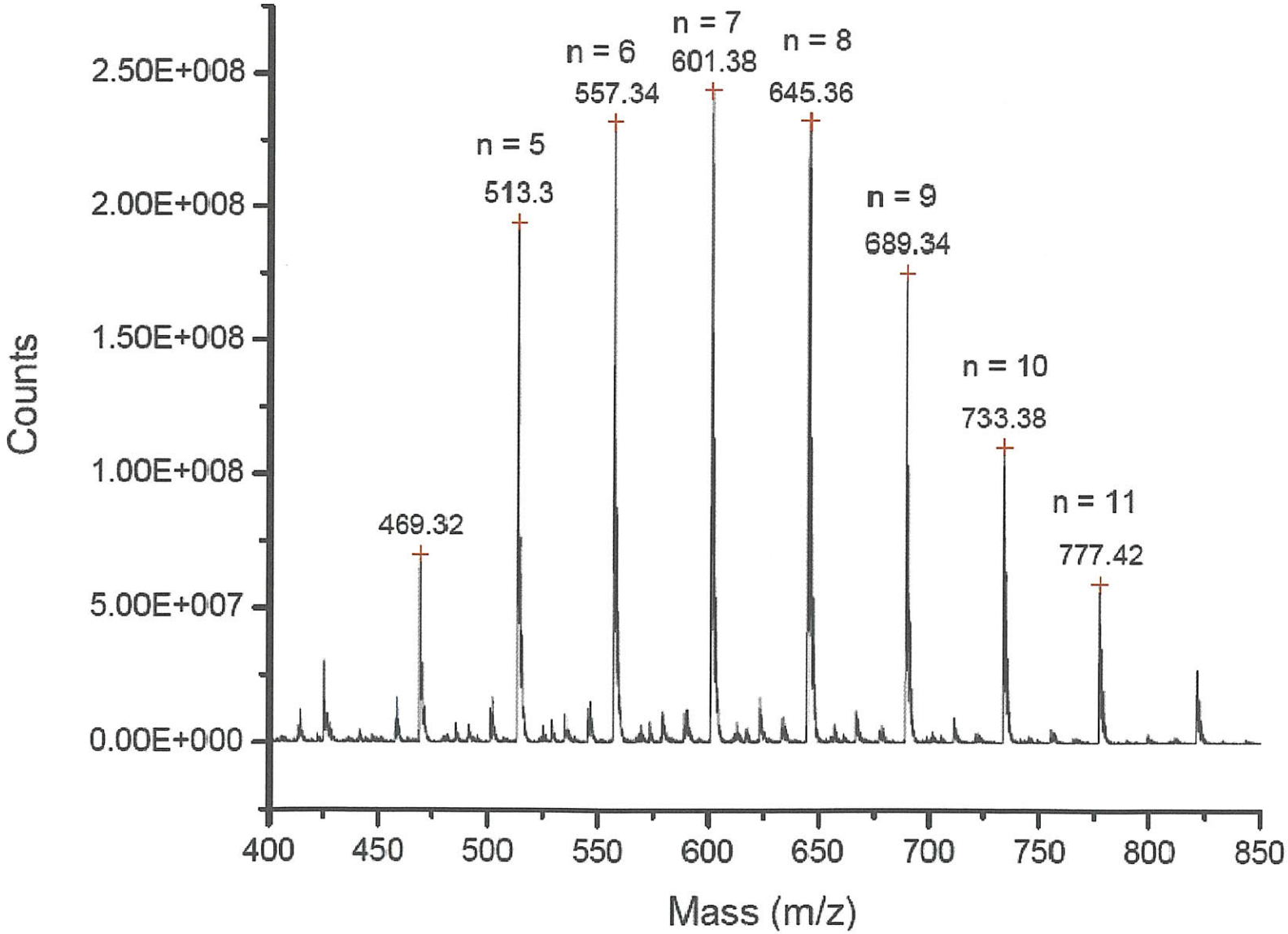

^{1}H-NMR (compound **2**)

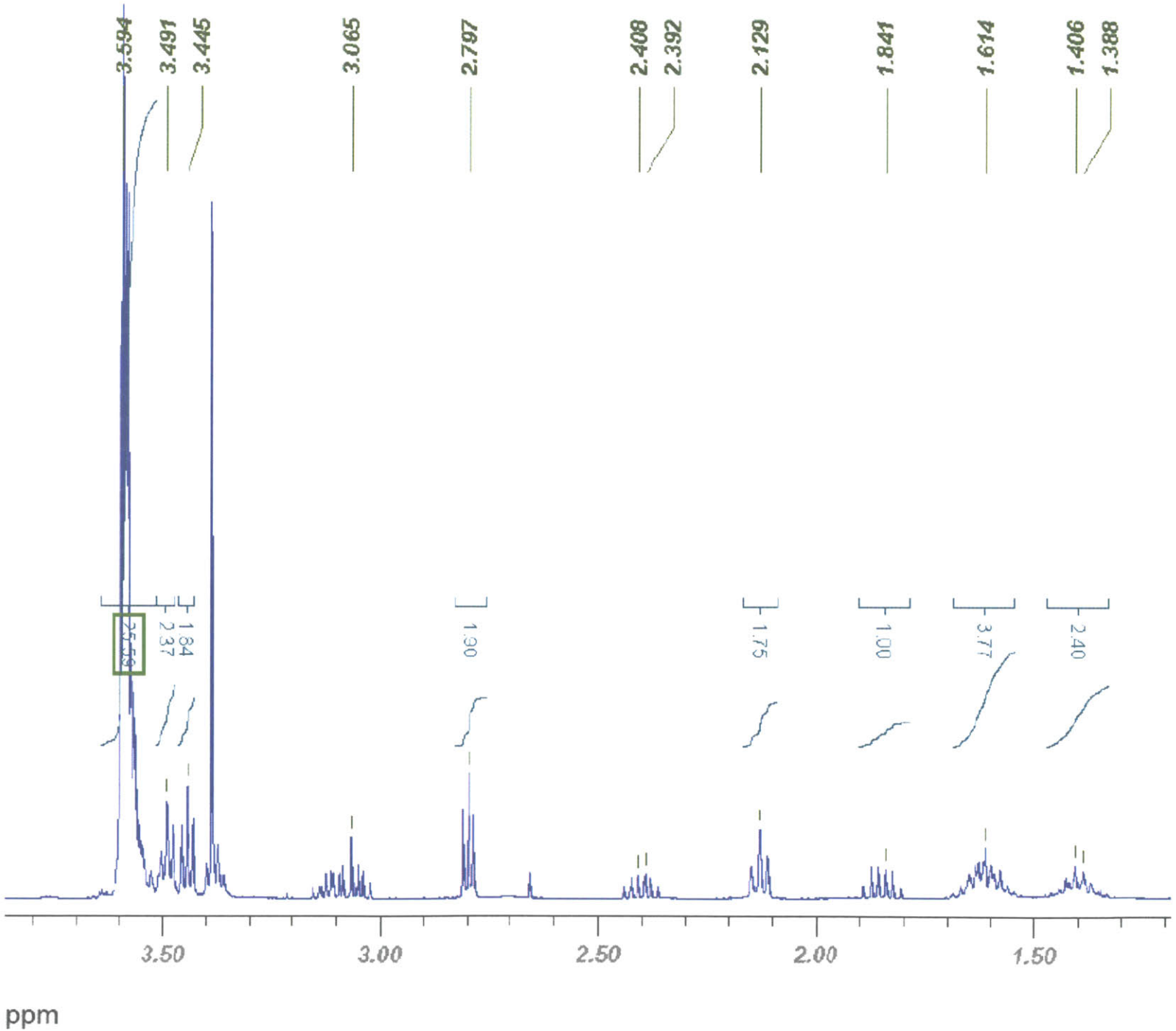

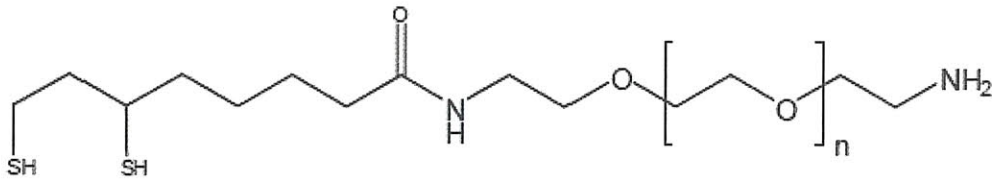

Chemical Formula: $C_{28}H_{58}N_2O_{10}S_2$
Molecular Weight (n = 8): 646.90

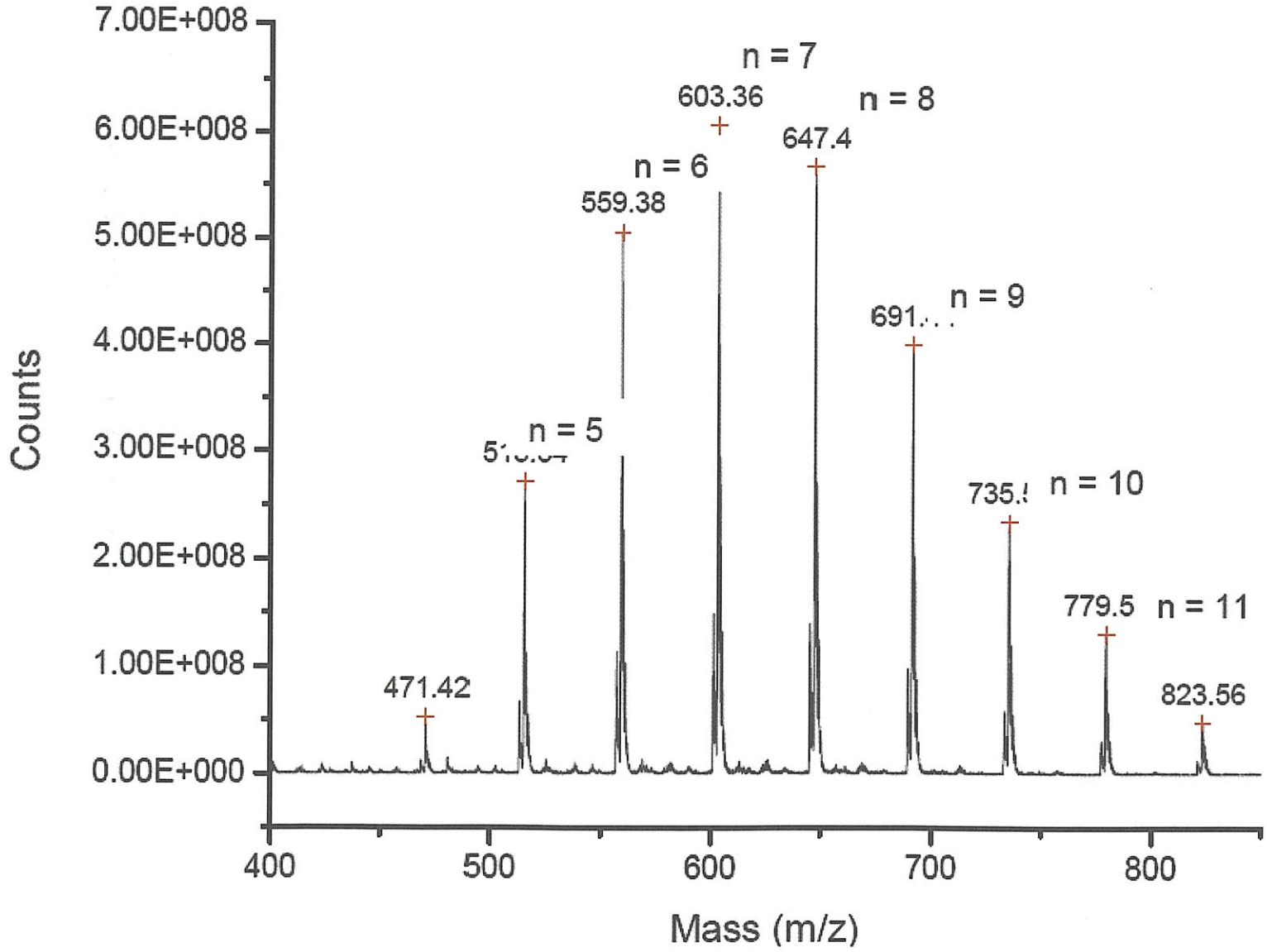

^{1}H-NMR (compound **3**)

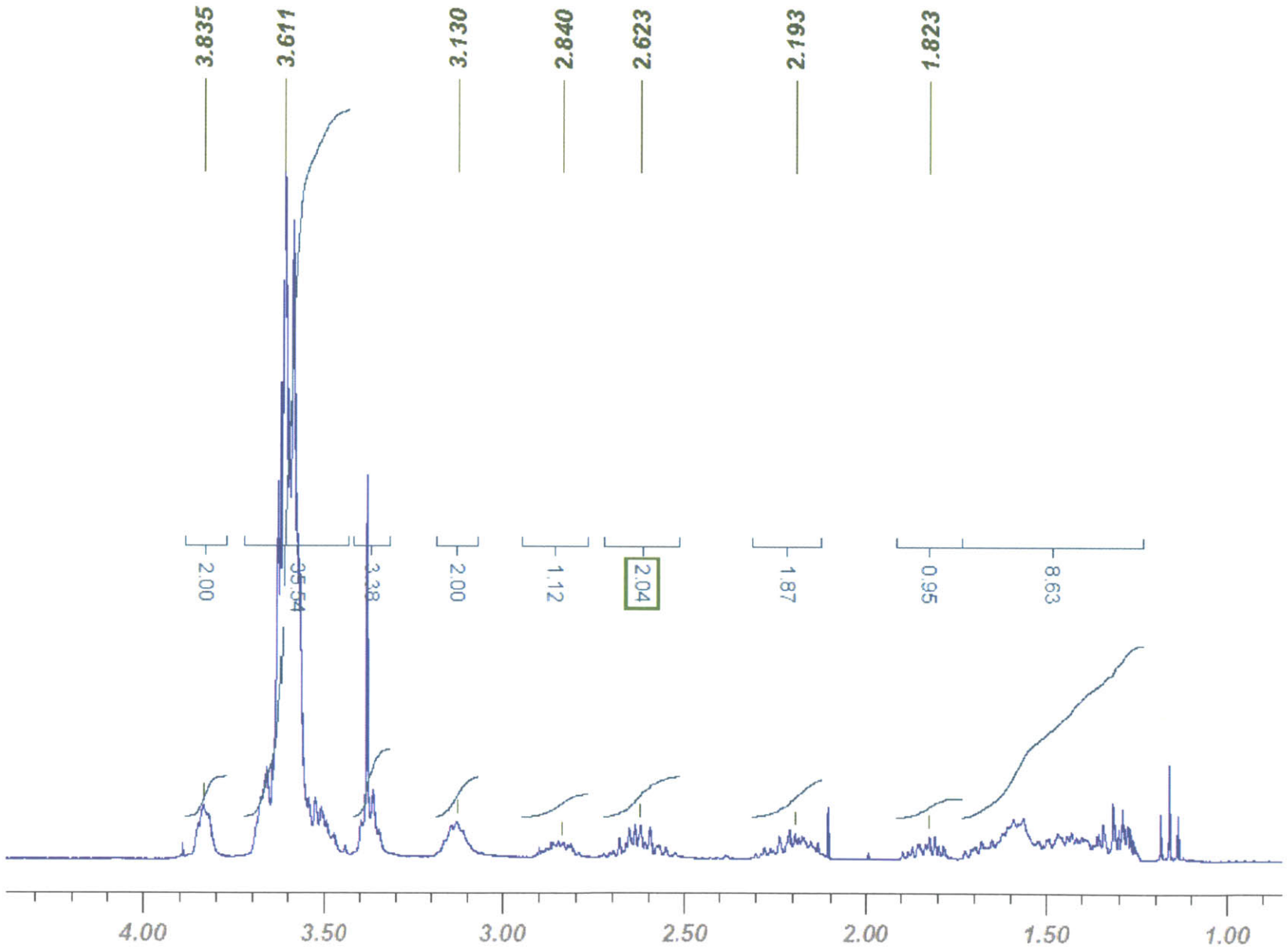

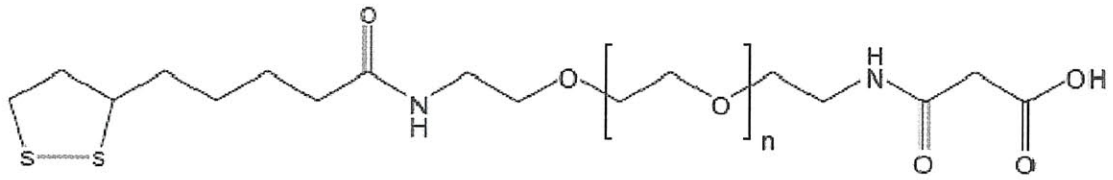

Chemical Formula: $C_{31}H_{58}N_2O_{13}S_2$
Molecular Weight (n = 8): 730.93

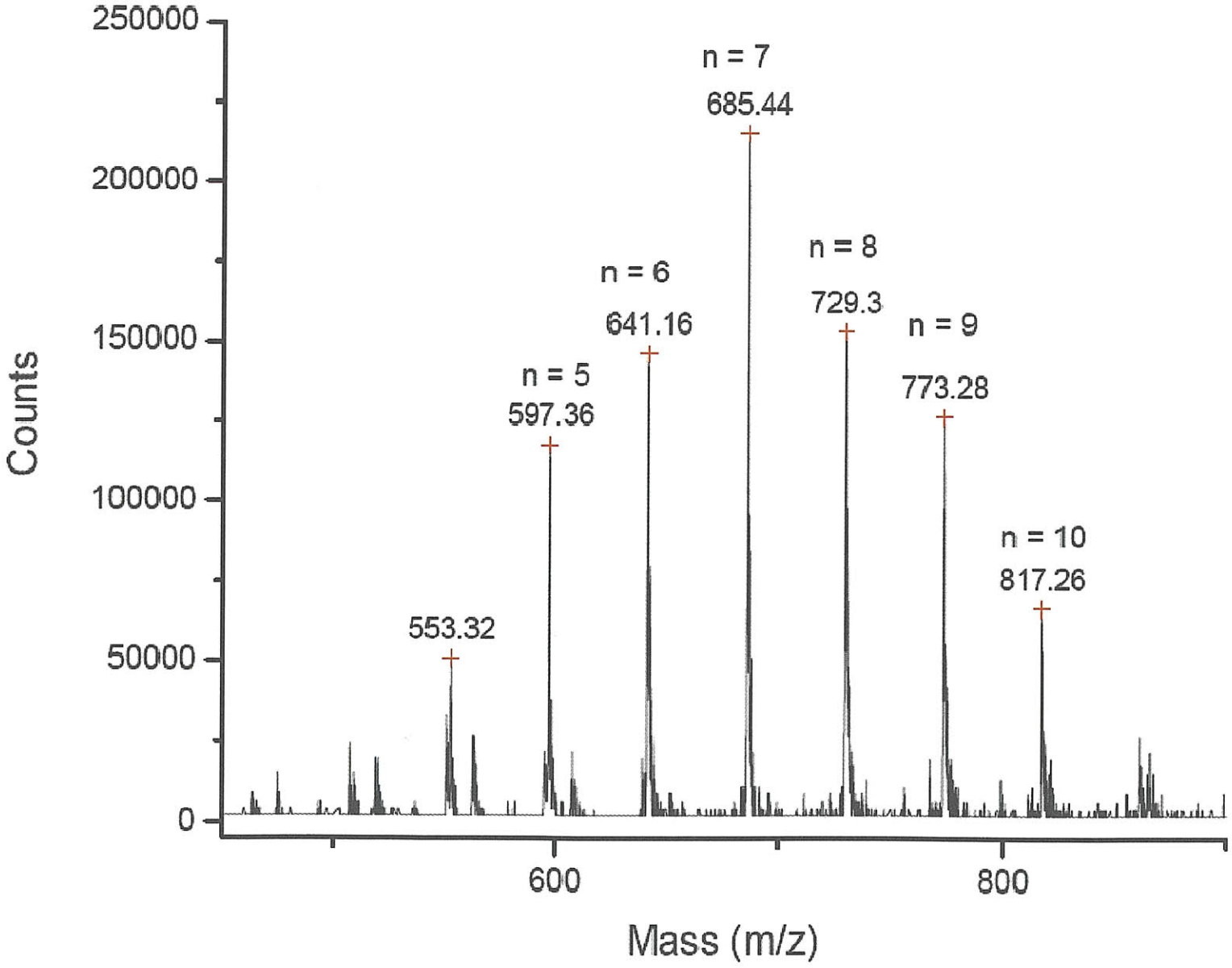

^{1}H-NMR (compound 5)

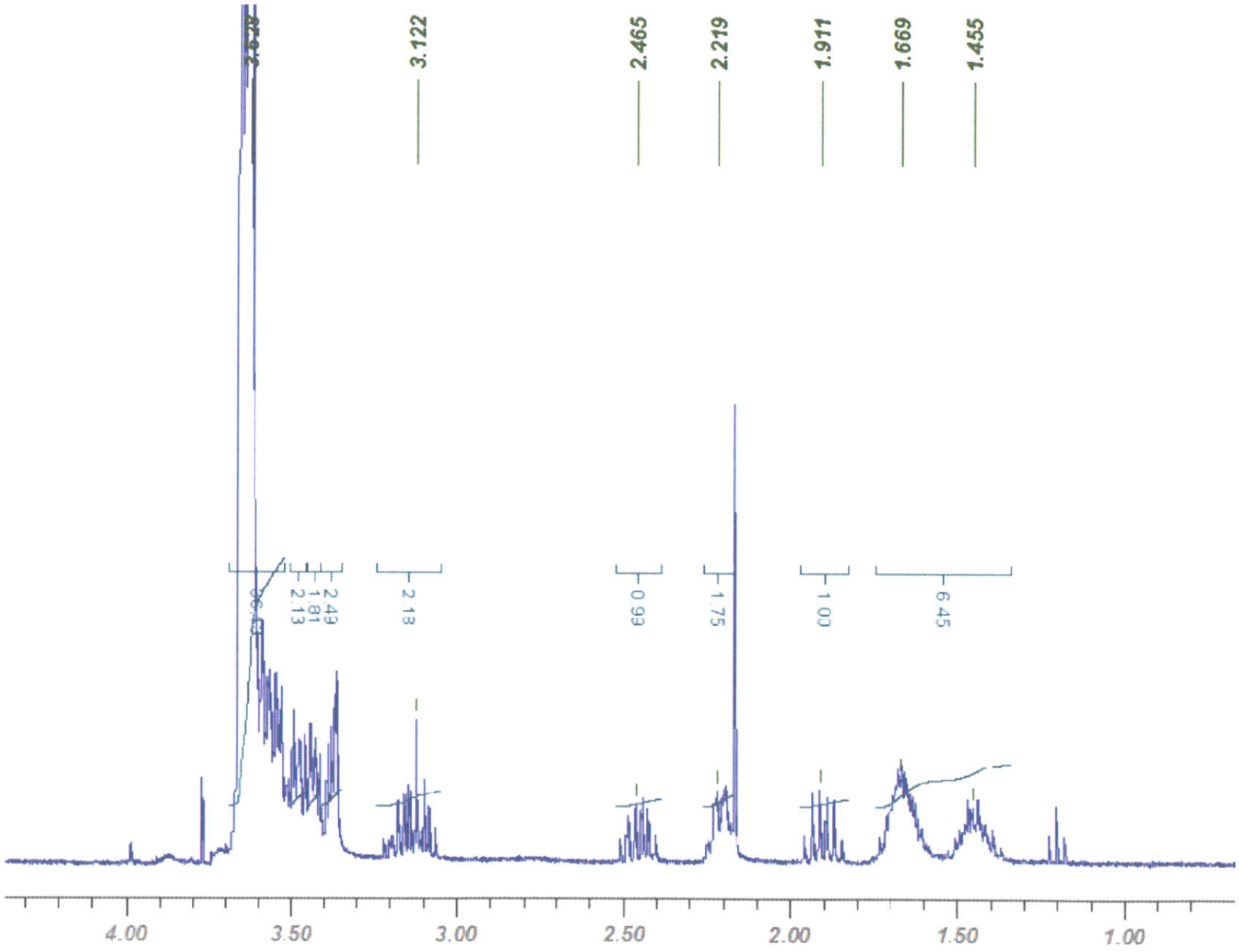

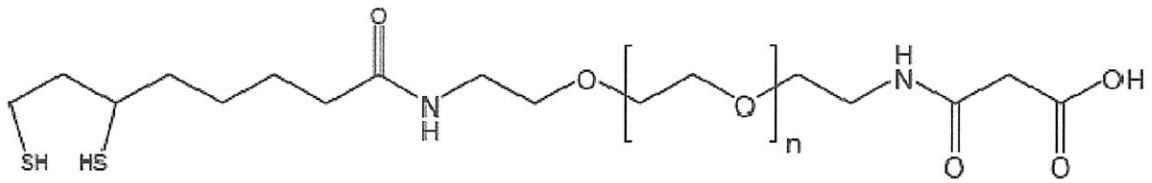

Chemical Formula: $C_{31}H_{60}N_2O_{13}S_2$
Molecular Weight (n = 8): 732.94

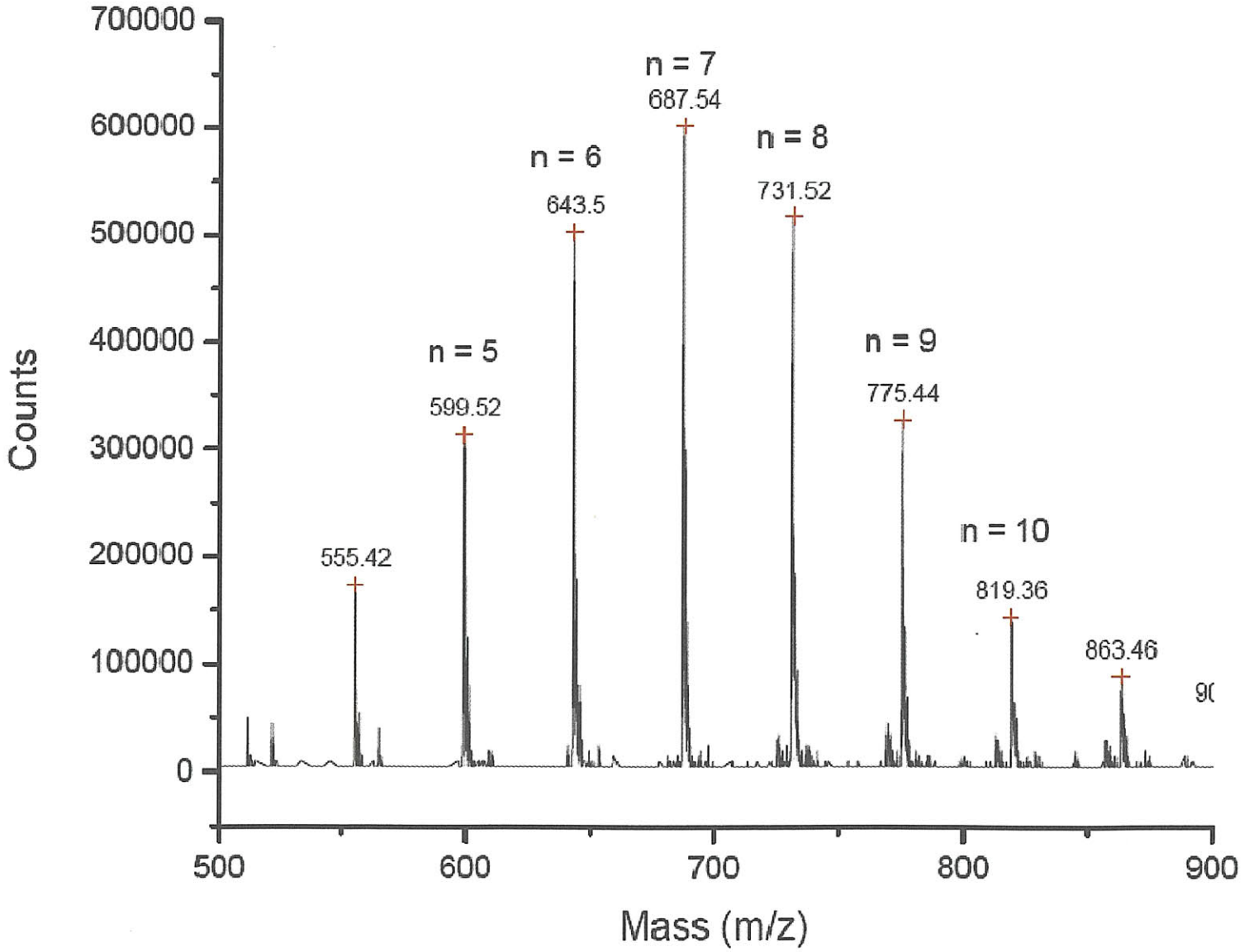

^{1}H-NMR (compound 6)

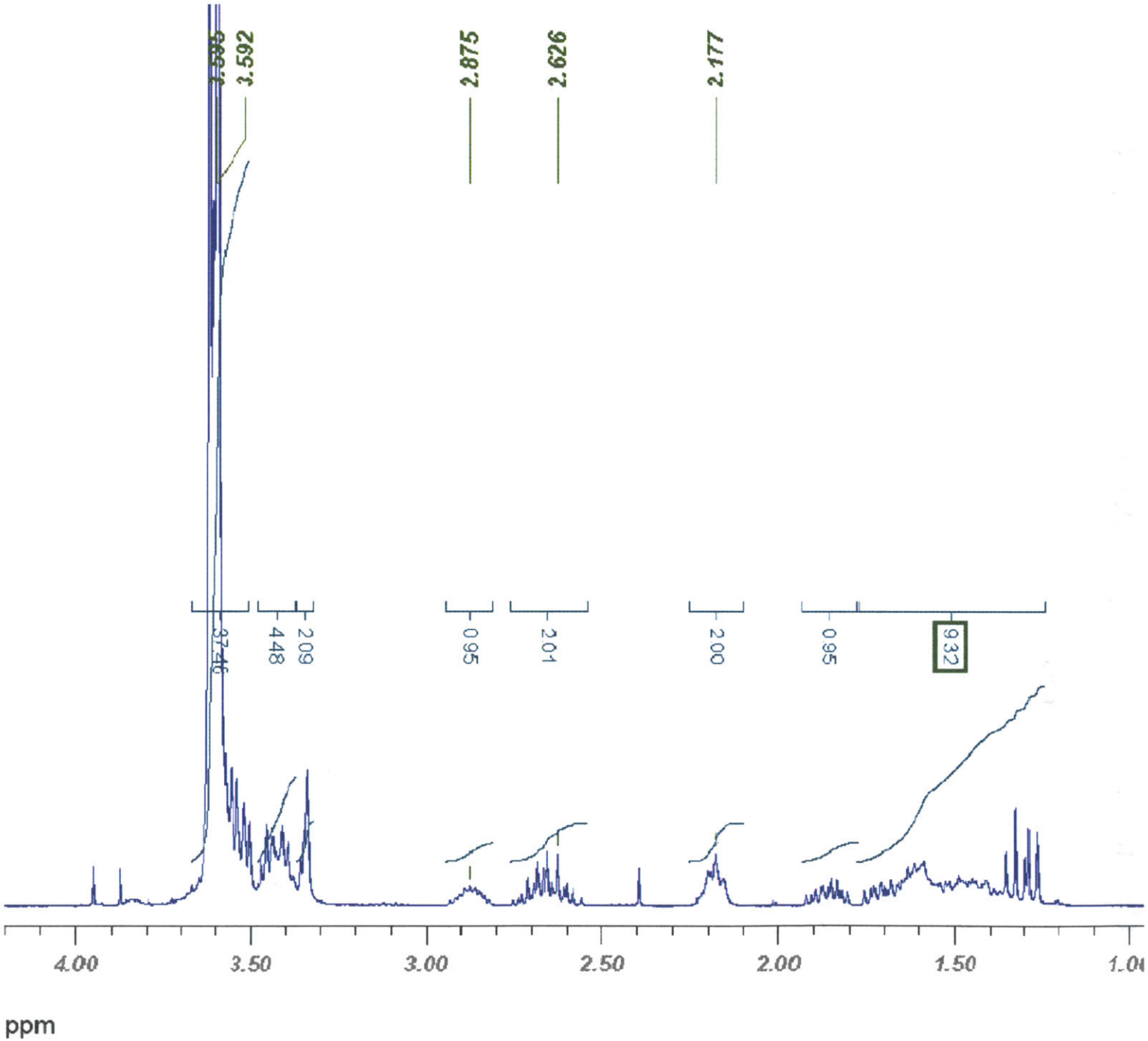

Chapter 5: Purification of valency-controlled QD-protein and QD-antibody conjugates*

5.1 *Background and Motivation*

In the previous chapter, we described a method of synthesizing compact biocompatible QDs using a hetero-bifunctional ligand system with a dithiol group for stable attachment to the QD surface, a PEG group for biocompatibility, and either an amine or carboxy group for derivatization. This system allowed QDs to achieve the numerous essential properties needed for live cell labeling, namely (1) small size, (2) derivatizability, (3) high QY, (4) biocompatibility, and (5) high colloidal stability. Using this system, we demonstrated high-affinity specific targeting by conjugating streptavidin to the QD surface both via poly-histidine induced self-assembly and via covalent conjugation. However, there is a fine point not discussed in the previous chapter with regards to labeling of cellular receptors, namely, the valency of the QD probe.

Typically, conjugation of QDs to proteins, small molecules, or antibodies for the purposes of targeting is done by reacting a stoichiometric ratio of the molecule to QD to achieve a desired average conjugation ratio. That is, some equivalent of the molecule or protein to be conjugated is mixed with the QD (i.e. 5:1 molecule to QD). The actual number of molecules coupled to each QD proceeds in a statistical fashion following a Poisson distribution

---

* Most figures in this chapter has appeared in print. It is reproduced with permission from *Nature Methods* 2008, **5**: 397-399. The cellular imaging data in this chapter were the result of a collaboration with the research group of Alice Y. Ting in the department of Biological Chemistry.

$$P(n, N) = \frac{N^n e^{-N}}{n!} \qquad (5\text{-}1)$$

where the function P(n, N) gives the population fraction of QDs with exactly n molecules bound given that the nominal average number of molecule(s) per QD is N.[1] Figure 5-1 shows a graphical representation of this statistical phenomenon. For instance, looking at the N = 3 (blue) graph, the population fraction of QDs with exactly 5 molecules (n = 5) bound is approximately 0.10, given an average molecule:QD ratio of 3:1 (N = 3).

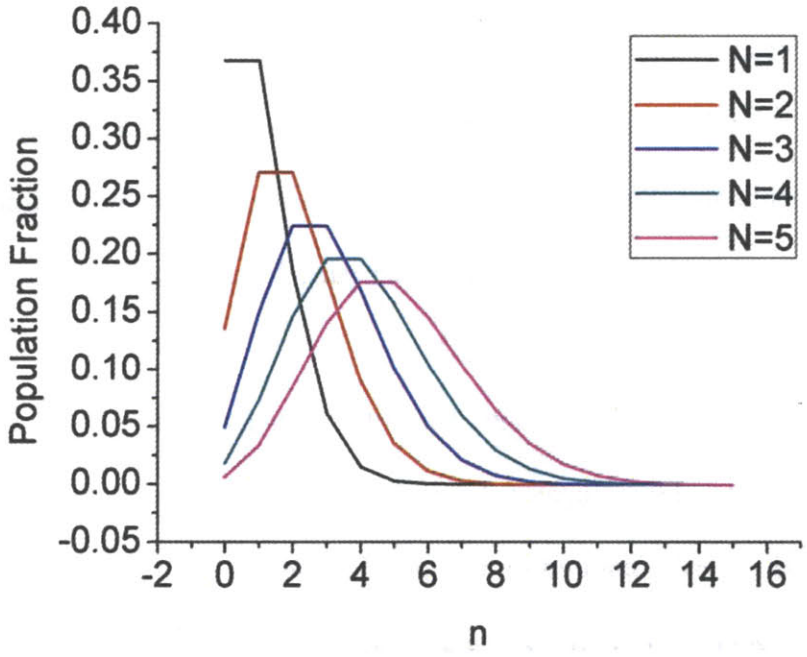

Figure 5-1 Poisson distribution showing the population fraction of QDs with exactly n moieties bound given an average QD:moiety ratio of N:1 for different values of N.

The main point is that the valency of molecules binding to the QDs is often left to probability, and there are advantages to performing the conjugation in a more controlled fashion. For example, if one could engineer a method to isolate a perfect 1:1 QD to DNA conjugate, this would facilitate the directed self-assembly of more complex superstructures.[2-4] One could

imagine linking exactly 2 QDs together, or forming a regular repeating lattice of QDs using precise 1:1, 2:1, 3:1, etc. DNA to QD constructs if one could control the valency of conjugation.

One previous attempt at preparing monovalent particles relied on the use of large polystyrene beads with a low density of surface functional groups, but yielded only moderately pure monovalency (~70%).[5, 6] In other works, valency-controlled gold nanoparticle-DNA conjugates were isolated using an electrophoretic separation method.[4, 7, 8] Gold nanoparticles (gNPs) were conjugated to DNA bearing thiol groups at the terminus, with the conjugation proceeding in a statistical fashion as described above. With sufficiently long strands of DNA, agarose gel electrophoresis of the mixture resulted in discrete bands corresponding to distinct gNP:DNA conjugates of defined valency. In this case, the addition of large DNA molecules added sufficient steric bulk and charge to the gNPs for the discrete conjugates within the mixture to be distinguished as separate bands on the gel. The particles could then be used further for directed self-assembly using DNA programming.[8]

Following this precedence, we sought a similar strategy using gel electrophoresis to purify monovalent QD:molecule conjugates. However, DNA is not a suitable molecule in our case, since the large size of DNA required for this purification to work will result in large size of the final construct. Our goal is to minimize the size, so a more compact biomolecule such as a protein is desired. In addition, the highly charged DNA backbone can induce non-specific binding and may not be compatible in a biological environment. In this chapter, I will describe the method we employed to isolate 1:1 QD:protein conjugates, in which the protein we relied on for purification simultaneously served as the functionality used for targeting. The question then is, why is it so important to use a monovalent probe for cell labeling?

In the context of cellular labeling, there is a severe downside to multivalent interactions. That is, when QDs target cell-surface receptors in a multivalent fashion (i.e. there are multiple targeting molecules per QD), the QD can link multiple near-by receptors together, and this crosslinking can trigger unwanted cellular signaling pathways[9] and reduce receptor mobility.[10] In order to solve this problem, monovalent QDs with a single binding site are required. Not only do the QDs have to be monovalent, but they must also remain small, bright stable, and biocompatible, which presents a significant challenge. This chapter will describe one method by which compact monovalent QDs can be synthesized and applied in a live-cell labeling context.

5.2 *Results and Discussion*

The key components enabling the purification of small monovalent QD using electrophoresis lies in the development of two key technologies: (1) a negatively charged PEGylated ligand that does not stick to cells and (2) monovalent streptavidin. The ligand utilized here (DHLA-carboxyPEG) was described in the previous chapter and comprises a dihydrolipoic acid moiety for QD binding, a PEG_8 group for water solubility and reduction of non-specific binding, and a carboxylic acid end-group for high electrophoretic mobility (Scheme 5-1). Streptavidin (SA) was used as the coupling partner, since it is a protein with sufficient molecular weight to produce conjugates that form distinct bands by gel electrophoresis, and SA also can be used for targeting. However, wild-type streptavidin is a tetramer with 4 biotin binding sites, so even 1:1 QD:SA conjugates will be multivalent.

In 2006, Howarth et al. reported a method by which monovalent streptavidin (mSA) could be engineered by disabling three of the four biotin binding sites, keeping only one active.[11] This was achieved via a targeted mutation on a SA subunit that disables the biotin binding site, producing a subunit that no longer binds biotin, but still engages in the self-assembly process that

forms the tetrametric SA protein. Thus, these "dead" (D) subunits would be mixed with the wild-type alive (A) subunits, forming statistical mixtures of A_xD_{4-x}, which could then be separated via a nickel-NTA column, as each D subunit also possessed a poly-histidine tag engineered for this purpose of purification. In this fashion, A1D3 monovalent streptavidin (mSA)

Scheme 5-1

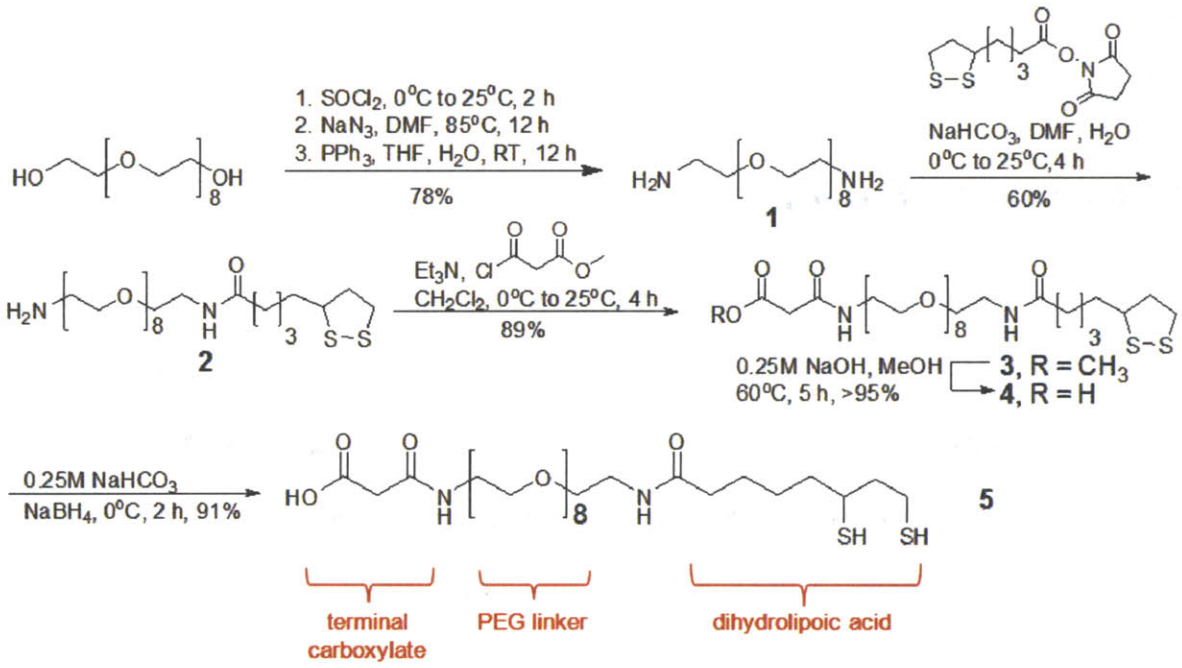

was synthesized, and the poly-histidine tags used for purification also served as a convenient method of conjugation to the QD surface. Thus, with the issue of multiple binding sites per SA solved, the challenge now lies in synthesis of the QD-mSA 1:1 conjugate.

Before going into the synthetic details, Figure 5-2 gives a big-picture overview of what is being achieved here relative to what has been accomplished previously. The state-of-the-art for cellular labeling using QDs prior to this thesis has been commercially available QDs that are large in size, multivalent, and required primary and secondary antibody interactions for targeting (Figure 5-2A). In this case, the entire targeting construct is on the order of 50 nm. The first

improvement came in the method of targeting, described in the previous chapter, which eliminated the need for bulky antibodies by directly utilizing the SA-biotin interaction with the development of the acceptor peptide (AP) and use of biotin ligase (BirA). Next, we re-engineered the QD surface coating to minimize its size, and now finally we are reducing the

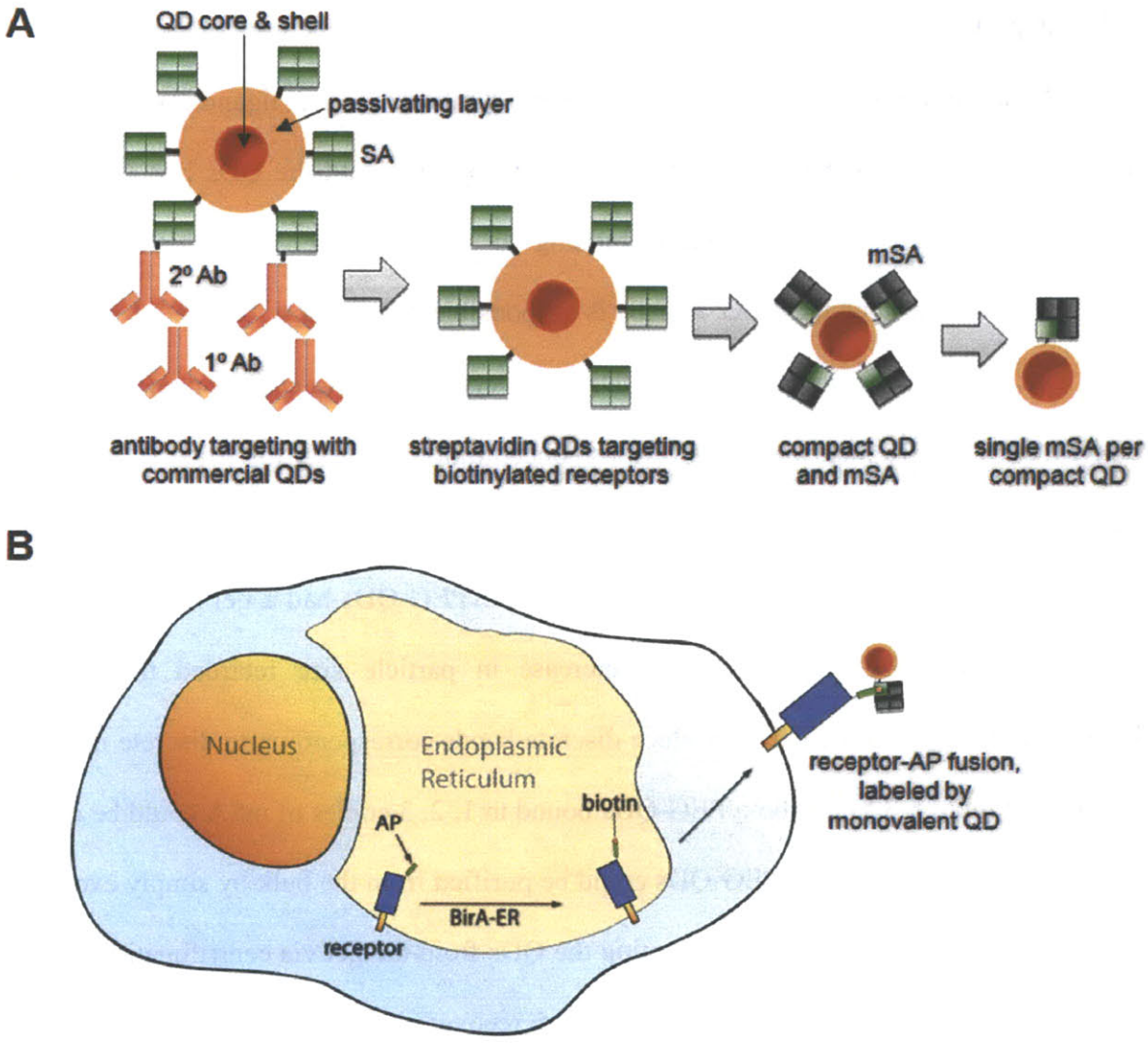

Figure 5-2 Evolution of QDs for cellular labeling. (A) Minimizing QD size and valency by going from large commercial multivalent QDs using anti-body interactions to small monovalent QDs bound to a single copy of mSA using only the SA-biotin interaction. (B) Site-specific biotinylation of AP-labeled receptors occurs within the ER using co-expressed BirA localized in the ER. Transport of labeled receptor to the cell surface then occurs, followed by labeling using QD-mSA.

number of binding sites per QD to just one. Figure 5-2B illustrates a further improvement in the labeling protocol described in the previous chapter. The receptor-AP construct is now biotinylated by co-expressed biotin ligase (BirA) localized in the ER, and the receptor is transported to the cell surface with the biotin already ligated, rather than by performing the biotin ligation with externally added BirA and biotin as was done previously. This advance improved the labeling protocol by reducing the number of steps required for labeling.[12]

605-nm emitting CdSe(CdZnS) QDs were synthesized and ligand exchanged using DHLA-CarboxyPEG. The HD in water was ~11 nm by DLS and the QDs had QY of ~40% while exhibiting negligible non-specific binding to cells, despite being highly negatively charged. We surmise that the PEG moiety is responsible for the low degree of non-specific binding, since negatively charged DHLA-QDs bind very strongly to cells non-specifically. The carboxyPEG-QDs were incubated with various concentrations of mSA for 1 h at RT and imaged by gel electrophoresis to probe the binding distribution. The gel mobility of QDs is determined by both particle size and charge. Unconjugated carboxyPEG-QDs had a gel mobility similar to 1kb DNA. Upon mSA conjugation, the increase in particle size retarded the motion of carboxyPEG-QDs within the gel to produce discrete bands corresponding to discrete numbers of mSA bound (Figure 5-3A). CarboxyPEG-QDs bound to 1, 2, 3 copies of mSA could be distinctly visualized. Monovalent carboxyPEG-QDs could be purified from the bulk by simply excising the band from the gel using a razor and extracting the QDs from the gel via centrifugation through a 200 μm filter. Generally this purification procedure recovers less than 35% of the gel, however, and the final QD concentration is ~500 nM with a volume of ~200 μL. This purified conjugate was found to be stable for at least 4 h under ambient conditions via repeated tests using gel electrophoresis.

In order to test that the purified conjugates were indeed monovalent, we performed a gel electrophoresis experiment using mono-biotinylated DNA (Figure 5-3B). Since DNA is highly negatively charged, a binding event between QD and DNA will cause a downward shift of the QD signal in the gel. At low biotin-DNA concentration, a single new band appeared and remained constant even with increasing biotin-DNA concentration. At the higher biotin-DNA concentrations, another band corresponding to excess DNA could also be visualized, but no additional QD bands appeared. This is consistent with the QDs being monovalent. If the carboxyPEG-QDs had 2 mSA attached, for example, then at higher biotin-DNA concentrations, one would expect the appearance of more bands, and this was not observed. Finally, to prove that the interaction is indeed specific between streptavidin and biotin, a QD sample pre-incubated with biotin showed no DNA binding even at high biotin-DNA concentration (Figure 5-3B, lane 6).

Another method we used to test whether the QDs were monovalent was by using atomic force microscopy (AFM). Both monovalent and multivalent carboxyPEG-QDs were incubated with mono-biotinylated DNA and deposited carefully onto freshly cleaved mica. Imaging with AFM under tapping mode revealed the height profiles of both QDs and DNA. In the case of the monovalent sample, most of the QDs in the field of view could be directly visualized as having a single DNA bound, while the multivalent QDs showed multiple DNA bound per QD. A height profile analysis shows heights of 5.8 nm and 0.8 nm for QDs and DNA, respectively, which is consistent with their expected values. Thus both the gel electrophoresis measurements and the AFM data are consistent with the QDs being truly monovalent.

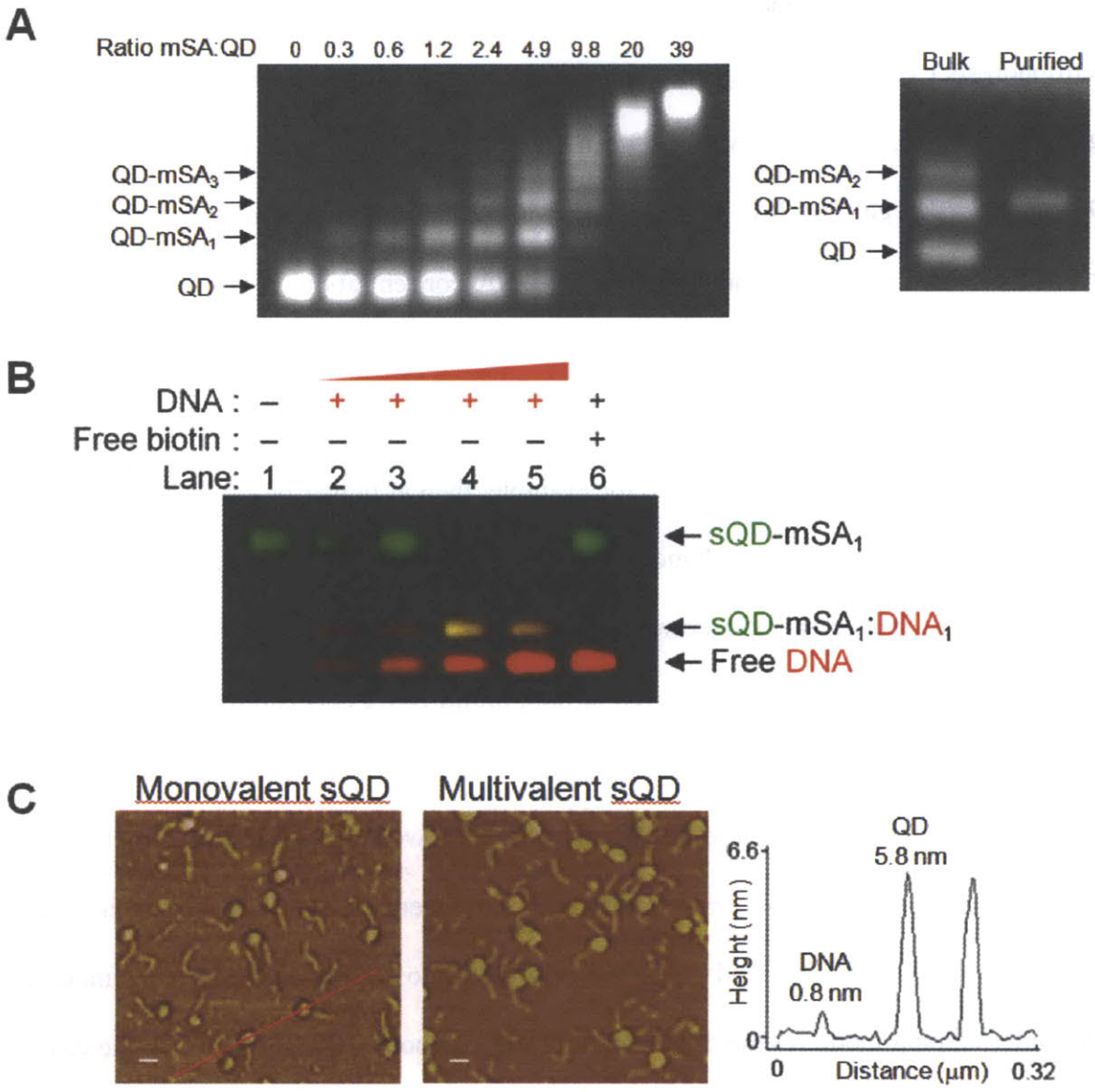

Figure 5-3 Generation and characterization of monovalent QDs. (A) Left: Change in carboxyPEG-QD mobility according to the number of mSA molecules attached. CarboxyPEG-QDs were incubated with mSA, separated on an agarose gel, and visualized under UV. Discrete bands corresponding to 0-3 copies of mSA per carboxyPEG-QD are indicated. Right: Monovalent carboxyPEG-QDs were purified from a bulk mixture of carboxyPEG-QD-mSA conjugates. (B) Testing valency by gel shift assay. QD-mSA_1 was incubated with varying amounts of mono-biotinylated DNA (for lanes 1-6: 0, 47, 95, 190, 380, and 190 nM DNA) and analyzed by agarose gel electrophoresis. As a control, QD-mSA_1 was pre-blocked with free biotin (lane 6), to show the specificity of QD-DNA binding. QD emission is colored green, DNA is colored red, and yellow shows the overlap. (C) Testing valency by AFM. Purified QD-mSA_1 (monovalent carboxyPEG-QDs) or multivalent carboxyPEG-QDs conjugated to ~6 copies of mSA were incubated with 3-fold excess mono-biotinylated DNA and imaged by AFM. The height profile along the red line is plotted in the right panel. Scale-bar, 25 nm.

The advantage being advertised here lies in having QDs that are both small and monovalent. Each part of the claim can be tested independently. In order to test whether smaller QDs are indeed better than their larger commercial counterparts, we performed a labeling experiment to see if smaller QDs could better access the crowded region between neuronal synapses. Howarth et al. attached an AP tag to the rat GluR2 subunit of the AMPA-type glutamate receptor, which localizes in the post-synaptic membrane. Labeling was performed with both commercially available Invitrogen QD-SA and carboxyPEG-QD-mSA and compared against a control Alexa-mSA conjugate.[12] In this case the QD-mSA were not purely monovalent,

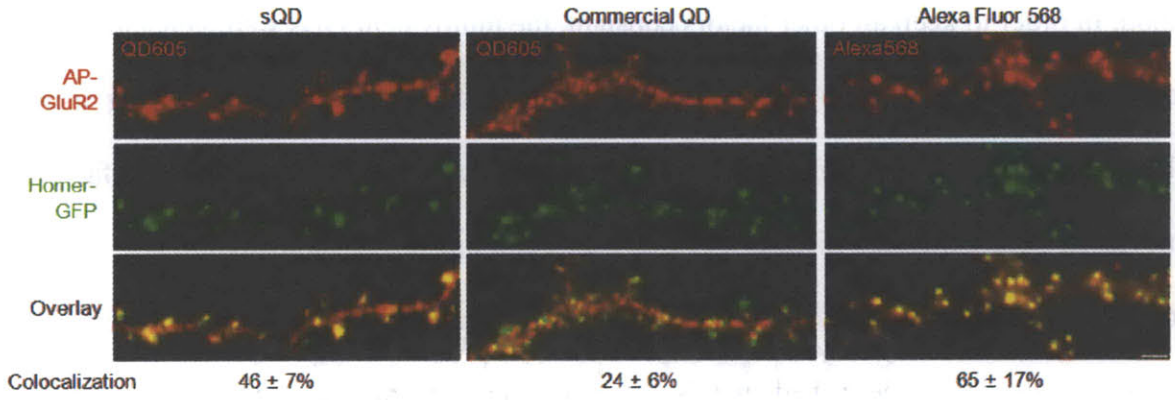

Figure 5-4 Fluorescence micrographs of hippocampal neurons transfected with plasmids encoding AP-GluR2, BirA-ER and the post-synaptic market Homer-GFP. Biotinylated AP-GluR2 was labeled at the cell surface with QD-mSA1, commercial QD605-SA, or mSA-Alexa Fluor 568 and imaged live. Yellow shows the overlap between red QD- or Alexa-labeled GluR2, and green Homer puncta. Scal bar, 1 μm. Error, ± 1 s.d. (n = 6)

but contained on average one mSA per QD. The Alexa dye conjugate represents the smallest possible probe and was used here as a best-case-scenario control. In addition, the synapse could be independently visualized via a post-synaptic marker, Homer-GFP. Thus, QDs which are able to enter the post-synaptic space will be colocalized with the GFP signal under fluorescence microscopy, and the degree of colocalization can be quantified by comparing the overlap between the QD and GFP channels.

The results of the labeling experiment are shown in Figure 5-4. The small QD-mSA construct showed ~46% colocalization with the post-synaptic marker, while the commercial QDs showed only ~24% colocalization. By comparison, the control Alexa-mSA construct showed ~65% colocalization, which represents the smallest possible labeling construct. By this measurement, the smaller carboxyPEG QDs offers much better access to the neuronal synapse vs commercial QDs and is even comparable to the Alexa dye control.

In order to test the hypothesis that receptor crosslinking can activate unwanted cellular signaling pathways, monovalent QDs were compared directly to multivalent QDs in the same work by Howarth et al.[12] where the EphA3 cell surface receptor was labeled using the AP-tag method. In order to keep all other factors constant, the multivalent QDs were generated from the same carboxyPEG-QDs bound to multiple copies of mSA (~6 copies). Labeling using the multivalent QDs produced clear clustering of the EphA3 receptor on the cell surface, while monovalent QDs generated diffuse labeling.[12] In addition, in the multivalent case, more QDs were internalized into the cell, which indicates receptor activation. In a separate experiment, the same monovalent QDs described in this thesis was used to measure the rate of diffusion of mutant vs wild-type low-density lipoprotein (LDL) receptors via single molecule imaging, demonstrating that the monovalent QD-mSA construct is not only able to achieve high affinity targeting, reduced receptor activation, and small size, but it was also bright enough and non-sticky enough to enable single molecule tracking, which was the ultimate goal.

In conclusion, we have developed a robust method for generating small QDs with a single copy of monovalent streptavidin for high affinity labeling and single molecule tracking. These new smaller QDs were able to better access tight spaces such as the neuronal synapse compared with commercial QDs and the use of monovalent QDs also prevented receptor

clustering and subsequent receptor activation compared to multivalent QDs in cell surface receptor targeting. In addition, the strategy used to make monovalent nanoparticles can be broadly generalized to purify to 1:1 QD-molecule conjugates using any molecule greater than 50 kDa by the gel electrophoresis method described here. The small size, combined with the monovalency represents an evolution in QD technology as probes for biological applications and will be used in the future for more unambiguous elucidation of complex biological problems.

5.3 *Experimental Methods*

Preparation of carboxyPEG-QDs and analysis of monodispersity. Exchange of the native TOPO/TOP surface ligands on QDs for the PEG-derivatized ligand **5** was carried out according to previously reported procedures[3], with several modifications. To 0.2 mL of QDs in growth solution was added MeOH to the point of turbidity. After centrifugation and decantation, 50 μL of neat **5** and 10 μL of MeOH were added. The mixture was stirred at 60 °C overnight and precipitated by adding 0.3 mL ethanol, 0.05 mL chloroform, and 0.5 mL hexane in succession. Centrifugation at 3,000 g for 4 min yielded a clear supernatant, from which the ligand was recovered. The pellet was dispersed in 0.5 mL of PBS and filtered through a 0.2 μm filter. The sample was purified using gel filtration chromatography (GFC) in order to narrow the size distribution and concentrated at 3,500 g using a Vivaspin-6 10,000 MWCO spin concentrator (Vivaproducts). GFC was performed using an ÄKTAprime Plus chromatography system (Amersham Biosciences) equipped with a Superose 6 10/300 GL column. PBS pH 7.4 was used as the mobile phase with a flow rate of 0.5 mL/min. Typical injection volumes were 500 μL. Detection was achieved by measuring the absorption at 280 nm, and the fluorescence spectrum at set time intervals was simultaneously recorded using a SD2000 fiber optic spectrometer with excitation at 460 nm from a LS-450 LED light source (Ocean Optics).

Purification of monovalent carboxyPEG-QDs. 8 μM carboxyPEG-QDs in PBS were incubated with the indicated volumes of monovalent streptavidin (mSA, 19 μM) or PEG-scFv antibody (13 μM) in PBS in a total volume of 5 μL for 1 h at 24 °C. mSA was prepared as described[4]. mSA and PEG-scFv each contained a single His_6-tag that stably binds to the ZnCdS shell[5]. Addition of 1-ethyl-3-diisopropylaminocarbodiimide did not change the conjugation efficiency (data not shown). Analysis of QD-protein conjugation was performed by electrophoresis using a Minicell Primo (Thermo) with 1% Omnipur agarose (EMD) in 10 mM $Na_2B_4O_7.10H_2O$ (adjusted to pH 8.0 using 1 M HCl) at 7.9 V/cm for 15 min. 6x loading buffer (16% sucrose in ddH_2O) was added to samples before loading. For purification, buffer was cooled on ice, the electrophoresis apparatus was surrounded in ice, and the gel was run at 6.4 V/cm for 20 min. Gels were visualized under 305 nm UV with a ChemiImager 5500 (Alpha Innotech Corporation) for analysis, or with the naked eye under ambient light for purification. Bands of interest were excised with a scalpel, placed in a Nanosep MF 0.2 μm filter (Pall), and centrifuged at 5,000 g for 1 min at 24 °C. This centrifugation eluted the buffer and QD-protein conjugates from the agarose into the collecting tube below. Band purity was quantified with ChemiImager 5500 software. Typically, QD-mSA_1 preps started from 120 pmol carboxyPEG-QDs and 120 pmol mSA. Conjugation with mSA is stochastic and so ~40 pmol were monovalent. Extraction efficiency from agarose was 30-50% (data not shown), giving a typical final yield of ~12-20 pmol QD-mSA_1.

Dynamic Light Scattering measurements of QD size. QD size was measured using a DynaPro™ Dynamic Light Scatterer (DLS) (Wyatt Technology Corporation). All samples were at 0.5-2 μM and filtered through a Nanosep MF 0.2 μm filter (Pall) before analysis. Typical count rates were 85-150 kHz. Each autocorrelation function was acquired for 10 s, and averaged

for 10 min per measurement. A software filter was employed to discard all autocorrelation function fits with sum of squares errors >15. The resulting autocorrelation function was fitted using Dynamics V6 software (Wyatt Technology Corporation), employing a non-negative least squares fitting algorithm. Hydrodynamic diameter was obtained from a mass-weighted size distribution analysis and reported as the mean of triplicate measurements. The antibody used for DLS was a mouse IgG1 to the truncated Nerve Growth Factor Receptor, obtained by Protein G affinity purification from the supernatant of B cell hybridoma 8737 (ATCC) and dialyzed into PBS.

Gel shift analysis of QDs with mono-biotinylated DNA. 236 bp mono-biotinylated DNA was generated by PCR from pIVEX-BirA (a gift from A. Griffiths, MRC Laboratory for Molecular Biology) using Taq DNA polymerase with the primers 5' biotin-triethylene glycol-GCGTTGATGCAATTTCT (Eurogentec) and primer S (5'TGGCTGCTGCCACCGCTG), using the conditions 95 °C 30 s, 50 °C 30 s, 72 °C 1 min for 27 cycles. The PCR product was purified from a 2% agarose gel using a QIAquick gel extraction kit (Qiagen). Varying amounts of 190 nM mono-biotinylated DNA were incubated in 100 mM sodium borate pH 8.0 for 10 min at 24 °C with 60 nM QD-mSA$_1$. To visualize QDs and DNA separately, we used carboxyPEG-QDs emitting at 545 nm, generated exactly as for carboxyPEG-QDs emitting at 605 nm but with smaller CdSe cores[11]. As a negative control to block DNA binding, QD-mSA$_1$ was pre-incubated for 5 min with 10 μM biotin. Samples were then mixed with 6x loading buffer (16% sucrose in ddH_2O) and run using a Minicell Primo (Thermo) on a 0.9 % Omnipur agarose (EMD) gel, cast with 0.5 μg/mL ethidium bromide, at 7.9 V/cm for 15 min in TAE buffer. Gels were visualized under 365 nm UV with a ChemiImager 5500, using an ethidium bromide filter (Alpha Innotech) to see DNA, and a GFP filter (Alpha Innotech) to see carboxyPEG-QDs.

AFM of QDs. 119 bp mono-biotinylated DNA was prepared by PCR as above, except primer S was replaced with primer XS (5'GTCGCCATGATCGCGTAGT). 9 nM of this mono-biotinylated DNA, prepared as above, was incubated with 3 nM QD sample for 1 h at 24 °C in 10 mM sodium borate pH 7.3. 20 μL 0.1 % poly-L-lysine (MW 500-2000) (Sigma) was pipetted on freshly cleaved muskovite mica V2 (Electron Microscopy Sciences). After incubation for 3 min, the mica was washed with 1 mL of water and dried in a nitrogen stream. 20 μL DNA-QD complex was pipetted onto the mica. After 6 min, the mica was rinsed with 1 mL of water and dried in a nitrogen stream. The mica was imaged using a Dimension 3100 AFM (Digital Instruments) in tapping mode, using an etched TESP silicon probe with a nominal tip radius of < 10 nm (Veeco Probes) operating at a resonant frequency of 273.3 kHz. Height and phase images were collected simultaneously across a 1 x 1 μm area, at a scan rate of 2 Hz and a resolution of 256 x 256 pixels. The resulting images were analyzed using Nanoscope v 5.30 software (Digital Instruments) and the phase image is displayed.

Receptor biotinylation. For biotinylation by recombinant biotin ligase, cells were incubated in PBS 5mM $MgCl_2$ with 2.6 μM biotin ligase and 10 μM biotin-AMP at 24 °C for 10 min, as previously described.[4] Cells were then washed 4x with PBS and incubated for 5 min at 24 °C with 20 nM QDs in PBS with 0.5% dialyzed bovine N,N-dimethyl casein (Calbiochem). Cells were washed 3x in PBS and imaged in PBS at 24 °C. For imaging of cells expressing BirA-ER[17, 18], cells were incubated in growth medium supplemented with 10 μM biotin (Tanabe USA) from 4 h after transfection. The next days cells were washed 4x in PBS and incubated for 5 min at 24 °C with 20 nM monovalent QDs in PBS with 0.5% casein. For specificity testing, cells were incubated with monovalent streptavidin-Alexa Fluor 568, prepared as described[4] at 100 nM

in PBS with 1% dialyzed Bovine Serum Albumin for 10 min at 4 °C. Cells were then washed 3x in PBS and imaged live.

5.4 *References*

1. Pons, T.; Medintz, I. L.; Wang, X.; English, D. S.; Mattoussi, H., Solution-phase single quantum dot fluorescence resonance energy transfer. *Journal of the American Chemical Society* **2006,** 128, (47), 15324-15331.

2. Claridge, S. A.; Liang, H. Y. W.; Basu, S. R.; Frechet, J. M. J.; Alivisatos, A. P., Isolation of discrete nanoparticle - DNA conjugates for plasmonic applications. *Nano Letters* **2008,** 8, (4), 1202-1206.

3. Pellegrino, T.; Sperling, R. A.; Alivisatos, A. P.; Parak, W. J., Gel electrophoresis of gold-DNA nanoconjugates. *Journal of Biomedicine and Biotechnology* **2007**.

4. Pellegrino, T.; Sperling, R. A.; Alivisatos, A. P.; Parak, W. J., Gel electrophoresis of gold-DNA nanoconjugates. *J Biomed Biotechnol* **2007,** 2007, 26796.

5. Worden, J. G.; Dai, Q.; Shaffer, A. W.; Huo, Q., Monofunctional group-modified gold nanoparticles from solid phase synthesis approach: Solid support and experimental condition effect. *Chemistry of Materials* **2004,** 16, (19), 3746-3755.

6. Sung, K. M.; Mosley, D. W.; Peelle, B. R.; Zhang, S. G.; Jacobson, J. M., Synthesis of monofunctionalized gold nanoparticles by Fmoc solid-phase reactions. *Journal of the American Chemical Society* **2004,** 126, (16), 5064-5065.

7. Zanchet, D.; Micheel, C. M.; Parak, W. J.; Gerion, D.; Alivisatos, A. P., Electrophoretic isolation of discrete Au nanocrystal/DNA conjugates. *Nano Letters* **2001,** 1, (1), 32-35.

8. Claridge, S. A.; Goh, S. L.; Frechet, J. M. J.; Williams, S. C.; Micheel, C. M.; Alivisatos, A. P., Directed assembly of discrete gold nanoparticle groupings using branched DNA scaffolds. *Chemistry of Materials* **2005,** 17, (7), 1628-1635.

9. Klemm, J. D.; Schreiber, S. L.; Crabtree, G. R., Dimerization as a regulatory mechanism in signal transduction. *Annual Review of Immunology* **1998,** 16, 569-592.

10. Iino, R.; Koyama, I.; Kusumi, A., Single molecule imaging of green fluorescent proteins in living cells: E-cadherin forms oligomers on the free cell surface. *Biophysical Journal* **2001,** 80, (6), 2667-2677.

11. Howarth, M.; Chinnapen, D. J. F.; Gerrow, K.; Dorrestein, P. C.; Grandy, M. R.; Kelleher, N. L.; El-Husseini, A.; Ting, A. Y., A monovalent streptavidin with a single femtomolar biotin binding site. *Nat Meth* **2006,** 3, (4), 267-273.

12. Howarth, M.; Liu, W.; Puthenveetil, S.; Zheng, Y.; Marshall, L. F.; Schmidt, M. M.; Wittrup, K. D.; Bawendi, M. G.; Ting, A. Y., Monovalent, reduced-size quantum dots for imaging receptors on living cells. *Nat. Methods* **2008,** 5, (5), 397-399.

Chapter 6: Design and Synthesis of Polymeric Imidazole-based Ligands (PILs) via RAFT Polymerization for Ultra-stable Compact Biocompatible QDs*

6.1 *Background and Motivation*

As discussed in Chapter 4, a major barrier towards the wide-spread use of QDs has been the presence of a trade-off among five desirable QD properties for fluorescence labeling in live cells and *in-vivo*: small size, high stability (both over time and in a wide pH range), high QY, facile derivatizabilty, and low non-specific binding. While it has been possible to achieve three or four of these criteria, achieving all five simultaneously has proven challenging for ligand design. Commercial QDs encapsulated with PEGylated amphiphilic polymer coatings are easily derivatizable and are suitable for single molecule imaging,[1, 2] but suffer from large hydrodynamic diameters (20 – 30 nm),[3] which can limit the access of QDs to crowded regions such as the neuronal synapse (as seen in Chapter 5), as well as potentially alter the native behavior of labeled receptors.[4-6] Smaller QDs have been achieved via ligand exchange with thiol-bearing molecules, but suffer from instability due to the weak interaction of mono-thiols with the QD surface.[7, 8] Recently, our group and others[9-12] have demonstrated increased interaction of thiol ligands with QDs by exploiting the bidentate binding motif using dihydrolipoic acid (DHLA) to furnish a new class of aqueous DHLA-PEG modified QDs that are compact, biocompatible, derivatizable, and exhibit very low non-specific binding. Notwithstanding, most

---

* Much of this chapter has appeared in print. It is reproduced with permission from *J Am Chem Soc* 2009, **132**: 472-483.

thiol-based coordinating ligands are inherently unstable owing to the oxidation and dimerization of the thiol groups, causing the ligands to detach from the QD surface over time (*vide infra*). We now report a new class of multidentate poly-imidazole ligands that obviate the need for thiols while maintaining the attractive properties of small size, low non-specific binding, derivatizability, and high QY. Here, we use the term multidentate to indicate a polymer with pendant groups that can bind to multiple sites on the QD surface, as opposed to multiple coordination of individual surface atoms, which has been posited in the case of poly-histidine coordination,[13] but is not necessarily apt to the present case.

Poly-histidine motifs have been shown to exhibit high affinity towards the Cd and Zn rich QD surface, and His_6-tags have been employed for facile and efficient derivatization of QDs with short peptides, dyes, and proteins.[13-16] Pendant imidazole groups in copolymer microgels have also been shown to stabilize organic soluble QDs.[17] From these observations, we hypothesized that a polymer that is rich in imidazole groups along the backbone should efficiently bind to the QD surface. Poly-imidazole is resistant to degradation by oxidation and its multidentate binding motif can greatly enhance stability.[18-20] To promote water solubility, prevent aggregation, and reduce non-specific binding,[21] we opted to pursue a strategy to co-polymerize a PEG-derived monomer, and described herein is the synthesis of a random brush copolymer architecture displaying both PEG and imidazole groups along the polymer backbone. Adding an additional monomer featuring either amine or biotin functional groups affords a 3-component multi-functional copolymer to yield QDs that are water soluble and derivatizable. Copolymer based ligands with multidentate pendant binding groups to the QD surface have been previously reported, but suffered from either limited water solubility, aggregation, low QY, and/or a lack of a functional handle for further covalent derivatization, or do not demonstrate the

low non-specific binding to cells or to serum proteins that are required for the most interesting biological applications.[17, 18, 22-24] In this report we seek to extend the previous work by optimizing our polymer system for biological compatibility as per the previously outlined desired properties for *in-vivo* and *in-vitro* applications. In order to achieve molecular weight control and narrow polydispersity of the proposed copolymer, we employed RAFT (radical addition fragmentation chain transfer) polymerization chemistry, which offers the further ability to mediate the controlled co-polymerization of a wide library of monomers.[25] By varying the ratio and composition of monomers, complex copolymers can be assembled to give compact, water-soluble QDs with tunable surface properties. QDs prepared with these new ligands exhibit extremely low non-specific binding to serum and greatly enhanced stability and long-term shelf-life, making them optimal for live cell and *in-vivo* imaging.

6.2 *Results and Discussion*

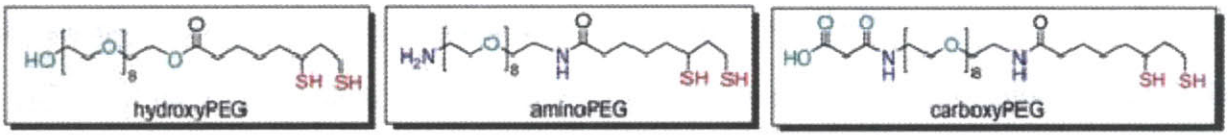

Figure 6-1 Chemical structures of DHLA-PEG derived ligands for QD water solubilization.

The design and synthesis of multidentate polymeric imidazole ligands (PILs) was undertaken to overcome the long-term instability of DHLA based ligands. Figure 6-2 shows the gel electrophoresis of various DHLA based carboxyPEG (Figure 6-1) coated QDs. When initially prepared, DHLA-carboxyPEG QDs exhibit sharp bands by gel electrophoresis, and a titration of increasing amounts of His_6-tagged monovalent streptavidin (mSA) produced discrete bands.[14] As reported, high-affinity cell labeling with low non-specific binding is achieved upon prompt use of the QD-mSA conjugates. However, the same conjugation experiment conducted

on DHLA-carboxyPEG QDs stored for ~1 week in the dark at 4 °C exhibits broadened bands, indicating a fluctuation in charge owing to a heterogeneous distribution of ligand density, most likely due to ligand detachment from the QD surface (Figure 6-2). Along with band broadening by gel electrophoresis, we observed a concomitant increase in non-specific binding to HeLa cells (data not shown), consistent with loss of ligand binding to the QDs. These deficiencies are ameliorated by the replacement of the thiol ligand with that of a polymeric imidazole ligand described below.

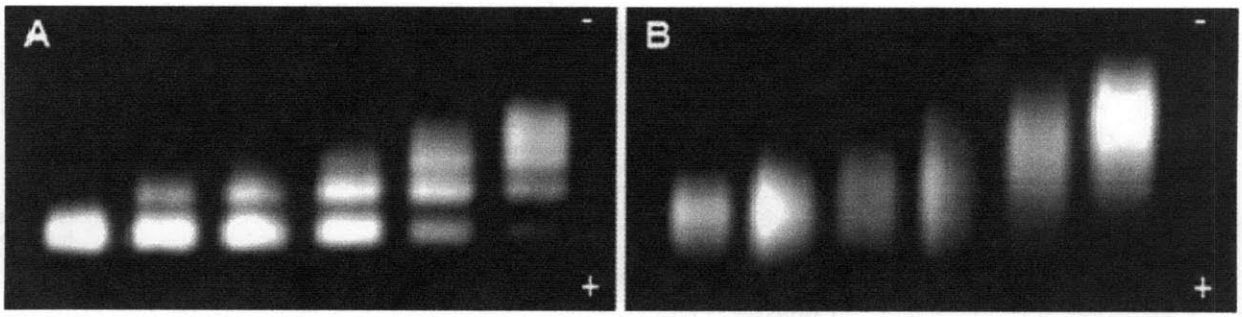

Figure 6-2 Instability of DHLA-PEG derived ligands over time. Gel electrophoresis of DHLA-carboxyPEG QDs (A) after initial ligand exchange and (B) after 1 week storage at 4 °C in the dark, with increasing titration of His6-Tagged monovalent streptavidin from left to right showing sharp and discrete bands in the initially prepared sample, but loss of fidelity after storage. QDs in (B) also exhibit increased non-specific binding to cells (data not shown).

6.1.1 Monomer Synthesis and Polymerization

Scheme 6-1 presents the synthetic strategy that was pursued to deliver the monomers for polymerization. Acrylic acid is coupled to primary amine bearing moieties via an amide bond forming reaction. Conjugate addition to the vinyl group was minimized by first preparing the NHS-ester of acrylic acid (**2**), and allowing the coupling reaction to proceed at 4 °C for only 30 min, upon which complete consumption of the starting materials was confirmed by TLC. Monomer **3** containing the imidazole group for QD binding was obtained from the reaction of

histamine with **2**. Since the trithiocarbonate RAFT agent **12** used in subsequent polymerization

Scheme 6-1

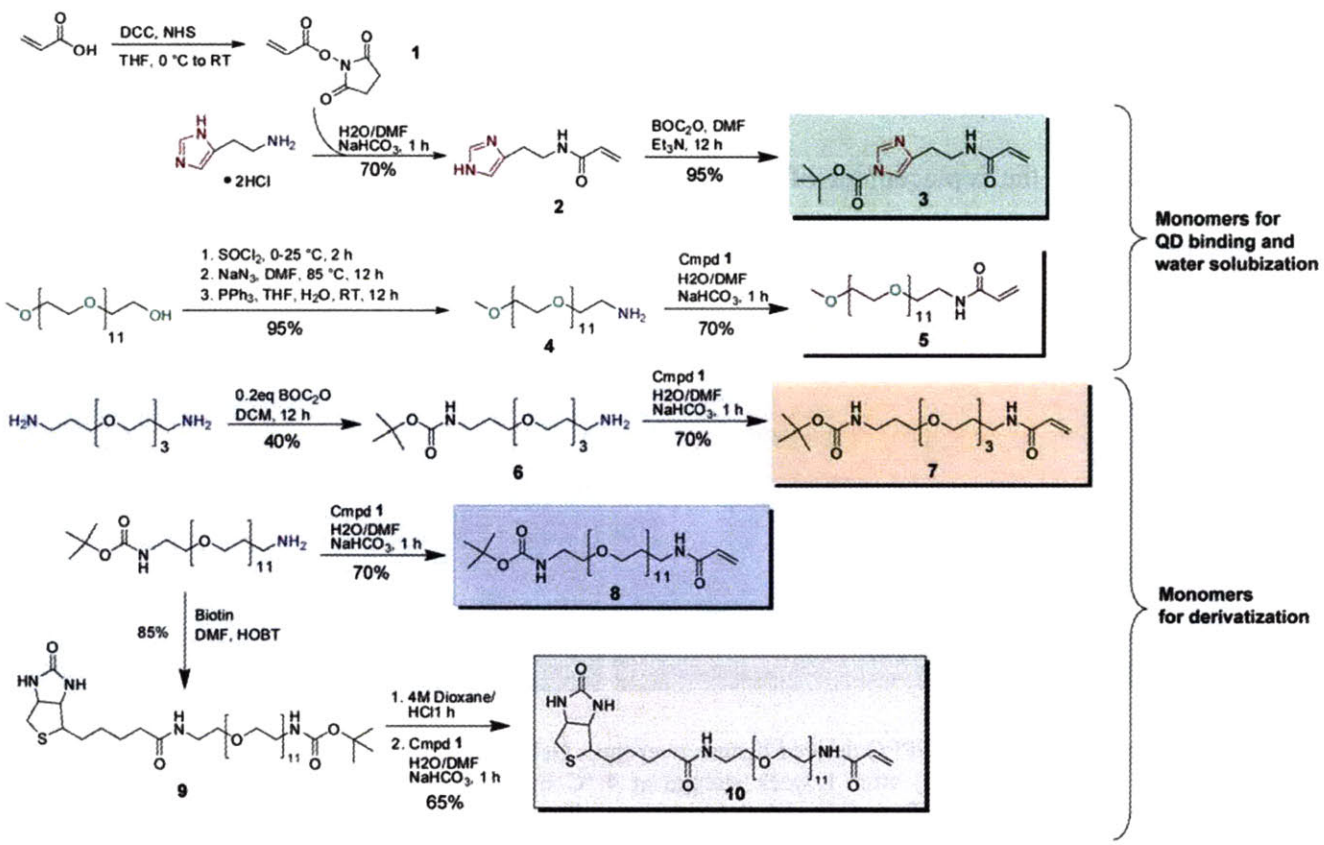

reactions[26] is highly sensitive towards degradation by aminolysis, the imidazole nitrogen was BOC protected to yield the final monomer **4**. Likewise, monomer **6** containing a PEG_{11} group for water solubility was obtained first via the conversion of the terminal hydroxyl group of mono-methoxy PEG to a primary amine **5**, followed by reaction with **2**. Monomers **8** and **9** with BOC-protected terminal amines were also synthesized in order to afford polymers bearing primary amine groups for derivatization with FRET dyes or proteins. Finally, to demonstrate the scope of monomer incorporation in the polymerization reaction scheme, monomer **11** was synthesized to

give polymers functionalized with biotin for binding assays. For each of the monomers, formation of an amide bond, as opposed to an ester bond, was necessary in order to circumvent the possibility of ester hydrolysis under the acidic BOC deprotection conditions following polymerization, and also to afford higher stability in the presence of hydrolytic enzymes for *in-vivo* and *in-vitro* applications. The reaction of monomers **4**, **6**, and **8** shown in Scheme 2 is representative of all polymerization reactions used in this study. The monomer mixture typically consists of 50% mole fraction of monomer **4** to ensure that there are enough imidazole groups for effective binding to the QD surface, with the remaining 50% mole fraction consisting of some mixture of monomer **6** (for water solubility), along with one of monomers **8**, **9**, or **11** (for derivatizability). In order to minimize the potential of long polymer chains cross-linking and aggregating QDs during ligand exchange, the polymer MW was kept low, with a targeted degree of polymerization (DP) below 30. test

6.1.2 RAFT Polymerization

One of the most versatile methods for controlled free radical polymerization is reversible addition fragmentation chain transfer (RAFT) polymerization, which has paved the way for the synthesis of complex architectures, including block copolymers, dendrimers, and star structures with low polydispersity and targeted molecular weights. The unprecedented flexibility of RAFT allows it to polymerize a wide range of monomers, including (meth)acrylics, vinyl alcohol, vinyl pyridine and acrylamides.[25] The mechanism, described in (Scheme 6-2), involves the introduction of a chain transfer agent (CTA) into an otherwise conventional free radical polymerization reaction. The CTA, typically a dithioester compound, undergoes degenerative chain transfer in the form of a fast equilibrium between the propagating radical species $P_n^{\bullet}$ and

Scheme 6-2

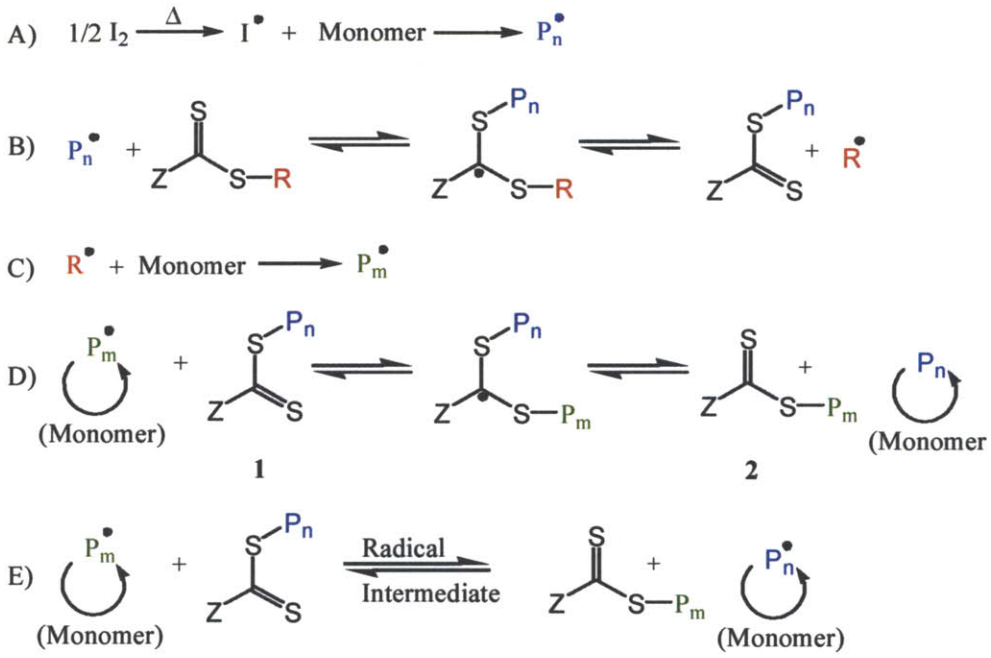

$P_m^{\bullet}$, and the dormant species **1** and **2** (Scheme 6-2, Step D). The rate of this chain transfer, determined largely by the radical stabilizing group **Z**, is on the same timescale as that of radical propagation, which gives the polymerization its controlled nature. This results in a polymer with a very narrow molecular weight distribution, and also leaves the polymer architecture with well defined end groups **R** and **Z-(S=C)-S-**. The polymer molecular weight can be tuned in one of two ways: (1) by changing the degree of polymerization (DP), or (2) by changing the [Monomer]:[RAFT] concentration ratio. The DP can be tuned by either changing the reaction time or reaction temperature. The monomer and RAFT concentration ratios can be used to estimate the final polymer molecular weight according to the following expression in the simplest case:

$$P_{MW} = \frac{[Monomer]}{[RAFT]} \times M_{mw} \times (\%\, Conversion) \qquad \textbf{(6-1)}$$

where the first term represents the ratio of concentrations of the monomer and RAFT agent, the second term is the molecular weight of the monomer, and the third term is the percent conversion from monomer to polymer. The percent conversion can be quantitatively measured via H^1 NMR spectroscopy by monitoring the disappearance of the vinyl peaks in the original monomer.

Scheme 6-3

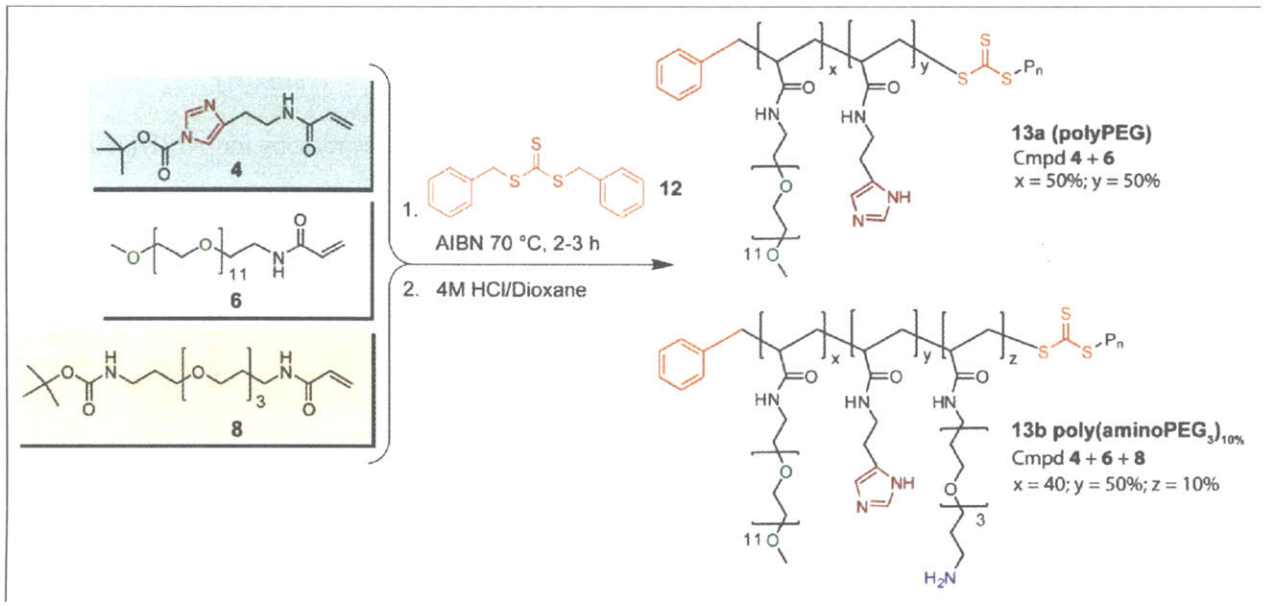

RAFT polymerization can be carried out with any number of conventional radical initiators. These are typically thermally activated and include AIBN, azobis(2-cyanopentanoic acid), and $K_2S_2O_8$.[27] In our case, AIBN was used as the initiator in the presence of the RAFT agent **12** to afford a controlled living polymerization.[26] Using an [AIBN] : [RAFT]:[Monomer] ratio of 0.25:1:28 and an equimolar mixture of monomers **4** and **6** (Scheme 6-3, polymer **13a**), the overall polymer conversion over time as monitored by ^{1}H-NMR spectroscopy (Figure 6-4) followed a linear relationship, achieving >80% conversion after 10 h (Figure 6-3A). Increasing the [AIBN] : [RAFT] ratio to 1:1 resulted in a non-linear conversion efficiency versus time, yielding >90% conversion after 2 h (Figure 6-4B); interestingly, a low PDI and good molecular

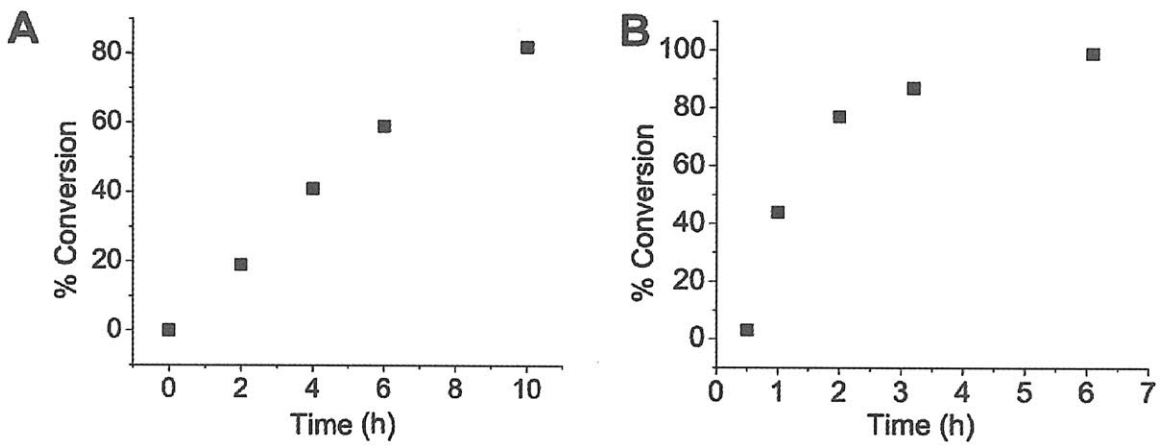

Figure 6-3 Polymerization Kinetics of poly(PEG) as monitored by 1H-NMR spectroscopy for [AIBN]/[RAFT] ratio of (A) 0.25:1 and (B) 1:1.

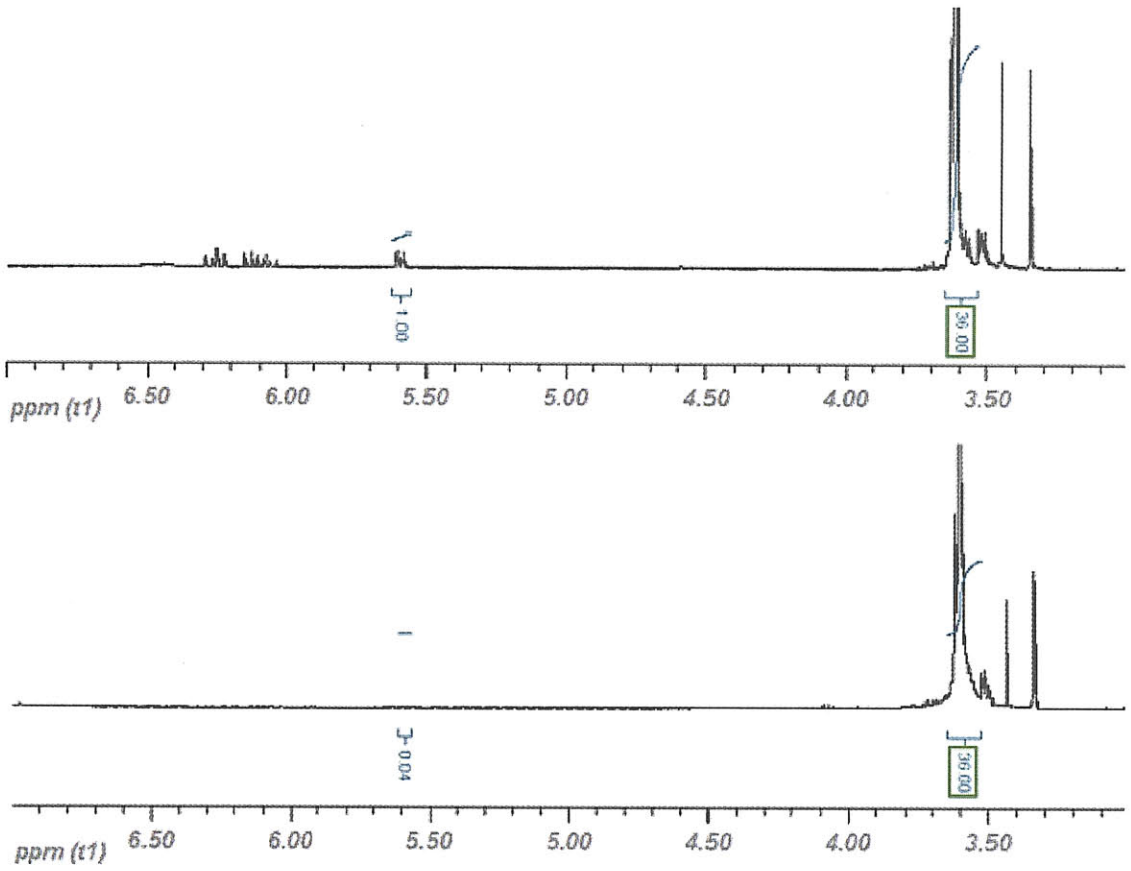

Figure 6-4 ^{1}H-NMR spectrum of monomers 4 and 6 mixed in a 1:1 molar ratio (top) before polymerization, and (bottom) after 4 h polymerization, showing >95% conversion.

weight control was maintained (*vide infra*). The plot of [Monomer] : [RAFT] ratio versus measured polymer DP using GPC followed a linear relationship, showing good MW control (Figure 6-5A), and a narrow PDI <1.2 (Figure 6-5B) was observed. Figure 2A shows that the targeted DP of <30 for copolymer **13a** was achieved using [Monomer]:[RAFT] ratios between 20 to 33:1, as measured by GPC. The same polymerization carried out in the absence of RAFT agent yielded a poorly controlled polymer (PDI > 3), confirming that the RAFT agent is responsible for mediating polymerization even under high relative initiator concentrations (Figure 6-5B). Because controlled polymerizations could be performed even under the relatively high [AIBN]/[RAFT] ratio of 1:1, new polymers could be rapidly prototyped due to the short reaction times required for near-complete polymer conversion.

Nomenclature for PILs	**Polymer ligand composition by mole %**
Poly(PEG)	50% Cmpd **6** / 50% Cmpd **4**
Poly(aminoPEG$_3$)$_{10\%}$	10% Cmpd **8** / 40% Cmpd **6** / 50% Cmpd **4**
Poly(aminoPEG$_{11}$)$_{25\%}$	25% Cmpd **9**/ 25% Cmpd **6**/ 50% Cmpd **4**
Poly(biotinPEG)$_{25\%}$	25% Cmpd **11**/ 25% Cmpd **6**/ 50% Cmpd **4**
Nomenclature for DHLA-based ligands	
hydroxyPEG	DHLA-PEG$_8$-OH
carboxyPEG	DHLA-PEG$_8$-COOH
aminoPEG	DHLA-PEG$_8$-NH$_2$

Table 6-1 Nomenclature of compounds used in this chapter.

The nomenclature of copolymer ligands used in this study is outlined in Table 6-1. For QD water solubilization, all polymer MWs were typically ~14 kDa with PDI <1.2 as measured by GPC calibrated using polystyrene MW standards. Since the relative reaction rates of the monomers within the co-polymerization mixture could not be determined due to overlapping NMR signals of the monomers, polymerizations were performed to >90% conversion efficiency to ensure the incorporation of all monomers in the mixture. It is not known whether the monomers are incorporated in a statistical fashion, or if there is some local ordering of monomer

units in the polymer microstructure. Further studies could be performed to measure the kinetics of each individual monomer unit in order to get a better idea of local ordering effects. An advantage of the class of polymers presented here for QD ligand exchange is that these ligands

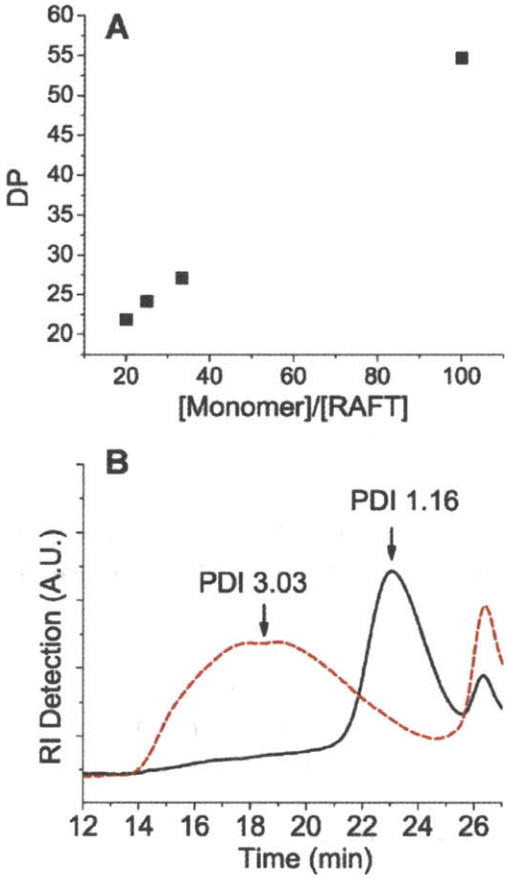

Figure 6-5 RAFT polymerization of 13a showing (A) tunable polymer DP as a function of [Monomer] to [RAFT] ratio. (B) GPC of polyPEG in DMF, showing narrow polydispersity with a [Monomer]:[RAFT] ratio of 30:1 and [AIBN]:[RAFT] ratio of 1:1 (—, black), and poor MW distribution without RAFT agent (---, red).

are amenable to long-term storage under ambient conditions without special precautions against degradation, unlike DHLA based ligands, which slowly oxidize over time and often need to be carefully stored in the dark at 4 °C.

6.1.3 Ligand Exchange and Characterization of Aqueous QDs

Ligand exchange of 605 nm emitting CdSe(CdZnS) core(shell) QDs[12] using poly(PEG)-PILs was performed by displacing the native hydrophobic ligands with the imidazole groups along the polymer backbone, which can participate in multiple binding interactions with the Cd and Zn rich QD surface. Ligand exchange conditions were relatively mild, and involved stirring a mixture of QDs and poly(PEG)-PILs in a solution of chloroform at RT, followed by addition of methanol and precipitation using chloroform and hexanes. The QDs were dispersed in water and then purified by dialysis. Complete ligand displacement was achieved within 1 h, and was

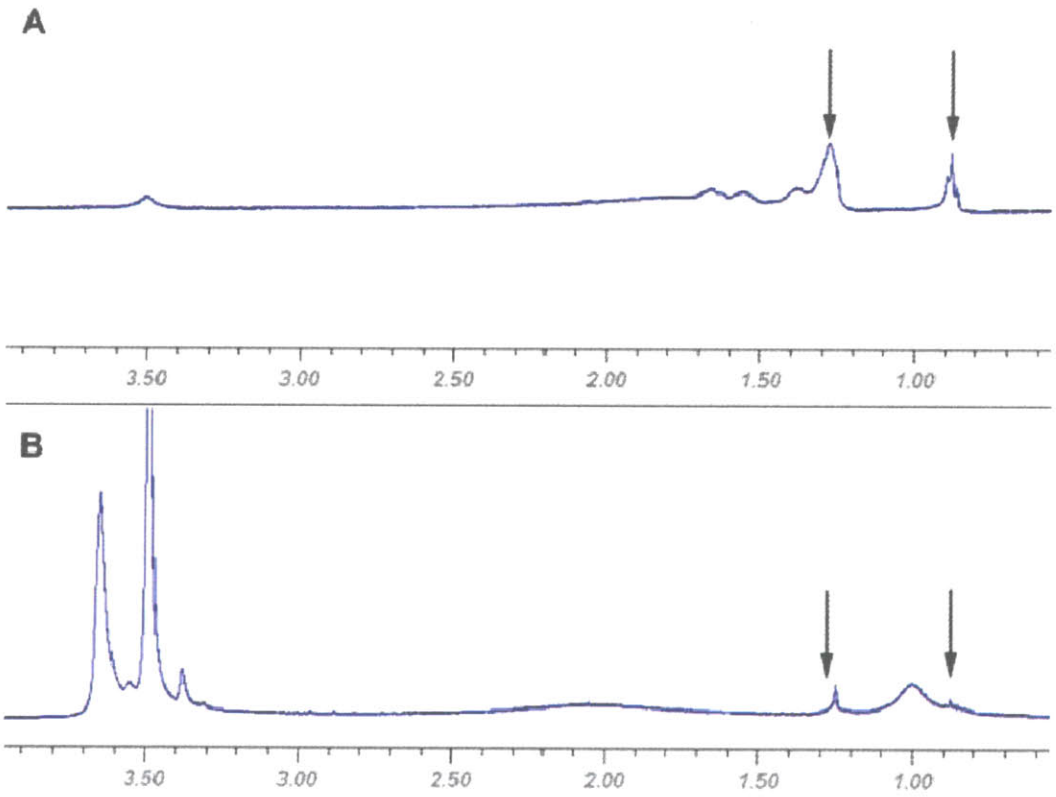

Figure 6-6 ^{1}H-NMR spectrum of QDs before and after ligand exchange. (A) Spectra of QDs in hexanes after 1x precipitation and (B) after ligand exchange with poly(PEG).

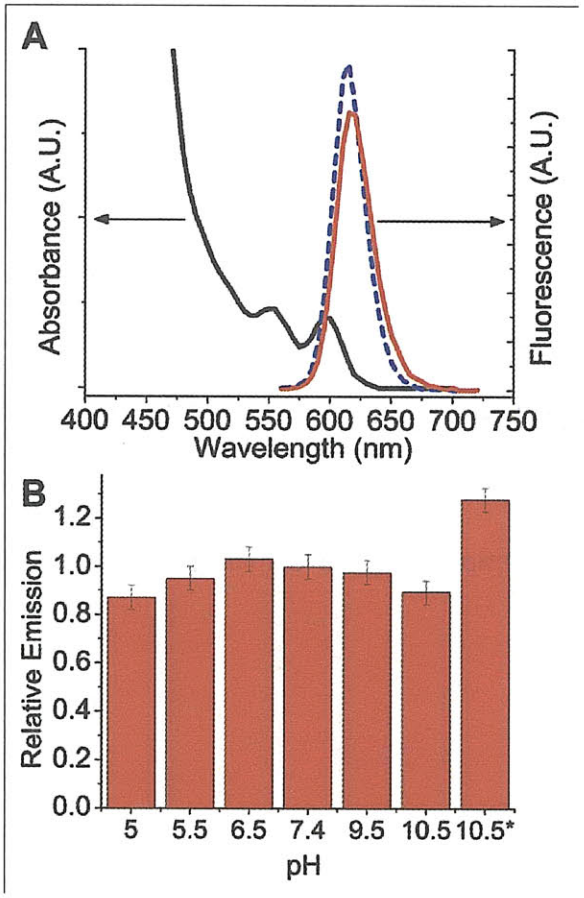

Figure 6-7 Spectra and stability of poly(PEG)-PIL. (A) Absorption spectra (—, black) and emission spectra of QDs before ligand exchange in octane (---, blue), and after ligand exchange in PBS (—, red), showing a slight decrease in fluorescence intensity with a final QY in water of >60%. (B) Stability of polyPEG QDs in various pH buffers after incubation at RT for 4 h. pH 10.5* refers to emission intensity after 5 minutes irradiation under 365nm UV light, showing ~20% photobrightening.

confirmed by ^{1}H NMR spectroscopy (Figure 6-6), which signaled the disappearance of the original aliphatic protons of TOP/TOPO coated QDs after ligand exchange with poly(PEG)-PILs, and the appearance of PEG protons from the polymer bound to the QD surface. A control experiment using a polymer of **6** alone did not yield water soluble QDs (data not shown). The emission peak of QDs after ligand-exchange with PILs exhibited a slight red-shift, while the line-width remained fairly constant (Table 6-2).

Ligand exchange of CdSe(CdS) core(shell) QDs with PEG)-PILs also proceeded smoothly. The presence of a high quality CdS shell applied using a modified selective ion layer

adsorption and reaction (SILAR) approach[28, 29] contributes significantly to the absorbance cross-section of QDs blue of 450 nm and is advantageous for increased brightness in single molecule imaging applications. In addition, a robust shell can greatly improve the QY of QDs after phase transfer to water. Indeed, the QY of CdSe(CdS) QDs ligand exchanged with poly(PEG)-PILs were in excess of 65% in water, a modest drop from a QY of 90% in octane (Figure 6-7A). The high QY of poly(PEG)-PIL QDs is maintained in buffers ranging from pH 5 to pH 10.5 after incubation at room temperature for 4 h (Figure 6-7B). Previous studies on the pH dependence of His_6-tag binding to Ni-NTA media show that the interaction is stable between pH 7-11,[13, 30] and becomes disrupted below pH 5 due to the protonation of the imidazole group. This is consistent with the binding of poly(PEG)-PILs to the surface of QDs via metal-affinity interactions. Below pH 5, the fluorescence intensity of QDs drops rapidly, but the QDs remain well dispersed in solution without any visible formation of macroscopic aggregation. In addition, a photobrightening effect was observed with poly(PEG)-PIL QDs. Photoannealing by illumination with 365 nm UV for 5 min increased the fluorescence intensity of poly(PEG)-PIL QDs by as much as 30%. Furthermore, this increase in fluorescence was retained for at least 24 h after the photoannealing treatment. This observation is consistent with previous studies of QD

QD Sample	Peak λ_{em} (nm)	FWHM (nm)
Organic solution	561.5	31.0
Poly(PEG)	563.3	30.8
Poly(aminoPEG$_3$)$_{10\%}$	563.4	30.8
Poly(aminoPEG$_3$)$_{25\%}$	565	30.3

Table 6-2 Comparison of emission spectra peaks and FWHM of the same CdSe(CdS) QDs coated with different polymers of various compositions.

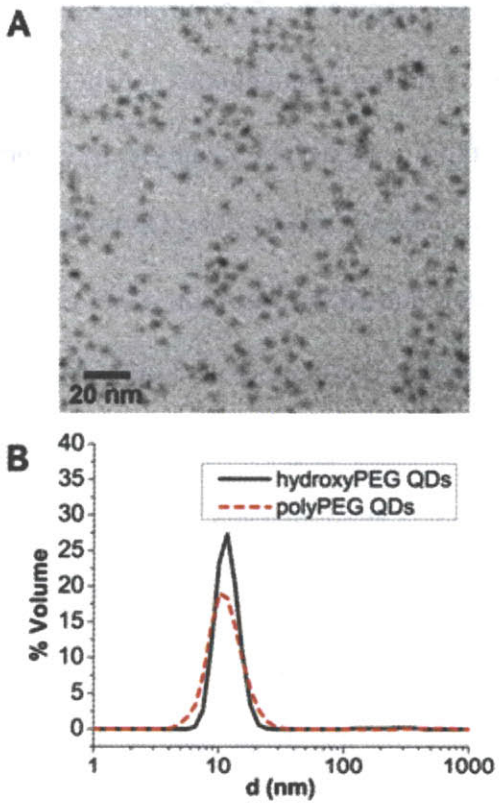

Figure 6-8 Size analysis of poly(PEG) QDs. (A) TEM of QDs ligand exchanged with polyPEG, showing non-aggregated mono-disperse samples. (B) Dynamic light scattering measurement of QDs ligand exchanged with hydroxyPEG (—, black) and QDs ligand exchanged with polyPEG (---, red), both showing an HD of ~11.5 nm.

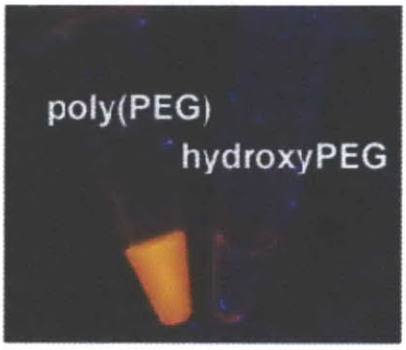

Figure 6-9 Qualitative stability of poly(PEG)-PIL QDs. Emission of poly(PEG) and hydroxyPEG QDs after purification by dialysis and 15 h storage at ambient conditions. HydroxyPEG QDs precipitated, while poly(PEG) QDs retained fluorescence for at least 2 months.

photobrightening upon conjugation with His_6-tagged proteins,[31] as the polymer in this case is binding to the QD surface via the same imidazole moiety. TEM analysis of QDs dropcast from water after ligand exchange with poly(PEG)-PILs shows that the QDs are well dispersed (Figure 6-8A), and dynamic light scattering analysis shows a single narrowly distributed population centered at ~11.5 nm hydrodynamic diameter for 605 nm emitting CdSe(ZnCdS) QDs (Figure 6-8B). This size is comparable to the hydrodynamic diameter of the same QDs ligand exchanged with DHLA-hydroxyPEG, likely due to the compact nature of the imidazole binding group, which is only a few carbons away from the polymer backbone. In addition, we observed that the multidentate binding motif employed in poly(PEG)-PILs results in an aqueous solution that is far more stable than DHLA-hydroxyPEG QDs. For instance, dilute DHLA-hydroxyPEG QDs and poly(PEG)-PIL QDs (<100 nM) were stored at RT under ambient room lighting. Both samples had been dialyzed to remove excess ligand in the solution. Within 15 h, the DHLA-hydroxyPEG QDs precipitated from the solution presumably due to photooxidation of the dithiol group, while poly(PEG)-PIL coated QDs remained stable under ambient conditions for at least 2 months (Figure 6-9D).

6.1.4 Three-Component Random Copolymers for Functionalized Biocompatible QDs

With robustness and compactness of poly(PEG)-PIL coated QDs established, we turned our attention to incorporating chemical functionality into the polymer so that the QDs can be subsequently derivatized for targeting and sensing applications. Multi-functional polymers can be synthesized from monomers **4** and **6**, along with one of monomers **8**, **9**, or **11**, to give functionalized QDs with primary amine or biotin groups upon water solubilization. Copolymerization with three monomers proceeded smoothly, with good size control and low

polydispersity (Figure 6-10), and functional monomers were incorporated at mole fractions ranging from 10-25%. As mentioned previously, the incorporation of all monomers was maximized by running the polymerization to >90% conversion, as overlapping ^{1}H signals made it difficult to determine the final polymer composition by NMR. Using the short aminoPEG$_3$ monomer **8**, polymers with amine functionalities were synthesized with the functional group

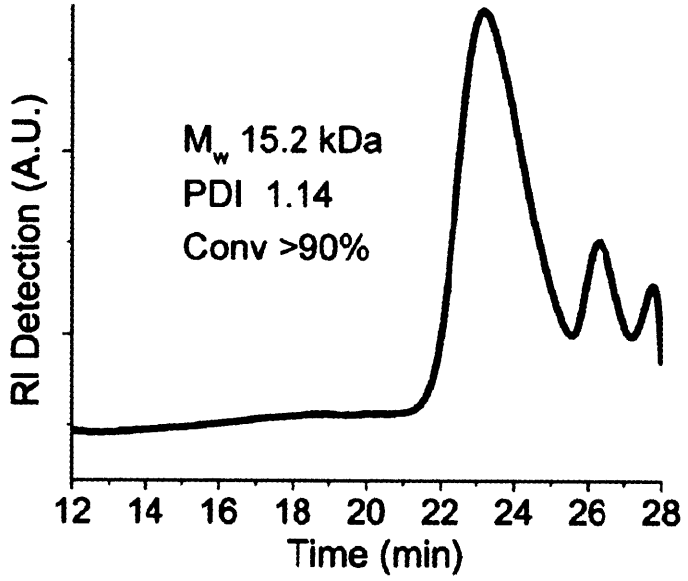

Figure 6-10 Characteristic GPC of a 3-component polymerization of poly (aminoPEG$_{11}$)$_{10\%}$, consisting of 50% imidazole (Cmpd 4), 40% methoxyPEG11 (Cmpd 6), and 10% aminoPEG11 (Cmpd 9).

close to the surface of the QD after ligand exchange, making this system ideal for dye conjugation and energy transfer sensing applications, as detailed below. Polymers with amine functionalities tethered by longer linkers were synthesized using the aminoPEG$_{11}$ monomer **9**. These polymers were found to be more suitable for the conjugation of QDs to larger

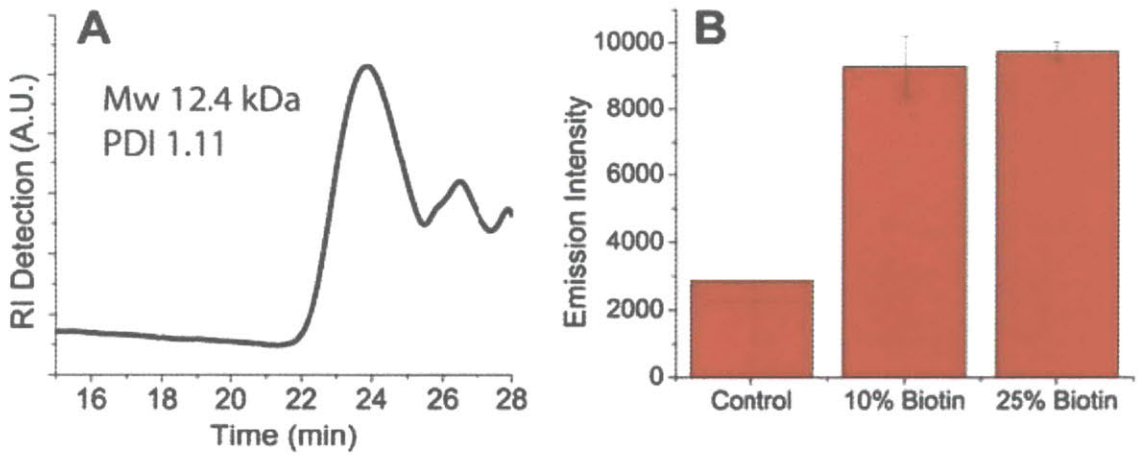

Figure 6-11 Characterization of biotin functionalized QDs. (A) GPC trace of poly(biotinPEG)10%-PILs. (B) Binding of poly(biotinPEG)10% and poly(biotinPEG)25% QDs to streptavidin-coated plates versus control poly(aminoPEG3)10% QDs. Fluorescence intensity at 605 nm was measured with excitation at 400 nm, in triplicate.

biomolecules such as proteins and antibodies, as the longer PEG_{11} linker makes the terminal amino groups more sterically accessible. Using the monomer **11**, polymers bearing a biotin functionality were also synthesized, giving water soluble QDs that bind readily to streptavidin coated plates (Figure 6-11). The synthesis of functional three-component copolymers affords a versatile and facile way of tuning the QD surface functionality for a wide range of potential applications.

6.1.5 Conjugation to an Energy Transfer Dye

A salient feature of the copolymer ligand strategy is the ability to incorporate side-chains that can be readily derivatized in aqueous solution. To demonstrate covalent derivatization, we conjugated 5-carboxy-X-rhodamine (ROX), a red-emitting fluorescent dye, to QDs ligand exchanged with poly(aminoPEG$_3$)$_{10\%}$-PILs via an amide linkage. The dye absorbance offers a convenient indication of the coupling yield. Additionally, the typical radial distance from the QD to the derivatization site may be determined from a Förster resonance energy transfer (FRET) analysis of the QD-dye pair.[32, 33]

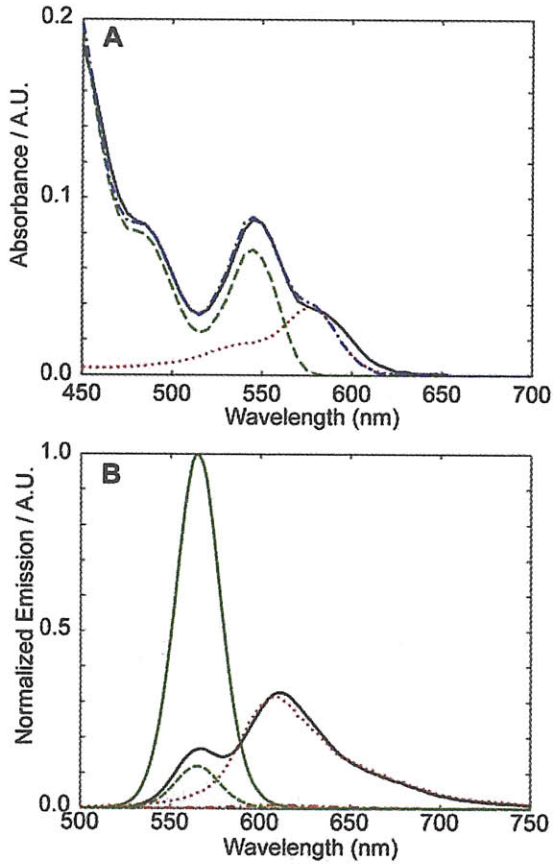

Figure 6-12 Covalent derivatization of poly(aminoPEG$_3$)$_{10\%}$ with ROX dye molecules. (A) Absorption spectrum of purified conjugate (—, black), least-squares fit of conjugate spectrum (– · – ·, blue), as sum of QD (---, green) and free ROX (····, red) contributions. (B) Photoluminescence spectrum of conjugate (—, black) and of control QD (—, green) and free dye (– · – ·, red), normalized to reflect the QD and ROX concentrations, respectively, present in the conjugate sample. Contributions of QD (---, green) and free ROX (····, red) to conjugate emission spectrum as obtained from a least-squares fit are also shown. All samples are excited at 450 nm, with dye emission showing 31 fold enhancement from the free dye vs. the conjugate.

To form conjugates, an aliquot of the amine-reactive succinimidyl ester of 5-ROX in dimethyformamide was added to a solution of the QDs in phosphate buffer at pH 7.6. Following the coupling reaction, the QDs were separated from unbound dye and NHS byproduct via size exclusion chromatography. Figure 6-12 shows the absorption and emission spectra of a purified QD-ROX conjugate made using 562 nm-emitting CdSe(CdS) QDs and 27 equivalents of the activated dye. The dye contribution to the sample absorbance is clearly visible in Figure 6-12A as a shoulder on the red side of the lowest energy exciton peak. A fit of the spectrum as a sum of QD and dye components reveals an average dye:QD ratio of 1.78:1. Figure 6-12B shows the

photoluminescence (PL) spectrum of the conjugate under 450 nm excitation. At this wavelength, ROX dye has minimal absorbance, allowing for the selective excitation of the QD. The QD PL peak is significantly quenched versus that of a control sample that was processed similarly but not modified with the ROX dye, while the ROX emission centered at 610 nm is significantly enhanced versus that of the free dye when normalized for the sample concentrations. Theseobservations are consistent with energy transfer; a fit of the emission spectrum reveals an energy transfer efficiency of 88%.

The high energy transfer efficiency suggests that the copolymer ligand system is able to poise small-molecule substituents in proximity to the QD core. Indeed, analysis of the observed efficiency and spectral overlap according to the Forster model suggests a characteristic separation distance of no more than 4.5 nm, which is consistent with observations of a small hydrodynamic radius for the ligand-exchanged QDs. The limited coupling yield observed here may indicate saturation of the available primary amine binding sites, suggesting that not all amine side-chains on the polymer are sufficiently accessible from the solvent, possibly due to the affinity of amines for the QD surface.

In order to gauge the number of free amines that are solution accessible, we probed the PIL-coated QDs with Fluorescamine, an amine-reactive fluorogenic probe (Figure 6-13). For QDs coated with poly(aminoPEG$_3$)$_{5\%}$, the average number of measured free amines exposed to solution per QD was only ~1. This low number suggests that most of the amines are in fact bound to the QD surface and are inaccessible to the solvent. Increasing the mole fraction of compound **8** from 5% to 20% (i.e. poly(aminoPEG$_3$)$_{20\%}$) increased the average amine:QD ratio to ~8:1. Indeed, using poly(aminoPEG$_3$)$_{25\%}$ coated QDs for dye conjugation yielded ~4 dyes/QD (data not shown).

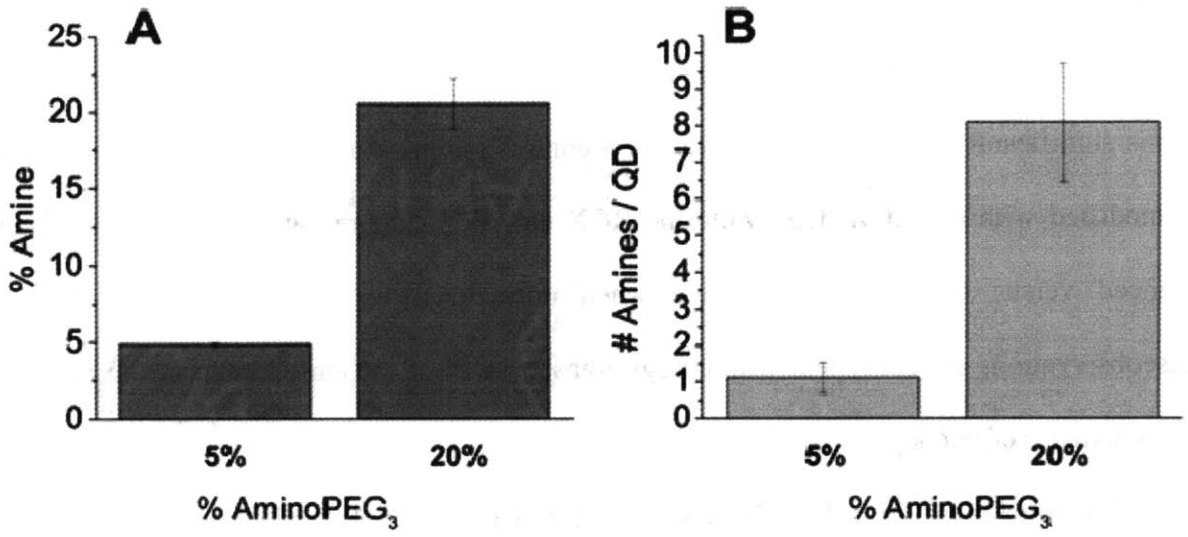

Figure 6-13 Fluroescamine assay of polymer amine reactivity in (A) the free polymer and (B) after ligand exchange on the surface of QDs using the same polymers as in (A).

Taken together, these results show that although some degree of amine binding is present, the incorporation of compound **8** into the polymer as a functional site for derivatization proved to be successful, and these initial results bode well for the derivatization of these QDs with dyes and other small molecules for applications in targeted biological imaging and sensing.

6.1.6 Non-specific Binding to HeLa Cells

An absence of non-specific binding is essential to reliable targeting and/or sensing applications involving QDs. To test the non-specific binding of poly(PEG)-PIL based QDs, we incubated HeLa cells with QDs of various surface compositions and subsequently washed the cells 4× with phosphate-buffered saline (PBS). Since the level of non-specific binding is inherently low for such PEGylated QDs, the cells were incubated at high QD concentrations (~500 nM) in order to highlight the differences between the coatings. Fluorescence and phase

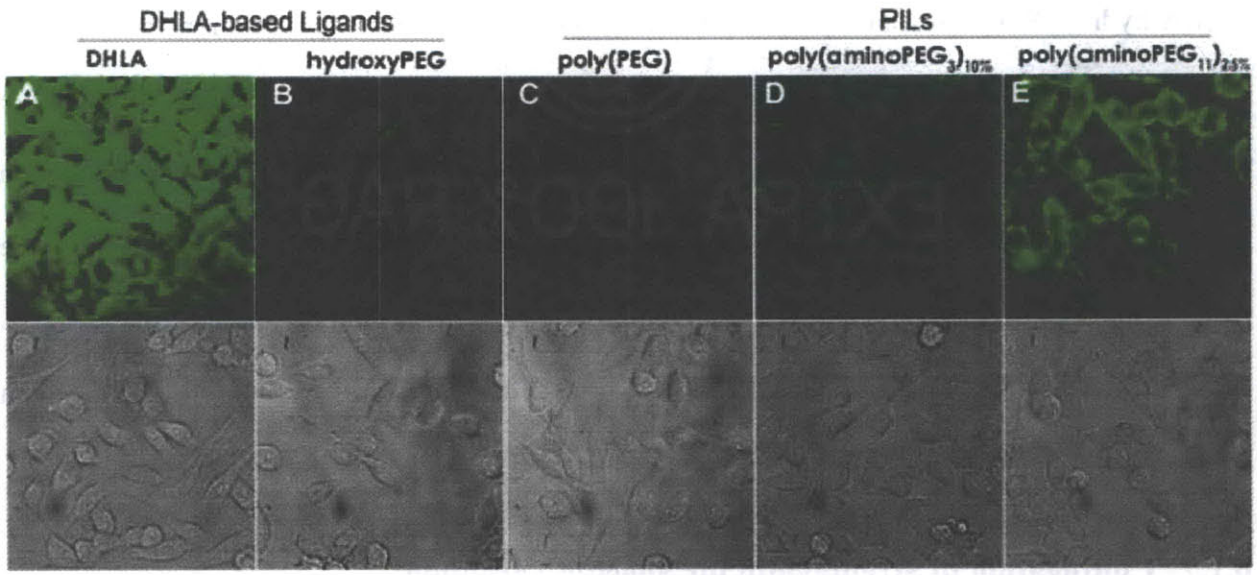

Figure 6-14 Non-specific binding of QDs on HeLa cells as a function of ligand coating, with incubation at 500 nM QD concentration for 5 min at 4 ℃ , followed by 4x wash with PBS buffer before imaging. Top: QD fluorescence at 565 nm with excitation at 488 nm. All images are scaled to the same contrast with the exception of (B) and (C), for which the left section has the same contrast as the other images, while the contrast has been boosted in the right section to highlight the difference between (B) and (C). Bottom: corresponding DIC image. QDs were ligand exchanged with (A) DHLA, (B) hydroxyPEG, (C) poly(PEG), (D) poly(aminoPEG$_3$)$_{10\%}$, and (E) poly(aminoPEG$_{11}$)$_{25\%}$.

contrast images of cells after washing are shown in Figure 6-14. As expected, DHLA coated QDs produced a high degree of non-specific binding to both cells and glass.[14] DHLA-hydroxyPEG coated QDs exhibited minimal non-specific binding, but some QD stickiness could be observed with enhanced contrast of the fluorescence images. Poly(PEG)-PIL QDs, when viewed under the same enhanced contrast, show virtually no non-specific binding, which may be attributed to several factors. First, the PEG chains of poly(PEG)-PILs are terminated in methoxy groups, which can further reduce non-specific binding versus PEG terminated with hydroxyl groups.[21, 34] Second, the PEG length of poly(PEG)-PILs is slightly longer versus that of DHLA-hydroxyPEG, and third, the methoxyPEG along the polymer backbone may offer a denser coverage of PEG groups to better passivate the QD surface. When amine groups are introduced in a three-component polymer (Figure 6-14D and E), we observe increasing levels of non-specific binding. Poly(aminoPEG$_3$)$_{10\%}$-PIL QDs show slightly more non-specific binding versus

DHLA-hydroxyPEG QDs, and poly(aminoPEG$_{11}$)$_{25\%}$-PIL QDs exhibit even more non-specific binding, consisting with an increase in the amount of amines on the QD surface. Although the non-specific binding for poly(aminoPEG$_{11}$)$_{25\%}$-PIL QDs appears to be non-trivial, the incubation for this particular experiment was performed at high QD concentration (500 nM). We demonstrate below that the covalent conjugation of streptavidin to poly(aminoPEG$_{11}$)$_{25\%}$-PIL QDs and their subsequent targeting to cells at low QD concentrations resulted in labeling with good signal to noise and allowed for single molecule tracking of QDs with minimal background.

6.1.7 Conjugation to Streptavidin for Specific Targeting

In order to demonstrate the capability of PIL-based QDs for targeted single molecule imaging in live cells, poly(aminoPEG$_{11}$)$_{25\%}$-PIL QDs were conjugated to streptavidin (SA) via 1-ethyl-3-(3- dimethylaminopropyl) carbodiimide (EDC) coupling chemistry. For targeting, HeLa cells were transfected with a plasmid for yellow fluorescent protein (YFP), fused to an extracellular acceptor peptide (AP) tag[5] and a transmembrane domain (TM) for cell surface targeting (AP-YFP-TM), as well as with a plasmid for endoplasmic reticulum-localized biotin ligase (BirA).[14, 35] The AP tag is specifically biotinylated by the co-expressed BirA and displayed on the cell surface along with YFP via the TM domain. The QD-SA conjugates were then added for labeling. At a high QD labeling concentration of 100 nM, excellent co-localization was observed between the YFP and QD channels, with very low levels of non-specific binding to non-transfected cells and glass (Figure 6-15A). A control experiment in which the QD-SA construct was pre-incubated with biotin showed no binding, confirming that the binding interaction was indeed between the QD-SA and biotin on the cell surface (Figure 6-15B).

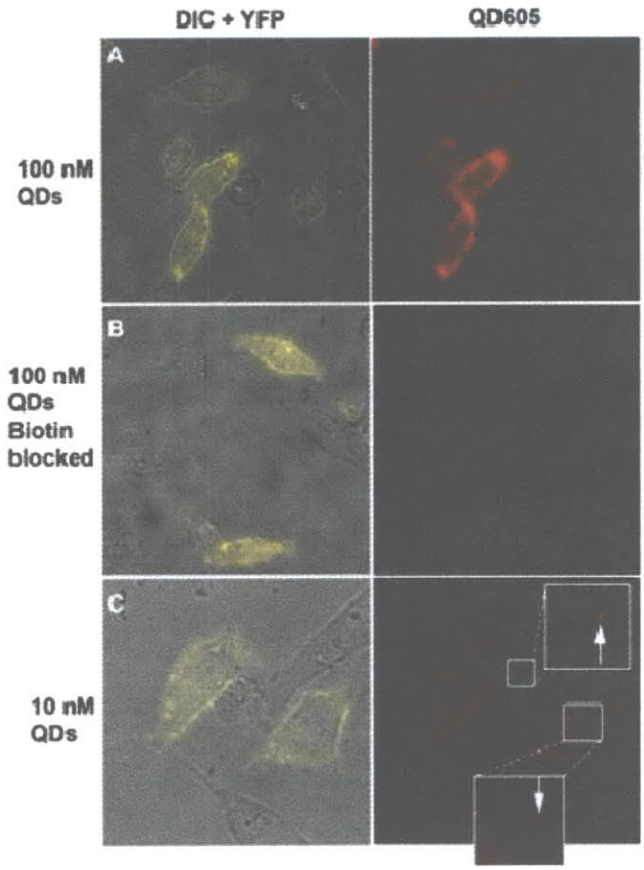

Figure 6-15 Targeting of poly(aminoPEG11)25% QD-SA conjugates to live HeLa cells transfected with AP-YFP-TM. (A) Ensemble labeling with 100 nM QDs. (B) Same as in (A), but with QDs pre-incubated with biotin. (C) Low-density labeling with 10 nM QD-SA reveals single QDs.

By reducing the QD labeling concentration to 10 nM, single QDs could be readily observed (Figure 6-15C), as identified by their fluorescence intermittency behavior (**Figure 6-16**). As previously discussed, DHLA-PEG based QDs are subject to degradation via loss of ligand coating after ~1 week and become increasingly sticky to cells. By contrast, in our experience, PIL-based QDs remain non-sticky and functional on the timescale of months.

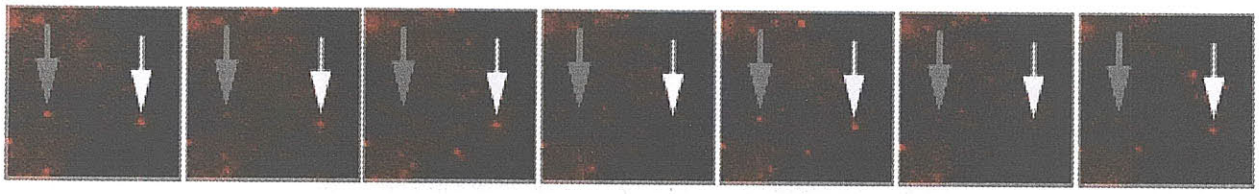

Figure 6-16 Time series (from left to right) of blinking of single QDs (white and gray arrows) targeted to the surface of HeLa cells, as shown in **Figure 6-15**C. Each frame was acquired with a 500 ms exposure time.

6.1.8 Non-specific Binding in Serum Proteins for in-vivo Applications

PEG_{11} monomer **6** is always present in a significant mole fraction within the polymer not only to provide water solubility, but also to mitigate nonspecific binding and prevent biofouling of QDs. To illustrate the stability of these QDs for *in-vivo* applications, we incubated various polymer-coated CdSe(CdZnS) 565-nm emitting QDs with mouse bovine serum at 37 °C for 4 h and analyzed the samples by size exclusion chromatography with fluorescence detection to

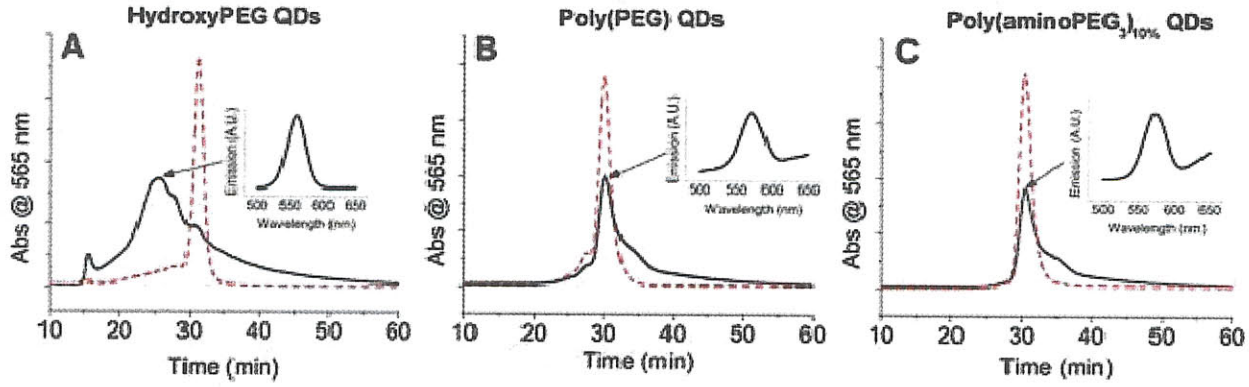

Figure 6-17 Non-specific binding of QDs with serum proteins after incubation with 95% mouse bovine serum for 4 h at 37 °C. QDs before incubation (- - -, red) and after incubation (—, black) for (A) hydroxyPEG QDs, (B) poly(PEG) QDs, and (C) poly(aminoPEG3)10% QDs. Insets show fluorescence spectrum of eluent at time indicated by the black arrow, showing QD emission.

determine the extent of non-specific binding to serum protein. In the case of QDs coated with DHLA-hydroxyPEG, significant serum protein binding was observed, as indicated by the formation of a large broad peak eluting at earlier times after serum incubation versus control

(Figure 6-17A). Previous serum binding experiments using DHLA-hydroxyPEG on InAs(ZnSe) QDs revealed low levels of non-specific binding to serum protein.[36] The discrepancy is likely due to the relative size of the QD cores. In the InAs(ZnSe) case, the inorganic cores were on the order of 2 nm in diameter, and the PEG_8 group of DHLA-hydroxyPEG provided sufficient passivation against non-specific binding. The CdSe(CdZnS) QDs used in this study are approximately twice the diameter and the relatively short PEG_8 chains of DHLA-hydroxyPEG are less able to provide full surface passivation. By contrast, QDs coated with poly(PEG)-PIL, exhibited negligible non-specific binding to serum proteins after incubation (Figure 6-17B), as indicated by the appearance of the peak position at the same position as the control. We surmise that the PEG units along the polymer backbone provide a denser coverage of PEG on the surface of the QDs, thus giving it enhanced anti-biofouling properties. Functionalized QDs ligand exchanged with poly(aminoPEG$_3$)$_{10\%}$-PIL also exhibited no detectable non-specific binding in serum (Figure 6-17C).

6.1.9 Probing the Tumor Microenvironment Using poly(PEG)-PIL QDs as a Diffusion Tracer

Taking advantage of the low serum binding of poly(PEG)-PIL QDs, we observed the distribution dynamics of these QDs within tumors in live mice (Figure 6-18). Using a breast tumor model grown beneath transparent windows in mice,[37-39] vascular transport of QDs after intravenous injection can be imaged via two-photon laser scanning microscopy as a function of time to observe QD distribution kinetics. The mouse vessel walls were visualized independently via green fluorescent protein (GFP) expressed under the promoter of the Tie2 receptor present on the surface of the vascular endothelial cells.[40] CdSe(CdS) poly(PEG)-PILs QDs emitting at 605

nm were injected retro-orbitally, and the tumor vasculature was imaged over 6 h. Initially, the

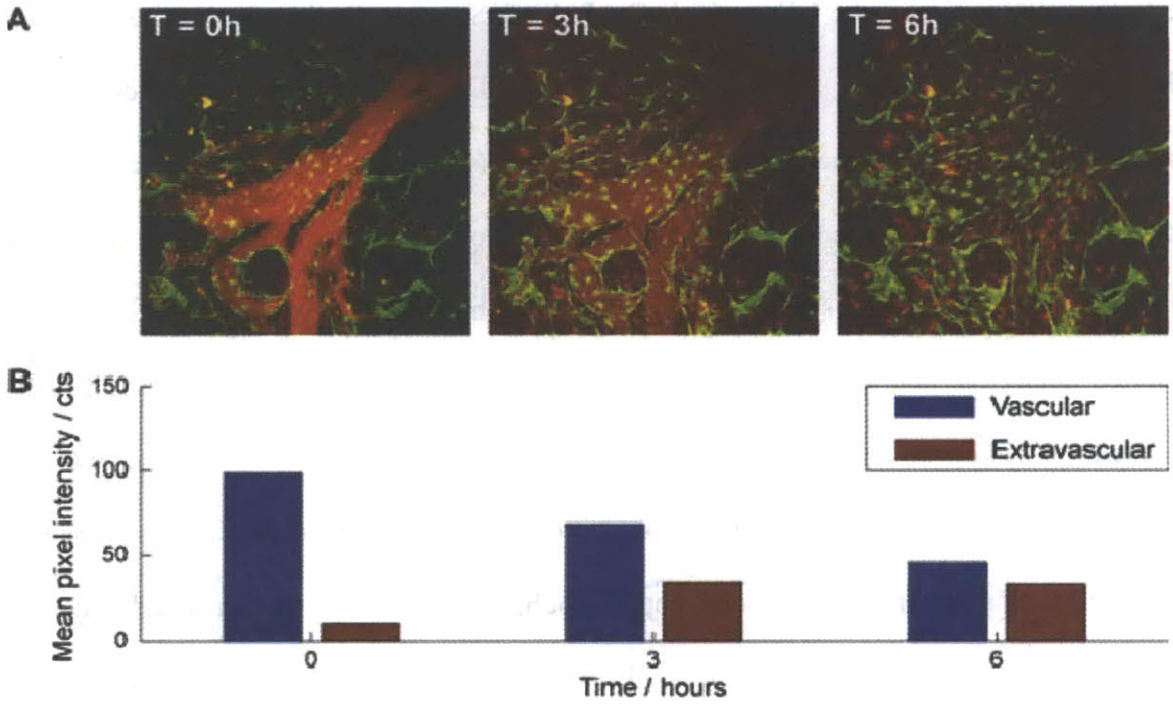

Figure 6-18 Poly(PEG)-PIL QDs in-vivo. (A) Time lapsed live QDs imaging of P008 tumor vasculature in Tie2-GFP/FVB mice. Red fluorescence corresponds to the signal from QDs within the vessel lumen (0 and 3h), or extravascular space in tumors (3 and 6h), while the green fluorescence is from the GFP in vascular endothelial cells that line the vessel wall. B, Mean QD (red channel) intensities within and outside of the blood vessels over time. Vessel regions are assigned by thresholding of the T=0h image. The QDs are initially confined within the vessels at T= 0. Images at later times reveal decreased vascular and increased extravascular fluorescence, indicative of clearance from the vessels and extravasation into tumor tissue, respectively.

QDs are confined within the vessel lumen. At 3 h, we observed clearance from the vasculature and the simultaneous appearance of QDs in the tumor tissue. After 6 h, the QDs had extravasated into the tumor tissue, appearing as a uniform signal spread throughout the field of view. The QDs appeared stable, and there was no indication of stickiness or aggregation on the lumen wall or in the tumor tissues. Having a stable, small, biocompatible QD scaffold should enable the use of these QDs as robust in vivo sensors.[33]

6.1.10 Conclusions

We have synthesized a new class of coordinating polymers that produce aqueous QDs with greater stability and shelf-life compared with previously reported DHLA-derived ligands, while maintaining the desirable QD properties of low non-specific binding, small size, facile derivatizability, and high QY. By using a three-monomer co-polymerization scheme, we were able to produce multi-functional aqueous QDs featuring imidazole groups for multidentate binding to the QD surface, PEG groups for water solubility and mitigation of non-specific binding, and either amine groups or biotin groups on the surface for derivatization. The monomer synthesis is facile and can be scaled to multi-gram quantities, and by utilizing RAFT polymerization, a wide variety of monomers were used to produce aqueous QDs with controllable surface properties and compositions. The enhanced QD stability enabled by these new polymers is crucial for cellular/*in-vivo* targeting and imaging/sensing applications in which the QDs must survive conjugation with dyes or proteins and subsequent purification steps in order to arrive at functional probes. Our poly-imidazole binding motif relieves the necessity to perform these steps in prompt succession. Often, weeks or months of time are needed to properly culture cells or raise animals for QD imaging studies, and these new QDs enable the long-term storage of functional sensing/targeting constructs for such studies. Furthermore, we demonstrate the utility of small non-sticky poly(PEG)-PIL QDs for achieving extravasation from the tumor vasculature in mice with uniform distribution, paving the way for studies of the tumor microenvironment. The modularity of the PIL system can potentially accommodate an even wider diversity of monomers, expanding the scope of functionalities achievable on QD surfaces well beyond the examples provided in this study.

6.2 *Experimental Details*

Materials and Instrumentation. All chemicals unless indicated were obtained from Sigma Aldrich and used as received. Air sensitive materials were handled in an Omni-Lab VAC glove box under dry nitrogen atmosphere with oxygen levels <0.2 ppm. All solvents were spectrophotometric grade and purchased from EMD Biosciences. Amine-bearing compounds were visualized on thin layer chromatography (TLC) plates using a ninhydrin solution. Acrylate compounds bearing terminal vinyl groups were visualized on TLC using $KMnO_4$. All other TLC plates were visualized by iodine staining. Flash column chromatography was performed on a Teledyne Isco CombiFlash Companion. ^1H NMR spectra were recorded on a Bruker DRX 401 NMR Spectrometer. UV-Vis absorbance spectra were taken using an HP 8453 diode array spectrophotometer. Photoluminescence and absorbance spectra were recorded with a BioTek Synergy 4 Microplate Reader. Dynamic light scattering analysis was performed on a Malvern Instruments ZetaSizer ZS90 in a low volume 12 μL quartz cuvette, with QD concentrations between 1-3 μM. Polymer molecular weights were determined in DMF solutions on an Agilent 1100 series HPLC/GPC system with three PLgel columns (103, 104, 105 Å) in series against narrow polystyrene standards.

Compound 2. To a stirred solution of acrylic acid (1.00 g, 13.88 mmol) and N-hydroxysuccinimide (NHS) (1.91 g, 16.65 mmol) in 40 mL of dry THF was added dropwise a solution of dicyclohexylcarbodiimide (DCC) (3.43g, 16.65 mmol) in 10 mL dry THF with stirring at 4 °C. The solution was warmed to room temperature and stirred for 2 h. Precipitates were removed by filtration, and the solvent was evaporated *in vacuo*. Ethylacetate (50 mL) was added to facilitate further precipitation of reaction byproducts, and the solution was filtered once more. The solvent was evaporated and the product dissolved in either 10 mL of anhydrous DMF

or dry THF to create a stock solution, which was used in later reaction steps without further purification.

Compound 4. To an aqueous solution of sodium bicarbonate (50 mL, 0.3 M) was added DMF (50 mL) and histamine dihydrochloride (2.50 g, 13.59 mmol). To this solution was added compound **2** (2.75 g, 16.3mmol) in a solution of DMF, with stirring at 4 °C. The reaction was monitored via TLC by ninhydrin stain for primary amines, and confirmed to be complete after 30 min to give the crude compound **3**. The solvent was removed *in vacuo*, and the product redissolved in DMF (50 mL). The solution was filtered, and triethylamine was introduced (2.27 mL, 16.30 mmol). Di-tert-butyl dicarbonate was added dropwise at 4 °C, and the solution was stirred overnight at RT. Water was added and the solution extracted with $CHCl_3$ (3 × 25 mL). The organics were combined and dried over sodium sulfate, and the solvent removed *in vacuo*. The crude product was purified by silica column (ethyl acetate/hexanes gradient 50:50 to 100:0, v/v) to give the pure product as a clear oil (2.59 g, 72% yield). ^{1}H NMR (400 MHz, $CDCl_3$): δ (ppm) 7.95 (s, 1H), 7.10 (s, 1H), 6.19 (dd, J1 = 1.8 Hz, J2 = 17.0 Hz, 1H), 6.07 (dd, J1 = 9.8 Hz, J2 = 17.0 Hz, 1H), 5.53 (dd, J_1 = 1.8 Hz, J_2 = 10.0 Hz, 1H), 3.53 (dt, 2H), 2.72 (t, 2H), 1.54 (s, 9H).

Compound 5. Neat methoxy poly(ethylene glycol) (10 g, 18.18 mmol, average MW 550 g/mol) was degassed at 80 °C for 1 h with stirring to remove traces of water. The flask was back-filled with N_2 and cooled on an ice bath before thionyl chloride (1.98 mL, 27.27 mmol) was slowly added. The solution was warmed to 25 °C and stirred for 2 h. The conversion was monitored by the disappearance of the broad O–H stretch at 3,500 cm^{-1} and the appearance of a C–Cl stretch at 730 cm^{-1} in the IR spectrum. The product was diluted with DMF (20 mL) and the solvent removed under reduced pressure. This was repeated three times to remove all residual

traces of thionyl chloride. The sample was dissolved in a solution of sodium azide (1.77 g, 27.27 mmol) in 100 mL DMF and stirred overnight at 85 °C. The solvent was removed under reduced pressure and 200 mL of dichloromethane was added. The precipitate was removed by vacuum filtration and the solvent evaporated *in vacuo* to yield the intermediate mono-azide. The sample was dissolved in 150 mL of tetrahydrofuran (THF), and triphenylphosphine (7.15 g, 27.27 mmol) was added. The solution was stirred at 25 °C for 4 h before adding 1 mL of water and stirring overnight. The THF was removed *in vacuo* and 100 mL of water was added. The precipitate was removed by vacuum filtration and the filtrate washed with toluene (3 × 50 mL). The water was removed *in vacuo* to yield the pure product as light yellow oil (9.67 g, 95%). ^{1}H NMR (400 MHz, $CDCl_3$): δ (ppm) 3.69 – 3.46 (m, 46H), 3.37 (s, 3H), 2.85 (t, 2H).

Compound 6. To a solution of compound **5** (2.20 g, 3.94 mmol) in dry THF was added compound **2** (1.00 g, 5.92 mmol) in a solution of dry THF, with stirring at 4 °C. The reaction was monitored via TLC by ninhydrin stain for primary amines, and confirmed to be complete after 30 min. The solution was filtered and the solvent evaporated *in vacuo*. The crude product was purified by silica column (methanol/ethyl acetate gradient 0:100 to 5:95, v/v) to give the pure product as a pale yellow oil (1.88 g, 78% yield). ^{1}H NMR (400 MHz, $CDCl_3$): δ (ppm) 6.68, 6.19 (dd, J_1 = 2.0 Hz, J_2 = 17.0 Hz, 1H), 6.08 (dd, J_1 = 9.8 Hz, J_2 = 17.0 Hz, 1H), 5.52 (dd, J_1 = 2.0 Hz, J_2 = 9.8 Hz, 1H), 3.56 – 3.37 (m, 48H), 3.27 (s, 3H).

Compound 8. To a solution of 4,7,10-trioxa-1,13-tridecanediamine (10.00 g, 45.45 mmol) in DCM (25 mL) was added dropwise di-tert-butyl dicarbonate (1.98 g, 9.09 mmol) at 4 °C. The solution was allowed to warm to RT and stirred overnight. The solution was washed with water (3 × 20 mL) to remove unreacted starting material. TLC analysis with ninhydrin staining shows mostly mono-substituted product in the organic phase. The organics were dried

over sodium sulfate and solvent removed *in vacuo.* The crude product (3.80 g, 17.27 mmol) was dissolved in a mixture of aqueous sodium bicarbonate buffer (20 mL, 0.3 M), and DMF (20 mL), to which compound **2** (3.38 g, 20.00 mmol) was added dropwise in a solution of DMF with stirring at 4 °C. The reaction was monitored via TLC by ninhydrin stain for primary amines, and confirmed to be complete after 30 min. Water was added and the solution extracted with $CHCl_3$ (3 × 25 mL). The organics were combined and dried over sodium sulfate, and the solvent removed *in vacuo.* The crude product was purified by silica column (ethyl acetate/methanol gradient 100:0 to 95:5, v/v) to give the pure product as a clear oil (4.52 g, 27% yield). ^{1}H NMR (400 MHz, $CDCl_3$): δ (ppm) 6.23 (dd, J_1 = 2.0 Hz, J_2 = 17.0 Hz, 1H), 6.08 (dd, J_1 = 9.8 Hz, J_2 = 17.0 Hz, 1H), 5.56 (dd, J_1 = 2.0 Hz, J_2 = 9.8 Hz, 1H), 3.65 – 3.44 (m, 14H), 3.17 (t, 2H), 1.83 – 1.65 (m, 4H), 1.39 (s, 12H).

Compound 9. To a solution of *O*-(2-Aminoethyl)-*O'*-[2-(Boc-amino)ethyl]decaethylene glycol (0.50 g, 0.78 mmol) in dry THF (25 mL) was added triethylamine (0.086 g, 0.85 mmol) and compound **2** (0.20 g, 1.16 mmol) dropwise in a solution of THF with stirring at 4 °C. The reaction was monitored via TLC by ninhydrin stain for primary amines, and confirmed to be complete after 30 min. The solution was filtered and the solvent removed *in vacuo.* The crude product was purified by silica column (DCM/MeOH gradient 100:0 to 95:5, v/v) to give the pure product as a clear oil (0.38 g, 70% yield). ^{1}H NMR (400 MHz, $CDCl_3$): δ (ppm) 6.28 (dd, J_1 = 2.0 Hz, J_2 = 17.0 Hz, 1H), 6.16 (dd, J_1 = 9.8 Hz, J_2 = 17.0 Hz, 1H), 5.59 (dd, J_1 = 2.0 Hz, J_2 = 9.8 Hz, 1H), 3.70 – 3.50 (m, 46H), 3.30 (q, 2H), 1.42 (s, 9H).

Compound 10. To a solution of *O*-(2-Aminoethyl)-*O'*-[2-(Boc-amino)ethyl] decaethylene glycol (0.50 g, 0.78 mmol) in DMF (150 mL) was added biotin (0.21 g, 0.86 mmol) and EDC (0.13 g, 0.86 mmol). The solution was stirred overnight, and the solvent removed *in-*

vacuo. The crude product was purified by silica column (DCM/MeOH 98:2, v/v) to give the pure product as a colorless oil (0.63 g, 85% yield). ^{1}H NMR (400 MHz, $CDCl_3$): δ (ppm) 4.23 (m, 1H), 4.43 (m, 1H), 3.48 (m, 4H), 3.52-3.61 (m, 40H), 3.24 (m, 2H), 3.35 (m, 2H), 2.82 (dd, J_1 = 12.8 Hz, J_2 = 4.9 Hz, 1H), 3.06 (m, 1H), 1.37 (s, 9H), 2.68 (d, J = 12.8 Hz, 1H), 2.16 (t, J = 7.5 Hz, 2H), 1.60 (m, 4H), 1.40 – 1.32 (m, 2H).

Compound 11. To compound **10** (0.50 g, 0.57 mmol) was added 4 M HCl in dioxane, and stirred for 1 h at room temperature. The solvent was removed *in vacuo*, and the crude product dissolved into a solution of 0.25 M aqueous sodium bicarbonate with DMF. To this solution was added dropwise a solution of compound **2**. The reaction was monitored via TLC by ninhydrin stain for primary amines and confirmed to be complete after 30 min. The solvent was removed *in vacuo*, and the crude product was purified by silica column chromatography (DCM:MeOH 98:2, v/v) to give the product as a colorless oil (0.31 g, 65% yield). ^{1}H NMR (400 MHz, $CDCl_3$): δ (ppm) 6.28 (dd, J_1 = 2.0 Hz, J_2 = 17.0 Hz, 1H), 6.17 (dd, J_1 = 9.8 Hz, J_2 = 17.0 Hz, 1H), 5.61 (dd, J_1 = 2.0 Hz, J_2 = 9.8 Hz, 1H), 4.49 (m, 1H), 4.30 (m, 1H), 3.48-3.72 (m, 44H), 3.42 (m, 2H), 3.13 (m, 1H), 2.89 (dd, J_1 = 12.8 Hz, J_2 = 4.9 Hz, 1H), 2.74 (d, J = 12.8 Hz, 1H), 2.22 (t, J = 7.4 Hz, 2H), 1.66 (m, 4H), 1.43 (m, 2H).

Typical PIL Polymerization. All monomers were kept as dilute stock solutions between 30-100 mg/mL in either ethylacetate or methanol. Stock solutions of RAFT agent **12** were prepared at 220 mg/mL in DMF, and AIBN was prepared at 50 mg/mL in DMF. All reagents were weighed out volumetrically. In a typical polymerization, monomers **4** (33 mg, 0.13 mmol) and **6** (77 mg, 0.13 mmol) were added to an 8 mL vial. The solvent was removed *in vacuo* and 50 μL of dry DMF along with RAFT agent **12** (2.53 mg, 0.0088 mmol), and AIBN (1.43 mg, 0.0088 mmol) were added. The contents of the vial were mixed, centrifuged at 5000 g for 2 min,

and then transferred to a 1 mL ampoule. The ampoule was subjected to 4 cycles of freeze-pump-thaw, and sealed under vacuum using a butane torch. The vial was heated to 70 °C on an oil bath for 1.5-3 h, after which 0.5 mL of a 4 M HCl in dioxane solution was added to cleave the BOC protecting groups. After 1 h at RT, the HCl was removed *in vacuo*. The deprotected polymer was dissolved in MeOH, to which a solution of NaOH in MeOH (1M) was added dropwise to adjust the pH to be between 8-9. The solvent was removed *in vacuo*, and then $CHCl_3$ was added to precipitate the salts. The solution was filtered through a 0.45 μm PTFE filter and the solvent removed *in vacuo* to yield the final polymer for QD ligand exchange.

Quantum Dot Synthesis. CdSe cores were synthesized according to previously reported procedures,[12, 41, 42] and were overcoated with either $Zn_{0.8}Cd_{0.2}S$ alloy shells or pure CdS shells. The alloy shell overcoating procedure has been described previously,[12, 42] and was used here to obtain QDs emitting at 565 and 605 nm with QYs of ~80% when diluted in hexane. For pure CdS shells, we developed a successive ion layer adsorption and reaction (SILAR) procedure that is modified from those reported by Peng et al and Mews et al (Xie JACS).[28, 29] Briefly, CdSe cores with a first exciton feature at 491 nm were synthesized by heating a mixture of trioctylphosphine (TOP), trioctylphosphine oxide (TOPO), CdO (0.9 mmol), and tetradecylphosphonic acid (TDPA, 2.0 mmol) to 340 °C under nitrogen, removing evolved water *in vacuo* at 160 °C, re-heating to 360 °C under nitrogen, and rapidly introducing trioctylphosphine selenide (TOPSe, 3.4 mmol) in trioctylphosphine (TOP), followed by cooling to room temperature. Cores isolated by repeated precipitations from hexane with acetone were brought to 180 °C in a solvent mixture of oleylamine (3 mL) and octadecene (6 mL). Aliquots of Cd and S precursor solutions were then introduced alternately starting with the metal (Cd), waiting 15 min between the start of each addition. The Cd precursor consisted of 0.6 mmol Cd-

oleate and 1.2 mmol decylamine in a solvent mixture of octadecene (3 mL) and TOP (3 mL). The S precursor consisted of 0.6 mmol hexamethyldisilathiane [$(TMS)_2S$] in 6 mL TOP. The dose of each overcoating precursor aliquot was calculated to provide a single monolayer of ions to the QD surface. Addition of a total of 4 aliquots each of Cd and S yielded QDs with emission at 562 nm and a QY close to unity when diluted in hexane. A similar procedure was performed on larger CdSe cores to obtain CdSe(CdS) QDs emitting at 610 nm.

Ligand Exchange with poly(PEG)-PIL. QDs (2 nmol) were precipitated using MeOH and brought into 50 μL of $CHCl_3$. The QD stock solution was mixed with solution of poly(PEG) (5 mg) in $CHCl_3$ (30 μL), and stirred for 10 min at RT, after which 30 μL of MeOH was added followed by stirring for an additional 20 min. QD samples were precipitated by the addition of EtOH (30 μL), $CHCl_3$ (30 μL), and excess hexanes. The sample was centrifuged at 4000 g for 2 min. The clear supernatant was discarded, and the pellet dried *in vacuo,* followed by the addition of PBS (500 μL, pH 7.4) was added. The aqueous sample was then filtered through a 0.2 μm filter syringe filter before use.

Fluorescamine assay of amines on surface of PIL-QDs. QDs emitting at 543 nm ligand-exchanged with various PILs were purified by dialysis 3× through a 50kDa MW cut-off spin concentrator. The QDs were adjusted to 1-2 μM concentration and placed into an eppendorf tube (240 uL). To the tube was added a solution of fluorescamine in acetone (10 uL, 28 mg/mL) followed by vigorous vortexing. The samples were incubated for 10 min at RT and the photoluminescence intensity of Fluorescamine was recorded at 480 nm with an excitation at 380 nm. The amine concentration versus fluorescence count was obtained via a calibration curve generated by performing the same assay on a serial dilution of a known concentration of compound **5**.

Covalent Conjugation of Streptavidin to poly(aminoPEG$_{11}$)$_{25\%}$-PIL QDs. Stretpavidin (50 μL, 10 mg/mL; Sigma Aldrich) was activated in MES buffer (pH 6.5) using Sulfo-NHS and EDC (20 eq) for 20 min at RT. The activated SA was mixed with poly(aminoPEG$_{11}$)$_{25\%}$-PIL QDs in sodium bicarbonate buffer at pH 8.4 at a SA:QD ratio of 5:1 and allowed to react for 1 h. The samples were dialyzed 2× through a 50 kDa MW cut-off spin concentrator and then used for labeling experiments.

Quantum Yield Measurement. QY of 605 nm emitting QDs was measured relative to Rhodamine 640 (λ_{ex} = 535 nm). Solutions of QDs in PBS and dye in ethanol were optically matched at the excitation wavelength. Fluorescence spectra of QD and dye were taken under identical spectrometer conditions in triplicate and averaged. The optical density was kept below 0.1 between 300-800 nm, and the integrated intensities of the emission spectra, corrected for differences in index of refraction and concentration, were used to calculate the QYs using the expression $QY_{QD} = QY_{Dye} \times (Absorbance_{dye}/Absorbance_{QD}) \times (Peak\ Area_{QD}/Peak\ Area_{Dye}) \times (n_{QD\ solvent})^2/(n_{Dye\ solvent})^2$.[43]

Gel Filtration Apparatus. GFC was performed using an ÄKTAprime Plus chromatography system from Amersham Biosciences equipped with a self-packed Superdex 200 10/100 glass column. PBS (pH 7.4) was used as the mobile phase with a flow rate of 1.0 mL/min. For amine functionalized polymers, the PBS buffer was supplemented with 50 mM of 2-(2-aminoethoxy)ethanol. Typical injection volumes were 100 μL. Detection was achieved by measuring the absorption at 280 nm.

Fluorescamine Assay of Amine Reactivity. Stock solutions of either amine-containing polymers were made at 20 mg/mL concentration. A serial dilution was made using 1, 2, and 4 uL of polymer stock into 240 uL of PBS buffer, followed by addition of 10 uL of a 30 mg/mL

solution of fluorescamine. This mixture was vortexed and incubated at room temperature for 10 min before fluorescence analysis on a BioTek plate reader with excitation at 380 nm and detection at 480 nm. The recorded fluorescence intensity signals were calibrated against solutions of known concentrations of compound **5** (methoxyPEG-NH_2).

Cell Culture. HeLa cells were grown in DMEM (Mediatech) with 10% Fetal Bovine Serum (Invitrogen), 50 U/mL penicillin and 50 μg /mL streptomycin (Invitrogen). The cells were transfected using 1 μL Lipofectamine 2000 (Invitrogen), 0.2 μg of BirA-ER plasmid[14, 35] and 0.2 μg of AP-YFP-TM plasmid per well of an 8-well chamber slide (LabTek). 1 mM biotin was added to the media during plasmid expression. Cells were imaged under 4 °C PBS the day after transfection. 1% Bovine Serum Albumin (Sigma) was added to block non-specific binding during specific binding studies of ligand-coated quantum dots. Commercial BSA is known to contain biotin, and the stock BSA solution was dialyzed with a 3 kDa cutoff dialysis tube three times for 8 h in PBS pH 7.4, in 4 °C.

Non-specific binding of QDs to serum. 565 nm emitting CdSe(CdZnS) QDs (5 μL) of various surface coatings were mixed with fetal bovine serum (95 μL) to a final concentration of ~0.5 μM. The mixture was incubated for 4 h at 37 °C with gentle mixing. The resultant QD size distribution was then measured using gel filtration chromatography. The mixture was injected into a Superose 6 GL10/300 column (GE Healthcare, Piscataway, NJ) on an Agilient 1100 series HPLC with an in-line degasser, autosampler, diode array detector, and fluorescence detector (Roseville, CA). PBS (pH 7.4) was used as the mobile phase with a flow rate of 0.5 mL/min and an injection volume of 50 μL. In order to selectively measure the signal from the QD rather than FBS, the fluorescence detection at 565 nm with 250 nm excitation was chosen.

Fluroescence and Phase Contrast Microscopy. Cells were imaged live using a Nikon TE2000-U inverted microscope with a 60× water-immersion lens and a Princeton Instruments MicroMAX Camera with an additional 1.5× magnification tube lens. Bright field images were collected using differential interference contrast and 10 ms exposure. Fluorescence images were collected with epifluorescent excitation provided by the 488 nm line of an Argon-Ion laser with the appropriate dichroic (Chroma, Z488RDC) and emission filters (QD605: D605/30M, YFP: D565/30m). Images were collected and analyzed using Image J version 1.41o. Typical exposure times were 0.1-0.5 s and fluorescence images were background-corrected.

Animal and tumor models. Orthotopic P008 mammary carcinoma models were prepared by implanting a small piece (1 mm^3) of viable tumor tissue from the source tumor animal into the mammary fat pad chamber[40] of 10 – 12 weeks old female Tie2-GFP/FVB mice. The tumors were allowed to grow up to 5 mm in diameter. All animal procedures were carried out following the Public Health Service Policy on Humane Care of Laboratory Animals and approved by the Institutional Animal Care and Use Committee of Massachusetts General Hospital.

Intravital Multiphoton Imaging. To study tumor vasculature using QDs and their distribution dynamic in live animals, 150 μL poly(PEG)-PIL QD600 at a concentration of 5 μM were injected retro-orbitally into the tumor bearing mice and imaged with multiphoton laser scanning microscope.[44] The images were recorded as 3D stacks (200 μm thickness, 1 μm step size) at 0 hour, 3 h and 6 h interval respectively and processed using the NIH ImageJ software. For the GFP channel, the emission filter used was 535±20 nm, and for QD600, the emission filter was 625±75 nm. All images were captured with a 20× water emersion lens (N.A. 0.95) and an excitation wavelength of 880 nm (500 mW).

6.3 *References*

1. Wu, X.; Liu, H.; Liu, J.; Haley, K. N.; Treadway, J. A.; Larson, J. P.; Ge, N.; Peale, F.; Bruchez, M. P., Immunofluorescent labeling of cancer marker Her2 and other cellular targets with semiconductor quantum dots. *Nat. Biotechnol.* **2003,** 21, (1), 41-46.

2. Dahan, M.; Levi, S.; Luccardini, C.; Rostaing, P.; Riveau, B.; Triller, A., Diffusion Dynamics of Glycine Receptors Revealed by Single-Quantum Dot Tracking. *Science* **2003,** 302, (5644), 442-445.

3. Smith, A. M.; Duan, H.; Rhyner, M. N.; Ruan, G.; Nie, S., A systematic examination of surface coatings on the optical and chemical properties of semiconductor quantum dots. *Phys. Chem. Chem. Phys.* **2006,** 8, 3895-3903.

4. Howarth, M.; Chinnapen, D. J. F.; Gerrow, K.; Dorrestein, P. C.; Grandy, M. R.; Kelleher, N. L.; El-Husseini, A.; Ting, A. Y., A monovalent streptavidin with a single femtomolar biotin binding site. *Nat Meth* **2006,** 3, (4), 267-273.

5. Howarth, M.; Takao, K.; Hayashi, Y.; Ting, A. Y., Targeting quantum dots to surface proteins in living cells with biotin ligase. *Proc Natl Acad Sci USA.* **2005,** 102, (21), 7583-7588.

6. Groc, L.; Heine, M.; Cognet, L.; Brickley, K.; Stephenson, F. A.; Lounis, B.; Choquet, D., Differential activity-dependent regulation of the lateral mobilities of AMPA and NMDA receptors. *Nat. Neurosci.* **2004,** 7, (7), 695-696.

7. Aldana, J.; Wang, Y. A.; Peng, X., Photochemical Instability of CdSe Nanocrystals Coated by Hydrophilic Thiols. *J. Am. Chem. Soc.* **2001,** 123, (36), 8844-8850.

8. Algar, W. R.; Krull, U. J., Adsorption and Hybridization of Oligonucleotides on Mercaptoacetic Acid-Capped CdSe/ZnS Quantum Dots and Quantum Dot-Oligonucleotide Conjugates. *Langmuir* **2006,** 22, (26), 11346-11352.

9. Mattoussi, H.; Mauro, J. M.; Goldman, E. R.; Anderson, G. P.; Sundar, V. C.; Mikulec, F. V.; Bawendi, M. G., Self-Assembly of CdSe-ZnS Quantum Dot Bioconjugates Using an Engineered Recombinant Protein. *J. Am. Chem. Soc.* **2000,** 122, (49), 12142-12150.

10. Uyeda, H. T.; Medintz, I. L.; Jaiswal, J. K.; Simon, S. M.; Mattoussi, H., Synthesis of Compact Multidentate Ligands to Prepare Stable Hydrophilic Quantum Dot Fluorophores. *J. Am. Chem. Soc.* **2005,** 127, (11), 3870-3878.

11. Susumu, K.; Uyeda, H. T.; Medintz, I. L.; Pons, T.; Delehanty, J. B.; Mattoussi, H., Enhancing the stability and biological functionalities of quantum dots via compact multifunctional ligands. *J. Am. Chem. Soc* **2007,** 129, (45), 13987-13996.

12. Liu, W.; Howarth, M.; Greytak, A. B.; Zheng, Y.; Nocera, D. G.; Ting, A. Y.; Bawendi, M. G., Compact Biocompatible Quantum Dots Functionalized for Cellular Imaging. *J. Am. Chem. Soc.* **2008,** 130, (4), 1274-1284.

13. Sapsford, K. E.; Pons, T.; Medintz, I. L.; Higashiya, S.; Brunel, F. M.; Dawson, P. E.; Mattoussi, H., Kinetics of Metal-Affinity Driven Self-Assembly between Proteins or Peptides and CdSe-ZnS Quantum Dots. *J. Phys. Chem. C.* **2007,** 111, (11528-11538).

14. Howarth, M.; Liu, W.; Puthenveetil, S.; Zheng, Y.; Marshall, L. F.; Schmidt, M. M.; Wittrup, K. D.; Bawendi, M. G.; Ting, A. Y., Monovalent, reduced-size quantum dots for imaging receptors on living cells. *Nat. Methods* **2008,** 5, (5), 397-399.

15. Medintz, I. L.; Pons, T.; Delehanty, J. B.; Susumu, K.; Brunel, F. M.; Dawson, P. E.; Mattoussi, H., Intracellular delivery of quantum dot-protein cargos mediated by cell penetrating peptides. *Bioconjugate Chem.* **2008,** 19, (9), 1785-1795.

16. Medintz, I. L.; Clapp, A. R.; Brunel, F. M.; Tiefenbrunn, T.; Uyeda, H. T.; Chang, E. L.; Deschamps, J. R.; Dawson, P. E.; Mattoussi, H., Proteolytic activity monitored by fluorescence resonance energy transfer through quantum-dot-peptide conjugates. *Nat. Mater.* **2006,** 5, (7), 581-589.

17. Shen, L.; Pich, A.; Fava, D.; Wang, M.; Kumar, S.; Wu, C.; Scholes, G. D.; Winnik, M. A., Loading quantum dots into thermo-responsive microgels by reversible transfer from organic solvents to water. *Journal of Materials Chemistry* **2008,** 18, (7), 763-770.

18. Yildiz, I.; McCaughan, B.; Cruickshank, S. F.; Callan, J. F.; Raymo, F. i. M., Biocompatible CdSe-ZnS Core-Shell Quantum Dots Coated with Hydrophilic Polythiols. *Langmuir* **2009,** 25, (12), 7090-7096.

19. Smith, A. M.; Nie, S., Minimizing the Hydrodynamic Size of Quantum Dots with Multifunctional Multidentate Polymer Ligands. *J. Am. Chem. Soc* **2008,** 130, (34), 11278-11279.

20. Kim, S.; Bawendi, M. G., Oligomeric Ligands for Luminescent and Stable Nanocrystal Quantum Dots. *J. Am. Chem. Soc.* **2003,** 125, (48), 14652-14653.

21. Bentzen, E. L.; Tomlinson, I. D.; Mason, J.; Gresch, P.; Warnement, M. R.; Wright, D.; Sanders-Bush, E.; Blakely, R.; Rosenthal, S. J., Surface modification to reduce nonspecific binding of quantum dots in live cell assays. *Bioconjugate Chemistry* **2005,** 16, (6), 1488-1494.

22. Wang, M.; Felorzabihi, N.; Guerin, G.; Haley, J. C.; Scholes, G. D.; Winnik, M. A., Water-Soluble CdSe Quantum Dots Passivated by a Multidentate Diblock Copolymer. *Macromolecules* **2007,** 40, (17), 6377-6384.

23. Wang, M.; Oh, J. K.; Dykstra, T. E.; Lou, X.; Scholes, G. D.; Winnik, M. A., Surface Modification of CdSe and CdSe/ZnS Semiconductor Nanocrystals with Poly(N,N-dimethylaminoethyl methacrylate). *Macromolecules* **2006,** 39, (10), 3664-3672.

24. Fang, C.; Qi, X.-Y.; Fan, Q.-L.; Wang, L.-H.; Huang, W., A facile route to semiconductor nanocrystal-semiconducting polymer complex using amine-functionalized rod–coil triblock copolymer as multidentate ligand. *Nanotechnology* **2007,** 18, (3), 035704-035704.

25. Chiefari, J.; Chong, Y. K.; Ercole, F.; Krstina, J.; Jeffery, J.; Le, T. P. T.; Mayadunne, R. T. A.; Meijs, G. F.; Moad, C. L.; Moad, G.; Rizzardo, E.; Thang, S. H., Living free-radical polymerization by reversible addition-fragmentation chain transfer: The RAFT process. *Macromolecules* **1998,** 31, (16), 5559-5562.

26. Naoto, A.; Bungo, O.; Hideharu, M.; Takeshi, E., Mild and Efficient One-Step Synthesis of Trithiocarbonates Using Minimum Amount of CS_2. *Syn. Lett.* **2006,** 4, 636-638.

27. Barner-Kowollik, C., *Handbook of RAFT Polymerization.* Wiley-VCH: 2008.

28. Li, J. J.; Wang, Y. A.; Guo, W. Z.; Keay, J. C.; Mishima, T. D.; Johnson, M. B.; Peng, X. G., Large-scale synthesis of nearly monodisperse CdSe/CdS core/shell nanocrystals using air-stable reagents via successive ion layer adsorption and reaction. *J. Am. Chem. Soc* **2003,** 125, (41), 12567-12575.

29. Xie, R.; Kolb, U.; Li, J.; Basche, T.; Mews, A., Synthesis and Characterization of Highly Luminescent CdSe-Core CdS/Zn0.5Cd0.5S/ZnS Multishell Nanocrystals. *J. Am. Chem. Soc.* **2005,** 127, (20), 7480-7488.

30. Ueda, E. K. M.; Gout, P. W.; Morganti, L., Current and prospective applications of metal ion-protein binding. *J. Chromatogr A.* **2003,** 988, (1), 1-23.

31. Medintz, I. L.; Clapp, A. R.; Mattoussi, H.; Goldman, E. R.; Fisher, B.; Mauro, J. M., Self-assembled nanoscale biosensors based on quantum dot FRET donors. *Nat. Mater.* **2003,** 2, (9), 630-638.

32. Snee, P. T.; Somers, R. C.; Nair, G.; Zimmer, J. P.; Bawendi, M. G.; Nocera, D. G., A Ratiometric CdSe/ZnS Nanocrystal pH Sensor. *J. Am. Chem. Soc.* **2006,** 128, (41), 13320-13321.

33. Somers, R. C.; Bawendi, M. G.; Nocera, D. G., CdSe nanocrystal based chem-/bio-sensors. *Chem. Soc. Rev.* **2007,** 36, 579-591.

34. Mei, B. C.; Susumu, K.; Medintz, I. L.; Delehanty, J. B.; Mountziaris, T. J.; Mattoussi, H., Modular poly(ethylene glycol) ligands for biocompatible semiconductor and gold nanocrystals with extended pH and ionic stability. *J. Mater. Chem.* **2008,** 18, (41), 4949-4958.

35. Howarth, M.; Ting, A. Y., Imaging proteins in live mammalian cells with biotin ligase and monovalent streptavidin. *Nat. Protoc.* **2008,** 3, (3), 534-545.

36. Zimmer, J. P.; Kim, S.-W.; Ohnishi, S.; Tanaka, E.; Frangioni, J. V.; Bawendi, M. G., Size Series of Small Indium Arsenide-Zinc Selenide Core-Shell Nanocrystals and Their Application to In Vivo Imaging. *J. Am. Chem. Soc.* **2006,** 128, (8), 2526-2527.

37. Jain, R. K.; Munn, L. L.; Fukumura, D., Dissecting tumour pathophysiology by intravital microscopy. *Nat. Rev. Cancer* **2002,** 2, 266-76.

38. Jain, R. K.; Brown, E. B.; Munn, L. L.; Fukumura, D., In *Live Cell Imaging: A Laboratory Manual*, Cold Spring Harbor Laboratory Press: Cold Spring Harbor, NY, 2004; pp 435-66.

39. Huang, P.; Dawson, M.; Lanning, R.; Jain, R. K.; Fukumura, D., Spontaneous Tumors in VEGF(P)-GFP/FVB and Tie2(P)-GFP/FVB Transgenic Mice. *Journal of the American Association for Laboratory Animal Science* **2008,** 47, (5), 170-170.

40. Duda, D. G.; Fukumura, D.; Munn, L. L.; Booth, M. F.; Brown, E. B.; Huang, P. G.; Seed, B.; Jain, R. K., Differential transplantability of tumor-associated stromal cells. *Cancer Res.* **2004,** 64, (17), 5920-5924.

41. Murray, C. B.; Norris, D. J.; Bawendi, M. G., Synthesis and characterization of nearly monodisperse CdE (E = sulfur, selenium, tellurium) semiconductor nanocrystallites. *J. Am. Chem. Soc.* **1993,** 115, (19), 8706-8715.

42. Snee, P. T.; Chan, Y.; Nocera, D. G.; Bawendi, M. G., Whispering-Gallery-Mode Lasing from a Semiconductor Nanocrystal/Microsphere Resonator Composite. *Adv. Mater.* **2005,** 17, (9), 1131-1136.

43. Eaton, D., Reference Materials for Fluorescence Measurement. *Pure Appl. Chem.* **1988,** 60, (7), 1107-1114.

44. Brown, E. B.; Campbell, R. B.; Tsuzuki, Y.; Xu, L.; Carmeliet, P.; Fukumura, D.; Jain, R. K., In vivo measurement of gene expression, angiogenesis and physiological function in tumors using multiphoton laser scanning microscopy. *Nature Medicine* **2001,** 7, (7), 864-868.

6.4 *Appendix: ^{1}H NMR Spectra of Compounds*

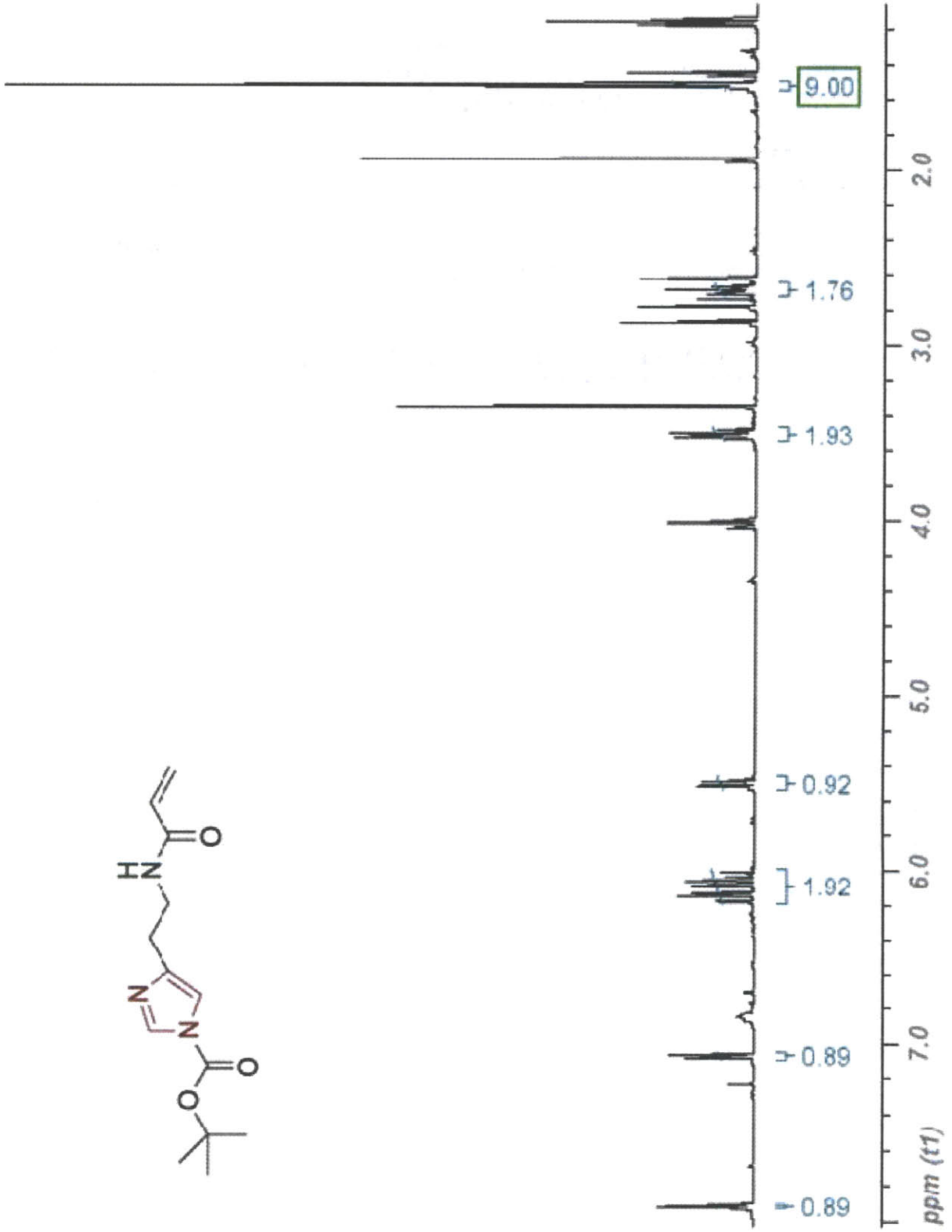

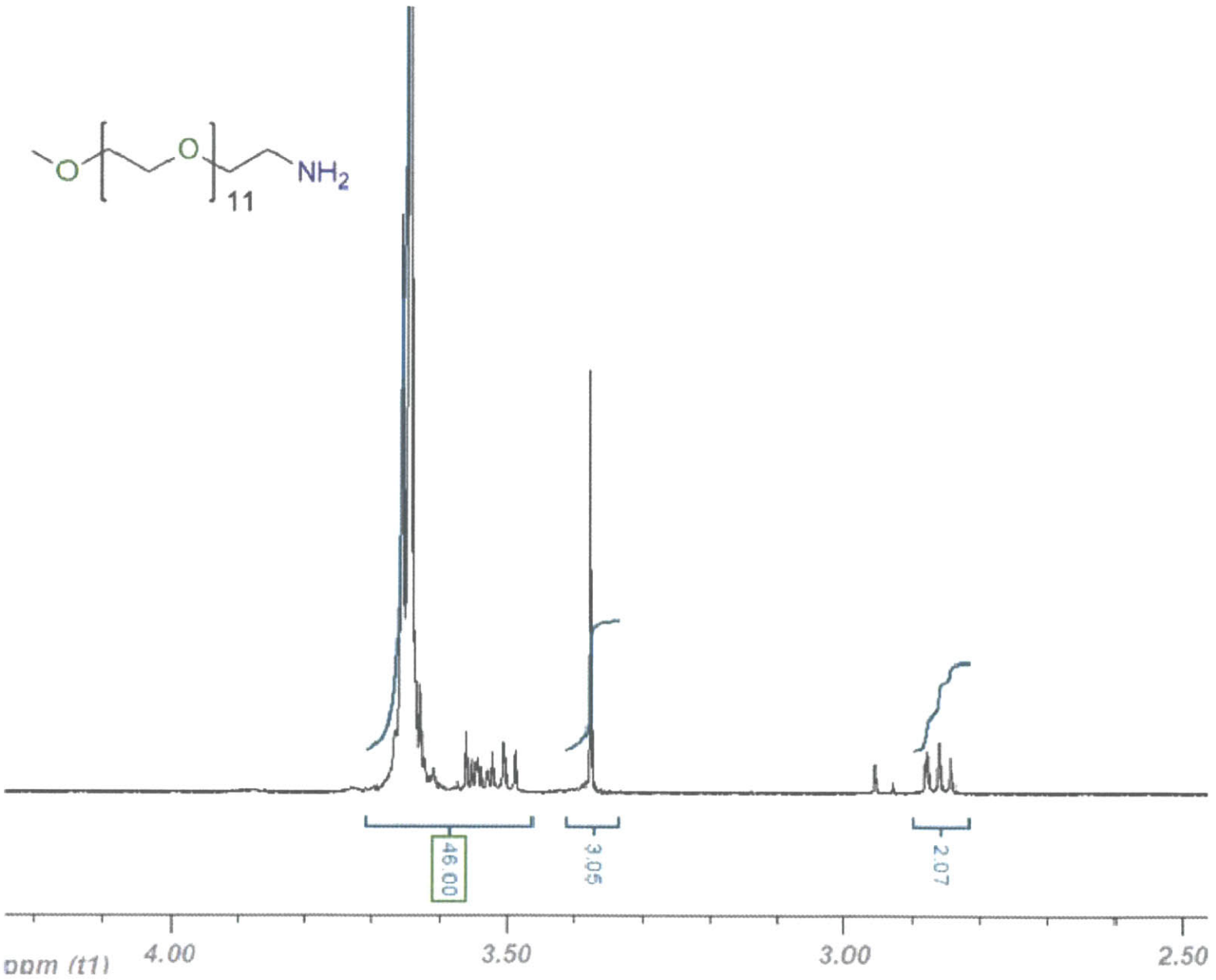
O
O
11
NH2
46.00
3.05
2.07
ppm (t1)
4.00
3.50
3.00
2.50

O
O
O
11
N
H
1.12
1.67
0.81
44.00
4.71
3.30
ppm (t1)
6.50
6.00
5.50
5.00
4.50
4.00
3.50
3.00

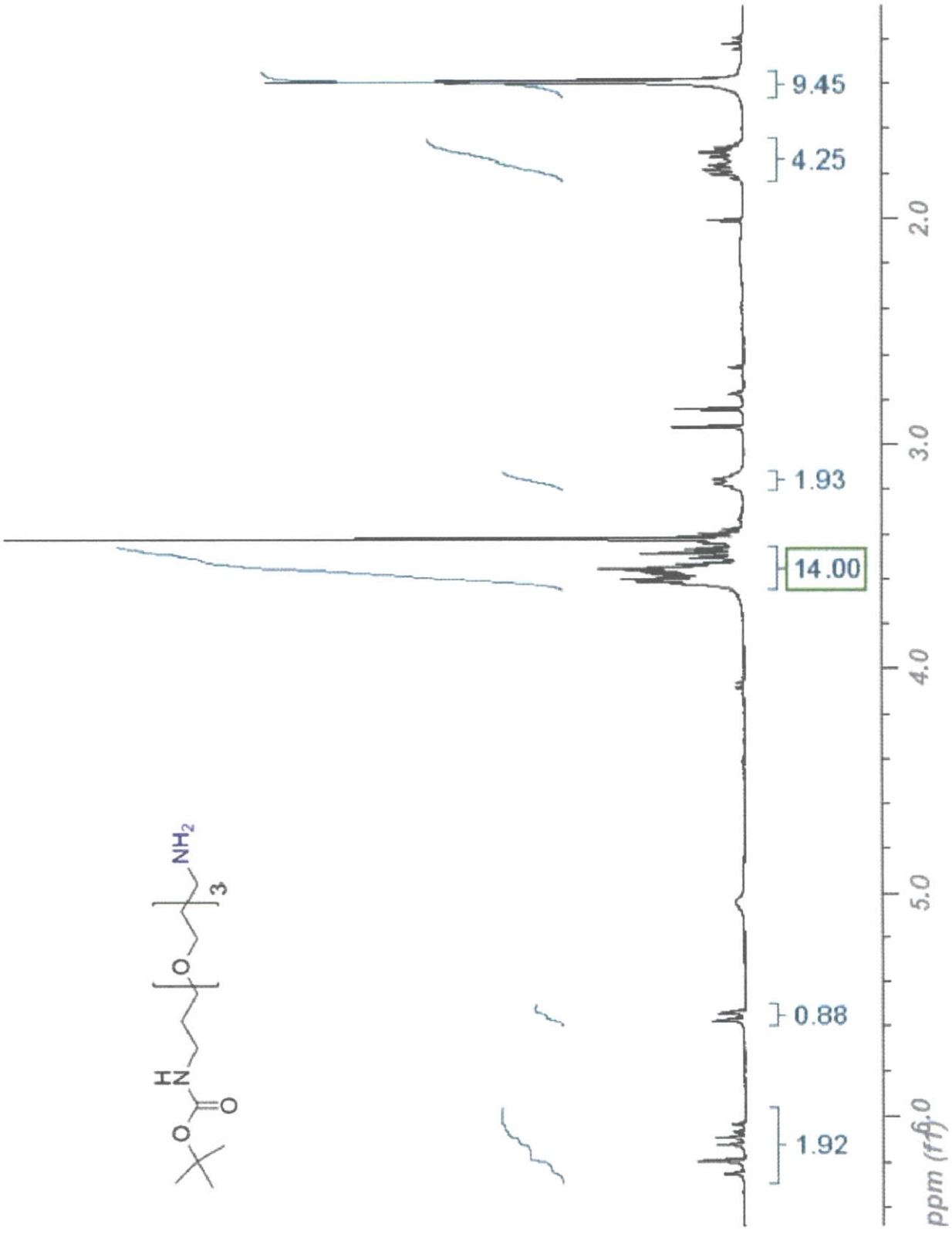
9.45
4.25
1.93
14.00
0.88
1.92
2.0
3.0
4.0
5.0
6.0
ppm (f1)
NH2
3
O
H
N
O
O

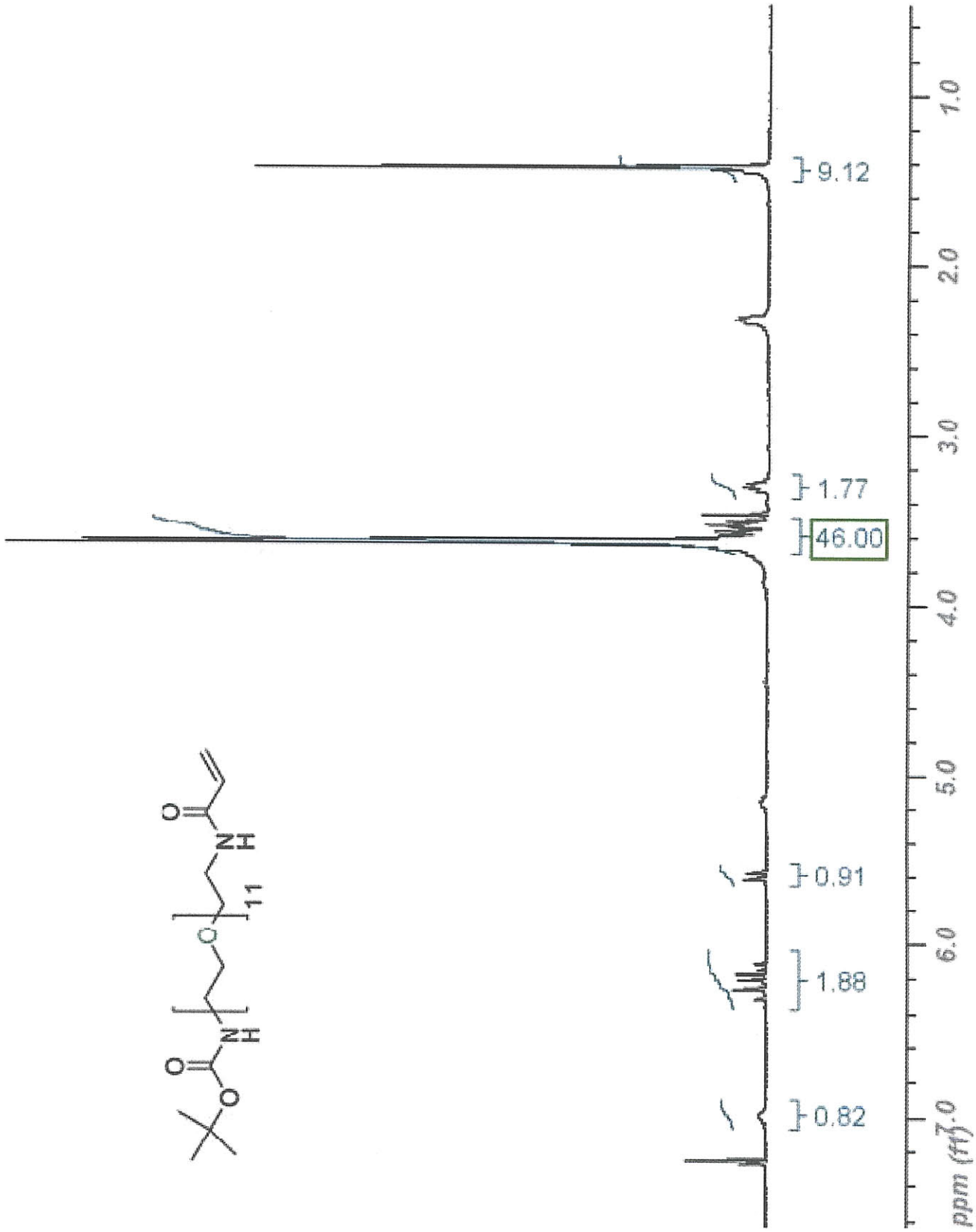
9.12
1.77
46.00
0.91
1.88
0.82
1.0
2.0
3.0
4.0
5.0
6.0
7.0
ppm (f1)
O
NH
11
O
NH
O
O

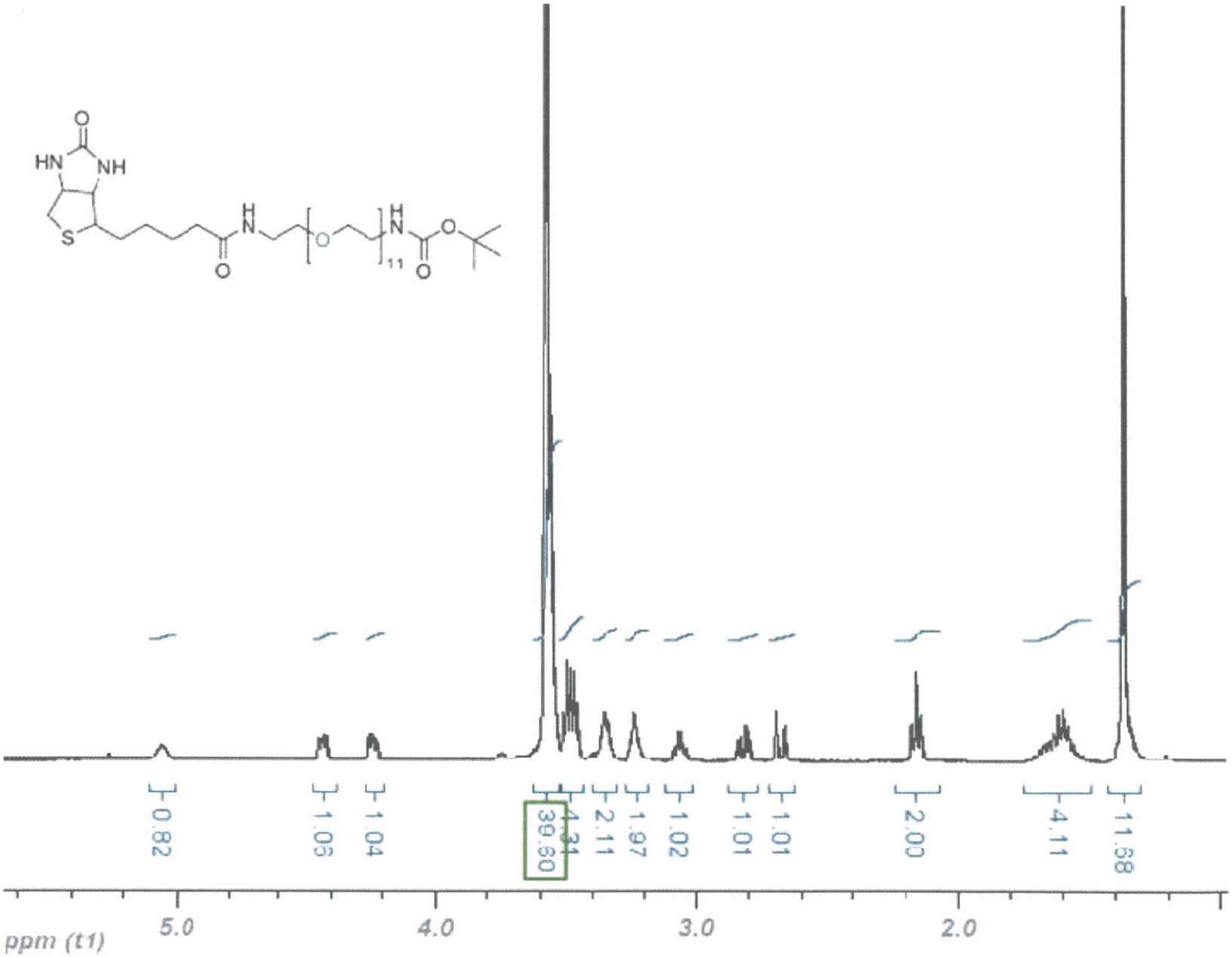
HN
NH
S
O
O
O
O
11
0.82
1.05
1.04
39.60
4.31
2.11
1.97
1.02
1.01
1.01
2.00
4.11
11.58
5.0
4.0
3.0
2.0
ppm (t1)

HN
NH
S
O
H
N
O
NH
11
O
2.26
0.81
0.91
0.88
44.0
1.81
1.04
1.29
1.01
1.87
4.42
2.07
2.27
7.0
6.0
5.0
4.0
3.0
2.0
1.0
ppm (t1)

Wenhao Liu

70 Pacific St. Apt 708 • Cambridge, MA 02139 • Phone: 224-558-2846 • E-mail: wenliu@mit.edu

---

Education

MASSACHUSETTS INSTITUTE OF TECHNOLOGY
Cambridge, MA
Candidate for Ph.D. in Chemistry, June 2010

- Designed and synthesized novel coordinating ligands for water-solubilization of fluorescent semiconductor nanocrystals (quantum dots, QDs), and demonstrated the efficacy of these new QDs for targeted imaging in tumor detection and for single molecule imaging on live cells
- Developed synthesis of novel imidazole-based polymer coating, achieving >10x increase in stability of water soluble QDs with impact in biological imaging and sensing applications (patents filed).

NORTHWESTERN UNIVERSITY
Evanston, IL
B.A. with Honors in Chemistry,
GPA: 3.9/4.0
B.A. in the Integrated Science Program, June 2005
Honors Thesis: Solid State Solvation of Donor-Acceptor Molecules in Amorphous Organic Thin Films.

Research Internships

IBM ALMADEN RESEARCH CENTER (6/2004 – 8/2004)
San Jose, CA

- Advisor: Craig Hawker. Developed novel polymer synthesis, achieving unprecedented control of chain-end functionality by combining RAFT polymerization with Click chemistry.
- Skills: Organic synthesis, living radical polymerization and polymer characterization, thin film deposition.

MIT LAB OF ORGANIC OPTICS AND ELECTRONICS (6/2003 – 8/2003)
Cambridge, MA

- Advisor: Vladimir Bulović. Led study on photo-induced rotation of polar molecules within optically active organic thin films.
- Developed understanding of the solid state solvation effect on tuning emission color of organic LEDs for potential commercial applications.
- Skills: N_2 glovebox handling, spin-coating, evaporative deposition under ultra-high vacuum, OLED device fabrication, electrical and optical characterization of OLED devices, AFM.

NORTHWESTERN UNIVERSITY CHEMISTRY DEPT (6/2002 – 8/2002)
Evanston, IL

- Advisor: Michael Wasielewski. Studied photo-induced electron transfer in donor-acceptor molecules using ultra-fast femtosecond transient absorption spectroscopy.
- Built Ti:Sapphire cavity dumped laser system as light source for fluorescence lifetime measurements.

Publications

Allen PM, **Liu W**, Chauhan VP, Lee J, Ting AY, Fukumura D, Jain RK, Bawendi MG. InAs(ZnCdS) Quantum Dots Optimized for Biological Imaging in the Near-Infrared. *J Am Chem Soc* 2010, **132**: 470-471.

Liu W, Greytak AB, Lee JM, Wong CR, Park J, Marshall LF, Jiang W, Ting AY, Nocera DG, Fukumura D, Jain RK, Bawendi MG. Compact biocompatible quantum dots via RAFT-mediated synthesis of imidazole-based random copolymer ligand. *J Am Chem Soc* 2009, **132**: 472-483.

Choi HS, **Liu W**, Liu F, Nasr K, Misra P, Bawendi MG, Frangioni JV. Design considerations for tumour-targeted nanoparticles. *Nature Nanotech* 2009, **5**: 42-47.

Halpert JE, Tischler JR, Nair G, Walker BJ, **Liu W**, Bulovic V, Bawendi MG. Electrostatic Formation of Quantum Dot/J-aggregate FRET Pairs in Solution. *J Phys Chem C* 2009, **113**: 9986–9992.

Liu W, Howarth M, Greytak AB, Zheng Y, Nocera DG, Ting AY, Bawendi MG. Compact Biocompatible Quantum Dots Functionalized for Cellular Imaging. *J Am Chem Soc* 2008, **130**: 1274 -1284.

Howarth M, **Liu W**, Puthenveetil S, Zheng Y, Marshall LF, Schmidt MM, Wittrup KD, Bawendi MG, Ting AY. Monovalent, reduced-size quantum dots for imaging receptors on living cells. *Nature Methods* 2008, **5**: 397-399.

Liu W, Choi HS, Zimmer JP, Tanaka E, Frangioni JV, Bawendi MG. Compact Cysteine-Coated CdSe(ZnCdS) QDs for In Vivo Applications. *J Am Chem Soc* 2007, **129**: 14530.

Choi HS, **Liu W**, Misra P, Tanaka E, Zimmer JP, Kandapallil B, Bawendi MG, Frangioni JV. Renal Clearance of Nanoparticles. *Nature Biotech* 2007, **25**: 1165 - 1170.

Sinks LE, Fuller MF, **Liu W**, Ahrens MJ, Wasielewski MR. Photoinduced electron transfer in a donor–acceptor dyad oriented by an aligned nematic liquid crystal solvent. *Chem Phys* 2005, **319**: 226-234

Goldsmith RH, Sinks LE, Kelley RF, Betzen LJ, **Liu W**, Weiss EA, Ratner MA, Wasielewski MR. Wire-like charge transport at near constant bridge energy through fluorene oligomers. *Proc Natl Acad Sci U S A.* 2005, **102**:3540-5.

Ahrens MJ, Sinks LE, Rybtchinski B, **Liu W**, Jones BA, Giaimo JM, Gusev AV, Goshe AJ, Tiede DM, Wasielewski MR. Self-assembly of supramolecular light-harvesting arrays from covalent multi-chromophore perylene-3,4:9,10-bis(dicarboximide) building blocks. *J Am Chem Soc* 2004, **126**:8284-94

Awards and Honors

National Science Foundation Graduate Research Fellowship (2006)
MIT Praecis Presidential Fellowship (2005)
Marple-Schweitzer Award (2005), awarded to top graduating senior in Chemistry
Sarrett Scholarship Award (2005), awarded to senior with best undergraduate thesis
Phi Beta Kappa (2004)
Undergraduate Research Grant (2004), awarded for original research proposal
Barry M. Goldwater Scholarship (2003)

Patents

"Imidazole-Based Random Co-Polymer for Synthesis of Water Soluble Biocompatible Semiconductor Nanocrystals", Provisional Patent submitted, August 16, 2009.

"Materials and Methods for Biological [NIR] Imaging", Provisional Patent Submitted, 2009

"Controlled Modification of Semiconductor Nanocrystals", US Patent Number 60/990,485 filed Nov 27, 2007, International Patent Number PCT/US2008/067649 filed June 20, 2008.

Conference Talks

RAFT mediated synthesis of imidazole-based random block copolymers as a chelating ligand for quantum dot water solubilization. American Chemical Society National Meeting 2010, Mar 21-25, San Francisco, CA. Podium Presentation.

RAFT mediated synthesis of imidazole-based random block copolymers as a chelating ligand for quantum dot water solubilization. American Chemical Society National Meeting 2009, Aug 15-20, Washington DC. Podium Presentation.

Compact Biocompatible Quantum Dots Functionalized for Cellular Imaging. Wenhao Liu. International Materials Research Society Conference 2008, Jun 9-12, Chongqing, China. Podium presentation.

Rapid total body clearance of nanosized objects. Wenhao Liu. American Chemical Society National Meeting 2007, Aug 19-23, Boston, MA. Podium presentation.

Community Involvement

WEB SYSTEMS DEVELOPER, OFFICE OF DEAN FOR STUDENT LIFE (11/2009 – 5/2010)

- Developed campus-wide housing management system for all on-campus dorms.
- Designed and implemented integrated system that manages student housing, building inventory, guest lists, package tracking, and customized content.
- On track to be adopted by all MIT on-campus dorms by the end of the year.

WEBMASTER, GRADUATE STUDENT COUNCIL (4/2009-4/2010)

- Re-designed GSC homepage to enhance ease of navigation
- Managed web commerce system for GSC Ski Trip and the Grad Gala
- Developed web applications to support the GSC internally in its mission to serve the community

WEB SYSTEMS DEVELOPMENT LEAD, MIT STUDENT ACTIVITIES OFFICE (9/2008 – 6/2009)

- Co-directed project that brought E-ticketing to MIT community.
- Led development of a flexible and extensible web-based ticketing manager, a custom shopping cart interface, an E-commerce system for credit processing and a print-at-home ticket and barcode scanning system.
- Resulted in over 3000 E-tickets sold for MIT community events in 2 months, including a concert where over 2000 people were admitted ~3x faster than in previous years using new electronic system, generating >50k in revenue.
- System continues to be widely used by over 20 student groups across campus.

CHIEF INFORMATION OFFICER, MIT CAREER FAIR (6/2008 – 9/2009)

- Managed hardware and deployed web technologies to support the MIT Career Fair.
- Worked closely in team with Career Fair Directors. Developed new E-commerce interface for credit processing and web tools to manage online company and student registration, resulting in an event attended by >300 companies and >3000 students, generating over 650K in revenue for MIT.

VICE PRESIDENT OF INFORMATION, SIDNEY PACIFIC EXECUTIVE COUNCIL (4/2008 – 4/2009)

- Managed team of 8 responsible for marketing and publicity of over 100 social

events, with two large events attracting an unprecedented attendance of >900 from MIT community.
- Directed the development of an online integrated publicity interface which streamlined a cumbersome procedure involving 4 steps into one interface for submitting publicity requests, greatly increasing throughput, efficiency, and accountability.

WEBMASTER, SIDNEY AND PACIFIC HOUSE GOVERNMENT (4/2005 – 4/2007)
- In charge of front-end and back-end database server.
- Developed applications to improve building security, increase resident interaction, and streamline government functions like publicity.

Personal

Interests: Piano, rock climbing, skiing, cooking, salsa dancing.
Languages: English, conversational ability in Mandarin.
Citizenship: United States of America.

Acknowledgements

I view these past 5 years as one of the most enriching times of my life. I feel that I have grown a great deal both as a person and as a scientist, and I couldn't have done it without the support of so many wonderful mentors and friends all around me. There are first of all some people who deserve special recognition, who throughout my life have nurtured my interest in science and have inspired me to pursue this path. One is Mr. Stanley, my high school science teacher, who brought chemistry alive in my mind. At Northwestern, I'd like to thank Ryan Hayes, a graduate student I met during my freshman year at a poster session who introduced me to his research and to his lab. Out of that friendship grew a 4 year long stint in the lab of Professor Michael Wasielewski, who became an important mentor in my life. He treated me like one of his graduate students, and always pushed me to do my best. Aaron Massari is another graduate student mentor I'd like to acknowledge, who spent many dozens of hours showing me the ins and outs of Ti:Sapph lasers ("you have to treat it like a woman").

At MIT, I'd like to first of all thank Moungi for giving me the opportunity to work in his lab. In addition to providing us with what seemed like unlimited funds to conduct research to our heart's content, he has also served as a wonderful mentor and friend. Moungi was always one to keep us focused on the big picture, and he has the gift of nudging us in the right direction while giving us the feeling that we have the freedom to pursue our own interests. In that sense, I could not have asked for a better advisor. He put his full trust in us, and I felt like I could not let him down. I believe that his style of management has contributed greatly to my success at MIT both inside and outside of the lab and for that I owe him a great debt of gratitude.

I'd like to acknowledge my first-year mentor John Zimmer for patiently instructing me in the ways of the lab and for tolerating my sometimes inconsiderate behavior with his lab space and hood. I'd like to also thank the following people who I met in lab during my first year who made me feel welcome and part of a family: Jon Halpert, Preston Snee (aka Dr. Chicken), Becky Somers, Johnny Steckel, Brian Yen, Venda Porter, Hao Huang, Numpon Insin, Gautham Nair, David Oertel, Jean-Michael Caruge and Yinthai Chan. I'll never forget the weekly adventures to "The Beast" and the No. 9 special with hot and sour soup.

What made my first year at MIT special were also the close friendships I formed with the people of my year in the Chemistry Department. That year, we must've tried nearly every good restaurant and partied at every club in Boston in our weekly Friday night outings. Of note are: birthday dinner at 33, motorcycle models at Avalon, international nights at Caprice, getting accused at Mantra of being underage, table dancing at Rumor, walks around the North End, and after-parties in my room where we stayed up all night karaoking cheesy love songs from the 90s. We kept each other sane and prevented each other from taking life too seriously under the pressure of classes and TAing. For my friends, I'd like to acknowledge Zhe Lu, Scott Geyer, Omar Ahmad, Brenda Goguen, Wendy Iskendarian, Nancy Yerkes, Montana Peterson, Lindsey McQuade, Cliff Wong, and Jennie Fong.

I'd like to also give special thanks to my collaborators, from whom I gained a tremendous amount of experience and support during my first year. I'd like to thank Dr. Hak-Soo Choi, Professor John Frangioni, Dr. Mark Howarth, and Professor Alice Ting for believing in me and for guiding me along both challenging and worthwhile projects. I'll always remember the summer where I rode my bike over to Beth Israel Hospital every other week with a QD size series and a picosecond diode laser strapped to my back. I never thought I would be so thrilled to see fluorescent mouse urine. I'll also remember the long nights with Mark trying to figure out how to AFM QDs with DNA, or painstakingly doing the same synthesis over and over again to try to reproduce results that had magically worked the very first time. Their dedication to science was a true inspiration to me and it made all the late nights in the lab enjoyable and worthwhile in

retrospect. I want to also thank Dr. Andrew Greytak, who I had the pleasure of working with on the QD sensor projects, for his meticulous approach to synthesis (and everything else) and for his amazing Matlab skills. I'd also like to thank Professor Dan Nocera for giving up his Sunday afternoons to help us go over our manuscripts and for always supporting us whenever we needed him.

Another part of the enriching experience I've had at MIT comes from the various activities and groups I became involved with outside of lab. In Sidney and Pacific (SP), where I lived for my entire tenure at MIT, I got a chance to experience the diversity and community spirit of MIT. Never have I seen such an impressive self-organized student government, and it was my privilege to have served with them for two years as Webmaster and one year on the Executive Council. I'd like to thank Dottie and Roger Mark, Roland Tang, and Annette Kim, who were the building's housemasters and served as wonderful mentors to myself and to the community. Their kindness and commitment to the students at MIT were an inspiration to me. They invited us into their homes and into their lives and made sure we had the resources and support we needed to carry out our vision in the House Council. For my friends and colleagues at SP, I would like to also acknowledge Ardavan Oskooi, Ben Mares, Matt Eddy, Sriram Krishnan, Nan Gu, Rob Wang, Jane Kim, Michelle Sander, Jiawen Chen, Matt Walker, Leslie Rogers, Hila Hashemi, Daniel Weller, Alex McCauley, Kasia Gora, Kai Iamsumang, Biliana Kaneva, James Hong, Alex Chan...the complete list is too long to list here. All of you have truly made SP the best place to live and brought the community to life. Some highlights include: the SP James Bond Dance Party, watching Roger being dropped into the Dunk Tank at the summer carnival, hanging up a 100 ft tarp off the side of the building for use as a giant outdoor movie screen, staying up until 6 one night with Ben rebuilding the SP webserver, spending a nice summer weekend at Roger and Dottie's house in the Cape, and cruising around the ocean in Roger's sailboat.

Through my involvement with Sidney Pacific, I was referred to a position (thanks, Nan) at the MIT Career Fair in my 3rd year, where I got to manage the web system that ran one of the largest student-organized career fairs in the country. Working with the other Career Fair Directors has reminded me of another amazing thing about MIT – the incredible organizational skills of the students here and what they can achieve on time volunteered out of their own schedules. For this experience, I'd like to acknowledge Victor Wang, Kaustuv DeBiswas, and Nathan Hammond for displaying commendable leadership and for teaching me a great deal about time management. My time at the Career Fair led to another collaboration where I got the chance to help develop an electronic ticketing system for MIT, which is now widely used by numerous student groups on campus. This led to another project for a campus-wide housing management system, which will hopefully be adopted by the MIT dorms later this year. Working in these large-scale projects has taught me how to think in a whole new way, and having a chance to create something of value to the community has been a tremendously satisfying experience. For this opportunity I'd like to thank Joshua Velasquez, who initially found me and believed in me when I didn't believe myself that it could be done. Some highlights include: weekend coding sessions that ran past midnight powered by Subway and techno, and watching a line of ~2000 students lined up outside the Ben Folds Five Spring concert as the first real-world test of our ticketing system and having that system actually working for the first time.

For all of these extracurricular activities, I'd like to especially acknowledge my first year room-mate Ardavan Oskooi, who encouraged me to apply to be Webchair at Sidney Pacific at the end of my first year. Without his advice and urging, I probably would never have done it and would have missed out on a great deal of opportunities. He also introduced me to Salsa dancing (which is how I met my fiancée) and to a wonderful group of people in the physics and math departments who I never would have interacted with otherwise. There was never a dull moment those first two years when we were roommates. To Ardavan, who has always stirred things up in my life, I thank you.

I'd also like to acknowledge the incoming waves of new students into the lab throughout the years with whom I have developed close friendships and shared many memories with both inside and outside of lab. I'd like express gratitude towards my mentees Hee-Sun Han for her always sunny disposition and positive attitude, and also Jungmin Lee for taking charge in leading the in-vitro QD research efforts. I will remember our food trips to Finale and fancy restaurants, and our fun hiking adventure to Franconia Ridge. I also want to give a shout-out to my "bro" Peter Allen, with whom I've shared an office for the past three years. The art of the "hand stamp", which we've perfected as a system for living large in the local Boston party scene even as poor graduate students, has contributed tremendously to our quality of life here. It was good to see Peter finally adjust to being out of California and to break out of his comfort zone. I'd like to give special acknowledgement to the oysters at Union Oyster house, the bachelorettes at the Liquor Store, the Little Black Dress Party, Wednesday nights at 33, the amazing lady at the Tam who pours us extraordinary drinks at sub-ordinary prices, and the late-night sausage stand outside of Gypsy Bar. These are sights, sounds, and feelings about Boston that I will never forget.

Life here has inevitably followed a sort of work hard/party hard philosophy, and I'm glad to say that the partying part was not without its purpose. I would like to thank that latter aspect of my life because it is how I met my fiancée and future wife. It was at a salsa club in Allston where I saw her for the first time, and the rest was history. I'd like to thank Fiona for sharing her life with me for her last year living in America before having to return to China. With her I have traveled the world, from Acadia National Park to Orlando, from Hong Kong to Thailand. It has not been easy to keep up the long distance relationship from opposite ends of the world this past year. We've been through a lot together, and I can't express enough how much I appreciate her kindness, support, and love. We have plans to get married in June and I look forward very much to spending my life with her together.

Last but not least I'd like to thank my parents for raising me and for everything they've sacrificed so that I could have the best possible start here in America. It was not easy for them to leave China and establish a life in the US. Many nights in those early days were spent washing dishes or taking orders at restaurants in Philadelphia's Chinatown, making just enough money to get by while they were also trying to earn their degrees in school. During that time I was happily in China being raised by my grandparents oblivious of the tremendous hardships they faced. My father made the biggest sacrifice of all by leaving for the US right around my 1st birthday. I met him for the first time at age 6 when I came to the US. While we were fairly poor in those days, he made sure I had plenty of mental stimulation and bought me many things that they could not afford, like model airplanes, chemistry sets, and RC cars. My mom spent countless hours tutoring me in English and helping with my homework, even while she was so busy with her own studies at the time. To my parents, I owe everything I have now. I feel that they have done a tremendous job in raising me and it was not until recently when I started thinking about starting a family of my own that I fully comprehended and appreciated the magnitude of the challenges they faced. I'd also like to thank my grandparents, and my aunt and uncle in China who nurtured me and raised me in my early years. It was later I learned that they suffered their own hardships during that time, but they were still able to provide me with the happiest childhood memories any kid could have.

Thanks again to all who have made my life possible up to this point, and to those who have made these past 5 years some of the best times of my life. I will miss you all dearly. I hope that we will keep in touch.

-Wen